UNIVERSITY OF BIRMINGHAM

INNOVATIONS IN FRAGRANCE ENCAPSULATION USING SILICA BASED PICKERING EMULSIONS

Mariana Benetti Terra Cardoso

A thesis submitted to The University of Birmingham for the degree of

DOCTOR OF PHILOSOPHY

School of Chemistry
College of Physical and Engineering Sciences
The University of Birmingham
August 2019

Abstract

Perfume microcapsules are essential components of laundry formulations to ensure perfume compatibility and provide a durable fragrant benefit, giving a sense of freshness to the consumer. In this context, the demand for sustainable perfume encapsulation techniques has been experiencing rapid growth as the industry investigates eco-friendly shell materials such as inorganic matrixes and biodegradable polymers as alternatives to conventional organic polymers. However, marrying the ecological demands with the technical challenges of having capsules that can retain and deliver the active ingredient in a complex formulated product is not straightforward.

In this work, a novel sustainable encapsulation method based on nanoparticle-stabilized emulsions, so-called Pickering emulsions, combined with silica-based sol-gel chemistry was developed and characterized using a perfume model (hexyl salicylate). The new technology was then tested for the encapsulation of a real-world perfume oil composition used in laundry applications. The obtained fully-inorganic silica capsules demonstrated outstanding mechanical stability, good resistance against perfume leakage and promising freshness performance in a complex liquid detergent formulation. By tuning the nanoparticles surface, it was also possible to successfully encapsulate other hydrophobic and hydrophilic actives, showing that the technology is flexible and has potential as an alternative to commercial organic polymer microcapsules for several industrial applications.

To my family and

in memory of my grandparents,

Leoni and Luli.

Acknowledgments

First of all, I would like to thank my academic supervisors Prof. Jon Preece and Prof. Zhibing Zhang and my industry supervisor Dr. Pierre Verstraete for the support and invaluable guidance throughout the PhD project. Your combined mentorship in chemistry, chemical engineering and formulations shaped me as a professional. I am looking forward to keeping working together in new and exciting projects.

I would also like to thank the laboratory and office friends that I have had the pleasure to meet during this journey. Thank you, Dennis, Greg, Michael and Owen, Andre and Peter, for always being there to help when needed. Thank you, Andy, Bianca, Bing, Dan, Javier and Xiaoting for your friendship and support both inside and outside the lab. I am also grateful for the amazing friends I made in Birmingham and are now just like family: Manue, Martina, Lies, Alfred, Francesco and Dorin.

I would like to thank School of Chemistry and School of Chemical Engineering, University of Birmingham for funding, administrative support and laboratory facilities, as well as Conselho Nacional de Pesquisa (CNPq) and Proctor and Gamble for the financial support.

To my family: Pai, Mae e Thi, obrigada por acreditar em mim, a distância é difícil, mas contar com o seu amor incondicional faz qualquer desafio parecer brincadeira. Se cheguei aqui e por que vocês me ensinaram a não desistir e sempre acreditar que é possível! Amo vocês.

Finally yet importantly, I would like to thank my adventure partner and best friend Ben for always being there for me. Your support made the difference, especially while writing this thesis. J'attends avec impatience les prochains chapitres de nos vies.

Table of Contents

List of Figures

List of tables

List of Equations

List of Abbreviations

1H NMR	Proton nuclear magnetic resonance
29Si NMR	Silicon nuclear magnetic resonance
A300	Aerosil 300 - hydrophlic fumed silica nanoparticles
AR	Allura red
CMC	Critical micelle concentration
CTAB	Cetylmethylammonium bromide
DB	Degree of branching
DFO	Dry fabric odour
DI water	Deionised water
EE	Encapsulation efficiency
ELS	Light scattering detector
FMCG	Fast Moving Consumer Goods
GC-MS	Gas chromatograph connected to a mass spectrometry detector
GPC	Gel permeation chromatography
HDL	Heavy-duty laundry detergents
HS	Hexyl salicylate
IPM	Isopropyl myristate
IR	Infrared spectroscopy
LFE	Liquid fabric enhances
LOC	Leave-on hair conditioners
MF	Melamine-formaldehyde
MML	Menthol menthyl lactate
Mw	Molecular weight
P&G	Procter & Gamble
PDI	Polydispersity index
PEOS	Hyperbranched polyethoxysiloxane
PM546	Difluoro[2-[1-(3,5-dimethyl-2H-pyrrol-2-ylidene-N)ethyl]-3,5-dimethyl-1H-pyrrolato-N]boron
PMC	Perfume microcapsule
PO	Commercial perfume oil provided by P&G
PRM	Perfume raw material
PSD	Particle size distribution
PZC	Point of zero charge
R816	Aerosil R816 - hydrophobic fumed silica nanoparticles
RFO	Rubbed fabric odour
ROC	Rinse-off hair conditioners
SEM	Scanning electron microscopy
SiO_2 NPs	Hydrophlic fumed silica nanoparticles
St Dev	Standard deviation
TEM	Transmission electron microcopy
TEOS	Tetraethoxysiloxane

Tg	Glass transition temperature
TMOS	Tetramethyl orthosilicate
UF	Urea-formaldehyde
UV-Vis	Ultraviolet-visible spectrocopy
VOCs	Volatile organic compounds
WFO	W+B14:C48et fabric odour

Scientific contributions

Patent applications

- Three patent applications submitted to the European and US patents offices (2019)

Conferences and Symposiums contributions

- Encapsulation of Hydrophilic/Hydrophobic Actives Using Silica Colloidosomes, RSC Chemical Nanosciences and Nanotechnology Meeting, Keele – UK (2016)
- Smart Microcapsules for Long-term Storage and Controlled Release of Strategic Actives for the Industry, Brazil Forum, Birmingham – UK (2017)
- Enhancing Consumer Goods Formulations Through University-Industry Collaboration – How to Promote Such Collaborations in Developing Countries? IX ABEP-U – London, UK (2017)
- Controlling the Nature of Pickering Emulsions by Varying the Surface Properties of Silica Colloidal Particles, 16th European Student Colloids Conference – ECIS, Florence -IT (2017)
- Silica Microcapsules for Controlled Release of Strategic Actives for Industry, School of Chemistry Postgraduate symposium 2017, Birmingham – UK (2017)
- Encapsulation and Trigger Release of Hydrophobic and Hydrophilic Actives Using Novel Silica Colloidosomes, Formula IX, Beijing – CH (2017)

- Encapsulation and Triggered Release of Hydrophobic and Hydrophilic Actives Using Silica Colloidosomes, Commercialisation of Pickering emulsions – RSC, London – UK (2017)
- Encapsulation and Triggered Release of Hydrophobic and Hydrophilic Actives Using Silica Colloidosomes, Innovations in Encapsulation – RSC, London – UK (2017)
- Encapsulation and Triggered Release of Hydrophobic and Hydrophilic Actives Using Silica Colloidosomes, Formulation Forum Launch Event 2018 -SCI , London – UK (2018)
- *Sustainable Encapsulation of Consumer Goods Actives*, School of Chemistry Postgraduate symposium 2018, Birmingham – UK (2018)

Thesis outline

Chapter 1– The literature review chapter begins by introducing the role of fragrances in consumer goods and highlighting current microencapsulation approaches to stabilised fragrances in formulations in general. Then, the current state-of-the-art for introducing fragrances to laundry products via microencapsulation is discussed including potential health and environmental safety issue related to current approaches. Finally, sustainable and environmentally friendly alternative encapsulation techniques are discussed followed by a more in deep review of Pickering emulsion-based encapsulation (so called, colloidosomes) and silica sol-gel chemistry encapsulation techniques.

Chapter 2 – An overview of the materials and microcapsule characterisation techniques is described in detail. Special attention is given to the different types of microscopy used throughout the project and the micromanipulation technique used for all mechanical properties measurements. The methods used in the industry for the performance and stability characterization of perfume microcapsules are also explored for the test of the silica capsules produced in this project.

Chapter 3 – The first result chapter describes the fundamentals of emulsion stability for oil-in-water emulsions using hydrophilic silica as Pickering emulsifier. Next, the preparation and characterization of the inorganic polymer used as silica precursor for the formation of the shell is presented. Finally, the mechanisms for the formation of Pickering emulsion-based silica capsules are fully discussed.

Chapter 4 – This chapter starts with the synthesis of silica capsules using a perfume model – hexyl salicylate – followed by a full technical characterisation of these capsules. Next, encapsulation parameters that can affect silicon-based capsules, for example: pH and the levels of the silica precursor and nanoparticles, are studied, including a summary of the mechanical properties of these capsules.

Chapter 5 – The preparation and characterization of silica capsules with a real-world consumer good perfume formulation is presented and discussed, including details of performance and stability testing using laundry product formulations.

Chapter 6 –In the first part of Chapter 6 methods to improve the stability and performance of perfume oil/silica are studied following two approaches: First using a hydrophobic co-solvent in the core (Isopropyl myristate) with high affinity to the perfume oil, to minimize leakage. Then, a process to mineralise silica capsules using sodium silicate and tetraethoxysiloxane is designed to improve stability in the finished product. In the second part of the chapter, the technology developed in this project is used for the encapsulation of other strategic actives for consumer goods products including a water-soluble dye model (other water-soluble actives can benefit from this, such as enzymes) and Menthyl menthol lactate (used for hair care applications).

Chapter 7 – Chapter 7 summarises the general conclusions from this project and proposes recommendations for future work and further development of the encapsulation process leading to better performance and stability in the finished product.

CHAPTER 1. Literature Review

Abstract

The aim of this chapter is four-fold:

(i) to understand the role of fragrances in consumer goods;

(ii) highlight the challenges when introducing perfumes into consumer products;

(iii) highlight current approaches to overcoming the challenges, via microencapsulation;

(iv) highlight the environmental and health safety issues related to the current perfume encapsulation techniques;

Building on the four points above and the current state-of-the-art for introducing perfumes into laundry products, this chapter will outline the hypothesis for the PhD research in this thesis for the microencapsulation of perfumes for introduction into laundry products.

Encapsulation strategies will also be introduced, looking into sustainable and environmentally friendly alternatives to the currently used polymeric based microcapsules. These sustainable capsules must perform and be stable in the finished product similarly to their polymeric counterparts. More specifically, encapsulation using colloidal particles, the so-called colloidosomes, combined with silica-based sol-gel chemistry is investigated as potential technologies, to produce consumer and environmentally friendly perfume capsules that comply with recent legislations limiting the levels of plastic-based technologies in consumer goods. Finally, colloidosomes and silica-based capsules will be discussed in detail, including

References to this Chapter on pages 50-59

the key parameters to enhance stability and performance of these capsules in consumer products.

1.1 Fragrances in laundry products: Why and the challenges

Fragrances are mixtures of natural or synthetic essential oils, which can contain a wide range of molecular structures including alcohols, aldehydes, hydrocarbons and terpenes.[1] Fragrances are widely found in consumer products such as:

(i) cosmetics;

(ii) heavy-duty laundry detergents (HDL);

(iii) liquid fabric enhancers (LFE), also known as fabric softeners;

(iv) leave-on hair conditioners (LOC) and,

(v) rinse-off hair conditioners (ROC).[2]

Fragrances are key components for such products as they can influence the consumer's decision when (i) first selecting a product, (ii) considering the perception of the products effectiveness, and (iii) repeat buying, or not, the product. Therefore, fragrances are important in product formulations in terms of sales enhancement, even if they do not play any role in improving the product properties.[3] Moreover, they represent a significant material cost to laundry products, with content ranging from 0.2 -1 wt% of laundry formulations.[4]

Fragrances used in laundry products are designed to:

(i) mask undesirable odours from cleansing agents within the formulation;

(ii) give the consumer a sense of freshness when opening and using the product; and

References to this Chapter on pages 50-59

(iii) deliver a fresh smell to the washed fabric, enhancing the experience of cleanliness.

When it comes to laundry applications, it can be very challenging to deliver fragrance to the fabric during and after the washing cycle. This challenge results from the following considerations the fact that fragrances:

(i) are a mixture of hydrophobic oils and these are the compound type that detergents are designed to remove from the fabric during the wash. This is somewhat mitigated by introducing fabric softeners, which contain the fragrance, at the end of the wash-cycle;

(ii) are volatile, so the post wash drying process, which involves heat, will lead to evaporative loss of the fragrance oils.[5]

(iii) can suffer chemical degradation when interacting with other components in the formulation (i.e. aldehyde or alkene moieties with peroxides);

(iv) in water-based formulations can lead to phase separation.[6]

(v) can undergo hydrolysis (i.e. ester moieties) when in alkaline (i.e. detergents) or acidic (i.e. fabric softeners) conditions.[7]

(vi) can undergo aerial oxidation (i.e. aldehyde and alkene moieties), accelerated by heat in the drying process when exposed on the fabric.[8]

Depending on the end use of the laundry product, specific levels of fragrances are desired. The five main factors that affect the volume of a fragrance in a formulation are:[5]

(i) odour contribution of the fragrance;

 References to this Chapter on pages 50-59

(ii) stability and performance in the finished product;

(iii) safety to consumer health;

(iv) impact on the environment; and

(v) cost.

Of course, the first two points have the potential to conflict with the last three points, in that to get to a desired consumer experience with regard to a pleasant odour of a product, may require so much fragrance, that it will be detrimental to consumer health, and/or the environment, as well as being prohibitively expensive to the cost of manufacture. Thus, technologies that use less fragrance, whilst maintaining a quality consumer experience are desirable.

1.1.1 Fragrance encapsulation

Encapsulation of fragrances has been a topic of extensive interest for both academia and industry in the past years.[4] More specifically, the consumer goods industry have identified encapsulation as a key technology when introducing fragrances to their formulations. Examples of consumer products that benefit from encapsulated fragrances are perfumes, personal care products, hair-care, laundry detergents and fabric softeners[4](**Table 1-1**).

The reason for the extensive interest has been that the microencapsulation of fragrances ensures, in principle that the perfume is:

(i) delivered at the right time;

(ii) to the right place;

References to this Chapter on pages 50-59

(iii) *via* a controlled release mechanism;

(iv) protecting the encapsulated perfume from the surrounding environment, avoiding degradation, evaporation and phase separation.[9]

***Table 1-1**. Shares of perfume encapsulation in consumer products.*[10]

Product type	Percentage (by volume) of the product type using perfume encapsulation
Laundry detergents	10-20%
Fabric softeners and scent boosters	~60%
Other cleaning products	<1%
Deodorants	<1%
Other cosmetic and personal care products	<1%

The main objective of using encapsulation in consumer products is to deliver a long-lasting fragrance experience to the users of laundry and personal care products, allowing to:

(i) maintain the sensory cues related to the important wellbeing, health and hygiene benefits that the use of these products provide to the consumer;

(ii) avoid the use of high perfume dosages that could be damaging to the environment;

(iii) avoid unnecessary repeated product application due to absence of sensory cue;

(iv) efficiently use resources as the perfume is delivered to the right place at the right time.

1.1.1.1 Fragrance encapsulation in laundry products

As observed in **Table 1-1**, encapsulation technologies are mostly used in laundry products such as detergents and fabric softeners. This is because the physical protection of fragrances

References to this Chapter on pages 50-59

using microcapsules comes as an advantageous way to protect the perfume not only during storage, but also through the fabric washing and drying process and ensure:

(i) perfume compatibility, by segregating the fragrance from other reactive components in the formulation, and hence increasing shelf-life.[10]

(ii) a more durable fragrant benefit after the fabric is dried, giving a sensation of freshness to the consumer, even when handling the fabric weeks or even months after the wash.

(iii) a more environmentally friendly approach, as a result of using less perfume in the formulation, resulting in less perfume being released into the drains during the wash,[4] or released to the atmosphere in the form of volatile organic compounds (VOCs).

In terms of fabric care formulations, the most successful encapsulation technologies are those based on aminoplast resins, such as urea-formaldehyde (UF) and melamine-formaldehyde (MF), due to their desirable mechanical properties and low wall permeability to fragrance molecules.[11]

In 2008, the microencapsulation specialist company Encapsys, in collaboration with Procter & Gamble (P&G), was the first to produce fragrance microcapsules for fabric softeners on a large scale. When the technology was first introduced, mainly UF and MF microcapsules were used.[12] Encapsys has now shown that it is capable of producing capsules with different wall chemistries, such as polyacrylate and gelatine.[13]

 References to this Chapter on pages 50-59

1.1.1.2 Polymer microcapsules in laundry products

Encapsulation is a costly technology, however is partially compensated by the lower volumes of fragrances required in the formulation as result of the stabilisation and segregation of expensive actives, coupled to the enabling of targeted delivery, which enhances consumer satisfaction and drives up revenue. Companies must understand the consumer needs to make sure that it is advantageous to introduce microcapsules to the product.

Health concerns are an important challenge. Although MF capsules are the lead technology when it comes to introducing fragrance capsules to fabric care products, these wall materials are formed from formaldehyde, which is suspected to be a carcinogenic compound and its concentration in the finished product is controlled by law.[14] Although the formaldehyde is chemically bound with the urea or melamine in the microcapsule product, it is in equilibrium with free formaldehyde, making it difficult to completely eliminate formaldehyde from the slurry, albeit at low levels which are designated as safe with respect to its carcinogenic activity.[15] In light of this, European and Asian governmental institutions have imposed restrictions on formaldehyde containing products in recent years. As a result, companies have been investing in research to identify potential alternatives to MF capsules, which are environmentally friendly and safe to human health, whilst also presenting good mechanical properties, and maintaining and stabilising the active within the capsule until the required application point.

The environmental safety challenge has come into sharp focus in the last two years, where there is a growing concern regarding pollution caused by single use plastic which is finding its way into water ways and the oceans at an alarming rate. Thus, regulations are starting to

References to this Chapter on pages 50-59

expand from the prohibition of single use items, such as plastic bags and straws, to other plastic products.[16] Microcapsules formed from organic polymer walls are in scope to be banned from Europe[17] and have already being banned for some countries in Asia, and hence legislation may be introduced to restrict or even prohibit their use. Clearly, and not withstanding a formal legal framework, replacement of these polymer microcapsules is the ethical course of action to protect an environment which is stressed by the population explosion of the last 100 years.

Therefore, alternatives to MF polymeric wall capsules which are eco-friendly and safe to human health are being actively investigated. Thus, innovations in polymer capsule wall materials have been around the use of biodegradable polymers (polylactide,[18] proteins,[19] and other biodegradable polyesters[20]).

1.1.1.3 Inorganic Polymer microcapsules

More recently inorganic matrixes (silicates,[21] clays,[22] and calcium carbonate[23]) have begun to be investigated as wall materials. However, marrying the ecological demands with the technical challenges of having capsules that can retain and deliver the active in a complex formulated product is not straight forward. In particular, the biggest challenges for these emergent shell materials is the stability and performance in the finished product, as their shells tend to be porous when compared to organic polymer counterparts, and scale-up of the encapsulation process is challenging.

1.2 Microencapsulation

Microencapsulation is a process where droplets of liquids, particles of solids or gasses are enclosed inside a solid shell in the micrometre size range (diameter 1-100 μm) (**Figure 1-1**).[24]

References to this Chapter on pages 50-59

Depending on the method, shell and core material the resulting morphology can be classified as mononuclear (single or multi-walled), polynuclear, matrix or irregular. The shell material can consist of plastics, biopolymer or inorganic matrix and the core material is physically separated from the surrounding environment.[4]

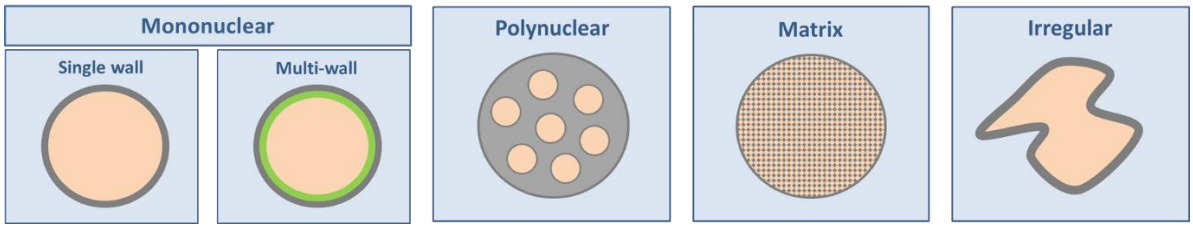

***Figure 1-1**. Schematic representation of a microcapsule and its key components: a core that contains an active material surrounded by a solid shell.*

The term microcapsule was first used in industry when the National Cash Register Company introduced carbonless copy paper in 1954 in Ohio, USA.[25] Encapsulation science has grown to take the basic idea of carbonless paper to make increasingly sophisticated encapsulation processes for use in a wide range of applications.

Today microcapsules are capable of:[26]

(i) providing stability of a formulation or material *via* the physical separation of incompatible components;

(ii) protecting the core material from the surrounding environment;

(iii) mixing incompatible or immiscible materials;

(iv) masking or hiding an undesirable attribute of the active;

(v) controlling or triggering the release of the active to a specific time or location.

References to this Chapter on pages 50-59

All of these attributes can lead to an increase of the shelf-life of a product and stabilisation of the "active ingredient" in liquid formulations.[26]

1.2.1 Controlled release

One of the principal features of the microencapsulation technology is the possibility of a controlled release of the encapsulated active. For microencapsulation, the controlled release is usually classified as sustainable release[27] or triggered release:[28]

- Sustainable release: the active is slowly released over time and the release is controllable by the permeability of the shell.
- Triggered release: the microcapsule shell should be formed from a material that is non-permeable to the active until a particular external stimulus is applied, such as mechanical rupture,[11, 29] light,[30] pH,[31, 32] temperature[33] or osmotic pressure.[34] When the trigger is applied, the active is released.

Both methods are extremely desirable for different industrial applications. For example, sustainable release is interesting for pharmaceutical applications, where a therapeutic agent must be delivered over a period of time. On the other hand, triggered release is interesting for food applications, whereas the encapsulated flavour must be released during chewing, providing the consumer with an enhanced sensation.

1.3 Emulsions

Formulated products may rely on oil-in-water emulsions to keep the materials dispersed.[35] An oil-in-water emulsion is formed when an oil is homogenised in an excess of water. This leads to the oil being dispersed in the water (continuous phase) as droplets.[36] The droplet size is dependent on a number of factors, including the energy input into the homogenisation

References to this Chapter on pages 50-59

(mixing process), with more energy leading to smaller droplets. Once the homogenisation process stops, *i.e.* the energy to sustain the dispersion of the oil in the continuous phase is removed; the oil and water will phase separate.[35] Due to the large interfacial area of emulsions, the systems tends to be thermodynamically unstable and undergoes phase separation if a stabilizing agent is not added to the system. The large interfacial area in the absence of surfactants leads to an increase in the interfacial Gibbs free energy (ΔG) according to **Equation 1-1**:

$$\Delta G \sim \gamma_{OW} \Delta A_{OW}, \qquad \textbf{\textit{Equation 1-1}}$$

where, γ_{OW} is the interfacial tension and ΔA_{ow} is the change in the interfacial area between oil and water. During emulsification ΔA_{ow} increases dramatically leading ΔG to be positive and the emulsion to be thermodynamically unstable. Several mechanisms lead to emulsion instability, such as coalescence, flocculation, creaming and Oswald ripening (**Figure 1-2**).[37] Of course, other parameters also play an import rule in the phase separation process such as the zeta potential, affecting the charged layer around the droplets hence their tendency to flocculate, as well as the viscosity and density of the oil which might affect the rates of creaming/ sedimentation. Surfactants and copolymers are commonly added to the system to increase emulsion stability, by decreasing the interfacial tension.[38]

References to this Chapter on pages 50-59

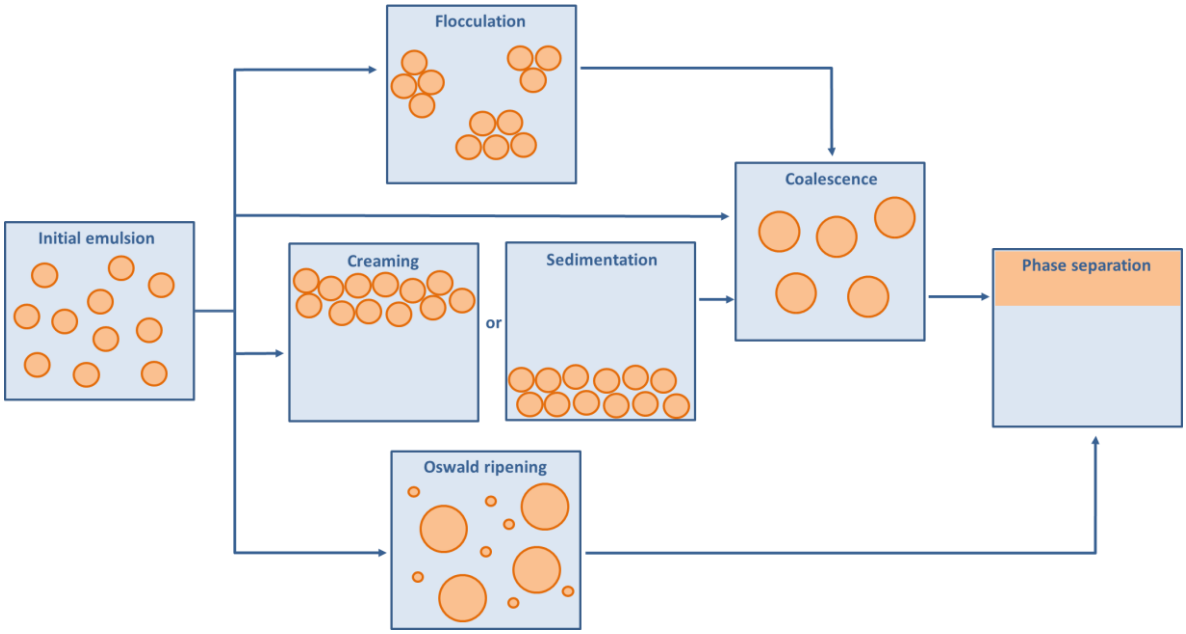

***Figure 1-2**. Schematic of mechanisms leading to phase separation of oil-in-water emulsions. Adapted from Lupetinsky et. al., 2006.*[36]

As discussed above, the reason for the phase separation is that the surface tension between water and oil is high, and thus energetically the oil-water interface is not favourable. However, the introduction of an organic surfactant can lead to a thermodynamically stable emulsion, by reducing the difference in surface free energies. This stabilisation results from:[39]

(i) the surfactant migrating to the interface between the oil droplet surface and the continuous phase,

(ii) the hydrophobic moiety of the surfactant embeds in the oil droplet because of dispersive interactions, and

(iii) the polar hydrophobic head-group embeds in the aqueous phase, stabilised by electrostatic and/or hydrogen bonding interactions with the water molecules.

References to this Chapter on pages 50-59

1.4 Pickering emulsions

Pickering emulsions are formed *via* self-assembly of solid particles at the interface between two immiscible phases such as oil and water (**Figure 1-3**).[40] These emulsions are produced as follows: first, two highly immiscible phases are emulsified in the presence of colloidal particles (Pickering emulsifier). These particles assemble spontaneously at the water-oil interface, lowering the interfacial energy between the phases and consequentially, stabilising the emulsion.[41] This type of emulsion was first identified by Ramsden[42] in 1903, but first fully described by Pickering in 1907.[43]

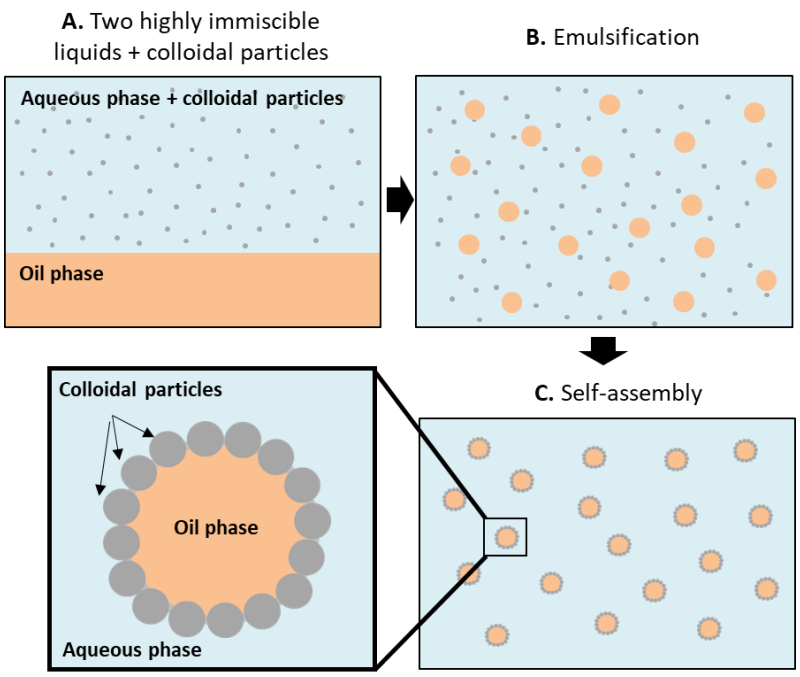

Figure 1-3. *Simplified scheme of Pickering emulsion formation. First, an aqueous dispersion containing colloidal particles is prepared and added to an oil phase (A). Then, the aqueous and oil phases are emulsified forming oil droplets in a continuous aqueous medium (B). The colloidal particles then self-assemble at the water-oil interface lowering the interfacial energy and stabilising the emulsion (C).*

References to this Chapter on pages 50-59

A number of different particles have been described in the literature as capable of stabilizing emulsions, for example, latex,[41] silica,[44] oxides[45] and clays.[46] Parameters such as the emulsion polarity and hydrophobicity, the particles wettability, shape and size, the surface properties and the interactions between the particles are important when defining how effective particles are in stabilizing emulsions.[47]

Some of the main benefits of Pickering emulsions over common organic amphiphilic surfactant-stabilized emulsions are:[48]

(i) higher resistance to coalescence;

(ii) mouldable permeability;

(iii) flexibility in terms of biocompatibility and environmentally friendly materials; and

(iv) facile and low-cost routes.

1.4.1 Pickering emulsion stability

To produce stable colloidal dispersions, it is essential to create an effective repulsion mechanism that is enough to overcome the van der Waals attraction between the particles. There are generally two types of colloidal stabilization mechanisms:[49]

<u>Electrostatic repulsion:</u> produced by creating an electrical double layer around the particles as a result of charge separation. When two particles with extended double layers approach each other to a distance where the double layers begin to overlap, strong repulsion occurs, thus overcoming van der Waals attractions.

<u>Steric repulsion:</u> produced by adsorbed non-ionic surfactant or polymer layers (stabilization groups) and can extend from the particle surfaces giving an adsorbed layer thickness. When two particles approach to a distance that this thickness begins to overlap, repulsion occurs.

References to this Chapter on pages 50-59

The stabilization mechanism also has a significant effect on the assembly to interfaces and on the formation, stability and properties of Pickering emulsions. Firstly, the surface of the particle is altered by the presence of the stabilization mechanism affecting the wetting properties and the equilibrium position of the particles at the interface. Secondly, the stabilization groups can lead to an activation barrier when a particle approaches the interface due to steric repulsion.[49]

The fundamental difference between the stabilization of emulsions using surfactants and solid particles, reside in the fact that the relatively large size of the stabilising units of the latter along with the presence of three phases in the system, results in a three-phase contact angle (**Figure 1-4)**. The stability of Pickering emulsions relies on the steric stabilization provided by the charged particle layer surrounding the droplet and preventing droplet aggregation and coalescence, therefore ideally, the particles exhibit partial wetting, assembling at interfaces, but remaining colloidal stable. To form Pickering emulsions that do not coalesce, the three-phase contact angle between the solid particle and the immiscible phases (**Figure 1-4**) should be close to 90°, where a high energy input is required for desorption, ΔG_d, of the particle from the interface according to **Equation 1-2**.[50]

$$\Delta G_d = \pi r^2 \gamma_{ow} (1 - cos\theta)^2, \qquad \textbf{\textit{Equation 1-2}}$$

where ΔG_d is the free energy difference due to desorption, r the particle radius, γ_{ow} the interfacial tension between the oil and water phases and θ the three-phase contact angle.

As explicit by the equation, the change of free energy of a spherical particle at the interface depends directly upon the water-oil interfacial tension and the radius of the particle.[51] The wettability of the particle and the polarity of the oil can also influence the stability of the

References to this Chapter on pages 50-59

emulsion *via* the contact angle. Thus, surface-active particles can spontaneously assemble at the oil-water interface and therefore lead to emulsion stability.[52]

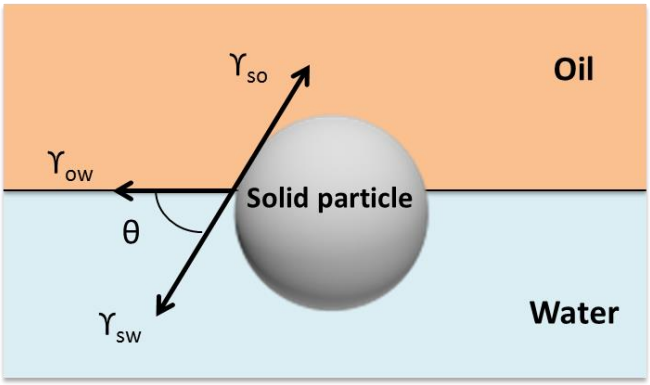

***Figure 1-4**. Scheme representing the three-phase contact angle Θ between a solid particle at the oil-water interface. Θ depends on the surface properties of the particle, particularly the wetting properties, and the particle-water, particle-oil and water-oil interface. γ_{SO}, γ_{OW} and γ_{SW} represent the interfacial tension between solid-oil, oil-water and solid-water, respectively.*

1.4.2 Effects of particles parameters on Pickering emulsions

1.4.2.1 Wettability of particles

Particle wettability was first studied by Schulman and Leja,[53] who described that depending on the contact angle, θ, of the particle with the water phase it would preferably form oil-in-water or water-in-oil emulsions.[54]

For particles with θ below 90°, the particle is more wetted by the water (hydrophilic particle) and an O/W emulsion is stabilized, as the particles minimise the energy by curving around the dispersed phase. The opposite is observed when the contact angle is above 90°, in this case the particle is more wetted by the oil phase (hydrophobic component) and a W/O emulsion is preferably formed **(Figure 1-5)**.[55, 56] If the contact angle is equal to 90 degrees, there is no

References to this Chapter on pages 50-59

preferentiality and the particles are wetted equally by both phases.[47] ΔG is maximum for θ = 90°, which is the maximum area of interface obliterated by placing the particles at it.[54]

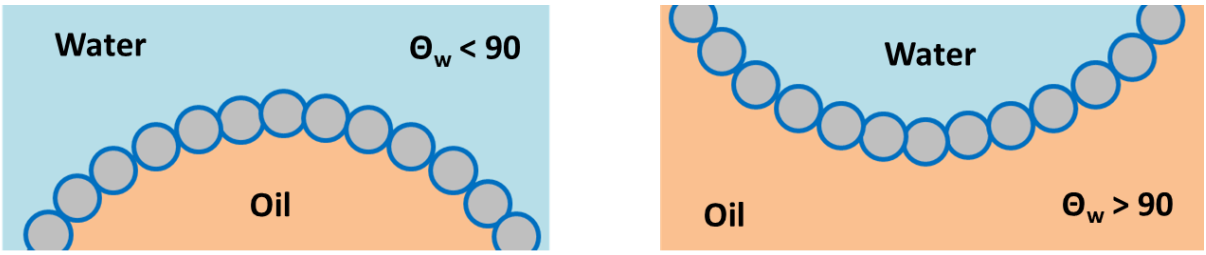

Figure 1-5. *Scheme representing the formation of O/W or O/W emulsions depending on the contact angle between the particle and water. If ϑw < 90°, the resulting emulsion is O/W and if ϑw < 90° the resulting emulsion is W/O.*

In a work conducted by Bink et al.,[51] silica nanoparticles with different hydrophilicities were used to study the stability of emulsions formed between toluene and water. The study identified that only particles with intermediate hydrophilicities (i.e. θ close to 90°) could spontaneously accumulate at the interface and stabilize the emulsion, which confirms that ΔG is maximum for θ = 90°.

1.4.2.2 Particle size

From **Equation 1-2**, it is possible to conclude that the size of the particle also has a great impact on their desorption energy. ΔG_d increases as a function of r^2, therefore bigger particles, in theory, can stabilize emulsions more efficiently. Bink *et al.*[57] have studied the effect of the particle size on Pickering emulsions using latex particles of diameter varying from 0.21 to 2.7 µm, and observed that they were all stable for more than six months, however their stability to sedimentation was higher for smaller particles (hence, more charged surfaces). In addition, average emulsion droplet increased with increasing the latex particle

References to this Chapter on pages 50-59

diameter when the volume fraction of water, oil and particles was unchanged. This is due to the larger surface area that can be stabilized by smaller particles.

However, Qi *et al.*[58] used poly(D,L-lactic-co-glycolic acid) particles in three different sizes to understand the effects of size on the stabilization of the Pickering emulsion. They noticed that when using smaller particles (330 nm), dense layers deposited at the droplet surface, which stabilized the emulsion more efficiently than when bigger particles were used (620 and 1150 nm). The explanation for the surprising results was that the adsorption kinetics of the larger particles was slow and resulted in less efficient packing at the droplet surface. At larger sizes the relationship is not observed anymore, probably because not all particles are located at the drop interface.

1.4.2.3 Particle shape

Most of the studies involving Pickering emulsifiers have used spherical shaped particles. However, a few studies have also demonstrated the possibility to stabilize emulsions using particles with different shapes such as rods and fibres,[59] nantubes,[60] ellipses and cubes.[61, 62] Madivala *et al*.[63] studied the effect of elliptical shaped polystyrene particles. The group noticed that elliptical particles could stabilize the emulsion more effectively when compared to spherical particles as they connected end-to-end forming triangular mesh structures preventing coalescence due to shape-induced capillary interactions.

Kalashnikova *et al*.[64] used rods as Pickering emulsifiers and noticed an improved stability of the emulsion. This improvement is because the rods connect forming a 2D network that give extra support to the structure. In terms of packing, non-spherical irregular particles should yield denser structures, which is advantageous when limited permeability is required.[65]

References to this Chapter on pages 50-59

1.4.2.4 Surface properties of the particles

Colloidal particles tend to aggregate in solution unless there are repulsive forces between them, such as electrostatic repulsion or steric stabilisation. However, this repulsive force between the particles can act as a barrier for their adsorption at the interface.[66] Multiple studies have shown that the stability of the Pickering emulsion directly depended on the electrostatic forces, which control the adsorption and desorption rate of particles at the oil-water interface.[67, 68]

The pH of the continuous phase, for example, can control the electrostatic repulsion between the particles and, in consequence, their adsorption at the interface.[69] In terms of silica, it was shown that the fraction of silanol surface groups could affect the structure of the emulsion in a more significant way than the contact angle.[70] Besides the surface charges of the particles, other surface properties of the particles can also have an effect on the Pickering emulsion stability, for example the roughness of the particle, which can reduce the contact surface hence reducing the emulsion stability.[71, 72]

1.4.2.5 Particle concentration

The particle concentration is important to ensure complete droplet coverage and avoid coalescence.[73] Usually, by increasing the particle concentration, stability is improved.[74] The droplet coverage can be calculated using **Equation 1-3**; it is defined as the ratio between the interfacial area that the particles can cover and the total interfacial area.

$$R_o = coverage\ x\ \pi\ x\ \left(\frac{W_o}{W_p}\right) x\ \left(\frac{\rho_p}{\rho_o}\right) x\ R_p \qquad \textbf{\textit{Equation 1-3}}$$

References to this Chapter on pages 50-59

Where, R_o and R_p are the radius of oil droplet and particle, W_o and W_P the weight of oil and particles, and ρ_p and ρ_o the density of particle and oil, respectively. For a dense monolayer of particles, the coverage is equal to 0.9, which corresponds to fractional area occupied by hexagonal closed-packed monodispersed particles.[73]

The concentration of particles can also influence the surface properties of the particles. For example, silica particles behave more hydrophobically at higher concentration, as the hydrophilic silanol groups are shielded and involved in siloxane bond formation between particles, which induces hydrophobic character and can improve emulsion stabilisation.[49] The concentration of particles also plays an important role in defining the droplet size *via* the so-called limited coalescence phenomenon discussed next.

1.4.3 Limited coalescence phenomenon

When using surfactants to stabilize an emulsion, the higher the surfactant concentration, the smaller the droplet, and usually an enhancement in stability of the emulsion is observed.[38] When the surfactant concentration reaches the critical micelle concentration (CMC), the droplet size remains constant. For Pickering emulsions, a similar phenomenon is observed; the increase of particle concentration decreases the droplet size, due to the limited coalescence phenomenon in emulsions stabilized solely by solid particles.[66]

Therefore, the limited coalescence phenomenon rationalises why an excess of oil-water interface is produced when compared to the area that can be covered by the particles, which must be irreversibly attached to the interface.[75] The droplets coalesce to a limited extent which reduces the interfacial area between the oil and water, and progressively increases the

References to this Chapter on pages 50-59

degree of coverage by the particles. As a result, a film of particles is formed at the interface, kinetically stabilizing the emulsion.[75]

The phenomenon is represented by **Figure 1-6** below: when the volume fraction of dispersed to continuous phase is fixed, by varying the concentration of particles it is possible to control the mean diameter of the formed droplet.

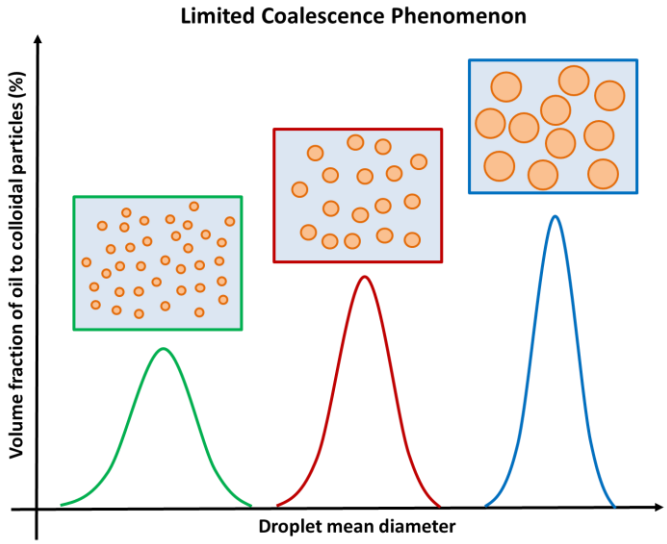

***Figure 1-6**. Representative graph of the limited coalescence phenomenon and its features: when an excess of oil- water interface is formed when compared to the particle coverable area, the droplets coalesce until all surfaces are covered. The mean droplet diameter increases as the particle concentration to the dispersed phase decreases.*

Another important feature of the limited coalescence phenomenon is the possibility to not only control the final droplet diameter, but also to obtain a narrow size distribution. In a particle poor system, the droplets will coalesce until all surfaces are completely covered, leading to remarkably monodisperse emulsions. It is possible to obtain a linear relationship between the droplet diameter and the particle concentration, with the slope dependant on

References to this Chapter on pages 50-59

the energy applied during the emulsification process.[76] The lower the particle concentration, the more narrowly distributed the size of the resultant emulsion (**Figure 1-6**).

Whitesides *et al*.[77] have conducted extensive mathematical modelling experiments using theoretical analyses of droplet collisions during emulsification and concluded that the final size distribution does not depend on the emulsification conditions and the initial droplet size. In addition, the droplet size becomes narrow at early stages of the limited coalescence process because the amount of irreversibly adsorbed particles is constant and independent of the droplet size, leading to a smaller degree of coverage in smaller droplets, which coalesce faster. As smaller droplets coalesce faster than bigger ones, the obtained size distribution is usually relatively narrow.

1.4.4 Pickering emulsion-based capsules – colloidosomes

Colloidosomes are shell-core (microcapsules) structures whose shell are composed of post-emulsification cross-linked colloidal particles and the core composed of a liquid or gel.[78] The colloidosome structure formation is achieved *via* the pre-formation of a Pickering emulsion[41].

This cross-linking can be achieved *via* physical or chemical stabilization, such as thermal annealing, where the polymer particles are heated up above the glass transition temperature, fusing the particles together[79] as well as covalent cross-linking.[80] Thus, the particles can be locked at the interface *via* mechanical stabilization; for example gel trapping, which involves the usage of a gel as internal phase, forming rigid capsules[81] and the polymerization of the droplet, which takes place after the formation of the Pickering emulsion, inside or at the surface of the particles, trapping the particles at the interface.[82, 83] These stabilisation methods can also be used to further reduce core leakage from the colloidosomes.

References to this Chapter on pages 50-59

Colloidosomes can be obtained using varies types of Pickering emulsifiers and preparation routes. Moreover, the wide range of particles and stabilization methods enable the capsules to be designed for a specific application,[41] which is extremely desirable, especially for bio-applications.[84] Colloidosomes formation can be achieved using multiple shell materials, for example: silica[85], polymers[86], oxides[87], and microgel particles[88]. In addition, there is much current research looking to find an effective mechanism to stabilise the particles within the colloidosomes shell and avoid the disruption of the microcapsule. This research will be discussed in the following sections.

The main advantage of colloidosomes for encapsulation is that the synthesis usually involves surfactant-free and environmental friendly conditions, which is extremely desirable for many industrial applications, such as pharmaceuticals and food.[89] However, due to the solid nature of the colloidal particles forming the shell and its high permeability, the technology is still struggling to have real commercial applications, especially in terms of small volatile molecules encapsulation, such as perfume oils.[41]

1.4.5 Permeability properties of colloidosomes

Colloidosomes are usually formed by the soft-template method,[41, 90] where the active to be encapsulated is loaded to droplets of an emulsion prior to the self-assembly of the colloidal particles. Colloidosomes are spherical, as the droplet will adopt a spherical shape in order the have the minimal interfacial energy.[90] Furthermore, with the adsorption of the particles at the interface the total interfacial energy of the droplet decreases. As the adsorption energy of the colloidal particles at the oil-water interface usually exceeds the thermal energy by many orders, the particle cannot leave the surface, and it is confined at the interface,[91] hence

spherical particles will organize in a hexagonal network at the interface, showing regular spaces (pores) between them.

Taking into account a monodispersed sphere planar-packing with diameter *d*, the interstitial diameter is approximately 0.15*d*.[87] However, when this packing is curved to form the shell of the capsule, additional defects must be present to fully cover the surface of the shell; leading to a higher permeability of the colloidosome as the defects are described to be approximately the size of 0.70*d* (**Figure 1-7)**.[92] The pores size can be adjusted by varying the shape or using a combination of different particle sizes. However, innovations in sealant mechanism would are highly sought after to avoid shell leakage.

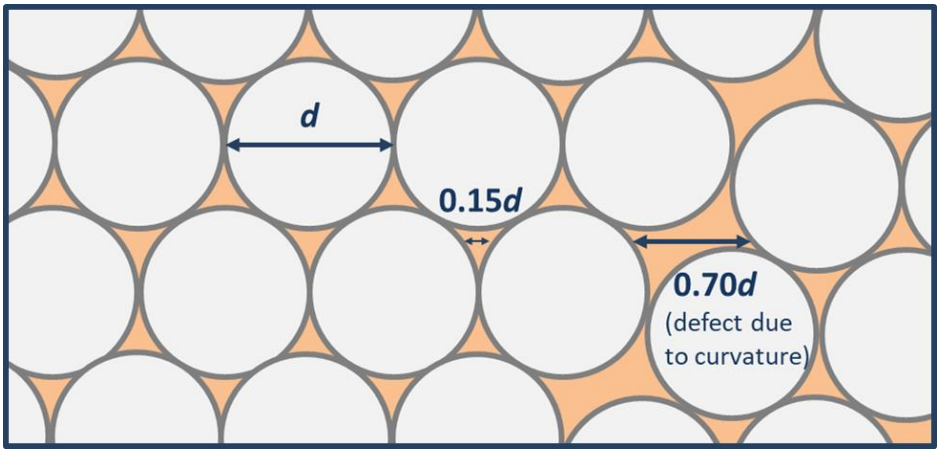

***Figure 1-7**. Scheme representing the possible pore sizes for closed-packed shell made of particles with diameter d.*

A model proposed by Rosenberg *et al.*,[93] demonstrated that for a colloidosome made of a monolayer of colloidal particles the diffusion of small molecules will be independent of the particle size. However, for multilayer shells, smaller particle sizes can reduce significantly the rate of transport. The study also shows that when compared to an uncoated system, colloidosomes can hinder the diffusion of small molecules.

References to this Chapter on pages 50-59

There are very few reports in the literature focusing on long-term retention using colloidosomes. Many of the techniques to make stable capsules are capable of only retaining actives for short periods (only minutes to hours). To be used in commercial applications, microcapsules must be able to retain actives on the time scale of months or years.

Thus, in conclusion, although colloidosomes have advantages over conventional encapsulation processes, their full potential as an encapsulation technique is yet to be fully realised, in particular in relation to minimize colloidosome permeability.

1.4.6 Approaches to minimize the permeability of colloidosomes

To form microcapsules from Pickering emulsions a mechanism for reducing/eliminating shell permeability and prevent the particles from detaching from the interface, releasing the core material, is required, and several mechanisms have been developed as shown in **Figure 1-8**, some of which also increase the capsules mechanical properties.

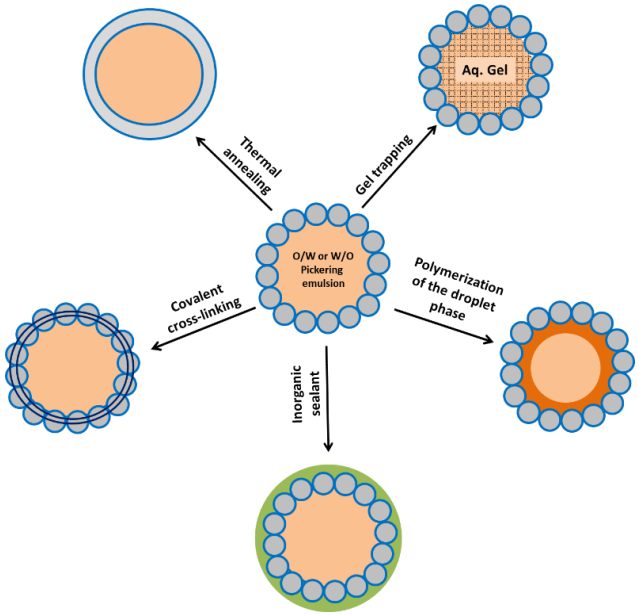

***Figure 1-8**. Scheme representing the possible ways of stabilizing colloidosomes from Pickering emulsions (Adapted from [41]).*

References to this Chapter on pages 50-59

1.4.6.1 Thermal annealing

The first method to lock the colloidosome shell in place was described by Dinsmore *et al.*,[86] by preparing latex particle colloidosomes and then heating up above the latex glass transition temperature (*Tg)* , to fuse them together. Using this method, the interstitial gaps between the particles could be controlled by varying the sintering time. Furthermore, the method was applicable for both hydrophobic and hydrophilic encapsulation. The authors suggested that the permeability of the colloidosome could be controlled, however this aspect was not demonstrated. The main drawback of this method is the high temperature necessary to fuse the particles together, which could be damaging to the active to be encapsulated.

1.4.6.2 Polymerization of the shell

The enhancement of the colloidosome shell stability can also be achieved *via* polymerization either at the outer and/or inner surface of the shell of the colloidosome. Many examples of such method can be found in the literature.[83] The first example was described using surface-modified silica particles comprising initiator sites for radical polymerization as Pickering emulsifier for paraffin oil in water.[82] Once the Pickering emulsion was formed, the initiator sites promote the *in situ* formation of the polymer on the surface of the colloidosome. The drawback for this method, according to the group, is that it is not suitable for scale-up and it is time consuming.

Alternative approaches were described with the polymerization occurring in the interior of the droplet using latex,[94] TiO_2,[95] SiO_2[96] or ZnO[97] as Pickering emulsifiers. The formation of the copolymer is possible *via* solvent evaporation, forming a thin layer of polymer in the inner surface of the shell. Long *et al*. [98] described a method using $CaCO_3$ particles and interfacial

References to this Chapter on pages 50-59

polymerization to form an organic polymer on the inner surface adjacent to the oil phase, and a second inorganic cross-linking with $CaCO_3$ on the outer surface adjacent to the continuous water phase. This method demonstrated reduced core leakage when compared to non-polymerized colloidosomes.

1.4.6.3 Covalent cross-linking

Stabilization of colloidosomes microcapsules can be achieved adding cross-linkers to the oil-water interface. William *et al*.[99] have described the formation of organic/inorganic colloidosomes encapsulating oils made of Magnafloc/Laponite nanoparticles coated by a cross-liked melamine formaldehyde film. Capsules formed were robust and could survive an alcohol challenge, which removes both the oil droplet phase and the aqueous continuous phase, keeping the capsules intact However, this study did not include a release profile data.

Thompson *et al*.[100, 101] have demonstrated a method to cross-link latex particles at the oil-water interface having the cross-linker initially in the inner oil phase, and therefore avoiding inter-colloidosome fusion. This work also included release data, which suggests that the leakage is minimized when compared to non-cross-linked samples. However, the colloidosomes still experienced complete release within hours.

The biggest advantage of the cross-linking method over the previous methods already described is that it can be achieved at ambient conditions, and therefore is suitable for the encapsulation of thermally sensitive actives, such as enzymes. However, for many methods the cross-linking is conducted from the continuous phase, which can possibly lead to inter-colloidosome fusion. Cross-linking can also be used in conjunction with another method such

as thermal annealing, avoiding inter-droplet cross-linking, thus enhancing the capsule synthesis efficiency.[102, 103]

1.4.6.4 Inorganic sealant

Keen *et al*.[104] have demonstrated that the colloidosomes can be sealed by the formation of a $CaCO_3$ external shell blocking the pores between the colloidal particles and therefore avoiding the leakage of large actives up to weeks. The method was also interesting because it could be conducted at ambient temperature and without harsh solvents.

For the formation of the $CaCO_3$ sealed colloidosomes, CO_3^{2-} was dissolved in the inner phase and the Ca^{2+} in the outer, continuous phase. During the synthesis, those salts meet at the channels between the particles, precipitating $CaCO_3$, which acts as a cement blocking the channel and therefore sealing the colloidosome to avoid core leakage. The method is extremely interesting, however, it was demonstrated using a W/O systems.

Wang and co-workers[105] also reported the formation of a calcite shell in a similar fashion whereby $CaCO_3$ nanoparticles were used as colloidal particles and nucleation sites and the capsules were further sealed using $CaCl_2$ and CO_2 gas to form a robust all $CaCO_3$ shell. This work was reported using oil-in-water emulsions and limonene flavour was encapsulated. Furthermore, the authors have demonstrated that an acid trigger release can be applied to release the active from the shell by dissolving the $CaCO_3$ wall.

In a similar way, Zhao *et al*. reported the formation of all-silica colloidosomes encapsulating hydrophobic liquids in two similar works.[89, 106] The group described the formation of Pickering emulsions formed from silica particles that could receive a further sol-gel treatment, gluing the particles at the O/W interface by a silica precursor polymer. Interestingly, the silica

References to this Chapter on pages 50-59

precursor used was dispersed in the inner oily phase, so the formation of the silica "glue" happened from the inner side of the colloidosome. Moreover, the authors suggested a 100% efficiency of encapsulation using this method, in a chemically inert system, which would be interesting for cosmetics applications for example. The drawback of this approached is that it requires a pre-synthesis of the silica precursor which is tedious and increases considerably the preparation time.

Also working with silica, Baillot *et al*.[107] described a method for sequential mineralization of Pickering emulsions formed with silica nanoparticles using tetraethoxyothosilicate (TEOS) and cetylmethylammonium bromide (CTAB) as the silica precursor and a cationic surfactant, respectively. As opposite to the method described by Zhao *et al*., TEOS was added to the dispersed phase and the silica particles worked as nucleation sites for the formation of silica from the outside of the emulsion surface. The group have demonstrated that the colloidosomes could have their shell thickness and mechanical properties controlled when multiple mineralization steps were applied. A limitation of this method is the usage of TEOS in the continuous aqueous phase can cause full gelation of the system if the conditions are not well controlled.

1.4.7 Trigger release mechanisms

There are several ways to trigger the active release from colloidosomes. The first example is pH triggered release, which is attractive for pharmaceutical applications as it could be applied, for example, for the differential pH found in the gastrointestinal system from the mouth. Miguel and co-workers, have reported stimulus-responsive colloidosomes using a pH trigger.[108] In this work, double emulsion templates of both W/O or O/W emulsions were used

References to this Chapter on pages 50-59

to form completely polymeric colloidosomes that had rapid and complete capsule dissolution in response to a mild pH stimulus. In addition, Sander and Studart[109] have demonstrated a methodology for the formation of complex colloidosomes that can release actives on-demand in single or multiple release events using a pH trigger.

Zhou and co-workers have demonstrated the synthesis of colloidosomes with a thermally switchable trigger based on the temperature dependent adsorption or desorption of a block copolymer dissolved in the core, onto or off the inner surface of the colloidosome.[110] Thermo-responsive colloidosomes were also reported by Cejkova *et al*.[111] The group described the formation of PNIPAM/silica colloidosomes that could show temperature dependent swelling/deswelling properties, leading to a trigger release of the active.

A trigger release based on the differential electrostatic interactions between oppositely charged ionic surfactants and particles was described by Zhu *et al*.[112] In this work, the O/W emulsion was formed with negatively charged silica nanoparticles, and could be stabilized or destabilized by the addition of anionic or cationic surfactants, respectively. The colloidosomes had then a switchable characteristic, what could be interesting for many commercial applications, such as phase change materials.[113]

As mentioned before, Keen *et al*.[104] reported the formation of $CaCO_3$-sealed colloidosomes using polystyrene as the colloidal particles. The authors described those capsules as having two different trigger release mechanisms: dilution and shear. It was investigated that how much shear would be necessary to break the capsules using a rheometer as a function of the thickness of the calcium carbonate shell, showing that a high shear can break the colloidosomes, releasing the active immediately. In addition, a very large dilution in water

References to this Chapter on pages 50-59

would also release the actives from the colloidosomes, but a small dilution would keep them intact, which is interesting for industrial applications such as laundry products.

Zhao[106] and Baillot[107] also reported colloidosomes made of silica alone, that had a mechanical force release trigger resulting from the brittle nature of silica. Those capsules were reported encapsulating hydrophobic liquids. Mechanical shear is interesting for consumer applications, for example, the active must be delivered when the consumer is handling the product.

1.5 Silica based microcapsules

In 1984, Avnir and co-workers published the first report demonstrating the possibility of entrapping organic molecules within an inorganic matrix.[114] Since, silica has been used as a shell material to form inorganic walled-capsules as an alternative to organic polymers, due to its mechanical and thermal stability, chemical inertness, inorganic nature, biocompatibility, easy functionalization and optical transparency.[115] In addition, silica can be manipulated to form dense walls, with well-defined porosity.[116]

The sol-gel process is a physicochemical method that assists in the formation of capsules whose shells are made of metal oxides.[117] Sol-gel encapsulation enables an effective controlled release, facility to manipulate the shell size and morphology and the possibility of room temperature processing, preventing degradation of the active material,[115, 116] all of which are desirable to the industry along with the physical protection of the entrapped active. On the other hand, the major drawback is that the gelling agent is generally a strong acid or base, what can potentially degrade the active compound.[118]

The main applications of silica capsules are in the health care,[119, 120] phase change materials,[121] food[122] and cosmetics industries.[123] as amorphous silica is considered as

References to this Chapter on pages 50-59

"generally recognized as Safe (GRAS)" by the US Food and Drugs Administration (FDA) and authorized as food additive in the European Union, including fumed and hydrated silica.[124]

Companies such as Sol-gel Technologies, based in Israel and CeramiSphere, based in Australia are examples of business fully dedicated to the commercialization of sol-gel entrapped products. The first commercial application of silica particles was by Merck in 2001 in collaboration with Sol-gel Technologies for sun protection application: silica capsules were loaded with UV molecular chromophores, under the tradename *Eusolex UV-Pearls.* These capsules were added to sunblock formulations to provide long-lasting protection while preventing skin contact with the irritant molecules.

1.5.1 The sol-gel process

Sol-gel chemistry was first intensively studied in the mid-1970s, when metal alkoxides solutions were found to be able to produce a variety of inorganic polymer networks and have continued to be extensively studied.[125] From metal alkoxide solutions, a variety of material types can be formed depending on the sol-gel process used, such as: aerogels, ceramics, uniform particles, films or fibres. Sol-gel materials are metastable solids formed in kinetically controlled reactions from molecular precursors. It consists of a dense amorphous network connecting the precursor molecules and their properties and final structure are directly influenced by several reaction parameters.[126]

A stable suspension of colloidal particles in a liquid is called *sol*. The colloidal particles can be crystalline or amorphous. Whereas a *gel* consists of a porous solid network embedded in a liquid phase ("wet gel"). Usually, the formation of a gel (gelation) results from the formation of covalent bonds between the sol particles. When other forces are involved, such as

References to this Chapter on pages 50-59

hydrogen bonds or van der Waals, gel formation can be reversible. The structure of the gel depends on the type, size and shape of the sol particles and can be densified when the solvent is (partially) removed, resulting in gel shrinkage (**Figure 1-8**).[127]

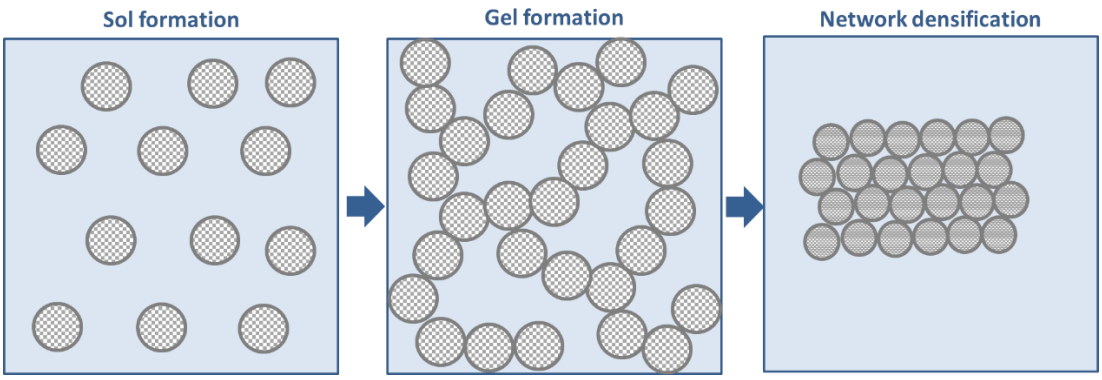

***Figure 1-9**. Colloidal network formation in sol-gel materials (adapted from [128]).*

The stability of the colloidal particles thus, ultimately controls the structure of the gel. The rate of agglomeration of sol particles can be determined by the van der Waals forces between these particles, such that electrolytes and organic additives can influence the gelation behaviour. Gelation can also be induced by fast drying of the solvent. This technique is particularly important for film and fibre formation. Moreover, at high pH values, where the particulates may have a high solubility in the sol, structures that are more porous are obtained. At low pH values, on the other hand, fine pore networks and dense structure are obtained due to low dissolution re-precipitation rate.[129]

1.5.2 Hydrolysis and condensation reactions for silica-based materials

The sol-gel process of silica-based materials relies upon the transformation of Si-OR (silicon alkoxides) and Si-OH (silanol) species to Si-O-Si (siloxane) *via* condensation reactions (loss of H_2O or alcohol).[128]

References to this Chapter on pages 50-59

The most common precursors are silicon alkoxides, $Si(OR)_4$, mostly tetraethoxysilane (TEOS), and aqueous solutions of silicates ("water glass"). Water glass solutions are a mixture of silicate species with an average composition of M_2SiO_3 (M= Na, K).[127] The stability of such species in solution is highly dependent on the pH. The point of zero charge (PZC) of silanol containing species is generally between pH 1.5 and 4.5. When the pH is brought down to below PZC the siliceous species are positively charged, and negatively charged when the pH is above the PZC (**Equations 1-4**).[130]

$$Si\text{-}OH + H^+ \rightarrow Si\text{-}OH_2^+$$

$$Si\text{-}OH + OH^- \rightarrow Si\text{-}O^- + H2O$$ ***Equations 1-4***

During the sol-gel process, the chemical reactions can be described by three equations (**Equations 1-5**). When silicon alkoxides are used as precursors, the hydrolysis reaction of Si-OR groups must precede condensation to generate Si-OH groups, which are necessary for condensation, which takes place by alcohol or water elimination:[130]

<u>Hydrolysis</u>: $\equiv Si{-}OR + H_2O \rightarrow \equiv Si{-}OH + ROH$

<u>Condensation:</u> $\equiv Si{-}OH + Si{-}OR \rightarrow \equiv Si{-}O{-}Si\equiv + ROH$

$\equiv Si{-}OH + Si{-}OH \rightarrow \equiv Si{-}O{-}Si\equiv + H2O$ ***Equations 1-5***

The most important differences between aqueous silicate and silicon alkoxides precursors are described in **Table 1-2**: [130]

References to this Chapter on pages 50-59

***Table 1-2**. Main differences between aqueous silicate and silicon alkoxides precursors*

	Aqueous silicates	**Silicon alkoxides**
Gelation initiation	pH change	Water addition (hydrolysis reactions)
Solvent	Always water	Neat or dissolved in an organic solvent (usually the alcohol produced during the condensation step)
Catalyst	Not necessary	Acidic or basic catalysts usually employed

Silicon alkoxides reactions are usually more complex and allow for a better control of the structure of the material formed. Moreover, the reaction can be catalysed by both acidic or basic conditions. When the pH is below the PZC (acidic conditions), the oxygen atom is protonated in a fast first step (**Equations 1-6** and **1-7**). Water or alcohol is then eliminated, and the electron density withdrawn from the central silicon atom making it more susceptible to attack by water (hydrolysis) or another silanol group (condensation).

Acidic conditions:

Hydrolysis

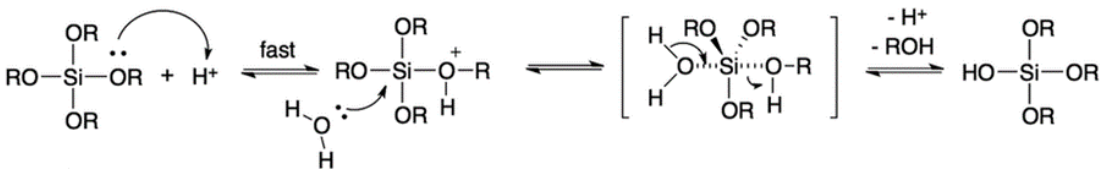

Equation 1-6

Condensation

References to this Chapter on pages 50-59

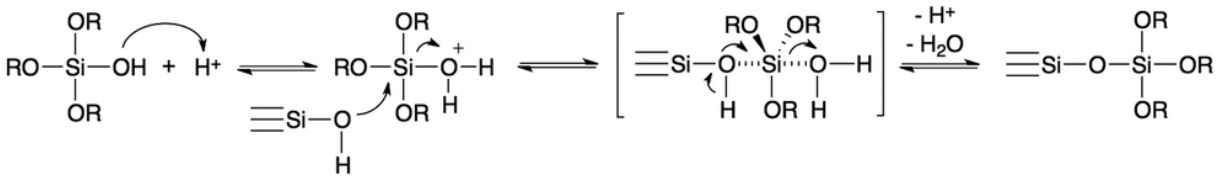

Equation 1-7

On the other hand, under basic conditions, the reaction proceeds *via* nucleophilic attack of OH^- (hydrolysis) or a ≡Si–O^- ion (condensation) by a deprotonation of water or a ≡Si–OH group (**Equation 1-8 and 1-9)**. Under strong alkaline conditions, the O-Si-O bonds can be cleaved again by OH^- molecules.[130]

Alkaline conditions:

<u>Hydrolysis</u>

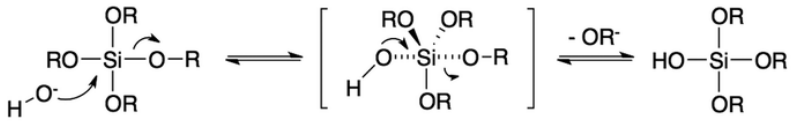

Equation 1-8

<u>Condensation</u>

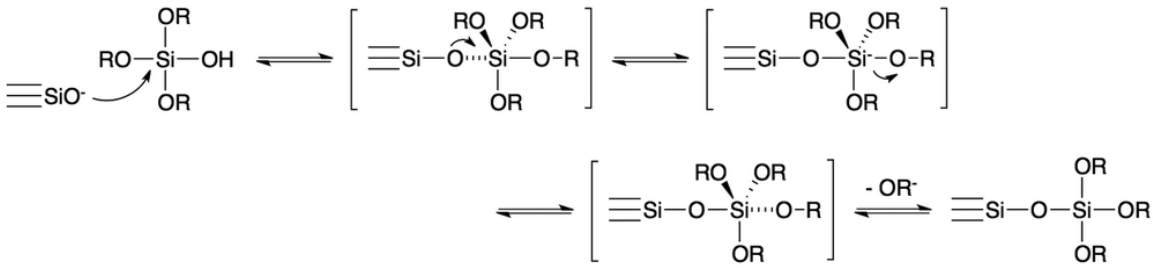

Equation 1-9

References to this Chapter on pages 50-59

Inductive effects are very important when stabilizing the intermediate states in the hydrolysis and condensation reactions, which is controlled by the substituents attached to the central silicon atom. The consequence is that the substituents will control the reactions rate and the final structure of the gel, and it is ultimately dependant on the pH of the reaction media.[130]

1.5.3 Factors influencing the rate of hydrolysis and condensation

The reactions described above can happen at different rates depending on the parameters influencing the hydrolysis and condensation reactions. The most important parameters are discussed in this section.

1.5.3.1 Type of precursor(s)

Silica precursors can be salts, oxides, hydroxides, complexes, alkoxides, acrylates and amines. Lower electronegativity and higher Lewis acidity leads to an increase in the reactivity towards water. Higher alkyls networks can lead to incomplete monomers reaction, which remain in solution.[131] For alkoxysilanes, branching and increasing the chain length of precursor substituent decreases the hydrolysis rate.[132]

1.5.3.2 pH (OH^- or H^+ catalysis), or other catalysts

As previously discussed, the reactions for base or acid-catalysed hydrolysis and condensation follow different mechanisms. Furthermore, silicon alkoxides react slowly with water, but the reaction rate can be increased by the use of acid or base catalysts.[133]

As observed in **Figure 1-10**, the reaction rate is minimal between pH 1.5 and 4.5 for condensation (PZC of silica) and pH 7 for hydrolysis.[130] At pH below 5, condensation is the limiting step and hydrolysis favoured. The opposite is observed for reactions at pH above 5, where the hydrolysis is the limiting step and Si-OH species are fast consumed due to the fast

References to this Chapter on pages 50-59

condensation. At very high pH conditions (pH > 12) the hydrolysis is again favoured and the condensation minimal, so in strongly alkaline conditions, silicon materials tend to be fully hydrolysed.[130]

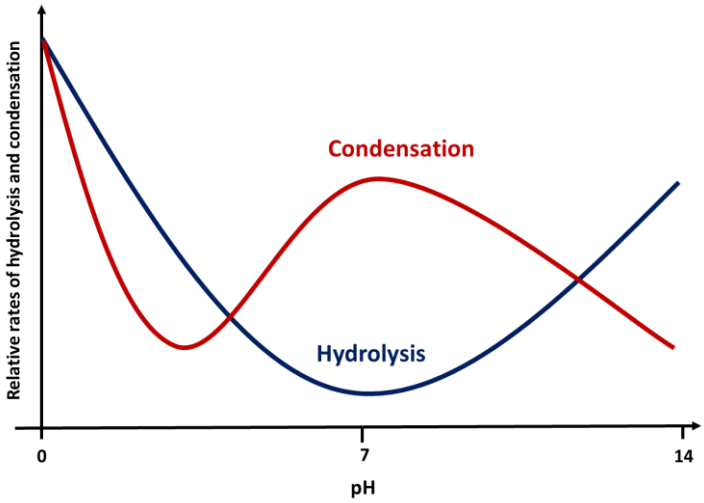

Figure 1-10. *Scheme representing the relative rates of the hydrolysis and condensation reaction as a function of the pH (Adapted from [130]).*

Overall, in acid-catalysed conditions, the hydrolysis rate is faster than condensation, which will generally start when hydrolysis is completed. The opposite is true for alkali-catalysed systems (below pH 12), where condensation is favoured instead of hydrolysis, leading to highly condensed species and usually lager pores when compared to acid-catalysed conditions.[128]

1.5.3.3 Alkoxides precursors to water ratio (R_w)

The quantity of available water during the sol-gel process strongly affects the hydrolysis and condensation kinetics. At a fixed alkoxides precursor concentration, an increase in the water content leads to an increase in the hydrolysis rate. For tetraalkoxysilanes for example, two equivalents of water (R_w = 2) are necessary for the formation of SiO_2, but four equivalents of

References to this Chapter on pages 50-59

water (R_w = 1) are necessary for the full hydrolysis of $Si(OR)_4$ to $Si(OH)_4$. So, in this case for a high quantity of water (lower R_w) hydrolysis is favourable over condensation.[130]

1.5.3.4 Type of solvent

The solvent used during the hydrolysis and condensation steps may vary in their polarity and be aprotic or protic.[128] Depending on the pH, the silanol groups involved in the condensation reaction might be protonated or deprotonated – protonated in base-catalysed reactions and deprotonated in acid-catalysed. In a protic solvent environment, hydrogen bonds will be formed between nucleophilic deprotonated silanol groups and the solvent, whereas aprotic solvents will form hydrogen bonds with electrophilic protonated silanol groups. As a result, protic solvents can promote acid-catalysed condensation and retard base-catalysed condensation reactions.[128]

1.5.3.5 Presence of electrolytes

Increasing the presence of electrolytes (salts) can accelerate the formation of the gel, as the electrical double layer around the sol particles is compressed causing the particles to coagulate as the attractive forces between the particles are uncharged and the repulsive barrier is reduced.[130] Due to this effect, most base-catalase reactions take place using ammonia, as it is not ionic, avoiding the introduction of unwanted electrolytes to the reaction. For acid-catalysed reactions on the other hand, the counterion is inevitably introduced to the reaction and influences the gelation rate and behaviour. [130]

1.5.3.6 Temperature

It is well known that temperature can fundamentally influence the kinetics of chemical reactions. Usually, the reaction happens faster at higher temperatures as there is an increase

References to this Chapter on pages 50-59

in molecule and collision kinetics. In sol-gel processes, the temperature influences primarily the gelling time, which decreases with increasing the temperature.[134]

Temperature may also influence the structure of the final material. It was observed that for TEOS-HCl systems, the pore size and pore percentage decrease with the increase of the gelation temperature until 60°C.[134, 135] As the temperature increases further, the pore percentage increases, which leads to the apparent density to decrease. This decrease is due to the high condensation rate at elevated temperatures, which leads to a more porous structure.[136]

1.5.4 Capsule structure

Different structures can be obtained depending on the desired properties of the silica capsule. In general, the active can be protected in a solid silica shell, which can be poly, mononuclear, double shell or a matrix.

1.5.4.1 Silica matrix structures

Silica matrix encapsulation is the most widely type of carrier used in industry nowadays.[117] During the encapsulation process the active is usually mixed directly with the silica precursor before the hydrolysis step. In the presence of a solvent such as ethanol, both the active and the precursor are soluble. The silicate material is then “doped” with the active during the gel process.[137, 138] TEOS is the main precursor used and this technique is used widely in the cosmetic, food and medical sectors, as it is easily scalable and the by-product , usually ethanol, is generally tolerable.[123] The active ingredient release kinetics is controlled by the material porosity and chemicals interactions with the silica cage.

References to this Chapter on pages 50-59

1.5.4.2 Core-shell structures from emulsion template

Core-shell structures comprised of a thin silica shell encapsulating actives can be formed using interfacial polymerization which combines sol-gel and emulsion chemistry. This method is attractive when a high encapsulated load of the active is necessary, as the core can have a weight as high as 90% of the final material.[123] The active release can be triggered using mechanical rupture or shell dissolution, releasing the content in a burst, or sustained manner, by controlling the pore sizes of the structures, which allows the active to be released over time.[139]

The emulsion droplet usually functions as a micro reactor for the hydrolysis and condensation of the silica precursor[117] *via* two methods that differ by the use of a hydrophilic or a hydrophobic precursor. For both methods an oil-in-water emulsion is formed containing the active and either the precursor or the gelling agent in the oil phase - depending of the hydrophobicity of the precursor. In the following step, the solid shell of the capsule is formed by adding the missing component (gelling agent or precursor).[118]

Low molecular weight silanes and alkylsilanes such as TEOS and tetramethylsiloxane (TMOS), are the main silica precursor used for the shell formation. Silica capsules with walls formed from condensed TEOS have been widely described in the literature.[140-143] The hydrolysis and condensation rates for these low molecular weight molecules occur relatively fast when compared to other alkyl structures, due to the retarding effect of the bulkier ethoxide groups,[126] which can be advantageous when forming a solid wall from an emulsion template.[117] Moreover, TEOS is interesting for industrial applications as it a relatively cheap

References to this Chapter on pages 50-59

and abundant starting material and is considered safe to be used in food and flavouring contact materials.[144]

To form the emulsion, ionic and non-ionic surfactants are used to stabilize the oil-in-water emulsion and define the structure of the final shell. Ionic surfactants, such as CTAB, usually yield pore sizes between 2-4 nm[117, 145] whereas non-ionic counterparts, such as Tween series (ethoxylated sorbitan esters), generate pores of around 10 nm.[146]

Silica has also been investigated as Pickering emulsifier between water and oils.[51] All silica microcapsules are typically formed when an additional silica precursor is added to the interface "sealing" the colloidal particles together. Typically TEOS is used as silica precursor, forming robust capsules that are mechanically stable as demonstrated by Jiang *et al*,[147] where a hydrophilic active was encapsulated in submicron capsules that released the active when triggered by an environmental signal such as surfactant or ethanol.

Wang *et al*. and Zhao *et al*.[106, 148] have demonstrated the possibility of using hyperbranched polyethoxysilane (PEOS) as precursor to "glue" the particles together forming nanocapsules with a narrow size distribution. Both studies have used organically modified silica nanoparticles and PEOS to encapsulate both hydrophilic and hydrophobic actives at high pH with 100% efficiency and mechanical stability.

The benefit of using PEOS over TEOS is that the former is a hydrophobic liquid that acts as a surfactant upon hydrolysis, which adheres to the water-oil interface, so the silica film formation is more efficient as less molecules are lost to the water phase (as happens to hydrolysed TEOS molecules).[89]

References to this Chapter on pages 50-59

The pH of the continuous phase can also greatly affect the final structure of the capsule, specially the porosity. Reports have demonstrated that acid-catalysed sol-gel reactions tend to have slower gelation times and the resulting silica material is significantly less porous and more mechanically robust than the base-catalysed counterparts.[143] Zhang and co-workers[121] for example, have demonstrated that the optimum pH to minimize porosity is between 2 and 3. Acidic conditions are, therefore, preferable for the formation of capsules with low porosity and basic conditions for the formation of mesoporous materials.[140]

1.5.4.3 Hybrid silica capsules (double-shell)

Silica-biopolymer hybrid capsules have also been studied as carriers for oily actives.[149] As described in a patent by Firmenich,[150] an oily active was first encapsulated in a gelatine/gum arabic shell, then TEOS is used to precipitate silica at the capsule surface forming a double shell. The company has demonstrated that the method is efficient for the encapsulation of fragrances and has enhanced mechanical properties when compared to conventional coacervate capsules. Sensory evaluation tests have also demonstrated that formulations containing encapsulated peppermint oil had superior performance than the non-encapsulated counterpart.

Other materials can be used to form a hybrid silica shell such as chitosan,[151] organic polymers[98, 152], alginate [149, 153, 154] and lipids.[155] The advantage of forming a hybrid or double shell is the possibility to enhance and tailor the properties of the capsule for specific applications. The resulting capsule could have a less porous wall or enhanced mechanical properties, for example.

References to this Chapter on pages 50-59

1.5.5 Fragrance encapsulation using silica capsules

Fragrance encapsulation using silica-based materials have been receiving a notable increase in attention from encapsulation and fragrances companies as can be observed in the increase in patents applications in recent years (**Figure 1-11**). Fragrance companies such as IFF, Givaudan and Firmenich are constantly innovating in fragrance encapsulation, along with consumer good companies, such as P&G, Henkel and Unilever, which have an interest in stabilising fragrances in their products.

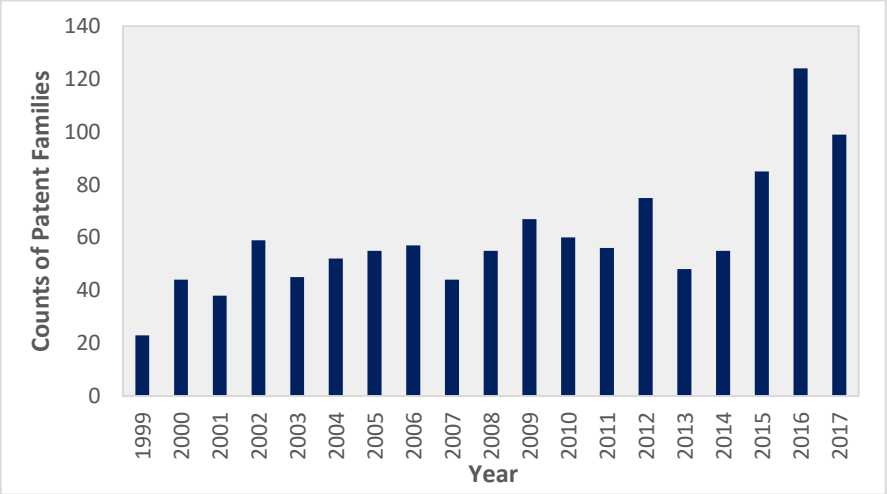

***Figure 1-11**. Number of patent applications disclosing fragrance encapsulation mentioning silica-based materials in the past 20 years (data obtained from patents search using Orbit software, key works: fragrance, encapsulation, silica).*

Ciriminna *et al*. have published a comprehensive review of sol-gel microencapsulation of odourants and flavours,[123] consisting mainly of porous silica-based materials, which is interesting for perfumes and personal care applications, as the silica matrix is doped with essential oils leading to controlled release.[156] Zuobing and co-workers, for example, have

References to this Chapter on pages 50-59

demonstrated the possibility to encapsulate lavender oil in organo-modified silica nanospheres.[157]

For fabric care applications, usually it is necessary to have a high load of perfume and a trigger release by mechanical force, leading to a burst release of the perfume on the fabric. Core-shell structures would be more interesting in this case; the limitation is the capability of retaining the oil inside the microcapsule during storage in detergent formulations. Currently, there is no fully inorganic silica-based encapsulation method capable of stabilizing fragrances in liquid detergent formulations as stated by the industrial partner in this project (P&G).

1.6 Conclusions

Microencapsulation techniques have been extensively studied as tools to improve the efficiency of fragrance delivery in consumer products. Encapsulation can make formulations more environmentally friendly by reducing the amount of perfume added to the product and reducing waste. Capsules can also improve the stability of fragrance, prolong formulations' shelf life and provide controlled release functions.

However, current microcapsules are made from organic based materials and can potentially be toxic. Thus, there is a clear necessity for technologies that are considered non-toxic to humans and the environment, by reducing the level of toxic materials and plastics used in the shell material. Although there are various wall chemistries available, such as biopolymers or inorganic matrixes, these still remain to be optimised in terms of stability in the finished product, performance, scaling up process and cost.

Particle stabilised emulsions (Pickering emulsions), are routes for the formation of microcapsules with improved mechanical properties and high stability without the use of

organic surfactants. However, due to the high permeability of these materials, their use as carriers of small molecules, such as fragrances, is still limited. Nevertheless, the permeability can be controlled using methodologies to seal the pores with gelatines, polymers or inorganic materials.

Silica has been studied as carrier for active materials for over a century and it is a promising material for a wide range of applications due to its thermal and mechanical stability, biocompatibility and chemical inertness. The health care, cosmetics and food industries, among others, already make use of silica-based materials as delivery systems in a large scale.

To make use of silica-based wall chemistries for the encapsulation of fragrances for detergent applications it is necessary to adjust the shell structure to obtain minimum porosity (avoiding perfume leakage during storage and shipping) and improved mechanical properties, so the fragrances survive the wash cycle and delivery freshness to the consumer. Other aspects are also important to make the technology usable for industrial application, for example, the scaling-up process and cost.

Overall, Pickering emulsions combined with sol-gel chemistry is a potential strategy for the formation of fully inorganic wall material for the encapsulation of fragrances with high payload. As described in the literature, the properties and structure of the shell can be tuned in order to minimise pore size, therefore leakage, and improve the materials mechanical properties.

The development of a fully inorganic shell technology capable of stabilising fragrances in detergent formulations is still a great challenge for the fabric care industry. Nevertheless, it offers an exciting new area for innovation, with the objective of bringing more

 References to this Chapter on pages 50-59

environmentally friendly formulations to the consumer, while maintaining an enhanced freshness experience.

1.7 Aim and Objectives

1.7.1 The challenge

Perfume microcapsules used in the fabric care industry today have their walls made of organic polymers. With the growing concerns regarding microplastics in the environment, alternative encapsulation technology must be explored. Some options available are technologies based on biopolymers, such as chitosan and alginate, which can be readily biodegraded in the environment or fully inorganic compositions, such as silica or calcium carbonate, where the formed shell is made of an inert material. The problem with these materials is that they are known for being porous, and therefore not able to stabilise perfume in surfactant-based formulations such as laundry detergents and fabric softeners.

1.7.2 The Aim and Objectives

The overall aim of this project is to formulate and characterise novel inorganic microcapsules with desirable structural and mechanical properties in order to provide stability, protection, long-term retention, and triggered release of strategic active ingredients in the Fast-Moving Consumer Goods (FMCG) industry, enhancing existing formulations as an alternative to organic polymer-based perfume microcapsules (PMCs).

More specifically, the project investigates the usage of silica microcapsules formed by the combination of sol-gel chemistry and silica Pickering emulsifiers for long-term encapsulation and protection of fragrances for fabric care applications that are able to protect the fragrance during storage and shipping of the product and deliver freshness when mechanical force is

References to this Chapter on pages 50-59

applied by the consumer. The objectives of this project are outlined below and summarized in **Figure 1-12**:

1. To study of the stabilization of perfume oil using hydrophilic silica nanoparticles as Pickering emulsifier, and preparation and characterization of hyperbranched polyethoxysiloxane (PEOS), which will be used as silica precursor. These are the building blocks for the preparation of the silica shell encapsulating perfume oil or hexyl salicylate in the following chapters (**Chapter 3**).

2. To development of an encapsulation strategy using a perfume model (hexyl salicylate) in order to understand the best approach to produce silica capsules from silica nanoparticles and PEOS, while minimizing leakage and enhancing mechanical properties (**Chapter 4**);

3. To apply the developed encapsulation technology to a real-world perfume oil formulation (**Chapter 5**);

4. To optimize the shell properties in order to enhance stability and performance in the finished product and improvement of the encapsulation process (**Chapter 6**);

5. To test the capsules produced using methods used in the industry in terms of performance and stability and applying the technology to other consumer goods strategic actives (**Chapters 5 and 6**).

References to this Chapter on pages 50-59

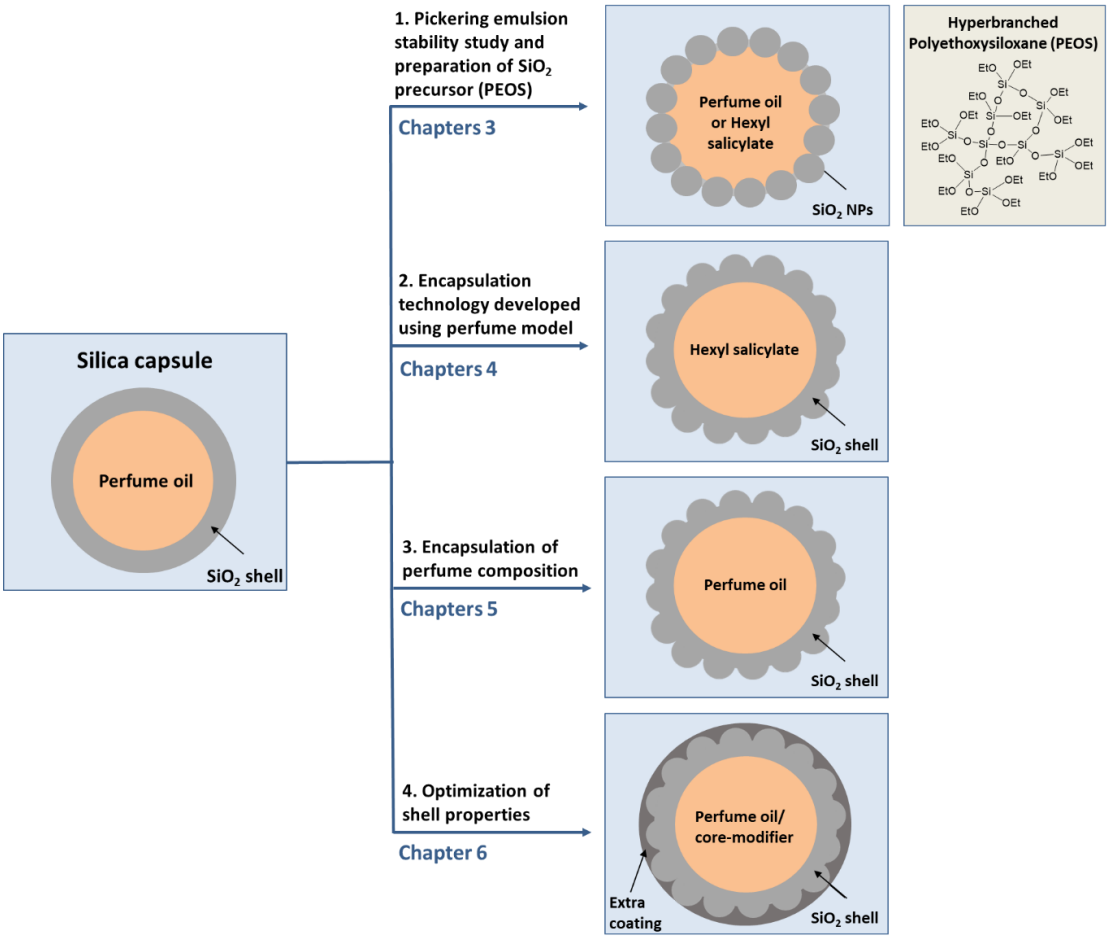

***Figure 1-12**. Scheme representing the key steps for the encapsulation of perfume oils in silica capsules.*

Table 1-3 below gives an overview of the core and shell materials studied in each of the results chapters. **Chapter 3** presents the Pickering emulsion stability between perfume oil or hexyl salicylate using SiO_2 NPs as Pickering emulsifier. Then, in the work presented in **Chapter 4**, silica capsules are formed using PEOS to cross-link the SiO_2 NPs encapsulating hexyl salicylate. **Chapter 5** investigates the encapsulation of the commercial perfume oil using PEOS and SiO_2 NPS to form the shell. Finally, in **Chapter 6** Isopropyl myristate is used as core-modifier to optimise the encapsulation of perfume oil studied in **Chapter 5,** as well as the addition of an extra silica coating to these capsules.

References to this Chapter on pages 50-59

***Table 1-3**. Overview of core and shell materials studied in each of the results chapters.*

		Chapter 3	Chapter 4	Chapter 5	Chapter 6
Core materials	**Hexyl salicylate**	X	X		
	Perfume oil	X		X	X
	Isopropyl myristate				X
Shell materials	**PEOS**		X	X	X
	SiO_2 NPs	X	X	X	X

1.8 References

1. G. Fráter, J. A. Bajgrowicz and P. Kraft, *Fragrance Chemistry*, *Tetrahedron*, **1998**, *54*, 7633-7703.
2. K. Bauer, D. Garbe and H. Surburg, *Common Fragrance and Flavor Materials: Preparation, Properties and Uses*, Wiley, **2008**.
3. D. Milotic, *The Impact of Fragrance on Consumer Choice*, *Journal of Consumer Behaviour*, **2003**, *3*, 179-191.
4. J. J. G. van Soest, in *Flavours and Fragrances: Chemistry, Bioprocessing and Sustainability*, ed. R. G. Berger, Springer Berlin Heidelberg, Berlin, Heidelberg, **2007**, pp. 439-455.
5. J. S. Jellinek, *The Use of Fragrance in Consumer Products*, Wiley, **1975**.
6. E. W. Flick, in *Cosmetic and Toiletry Formulations*, ed. E. W. Flick, William Andrew Publishing, Oxford, **1989**, pp. 327-333.
7. A. Herrmann, *Controlled Release of Volatiles under Mild Reaction Conditions: From Nature to Everyday Products*, *Angewandte Chemie International Edition*, **2007**, *46*, 5836-5863.
8. D. Lenoir, *Organic Reaction Mechanisms. Edited by A. C. Knipe*, *Angewandte Chemie International Edition*, **2006**, *45*, 3204-3205.
9. G. Nelson, *Application of Microencapsulation in Textiles*, *International Journal of Pharmaceutics*, **2002**, *242*, 55-62.
10. C. Larote, C. Gonzalez, *Fragrance Encapsulation in Consumer Products*, IFRA Europe report, **2018** (available from: https://echa.europa.eu/documents/10162/23964241/02_ifra-laroche_and_gonzales_en.pdf/2f1585db-13d3-4756-4911-7422a4d7381c) - Acessed 10/12/2018)
11. G. Sun and Z. Zhang, *Mechanical Strength of Microcapsules Made of Different Wall Materials*, *International Journal of Pharmaceutics*, **2002**, *242*, 307-311.
12. J. O. D. J Smets, A Pintens, S J Guinebretiere, A K Druckrey ,P D Sands Procter and Gamble Co *Benefit Agent Containing Delivery Particle,* **2007**
13. T. A. S. H Zhang, K A Hobart, D J Williamson Encapsys Inc, *Encapsulation,* **2015**
14. B. Sumiga, E. Knez, M. Vrtacnik, V. Ferk-Savec, M. Staresinic and B. Boh, *Production of Melamine-Formaldehyde Pcm Microcapsules with Ammonia Scavenger Used for Residual Formaldehyde Reduction*, *Acta Chim Slov*, **2011**, *58*, 14-25.

15. J. K. McLaughlin, *Formaldehyde and Cancer: A Critical Review*, *International Archives of Occupational and Environmental Health*, **1994**, *66*, 295-301.
16. E. MacArthur, *Beyond Plastic Waste*, *Science*, **2017**, *358*, 843-843.
17. E. Kentin, *Restricting Microplastics in the European Union: Process and Criteria Under REACH*, E. Euer. Phys. J. Plus **2018**, 133, 425.
18. H. Sawalha, K. Schroën and R. Boom, *Biodegradable Polymeric Microcapsules: Preparation and Properties*, *Chemical Engineering Journal*, **2011**, *169*, 1-10.
19. M. Jaganathan, D. Madhumitha and A. Dhathathreyan, *Protein Microcapsules: Preparation and Applications*, *Advances in Colloid and Interface Science*, **2014**, *209*, 1-7.
20. Y. Xiao, B. Wu, X. Fu, R. Wang and J. Lei, *Preparation of Biodegradable Microcapsules through an Organic Solvent-Free Interfacial Polymerization Method*, *Polymers for Advanced Technologies*, **2019**, *30*, 483-488.
21. M. Fujiwara, K. Shiokawa, Y. Tanaka and Y. Nakahara, *Preparation and Formation Mechanism of Silica Microcapsules (Hollow Sphere) by Water/Oil/Water Interfacial Reaction*, *Chemistry of Materials*, **2004**, *16*, 5420-5426.
22. Y. Cui and J. S. van Duijneveldt, *Microcapsules Composed of Cross-Linked Organoclay*, *Langmuir*, **2012**, *28*, 1753-1757.
23. M. Fujiwara, K. Shiokawa, K. Morigaki, Y. Zhu and Y. Nakahara, *Calcium Carbonate Microcapsules Encapsulating Biomacromolecules*, *Chemical Engineering Journal*, **2008**, *137*, 14-22.
24. P. T. d. Silva, L. L. M. Fries, C. R. d. Menezes, A. T. Holkem, C. L. Schwan, É. F. Wigmann, J. d. O. Bastos and C. d. B. d. Silva, *Microencapsulation: Concepts, Mechanisms, Methods and Some Applications in Food Technology*, *Ciência Rural*, **2014**, *44*, 1304-1311.
25. R. Arshady, *Microspheres Microcapsules & Liposomes: Preparation & Chemical Applications*, Citus Books, **1999**.
26. R. Dubey, *Microencapsulation Technology and Applications*, *2009*, **2009**, *59*, 14.
27. M. N. Singh, K. S. Y. Hemant, M. Ram and H. G. Shivakumar, *Microencapsulation: A Promising Technique for Controlled Drug Delivery*, *Research in pharmaceutical sciences*, **2010**, *5*, 65-77.
28. H.-C. Wang, Y. Zhang, C. M. Possanza, S. C. Zimmerman, J. Cheng, J. S. Moore, K. Harris and J. S. Katz, *Trigger Chemistries for Better Industrial Formulations*, *ACS Applied Materials & Interfaces*, **2015**, *7*, 6369-6382.
29. C. P. Molloy, Y. Yao, H. Kammoun, T. Bonnard, T. Hoefer, K. Alt, F. Tovar-Lopez, G. Rosengarten, P. A. Ramsland, A. D. van der Meer, A. van den Berg, A. J. Murphy, C. E. Hagemeyer, K. Peter and E. Westein, *Shear-Sensitive Nanocapsule Drug Release for Site-Specific Inhibition of Occlusive Thrombus Formation*, *Journal of Thrombosis and Haemostasis*, **2017**, *15*, 972-982.
30. N. Fomina, J. Sankaranarayanan and A. Almutairi, *Photochemical Mechanisms of Light-Triggered Release from Nanocarriers*, *Advanced drug delivery reviews*, **2012**, *64*, 1005-1020.
31. A. Abbaspourrad, S. S. Datta and D. A. Weitz, *Controlling Release from Ph-Responsive Microcapsules*, *Langmuir*, **2013**, *29*, 12697-12702.

32. S. E. Paramonov, E. M. Bachelder, T. T. Beaudette, S. M. Standley, C. C. Lee, J. Dashe and J. M. J. Fréchet, *Fully Acid-Degradable Biocompatible Polyacetal Microparticles for Drug Delivery*, *Bioconjugate Chemistry*, **2008**, *19*, 911-919.
33. S. P. Friedman and Y. Mualem, *Diffusion of Fertilizers from Controlled-Release Sources Uniformly Distributed in Soil*, *Fertilizer research*, **1994**, *39*, 19-30.
34. L. Shang, Y. Cheng, J. Wang, Y. Yu, Y. Zhao, Y. Chen and Z. Gu, *Osmotic Pressure-Triggered Cavitation in Microcapsules*, *Lab on a Chip*, **2016**, *16*, 251-255.
35. F. Goodarzi and S. Zendehboudi, *A Comprehensive Review on Emulsions and Emulsion Stability in Chemical and Energy Industries*, *The Canadian Journal of Chemical Engineering*, **2019**, *97*, 281-309.
36. R. J. G. Lopetinsky, J. H. Masliyah and Z. Xu, in *Colloidal Particles at Liquid Interfaces*, eds. B. P. Binks and T. S. Horozov, Cambridge University Press, Cambridge, **2006**, pp. 186-224.
37. in *Emulsion Formation and Stability*.
38. D. J. McClements and S. M. Jafari, *Improving Emulsion Formation, Stability and Performance Using Mixed Emulsifiers: A Review*, *Advances in Colloid and Interface Science*, **2018**, *251*, 55-79.
39. in *Applied Surfactants*, pp. 115-185.
40. S. Shilpi, A. Jain, Y. Gupta and S. K. Jain, *Colloidosomes: An Emerging Vesicular System in Drug Delivery*, **2007**, *24*, 361-391.
41. K. L. Thompson, M. Williams and S. P. Armes, *Colloidosomes: Synthesis, Properties and Applications*, *Journal of Colloid and Interface Science*, **2015**, *447*, 217-228.
42. W. Ramsden and F. Gotch, *Separation of Solids in the Surface-Layers of Solutions and 'Suspensions' (Observations on Surface-Membranes, Bubbles, Emulsions, and Mechanical Coagulation).—Preliminary Account*, *Proceedings of the Royal Society of London*, **1904**, *72*, 156-164.
43. S. U. Pickering, *Cxcvi.-Emulsions*, *Journal of the Chemical Society, Transactions*, **1907**, *91*, 2001-2021.
44. B. P. Binks and C. P. Whitby, *Nanoparticle Silica-Stabilised Oil-in-Water Emulsions: Improving Emulsion Stability*, *Colloids and Surfaces A: Physicochemical and Engineering Aspects*, **2005**, *253*, 105-115.
45. X.-F. Guo, Y.-S. Kim and G.-J. Kim, *Fabrication of Sio2, Al2o3, and Tio2 Microcapsules with Hollow Core and Mesoporous Shell Structure*, *The Journal of Physical Chemistry C*, **2009**, *113*, 8313-8319.
46. M. Williams, S. P. Armes and D. W. York, *Clay-Based Colloidosomes*, *Langmuir*, **2012**, *28*, 1142-1148.
47. T. N. Hunter, R. J. Pugh, G. V. Franks and G. J. Jameson, *The Role of Particles in Stabilising Foams and Emulsions*, *Advances in Colloid and Interface Science*, **2008**, *137*, 57-81.
48. Y. Chevalier and M.-A. Bolzinger, *Emulsions Stabilized with Solid Nanoparticles: Pickering Emulsions*, *Colloids and Surfaces A: Physicochemical and Engineering Aspects*, **2013**, *439*, 23-34.
49. T. Tadros. *Electrostatic and Steric Stabilization of Colloidal Dispersions. In Electrical Phenomena at Interfaces and Biointerfaces,***2012**, H. Ohshima (Ed.)

50. R. Aveyard, B. P. Binks and J. H. Clint, *Emulsions Stabilised Solely by Colloidal Particles*, *Advances in Colloid and Interface Science*, **2003**, *100–102*, 503-546.
51. B. P. Binks, P. D. I. Fletcher, B. L. Holt, P. Beaussoubre and K. Wong, *Phase Inversion of Particle-Stabilised Perfume Oil-Water Emulsions: Experiment and Theory*, *Physical Chemistry Chemical Physics*, **2010**, *12*, 11954-11966.
52. S. Björkegren, L. Nordstierna, A. Törncrona and A. Palmqvist, *Hydrophilic and Hydrophobic Modifications of Colloidal Silica Particles for Pickering Emulsions*, *Journal of Colloid and Interface Science*, **2017**, *487*, 250-257.
53. J. H. Schulman and J. Leja, *Control of Contact Angles at the Oil-Water-Solid Interfaces. Emulsions Stabilized by Solid Particles (Baso4)*, *Transactions of the Faraday Society*, **1954**, *50*, 598-605.
54. M. Destribats, S. Gineste, E. Laurichesse, H. Tanner, F. Leal-Calderon, V. Héroguez and V. Schmitt, *Pickering Emulsions: What Are the Main Parameters Determining the Emulsion Type and Interfacial Properties?*, *Langmuir*, **2014**, *30*, 9313-9326.
55. B. P. Binks, *Particles as Surfactants—Similarities and Differences*, *Current Opinion in Colloid & Interface Science*, **2002**, *7*, 21-41.
56. M. Williams, N. J. Warren, L. A. Fielding, S. P. Armes, P. Verstraete and J. Smets, *Preparation of Double Emulsions Using Hybrid Polymer/Silica Particles: New Pickering Emulsifiers with Adjustable Surface Wettability*, *ACS Applied Materials & Interfaces*, **2014**, *6*, 20919-20927.
57. B. P. Binks and S. O. Lumsdon, *Pickering Emulsions Stabilized by Monodisperse Latex Particles: Effects of Particle Size*, *Langmuir*, **2001**, *17*, 4540-4547.
58. F. Qi, J. Wu, G. Sun, F. Nan, T. Ngai and G. Ma, *Systematic Studies of Pickering Emulsions Stabilized by Uniform-Sized Plga Particles: Preparation and Stabilization Mechanism*, *Journal of Materials Chemistry B*, **2014**, *2*, 7605-7611.
59. S. Fujii, M. Okada and T. Furuzono, *Hydroxyapatite Nanoparticles as Stimulus-Responsive Particulate Emulsifiers and Building Block for Porous Materials*, *Journal of Colloid and Interface Science*, **2007**, *315*, 287-296.
60. H. Liu, Y. Xu, C. Zhou, S. Geng, C. Wei and C. Yu, *Facile Fabrication and Property of Biocompatible and Biodegradable Cellulose-Coated Pmma Composite Microspheres by Pickering Emulsion System*, *International Journal of Polymeric Materials and Polymeric Biomaterials*, **2017**, *66*, 773-780.
61. D. J. Kraft, J. W. J. de Folter, B. Luigjes, S. I. R. Castillo, S. Sacanna, A. P. Philipse and W. K. Kegel, *Conditions for Equilibrium Solid-Stabilized Emulsions*, *The Journal of Physical Chemistry B*, **2010**, *114*, 10347-10356.
62. J. W. J. de Folter, E. M. Hutter, S. I. R. Castillo, K. E. Klop, A. P. Philipse and W. K. Kegel, *Particle Shape Anisotropy in Pickering Emulsions: Cubes and Peanuts*, *Langmuir*, **2014**, *30*, 955-964.
63. B. Madivala, J. Fransaer and J. Vermant, *Self-Assembly and Rheology of Ellipsoidal Particles at Interfaces*, *Langmuir*, **2009**, *25*, 2718-2728.
64. I. Kalashnikova, H. Bizot, B. Cathala and I. Capron, *New Pickering Emulsions Stabilized by Bacterial Cellulose Nanocrystals*, *Langmuir*, **2011**, *27*, 7471-7479.
65. T. Bollhorst, K. Rezwan and M. Maas, *Colloidal Capsules: Nano- and Microcapsules with Colloidal Particle Shells*, *Chemical Society Reviews*, **2017**, *46*, 2091-2126.

66. J. Wu and G.-H. Ma, *Recent Studies of Pickering Emulsions: Particles Make the Difference*, *Small*, **2016**, *12*, 4633-4648.
67. F. Reincke, W. K. Kegel, H. Zhang, M. Nolte, D. Wang, D. Vanmaekelbergh and H. Möhwald, *Understanding the Self-Assembly of Charged Nanoparticles at the Water/Oil Interface*, *Physical Chemistry Chemical Physics*, **2006**, *8*, 3828-3835.
68. M. E. Flatté, A. A. Kornyshev and M. Urbakh, *Electrovariable Nanoplasmonics and Self-Assembling Smart Mirrors*, *The Journal of Physical Chemistry C*, **2010**, *114*, 1735-1747.
69. M. Luo, G. K. Olivier and J. Frechette, *Electrostatic Interactions to Modulate the Reflective Assembly of Nanoparticles at the Oil–Water Interface*, *Soft Matter*, **2012**, *8*, 11923-11932.
70. J. S. Weston, R. E. Jentoft, B. P. Grady, D. E. Resasco and J. H. Harwell, *Silica Nanoparticle Wettability: Characterization and Effects on the Emulsion Properties*, *Industrial & Engineering Chemistry Research*, **2015**, *54*, 4274-4284.
71. A. San-Miguel and S. H. Behrens, *Influence of Nanoscale Particle Roughness on the Stability of Pickering Emulsions*, *Langmuir*, **2012**, *28*, 12038-12043.
72. E. Vignati, R. Piazza and T. P. Lockhart, *Pickering Emulsions: Interfacial Tension, Colloidal Layer Morphology, and Trapped-Particle Motion*, *Langmuir*, **2003**, *19*, 6650-6656.
73. J. Frelichowska, M.-A. Bolzinger and Y. Chevalier, *Effects of Solid Particle Content on Properties of O/W Pickering Emulsions*, *Journal of Colloid and Interface Science*, **2010**, *351*, 348-356.
74. S. A. P. W. P. B. S. Leal-Calderon, *Some General Features of Limited Coalescence in Solid-Stabilized Emulsions*, *The European Physical Journal E*, **2003**, *11*, 273-281.
75. S. Arditty, C. P. Whitby, B. P. Binks, V. Schmitt and F. Leal-Calderon, *Some General Features of Limited Coalescence in Solid-Stabilized Emulsions*, *The European Physical Journal E*, **2003**, *11*, 273-281.
76. S. S. Datta, H. C. Shum and D. A. Weitz, *Controlled Buckling and Crumpling of Nanoparticle-Coated Droplets*, *Langmuir*, **2010**, *26*, 18612-18616.
77. T. H. Whitesides and D. Ross, *Experimental and Theoretical Analysis of the Limited Coalescence Process: Stepwise Limited Coalescence*, **1995**.
78. H. N. Yow and A. F. Routh, *Formation of Liquid Core-Polymer Shell Microcapsules*, *Soft Matter*, **2006**, *2*, 940-949.
79. H. N. Yow and A. F. Routh, *Release Profiles of Encapsulated Actives from Colloidosomes Sintered for Various Durations*, *Langmuir*, **2009**, *25*, 159-166.
80. P. Arumugam, D. Patra, B. Samanta, S. S. Agasti, C. Subramani and V. M. Rotello, *Self-Assembly and Cross-Linking of Fept Nanoparticles at Planar and Colloidal Liquid−Liquid Interfaces*, *Journal of the American Chemical Society*, **2008**, *130*, 10046-10047.
81. O. J. Cayre, P. F. Noble and V. N. Paunov, *Fabrication of Novel Colloidosome Microcapsules with Gelled Aqueous Cores*, *Journal of Materials Chemistry*, **2004**, *14*, 3351-3355.
82. Y. Chen, C. Wang, J. Chen, X. Liu and Z. Tong, *Growth of Lightly Crosslinked Phema Brushes and Capsule Formation Using Pickering Emulsion Interface-Initiated Atrp*, *Journal of Polymer Science Part A: Polymer Chemistry*, **2009**, *47*, 1354-1367.
83. S. A. F. Bon, in *Encyclopedia of Polymeric Nanomaterials*, eds. S. Kobayashi and K. Müllen, Springer Berlin Heidelberg, Berlin, Heidelberg, **2014**, pp. 1-6.

84. Y. Liu, X. Chen and J. H. Xin, *Silica Nanoparticles-Walled Microcapsules*, *Journal of Materials Science*, **2006**, *41*, 5399-5401.
85. M. Li, R. L. Harbron, J. V. M. Weaver, B. P. Binks and S. Mann, *Electrostatically Gated Membrane Permeability in Inorganic Protocells*, *Nat Chem*, **2013**, *5*, 529-536.
86. A. D. Dinsmore, M. F. Hsu, M. G. Nikolaides, M. Marquez, A. R. Bausch and D. A. Weitz, *Colloidosomes: Selectively Permeable Capsules Composed of Colloidal Particles*, *Science*, **2002**, *298*, 1006-1009.
87. H. Duan, D. Wang, N. S. Sobal, M. Giersig, D. G. Kurth and H. Möhwald, *Magnetic Colloidosomes Derived from Nanoparticle Interfacial Self-Assembly*, *Nano Letters*, **2005**, *5*, 949-952.
88. D. B. Lawrence, T. Cai, Z. Hu, M. Marquez and A. D. Dinsmore, *Temperature-Responsive Semipermeable Capsules Composed of Colloidal Microgel Spheres*, *Langmuir*, **2007**, *23*, 395-398.
89. Y. Zhao, Z. Chen, X. Zhu and M. Moller, *Silica Nanoparticles Catalyse the Formation of Silica Nanocapsules in a Surfactant-Free Emulsion System*, *Journal of Materials Chemistry A*, **2015**, *3*, 24428-24436.
90. F. J. Rossier-Miranda, C. G. P. H. Schroën and R. M. Boom, *Colloidosomes: Versatile Microcapsules in Perspective*, *Colloids and Surfaces A: Physicochemical and Engineering Aspects*, **2009**, *343*, 43-49.
91. P. Pieranski, *Two-Dimensional Interfacial Colloidal Crystals*, *Physical Review Letters*, **1980**, *45*, 569-572.
92. P. Lipowsky, M. J. Bowick, J. H. Meinke, D. R. Nelson and A. R. Bausch, *Direct Visualization of Dislocation Dynamics in Grain-Boundary Scars*, *Nat Mater*, **2005**, *4*, 407-411.
93. R. T. Rosenberg and N. R. Dan, *Diffusion through Colloidosome Shells*, *Journal of Colloid and Interface Science*, **2011**, *354*, 478-482.
94. S. A. F. Bon, S. Cauvin and P. J. Colver, *Colloidosomes as Micron-Sized Polymerisation Vessels to Create Supracolloidal Interpenetrating Polymer Network Reinforced Capsules*, *Soft Matter*, **2007**, *3*, 194-199.
95. T. Chen, P. J. Colver and S. A. F. Bon, *Organic–Inorganic Hybrid Hollow Spheres Prepared from Tio2-Stabilized Pickering Emulsion Polymerization*, *Advanced Materials*, **2007**, *19*, 2286-2289.
96. D. Yin, Q. Zhang, C. Yin, X. Zhao and H. Zhang, *Hollow Microspheres with Covalent-Bonded Colloidal and Polymeric Shell by Pickering Emulsion Polymerization*, *Polymers for Advanced Technologies*, **2012**, *23*, 273-277.
97. W. Chen, X. Liu, Y. Liu and H.-I. Kim, *Synthesis of Microcapsules with Polystyrene/Zno Hybrid Shell by Pickering Emulsion Polymerization*, *Colloid and Polymer Science*, **2010**, *288*, 1393-1399.
98. Y. Long, B. Vincent, D. York, Z. Zhang and J. A. Preece, *Organic–Inorganic Double Shell Composite Microcapsules*, *Chemical Communications*, **2010**, *46*, 1718-1720.
99. M. Williams, B. Olland, S. P. Armes, P. Verstraete and J. Smets, *Inorganic/Organic Hybrid Microcapsules: Melamine Formaldehyde-Coated Laponite-Based Pickering Emulsions*, *Journal of Colloid and Interface Science*, **2015**, *460*, 71-80.

100. K. L. Thompson and S. P. Armes, *From Well-Defined Macromonomers to Sterically-Stabilised Latexes to Covalently Cross-Linkable Colloidosomes: Exerting Control over Multiple Length Scales*, *Chemical Communications*, **2010**, *46*, 5274-5276.
101. K. L. Thompson, S. P. Armes, J. R. Howse, S. Ebbens, I. Ahmad, J. H. Zaidi, D. W. York and J. A. Burdis, *Covalently Cross-Linked Colloidosomes*, *Macromolecules*, **2010**, *43*, 10466-10474.
102. Q. Yuan, O. J. Cayre, S. Fujii, S. P. Armes, R. A. Williams and S. Biggs, *Responsive Core−Shell Latex Particles as Colloidosome Microcapsule Membranes*, *Langmuir*, **2010**, *26*, 18408-18414.
103. O. J. Cayre, J. Hitchcock, M. S. Manga, S. Fincham, A. Simoes, R. A. Williams and S. Biggs, *Ph-Responsive Colloidosomes and Their Use for Controlling Release*, *Soft Matter*, **2012**, *8*, 4717-4724.
104. P. H. R. Keen, N. K. H. Slater and A. F. Routh, *Encapsulation of Amylase in Colloidosomes*, *Langmuir*, **2014**, *30*, 1939-1948.
105. X. Wang, W. Zhou, J. Cao, W. Liu and S. Zhu, *Preparation of Core–Shell Caco3 Capsules Via Pickering Emulsion Templates*, *Journal of Colloid and Interface Science*, **2012**, *372*, 24-31.
106. Y. Zhao, Y. Li, D. E. Demco, X. Zhu and M. Möller, *Microencapsulation of Hydrophobic Liquids in Closed All-Silica Colloidosomes*, *Langmuir*, **2014**, *30*, 4253-4261.
107. M. Baillot, A. Bentaleb, E. Laurichesse, V. Schmitt and R. Backov, *Triggering the Mechanical Release of Mineralized Pickering Emulsion-Based Capsules*, *Langmuir*, **2016**, *32*, 3880-3889.
108. A. San Miguel, J. Scrimgeour, J. E. Curtis and S. H. Behrens, *Smart Colloidosomes with a Dissolution Trigger*, *Soft Matter*, **2010**, *6*, 3163-3166.
109. J. S. Sander and A. R. Studart, *Nanoparticle-Filled Complex Colloidosomes for Tunable Cargo Release*, *Langmuir*, **2013**, *29*, 15168-15173.
110. S. Zhou, J. Fan, S. S. Datta, M. Guo, X. Guo and D. A. Weitz, *Thermally Switched Release from Nanoparticle Colloidosomes*, *Advanced Functional Materials*, **2013**, *23*, 5925-5929.
111. J. Čejková, J. Hanuš and F. Štěpánek, *Investigation of Internal Microstructure and Thermo-Responsive Properties of Composite Pnipam/Silica Microcapsules*, *Journal of Colloid and Interface Science*, **2010**, *346*, 352-360.
112. Y. Zhu, J. Jiang, K. Liu, Z. Cui and B. P. Binks, *Switchable Pickering Emulsions Stabilized by Silica Nanoparticles Hydrophobized in Situ with a Conventional Cationic Surfactant*, *Langmuir*, **2015**, *31*, 3301-3307.
113. E. M. Shchukina, M. Graham, Z. Zheng and D. G. Shchukin, *Nanoencapsulation of Phase Change Materials for Advanced Thermal Energy Storage Systems*, *Chemical Society Reviews*, **2018**, *47*, 4156-4175.
114. D. Avnir, D. Levy and R. Reisfeld, *The Nature of the Silica Cage as Reflected by Spectral Changes and Enhanced Photostability of Trapped Rhodamine 6g*, *The Journal of Physical Chemistry*, **1984**, *88*, 5956-5959.
115. M. A. Ashraf, A. M. Khan, M. Ahmad and M. Sarfraz, *Effectiveness of Silica Based Sol-Gel Microencapsulation Method for Odorants and Flavors Leading to Sustainable Environment*, *Frontiers in chemistry*, **2015**, *3*, 42-42.

116. K. Bean, C. F. Black, N. Govan, P. Reynolds and M. R. Sambrook, *Preparation of Aqueous Core/Silica Shell Microcapsules*, *Journal of Colloid and Interface Science*, **2012**, *366*, 16-22.
117. R. Ciriminna, M. Sciortino, G. Alonzo, A. d. Schrijver and M. Pagliaro, *From Molecules to Systems: Sol–Gel Microencapsulation in Silica-Based Materials*, *Chemical Reviews*, **2011**, *111*, 765-789.
118. B. Y. Ahn, S. I. Seok and I. C. Baek, *Sol–Gel Microencapsulation of Hydrophilic Active Compounds from the Modified Silicon Alkoxides: The Control of Pore and Particle Size*, *Materials Science and Engineering: C*, **2008**, *28*, 1183-1188.
119. C. Barbé, J. Bartlett, L. Kong, K. Finnie, H. Q. Lin, M. Larkin, S. Calleja, A. Bush and G. Calleja, *Silica Particles: A Novel Drug-Delivery System*, *Advanced Materials*, **2004**, *16*, 1959-1966.
120. K. S. Finnie, J. R. Bartlett, C. J. A. Barbé and L. Kong, *Formation of Silica Nanoparticles in Microemulsions*, *Langmuir*, **2007**, *23*, 3017-3024.
121. H. Zhang, X. Wang and D. Wu, *Silica Encapsulation of N-Octadecane Via Sol–Gel Process: A Novel Microencapsulated Phase-Change Material with Enhanced Thermal Conductivity and Performance*, *Journal of Colloid and Interface Science*, **2010**, *343*, 246-255.
122. P. Corell Escuin, A. García-Bennett, J. V. Ros-Lis, A. Argüelles Foix and A. Andrés, *Application of Mesoporous Silica Materials for the Immobilization of Polyphenol Oxidase*, *Food Chemistry*, **2017**, *217*, 360-363.
123. R. Ciriminna and M. Pagliaro, *Sol–Gel Microencapsulation of Odorants and Flavors: Opening the Route to Sustainable Fragrances and Aromas*, *Chemical Society Reviews*, **2013**, *42*, 9243-9250.
124. a. US Food and Drug Administration GRAS Substances (SCOGS) Database—Select Committee on GRAS Substances (SCOGS) Opinion: Silicates. [(accessed on 1/12/2019)]; Available: https://www.fda.gov/food/ingredientspackaginglabeling/gras/scogs/ucm260849.htm.
b.M. Younes *et al*.- EFSA Panel on Food Additives and Nutrient Sources added to Food. *Scientific Opinion on the re-evaluation of silicon dioxide (E 551) as a food additive*. EFSA Journal 2018;16(1):5088, 70 pp.
125. M. Nogami and Y. Moriya, *Glass Formation through Hydrolysis of Si(Oc2h5)4 with Nh4oh and Hcl Solution*, *Journal of Non-Crystalline Solids*, **1980**, *37*, 191-201.
126. Z. Jianing and R. Hans, *Sol–Gel Science, the Physics and Chemistry of Sol–Gel Processing, Ed. By C. J. Brinker and G. W. Scherer, Academic Press, Boston 1990, Xiv, 908 Pp., Bound—Isbn 0-12-134970-5*, *Advanced Materials*, **1991**, *3*, 522-522.
127. in *The Sol-Gel Handbook*.
128. C. J. Brinker, *Hydrolysis and Condensation of Silicates: Effects on Structure*, *Journal of Non-Crystalline Solids*, **1988**, *100*, 31-50.
129. B. Topuz and M. Çiftçioğlu, *Preparation of Particulate/Polymeric Sol–Gel Derived Microporous Silica Membranes and Determination of Their Gas Permeation Properties*, *Journal of Membrane Science*, **2010**, *350*, 42-52.
130. D. Levy and M. Zayat, *The Sol-Gel Handbook: Synthesis, Characterization, and Applications*, Wiley, **2015**.

131. D. Wang and G. P. Bierwagen, *Sol–Gel Coatings on Metals for Corrosion Protection*, *Progress in Organic Coatings*, **2009**, *64*, 327-338.
132. C.-L. Chiang, C.-C. M. Ma, D.-L. Wu and H.-C. Kuan, *Preparation, Characterization, and Properties of Novolac-Type Phenolic/Sio2 Hybrid Organic–Inorganic Nanocomposite Materials by Sol–Gel Method*, *Journal of Polymer Science Part A: Polymer Chemistry*, **2003**, *41*, 905-913.
133. M. A. Fardad, *Catalysts and the Structure of Sio2 Sol-Gel Films*, *Journal of Materials Science*, **2000**, *35*, 1835-1841.
134. M. W. Colby, A. Osaka and J. D. Mackenzie, *Temperature Dependence of the Gelation of Silicon Alkoxides*, *Journal of Non-Crystalline Solids*, **1988**, *99*, 129-139.
135. M. W. Colby, A. Osaka and J. D. Mackenzie, *Effects of Temperature on Formation of Silica Gel*, *Journal of Non-Crystalline Solids*, **1986**, *82*, 37-41.
136. O. K. Filho and M. A. Aegerter, *Rheology of the Gelation Process of Silica Gel*, *Journal of Non-Crystalline Solids*, **1988**, *105*, 191-197.
137. D. Avnir, *Organic Chemistry within Ceramic Matrixes: Doped Sol-Gel Materials*, *Accounts of Chemical Research*, **1995**, *28*, 328-334.
138. T. Yamamoto, Nakato Laboratory, **1987**
139. S. Radin, T. Chen and P. Ducheyne, *The Controlled Release of Drugs from Emulsified, Sol Gel Processed Silica Microspheres*, *Biomaterials*, **2009**, *30*, 850-858.
140. S. P. Meaney, R. F. Tabor and B. Follink, *Synthesis and Characterisation of Robust Emulsion-Templated Silica Microcapsules*, *Journal of Colloid and Interface Science*, **2017**, *505*, 664-672.
141. C. I. Zoldesi and A. Imhof, *Synthesis of Monodisperse Colloidal Spheres, Capsules, and Microballoons by Emulsion Templating*, *Advanced Materials*, **2005**, *17*, 924-928.
142. M. O'Sullivan, Z. Zhang and B. Vincent, *Silica-Shell/Oil-Core Microcapsules with Controlled Shell Thickness and Their Breakage Stress*, *Langmuir*, **2009**, *25*, 7962-7966.
143. J.-H. Park, C. Oh, S.-I. Shin, S.-K. Moon and S.-G. Oh, *Preparation of Hollow Silica Microspheres in W/O Emulsions with Polymers*, *Journal of Colloid and Interface Science*, **2003**, *266*, 107-114.
144. Panel on Food Contact Materials, Enzymes, Flavourings and Processing Aids *Scientifict Opinion on the safety assessment of the substances tetraethyl orthosilicate, CAS No. 78-10-4, and hexamethyldisilazane, CAS No. 99-97-3, for use in food contact materials.* (available: http://www.efsa.europa.eu/en/efsajournal/pub/4337) Acessed 1/12/2019
145. Z. Teng, Y. Han, J. Li, F. Yan and W. Yang, *Preparation of Hollow Mesoporous Silica Spheres by a Sol–Gel/Emulsion Approach*, *Microporous and Mesoporous Materials*, **2010**, *127*, 67-72.
146. C. J. Brinker, W. D. Drotning and G. W. Scherer, *A Comparison between the Densification Kinetics of Colloidal and Polymeric Silica Gels*, *MRS Proceedings*, **1984**, *32*, 25.
147. H. Jiang, L. Hong, Y. Li and T. Ngai, *All-Silica Submicrometer Colloidosomes for Cargo Protection and Tunable Release*, *Angewandte Chemie International Edition*, **2018**, *57*, 11662-11666.
148. H. Wang, X. Zhu, L. Tsarkova, A. Pich and M. Möller, *All-Silica Colloidosomes with a Particle-Bilayer Shell*, *ACS Nano*, **2011**, *5*, 3937-3942.

149. T. Coradin, N. Nassif and J. Livage, *Silica–Alginate Composites for Microencapsulation*, *Applied Microbiology and Biotechnology*, **2003**, *61*, 429-434.
150. P. E. G Dardelle, Firmenich Sa, *Core-Shell Capsules,* **2011**
151. H.-Y. Kang and H.-H. Chen, *Preparation of Thermally Stable Microcapsules with a Chitosan–Silica Hybrid*, *Journal of Food Science*, **2014**, *79*, E1713-E1721.
152. K. Zhang, W. Wu, K. Guo, J. Chen and P. Zhang, *Synthesis of Temperature-Responsive Poly(N-Isopropyl Acrylamide)/Poly(Methyl Methacrylate)/Silica Hybrid Capsules from Inverse Pickering Emulsion Polymerization and Their Application in Controlled Drug Release*, *Langmuir*, **2010**, *26*, 7971-7980.
153. M. Boissière, P. J. Meadows, R. Brayner, C. Hélary, J. Livage and T. Coradin, *Turning Biopolymer Particles into Hybrid Capsules: The Example of Silica/Alginate Nanocomposites*, *Journal of Materials Chemistry*, **2006**, *16*, 1178-1182.
154. J.-Y. Wang, H.-R. Yu, R. Xie, X.-J. Ju, Y.-L. Yu, L.-Y. Chu and Z. Zhang, *Alginate/Protamine/Silica Hybrid Capsules with Ultrathin Membranes for Laccase Immobilization*, *AIChE Journal*, **2013**, *59*, 380-389.
155. S. Simovic, P. Heard, H. Hui, Y. Song, F. Peddie, A. K. Davey, A. Lewis, T. Rades and C. A. Prestidge, *Dry Hybrid Lipid–Silica Microcapsules Engineered from Submicron Lipid Droplets and Nanoparticles as a Novel Delivery System for Poorly Soluble Drugs*, *Molecular Pharmaceutics*, **2009**, *6*, 861-872.
156. B. Mahltig, H. Haufe and H. Böttcher, *Functionalisation of Textiles by Inorganic Sol–Gel Coatings*, *Journal of Materials Chemistry*, **2005**, *15*, 4385-4398.
157. Z. Xiao, M. Liu, Y. Niu, G. Zhu, J. Deng and S. Liu, *Lavender Fragrance Sol-Gel Encapsulated in Ormosil Nanospheres*, *Flavour and Fragrance Journal*, **2019**, *34*, 21-27.

CHAPTER 2. Materials and Methods

Abstract

This chapter introduces the chemicals, equipment and methods used throughout the PhD project. It is divided in four sections:

1. The first section concerns the chemicals, including the perfume oil and Pickering emulsifier used.
2. The second section describes the technique to produce the Pickering emulsions and the various emulsification methods used in this project.
3. The third section describes the equipment used for capsule characterisation.
4. The final section concerns the methods used in the industry to evaluate the stability and performance of perfume microcapsules (PMCs) in real-world consumer products.

2.1 Chemicals

Perfume oil and isopropyl myristate (IPM) were kindly provided by Procter and Gamble Brussels Innovation Centre. Hexyl salicylate (HS), acetic anhydride, titanium trimethylsilane (TETRAKIS), difluoro[2-[1-(3,5-dimethyl-2H-pyrrol-2-ylidene-N)ethyl]-3,5-dimethyl-1H-pyrrolato-N]boron (PM546 – fluorescent dye) and Allura red dye (AR) were supplied by Sigma-Aldrich, UK. Tetraethoxysilane (TEOS) and absolute ethanol were supplied by VWR, UK. Fumed silica nanoparticles (SiO_2 NPs) - Aerosil 300 (A300) and Aerosil R816 were supplied by Evonik Industries. All Chemicals were used as received without further purification.

References to this Chapter on pages 89-90

2.1.1 Perfume oil

The perfume oil provided by P&G is a mixture of 13 different components, which includes aldehydes, esters, alcohols and hydrocarbons. The composition was not disclosed by P&G so the perfume activity and perfume leakage experiments were done at the company where the characterization methods are already established for the encapsulated perfume composition. These methods will be described and discussed later in Section 2.5.

A fluorescent dye (PM546, excitation and emission 493 nm and 504 nm, respectively - **Figure 2-1**) was dissolved in the oil that was to be encapsulated, in order to follow the oil encapsulation process. The level of dye used was kept at 0.1 wt% to the oil phase for all experiments throughout the project.

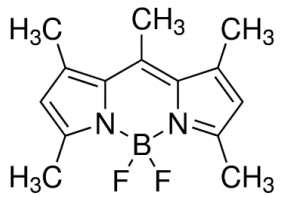

***Figure 2-1**. PM546 structure.*

2.1.2 Aerosil 300 fumed silica (A300)

Commercial silica nanoparticles (SiO_2 NPs) were selected for this project due to low cost and commercial availability. For industrial applications, these features are essential, as the availability and cost of raw materials are key points when it comes to bring a new technology to the market.

The fumed silica particles used (A300) were produced by pyrolysis of silicon tetrachloride in an oxygen-hydrogen flame at high temperature (> 1500°C),[1] according to **Equation 2-1**. In the

References to this Chapter on pages 89-90

flame process, molecules of SiO_2 collide and coalesce to form smooth and approximately spherical primary nanoparticles 10 - 20 nm in diameter. These primary nanoparticles collide and fuse at lower temperatures to form stable aggregates of 100 - 200 nm in diameter that can further agglomerate when at rest (**Figure 2-2A**).[2]

$$SiCl_4 + 2H_2 + O_2 \rightarrow SiO_2 + 4HCl \qquad \textbf{\textit{Equation 2-1}}$$

The resulting fumed silica nanoparticles are amorphous and possess a surface area of 300 m^2 g^{-1}. The surface of these particles is covered by silanol groups (SiOH), which provide a hydrophilic character to the nanoparticles so they are easily dispersed in aqueous solutions.[3] **Figure 2-2B** shows a TEM image of the A300 nanoparticles used throughout the project. In terms of porosity, A300 possess pore volume of 0.56 (cm^3g^{-1}). Full characterisation of Aerosil silica particles can be found in the Evonik webpage (www.aerosil.com).

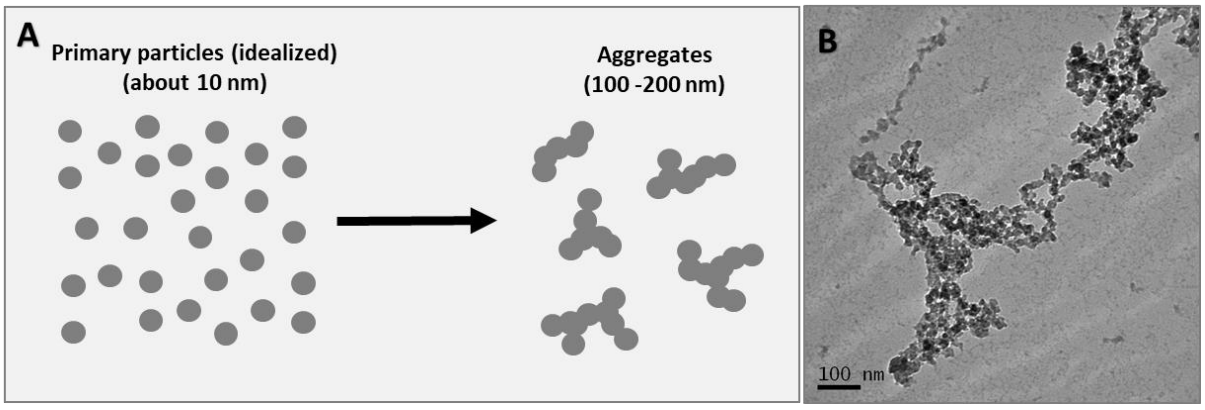

***Figure 2-2**. (A) Scheme representing the aggregation of the primary particles during the synthesis of fumed silica and (B) TEM micrograph of the Aerosil 300 nanoparticles as received by Evonik. Scale bar: 100 nm.*

References to this Chapter on pages 89-90

2.2 Pickering emulsion preparation

Two homogenisers were used to prepare Pickering emulsions throughout the project, based at the University of Birmingham and Proctor and Gamble Brussels Innovation Centre.

At the University of Birmingham (UoB):

- Stuart Vortex mixer SA8 – variable speed (Boibby Stelin LTD – UK) operating at 2500 RPM for 5 minutes.

The Vortex was selected for the first studies due to its ability to mix millilitre volumes of liquids. It consists of an electric motor attached to a rubber cup that oscillates rapidly in a circular motion. As the vial is pressed to the top of the rubber cup, the motion is transferred to the mixture inside the vial generating a vortex and leading to emulsification of the mixture. The main limitation of using the vortex mixer is that the maximum speed for this equipment is 2500 RPM, which limits the droplet size range formed during emulsification.

At Procter and Gamble (P&G):

- IKA Ultra-Turrax T25 basic homogeniser (IKA-Werke GmbH & Co – Germany) equipped with a dispersing head of 10- or 25-mm diameter operating at 8500 RPM for 5 minutes (standard speed for perfume emulsification at the company).

The Ultra-Turrax consists of rotor within a stationary stator (dispersion head). The rotor is attached to an electric motor that provides high circumferential speed; the liquid is drawn axially into the dispersing head and then forced radially through the voids in the motor-stator arrangement, providing strong shear forces to form the emulsion (**Figure 2-3**). The operation

References to this Chapter on pages 89-90

volume varies between 1 to 2000 mL depending on the dispersing head used and it can operate in a wide range of speeds (3000 – 25000 RPM).

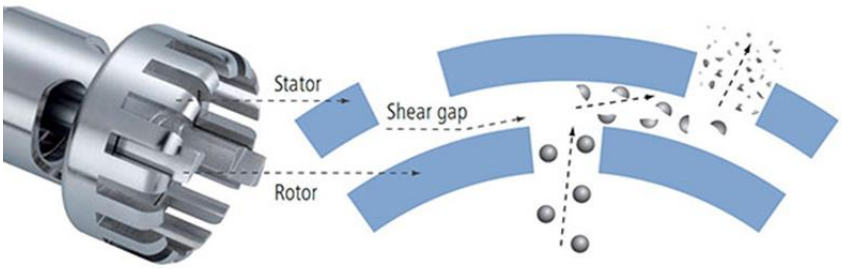

***Figure 2-3**. Ultra-turrax main components. Images from IKA website (https://www.ika.com/laboratory-equipment/products/dispersers/products/2098/t-25-digital-ultra-turrax)*

2.3 Capsule characterization techniques

Capsules and materials were characterized using facilities in both UoB and P&G.

(i) *Mean size and size distribution* of capsules and emulsions were characterised by laser diffraction.

(ii) *Capsule morphology, structure and shell thickness* were characterized using optical microscopy, SEM and TEM.

(iii) *Mechanical properties* were studied by micromanipulation *via* compression of single capsules to rupture.

(iv) *Encapsulation efficiency and leakage* were characterized using UV/visible spectrometry.

Details of each technique are presented in this section.

References to this Chapter on pages 89-90

2.3.1 Laser diffraction particle sizing

Laser diffraction technique is a non-destructive method well-established in industry to obtain the size distribution of particles and emulsion droplets. It uses the principles of static light scattering (SLS) and the Mie theory of light to calculate the size of the particles present.[4]

The laser diffraction technique is based on the principle that particles interacting with a laser beam leads to light being *diffracted*, *refracted*, *reflected* or *absorbed*, which will result in characteristic scattering of light that is directly related to particle size (**Figure 2-4**).[5] A wide range of scattered light angles and intensities are measured by detectors positioned around the sample in order to obtain the sample's size distribution curve.

The particle size is directly related to the light scattering angle and intensity; as the particle size increases, the scattering angle decreases logarithmically[5] and the intensity of the light increases[6]. When the particles are considerably bigger than the light wavelength, diffraction will be the main source of light, hence the name of the technique.

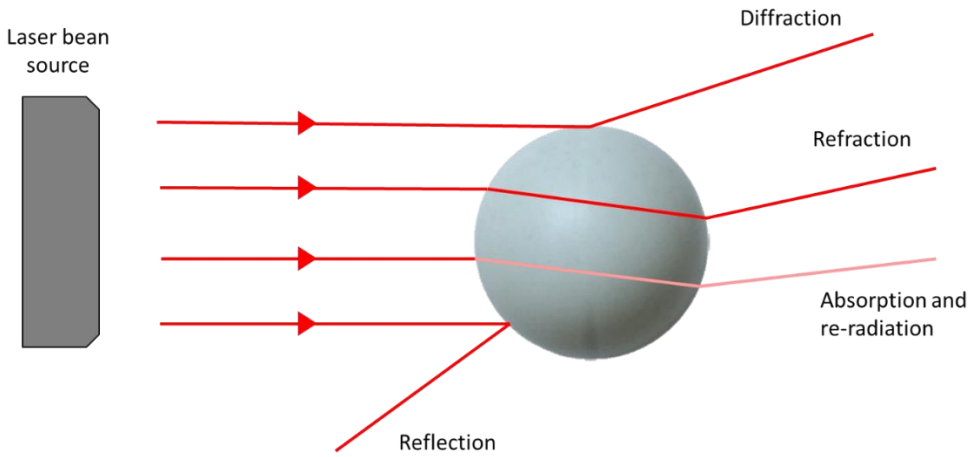

***Figure 2-4**. Scheme representing the possible light interactions with the particle: the light can suffer diffraction, refraction, absorption and re-radiation, and reflection, which will result in a*

References to this Chapter on pages 89-90

characteristic light scattering pattern for the particle. The information is collected by detectors and the particles size calculated using the Mie theory.

A typical laser diffraction apparatus is represented by **Figure 2-5.** The apparatus operates with a laser source with a fixed wavelength, which is focused before reaching the sample. Some techniques use two different light sources, usually red and blue, for the measurement of particles of different sizes. The sample is homogenised using a dispersion unit to ensure that a constant stream of particles is passing thought the laser beam. As the laser passes through the sample and interacts with the particles as shown in **Figure 2-4**, the light is scattered, and an array of detectors can measure scattered light in a wide range of angles. Some apparatus also includes backscatter detectors, enabling the detection of particles as small as 20 nm.

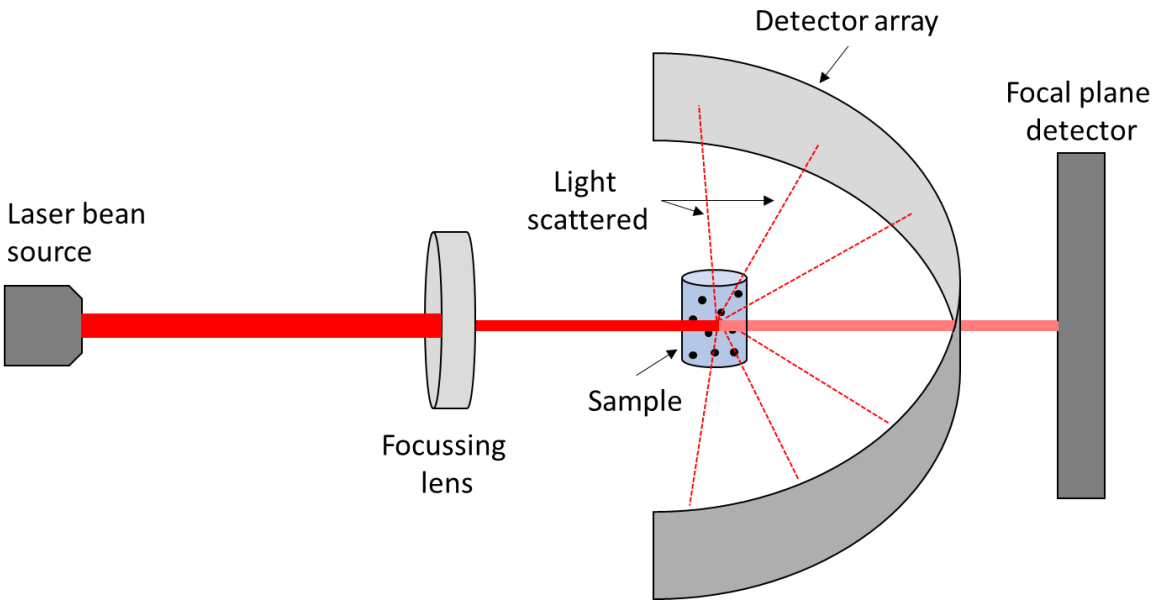

***Figure 2-5**. Scheme representing a laser diffraction optical system. The single-wavelength light originates from the laser beam source and interacts with the particles in the dispersing unit. The scattered light is detected and calculated by an array of detectors and the patters calculated using the Mie theory.*

References to this Chapter on pages 89-90

For this project, a Mastersizer 2000 instrument (Malvern Instruments Ltd, Malvern - UK) was used. The instrument measures the volume fraction of the capsules in different size bands in the size range of 20 nm to 2000 µm. The refractive index used was 1.46 (for amorphous silica[7]) and the data analysed using Excel®.

2.3.1.1 Particle size distribution

The particle size distributions are calculated by comparing the sample's scattering pattern with the Mie Theory using a mathematical inversion process. The Mie Theory is based on Maxwell's electromagnet field equations and is capable of predicting scattering intensities for different types of particles using the following assumptions[8]:

- The particles being measured are homogeneous and spherical (for non-spherical particles the size is expressed in terms of spherical equivalent diameter based on volume).
- The refractive index of both the particles and dispersed phase are known.
- The suspension is dilute, to reduce the probability that scattered light undergoes secondary scattering by other particles in the dispersion.

An example of size distribution curve for microcapsules can be found in **Figure 2-6.** Laser diffraction results are reported in terms of volume, so the mean diameter over volume (D[4,3]) was used to define the size distribution of the capsules. The volume moment mean (De Brouckere Mean Diameter) is relevant for many samples as it reflects the size of those particles which constitute the bulk of the sample volume.[9] It is most sensitive to the presence of large particulates in the size distribution. **Equation 2-2** below defines the volume moment mean. It is interesting to note that although both **A** and **B** curves have the same mean particle

References to this Chapter on pages 89-90

diameter, curve B shows a much narrow particle size distribution as the frequency is limited to smaller number of particle sizes.

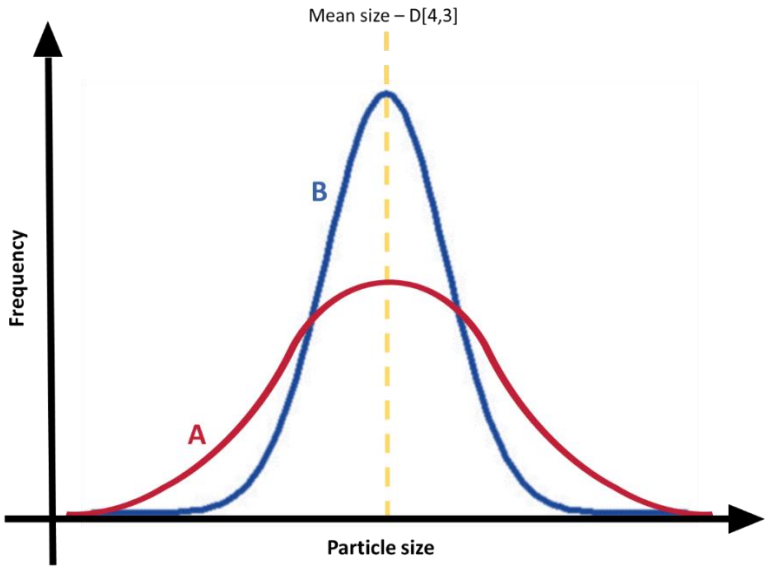

Figure 2-6. *Example of a symmetric size distribution curve obtained using the laser diffraction technique. The result is typically obtained in terms of volume frequency for different size channels. The mean size is defined as the mean diameter over volume D[4,3].*

$$D[4,3] = \frac{\sum_{i=1}^{N} d_i^4}{\sum_{i=1}^{i=N} d_i^3}$$ ***Equation 2-2***[9]

where, D_i is the geometric mean: the square root of upper x lower capsule diameters for each size channel measured along with its percentage and N is the total number of capsules tested: For the numerator the geometric D_i is taken to the fourth power multiplied by the percent in that channel, summed over all channels. For the denominator the geometric *D* taken to the third power multiplied by the percent in that channel, summed over all channels.[9]

One of the common values used to define size distribution of a sample in laser diffraction is the SPAN, which describes the distribution width and is given by **Equation 2-3**. The lower the

References to this Chapter on pages 89-90

SPAN value, the more narrowly distributed the sample is in terms of size. In the case of the example in **Figure 2-6**, Curve B has a smaller SPAN value than curve A.

$$SPAN = \frac{D[0.9]-D[0.1]}{D[0.5]}$$ ***Equation 2-3***

where, D[0.9], D[0.1] and D[0.5] represent the cumulative particle diameter that falls below 90, 10 and 50% of the total population, respectively (**Figure 2-7**).

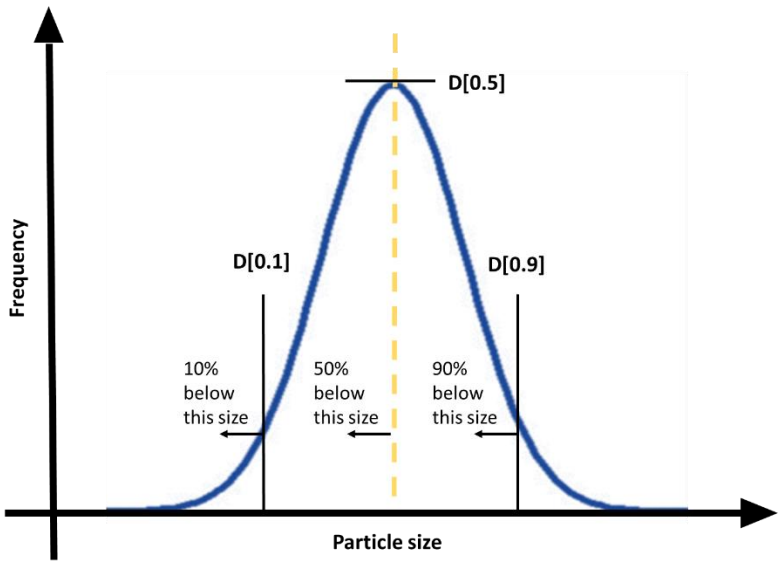

Figure 2-7. *Schematic representation of D[0.1], D[0.5] and D[0.9] for SPAN calculation. D[0.5] is defined as the diameter where half the population lies below this value. In the same way, 90% of the distribution lies below D[0.9] and 10% below D[0.1].*

2.3.2 Optical microscopy

Optical microscopy is a powerful tool to assess emulsion stability and capsule formation. An optical microscope uses visible light combined with a series of lenses to magnify objects. Usually, the resolution limit of optical microscopes is 200 nm due to the light wavelength.[10] This type of microscope can also be equipped with special light sources such as UV which is a

References to this Chapter on pages 89-90

powerful tool to observe different components in a sample when one or more are marked with a fluorescent probe.

For the formation of an image using an optical microscope two components are indispensable: the objective lens, which collects light and forms an image and the condenser lens, which focuses the light in a small section of the sample.[10] The diagram found in **Figure 2-8** shows the main components of a typical optical microscope: visible light is irradiated by a source and focused by the condenser lens before reaching the glass slide containing the sample. The image of the specimen is magnified by the objective lenses and with the help of the projection lens the operator can observe the magnified image using the eye piece.[11]

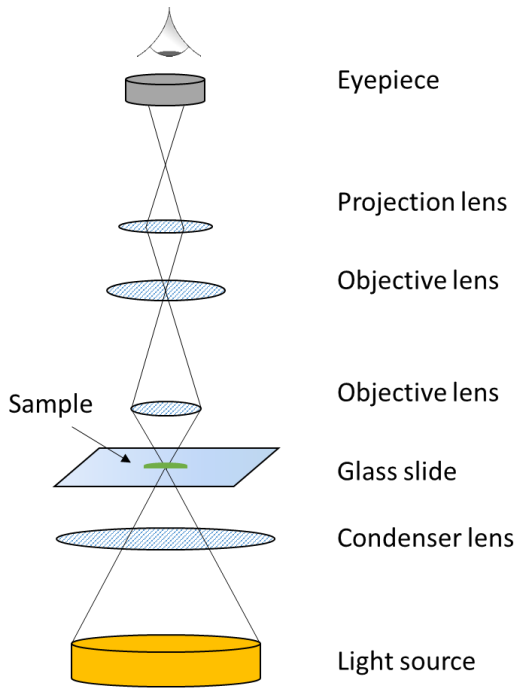

Figure 2-8. *Diagram representing the different components found in an optical microscope.*

At the University of Birmingham, an optical microscope (Leica DMRBE, Leica Microscope & Systems GmbH) equipped with a software package Moticam Pro 3.0 was used. In addition, a

References to this Chapter on pages 89-90

CoolLED pE-300 white light source was attached to the microscope to observe capsules and emulsions filled with the fluorescence dye. The resolution of the microscope was 200 nm.

When the research was undertaken in P&G, the microscope used was a Zeiss Axio imager 2 pol (Carl Zeiss Microscopy – Germany, resolution 200 nm) also equipped with a UV light source (Kubler codex HXP 120C).

2.3.3 Scanning electron microscopy (SEM)

Scanning electron microscopy is a useful tool for the study of surfaces, giving great insight about the structure and morphology of capsules, as well as the shell thickness.

Figure 2-9 presents a scheme representing the key components of a scanning electron microscope, which are: source of electrons, condenser and object lenses. First, a sample is placed in the sample holder; the sample can be coated with a nano-scaled layer of platinum or gold to improve contrast and the signal-to-noise ratio.[12] The sample is then submitted to a high vacuum inside the microscope chamber, before being irradiated with a high-energy electron beam. The electrons are accelerated downwards passing through the lenses that make the beam focused allowing the sample to be scanned by moving the deflection coils.[13]

References to this Chapter on pages 89-90

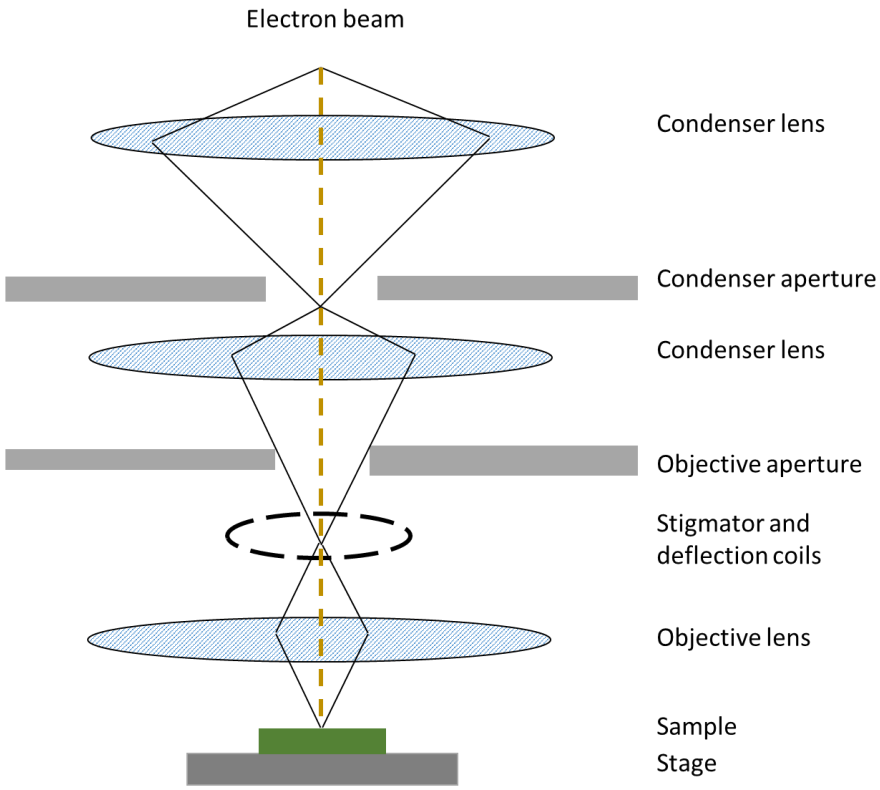

***Figure 2-9**. Schematic representation of the key components of a scanning electron microscope.*

The interaction between the beam and sample surface generates a series of signals that can be detected by the backscattered electron detector (**Figure 2-10**), X-rays and secondary electrons are also ejected from the sample. Secondary electrons have much lower energy when compared to backscattered electrons and can be used for topographic imaging as they are close to the surface. The difference in contrast of SEM images is due to the different atomic number of the elements present on the surface of the sample. Higher atomic number elements produce brighter images.[14]

References to this Chapter on pages 89-90

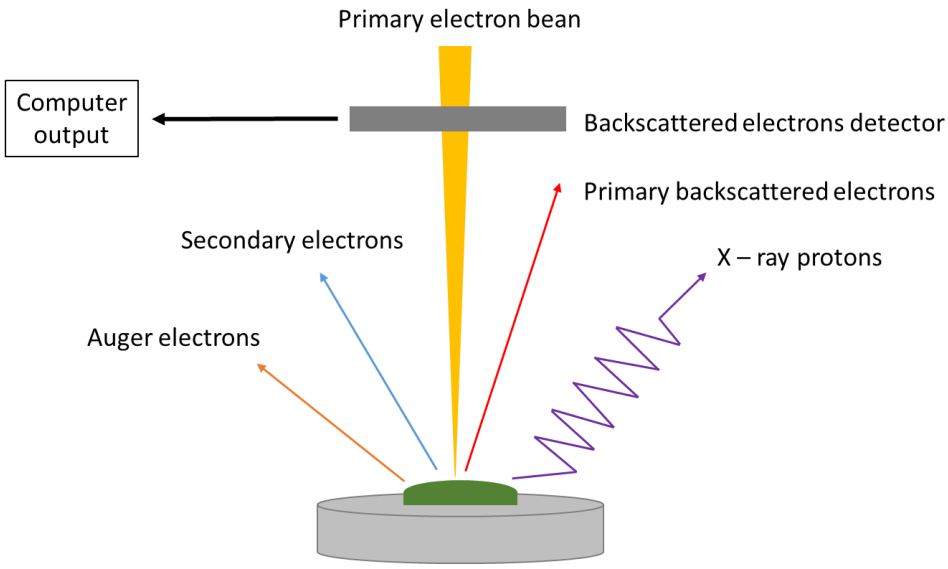

***Figure 2-10**. Scheme representing the interactions between the high-energy electron beam and the sample surface. As the beam reaches the sample surface, X-ray protons, Auger electrons, secondary electrons and primary electrons are emitted. Primary electrons are detected, and the patterns transmitted to a computer output.*

The main advantages of using SEM is that the equipment can be connected to a wide range of detectors, providing valuable information about the sample, such as surface structure and morphology. In contrast, SEM is usually a more expensive and time-consuming technique relatively to optical microscopy. Another limitation is the necessity to operate under high vacuum, so the sample must be mechanical stable and dry. Typical SEM images are represented in **Figure 2-11**.

Two different SEM types are used in this PhD project.

1. At P&G a TM-1000 Tabletop Microscope (Hitachi, Ltd – Japan), magnification 1500X.

References to this Chapter on pages 89-90

2. at UoB a Philips XL-30 FEG Environmental SEM with Oxford Inca EDS (Philips UK ltd, Guildford – UK), magnification 3500X.

When preparing the sample, a drop of water containing the microcapsules was allowed to dry on the surface of a mount containing a carbon impregnated self-adhesive disc. For shell thickness characterisation, a razor blade was used to break the capsules prior to placing the sample holder in the SEM vacuum chamber. **Figure 2-11** shows examples of images obtained using the tabletop SEM at P&G (A) and the SEM used at UoB (B).

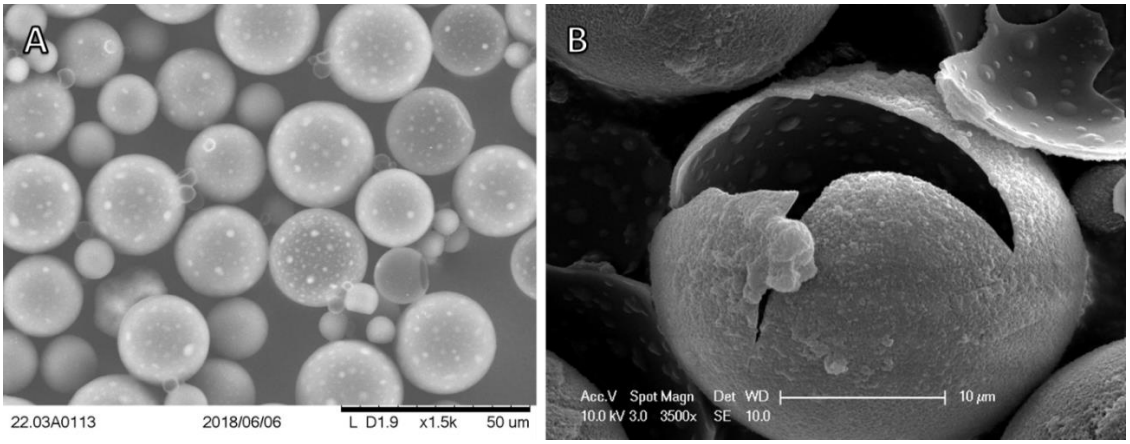

***Figure 2-11**. SEM micrographs of the same capsule sample produced in this project. (A) was obtained using the TM – 1000 tabletop microscope at P&G (1500x magnification - scale bar: 50 µm) and (B) using the Philips XL-30 FEG Environmental SEM at UoB (3500x magnification scale bar: 10 µm).*

2.3.4 Transmission electron microscopy (TEM)

A transmission electron microscope (TEM) works in a similar way as a slide projector: the electron gun produces a monochromatic electron stream, which is transmitted through the sample, projecting onto the viewing screen an enlarged image of the specimen.[15]

References to this Chapter on pages 89-90

A typical TEM layout is shown in **Figure 2-12.** The electron gun produces an electron beam, which passes through a pair of condenser lenses that determine the spot size and brightness. A condenser aperture then restricts the beam before it strikes the sample. At this point, part of the beam will be transmitted and focused by the objective lens into an image; the other part will be deflected.

The image generated by the objective lens passes through intermediate and projector lenses to be enlarged when it reaches a fluorescent screen, generating light and allowing the user to view the image through the viewing window. Areas where fewer electrons are transmitted appear darker and the opposite is observed for light areas. Information about the structure of the sample in terms of density and thickness can thus be extracted.[16]

As the wavelength of electrons are about 1 nm, the resolution attainable for TEM is much higher than that for optical microscopy, which uses visible light as source of radiation (wavelength of approximately 400 - 700 nm). The resolution observed for TEM is about 0.5 nm which is 400 times smaller than for an optical microscope (200 nm).[17]

References to this Chapter on pages 89-90

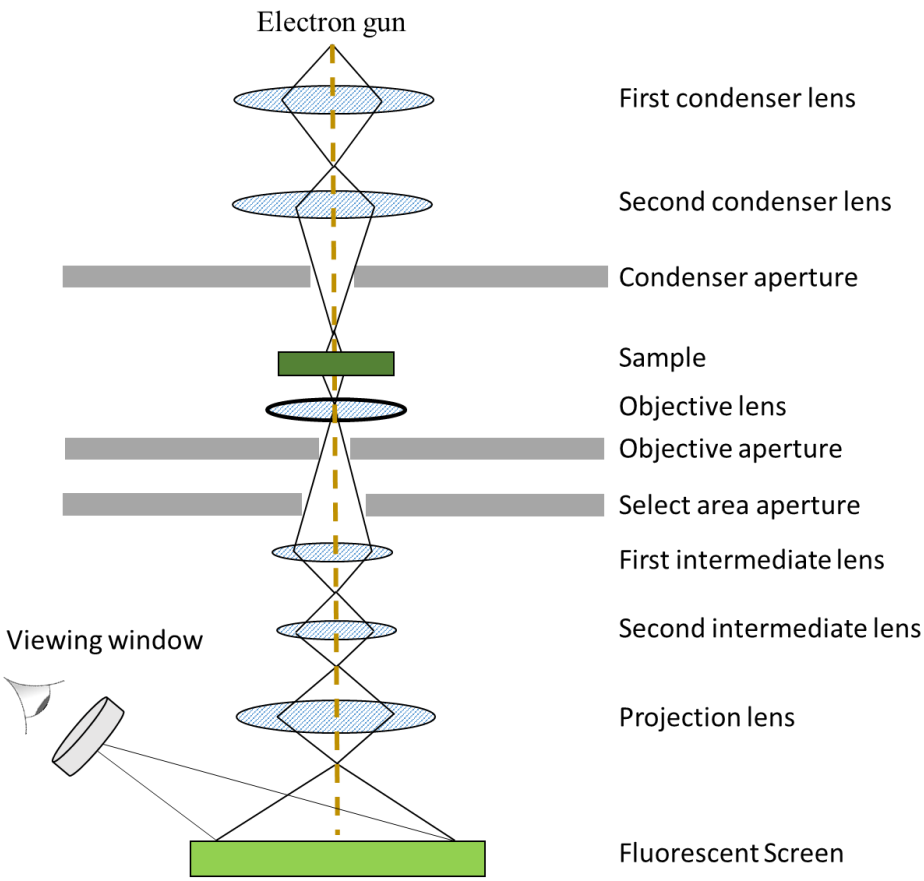

***Figure 2-12**. Scheme representing the key components of a transmission electron microscope.*

For this project, TEM images were obtained using a Jeol 1200EX TEM (Jeol Ltd., Welwyn Garden City, UK). The sample aqueous dispersion was diluted 500x in DI water and a drop was placed onto a copper/carbon 200 mash grid and left to settle for 5 minutes before the excess of water was removed. The mash was then allowed to air dry and placed in the TEM chamber.

2.3.5 Micromanipulation technique

The micromanipulation technique is a well-established method to compress bacteria, animal and vegetable cells,[18-20] yeast,[21] and capsules[22, 23] between two parallel surfaces. The information obtained is valuable to understand the mechanical properties of micro-sized structures[22]. For this project, the technique was used to obtain the force versus displacement

References to this Chapter on pages 89-90

curves up to the rupture of individual capsules of known diameter, in order to compare mechanical properties as function of size, shell thickness and method of production.

A schematic diagram of the micromanipulation rig can be found in **Figure 2-13**. For this experiment, the capsules were first diluted 500x in DI water, then a drop of the diluted dispersion was added to a glass slide and left to air dry. The glass containing the capsules was then positioned on the micromanipulation rig stage equipped with an electronically controlled force transducer (Model 403A, Aurora Scientific Inc., Canada, with a maximum operation limit of 5 mN) with a glass probe attached, capable of measuring the rupture force and the deformation suffered by the capsule as a known force is applied.

The capsules are observed using the side view microscope connected to a camera and a monitor, this is to ensure that a single capsule is being compressed, and that the capsule is properly positioned under the glass probe prior to compression. The image obtained is also used to measure and record the size of the microcapsule. The probe travels down at 2 µm $s.^{1}$ The voltage data is obtained by the transducer and the data converted to force using an Excel® macro. The system measures the force with a precision to 0.1 µN and displacement to 0.2 µm.[23] At least 10 individual capsules were tested for statistical analysis.

References to this Chapter on pages 89-90

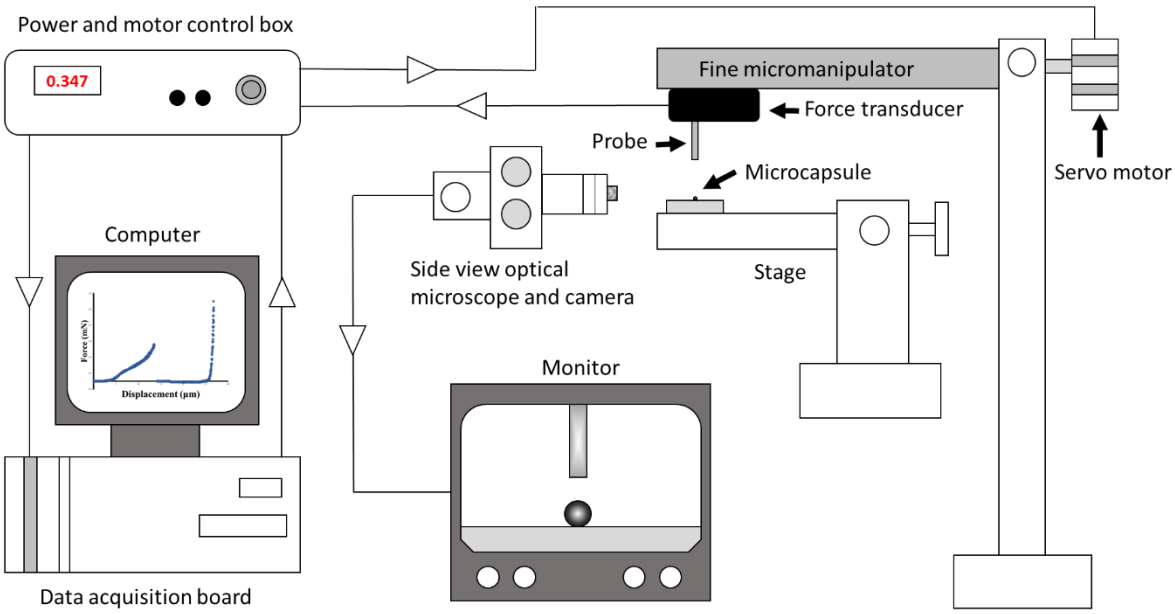

***Figure 2-13**. Schematic diagram of the micromanipulation rig (Adapted from[23])*

2.3.5.1 Preparation of Transducer Probes

A glass puller (Micro Forge, MF-900 Narishige, Japan) was used to heat and pull a borosilicate glass capillary with an inner diameter of 0.58 mm and outer diameter of 1.0 mm, to produce two glass needles. These needles were ground on their contact surface using a grinding machine (EG-40, Narishige, Japan) for 24 hours, to obtain a probe of the correct diameter and a flat surface. After grinding, the probe was fixed to a glass slide and observed under an optical microscope to measure the surface diameter and check if a flat surface was obtained (**Figure 2-14**). The probe was then attached to the force transducer using a commercial superglue (Loctite, UK) and allowed to dry for 24h.

References to this Chapter on pages 89-90

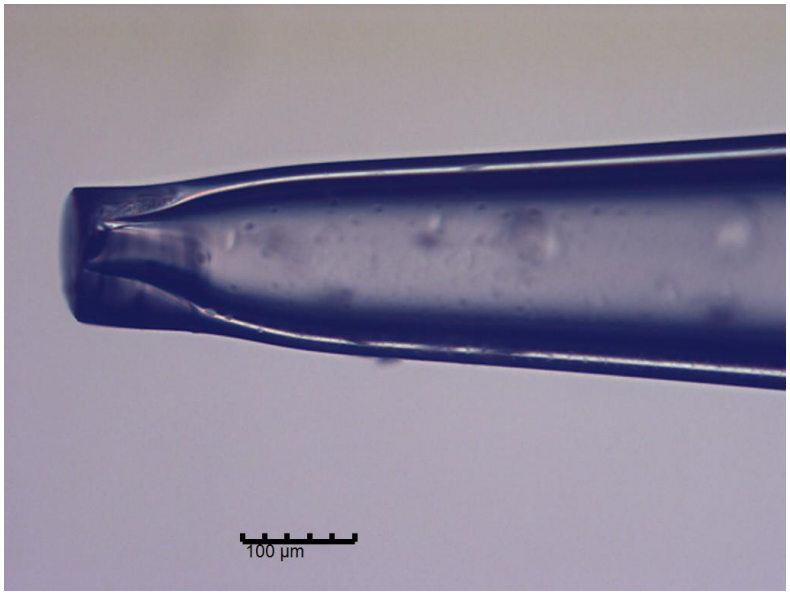

***Figure 2-14**. Optical microscopy micrograph of a glass probe prepared in our laboratory. The tip diameters is about 120 µm. Scale bar: 100 µm.*

To ensure that the capsule is compressed between two flat surfaces, the probe diameter should be at least twice the diameter of the microcapsules to be tested. The probes used in this project had a diameter between 50 to 150 µm.

2.3.5.2 Data obtained

Typical data obtained from the micromanipulation rig when compressing a single microcapsule is shown in **Figure 2-15** below. **A** corresponds to no contact between the particle and the probe – the probe is travelling in air prior to making contact with the microcapsule surface, so there is no force being measured. At point **B** the probe contacts the microcapsule and the force increases until point **C**, where the capsule suffers rupture – at this point the rupture force of the capsule is recorded. As the capsule is now ruptured there is no force applied to the probe so the force is back to the baseline as seen on point **D**. The probe continues to move down with no force registered until it begins to compress the capsule

References to this Chapter on pages 89-90

debris and the glass slide at point **E**, and the force increases rapidly as the probe pushes against the glass surface. The motor stops automatically when the force reaches a maximum to avoid breakage of the probe and transducer.

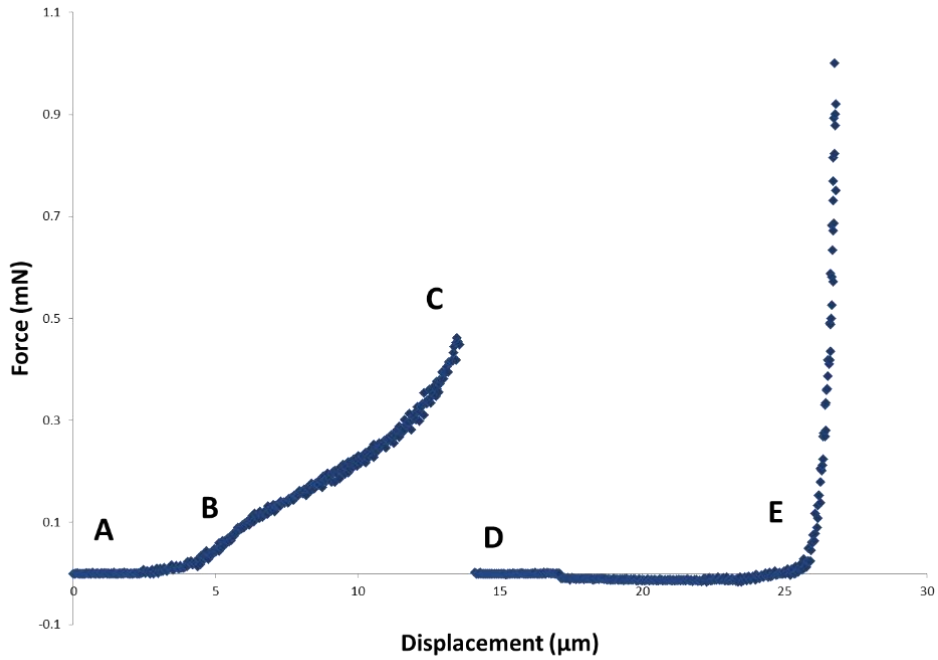

***Figure 2-15**. Typical Force vs. displacement graph obtained when compressing single capsules to rupture. A represents the baseline, B the first contact with the capsule when the force increases, at C the capsule is ruptured. At point D the probe begins to compress the capsule debris and E it reaches the glass slide.*

2.3.6 Ultraviolet-visible spectroscopy (UV-Vis)

Solution state Ultraviolet-Visible (UV-Vis) spectroscopy is a facile and convenient technique to obtain the concentration of organic compounds that contain a chromophore,[24] which makes use of the Beer-Lambert law[25] (**Equation 2-4**).

$$A = log\frac{I_0}{I_t} = \varepsilon lc$$ ***Equation 2-4***

References to this Chapter on pages 89-90

where, A is the sample absorbance, I_0 is the incident light intensity, I_t the transmitted light intensity, ε is the extinction coefficient (mL g^{-1} cm^{-1}), l is the optical path length (cm) and c the sample concentration (g mL^{-1}). The concentration of a compound in solution can then be obtained by measuring the absorbance of the unknown concentration using **Equation 2-4**, if the extinction coefficient ε is known for the compound.

In order to obtain an unknown concentration of a compound in solution a calibration curve of the compound λ_{max} absorbance versus known concentrations is required as shown in **Figure 2-16** for hexyl salicylate (HS), where the slope is proportional to the extinction coefficient ε (mL g^{-1} cm^{-1}).

For all UV-Vis measurement of HS, a binary miscible solvent mixture of 36% v/v propan-1-ol in water was used. This co-solvent mixture was used as suggested previously by Mercade-Prieto *et al.*[26] to increase the HS solubility in the continuous phase, enabling a direct measurement of HS absorbance.[26]

References to this Chapter on pages 89-90

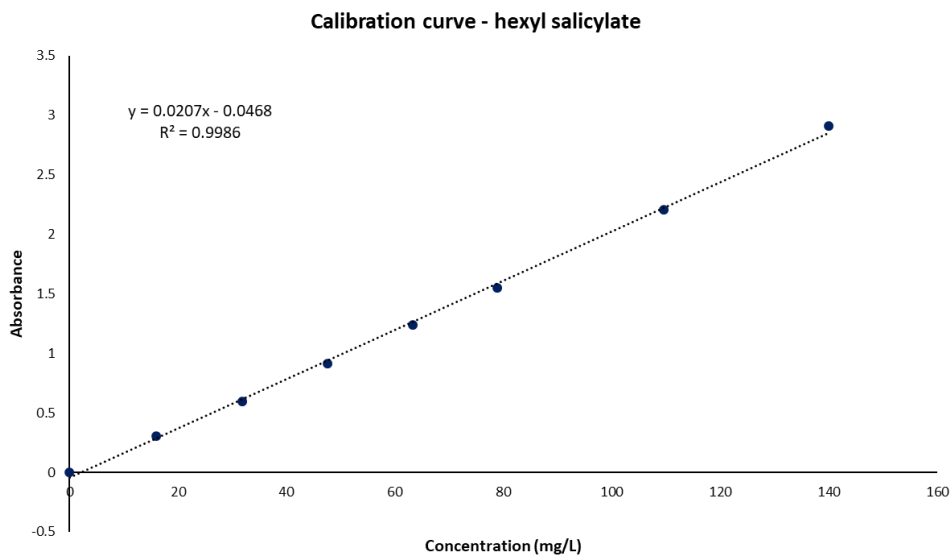

***Figure 2-16**. Calibration curve obtained at 305 nm for different levels of hexyl salicylate in 36% propan-1-ol aqueous solution. The data points represent the absorbance max (λmax) for each concentration (g mL-1). The linear fit obtained was y=0.0207x-0.0468.*

In this project, a UV-Vis spectrophotometer (Cecil Instruments, Cambridge, UK) was used to measure both the encapsulation efficiency and HS release from the microcapsules as a function of time. The absorbance was measured using quartz cuvettes with 3 mL volume capacity and 1 cm of optical path length.

2.3.6.1 Encapsulation Efficiency

The encapsulation efficiency was obtained using the calibration curve for HS and a UV-Vis spectrophotometer: a capsule sample was prepared containing a known HS mass. The capsules were then centrifuged at 2500 RPM per 10 min and the sediment (capsules) was redispersed in 36% propanol aqueous solution. Then, glass microbeads (50 µm in diameter) were added to the vial, which was put under vigorous magnetic stirring (500 RPM) for three days to break the microcapsules and free the HS. The sample was then centrifuged once again

References to this Chapter on pages 89-90

to remove any capsule shell debris and the supernatant analysed using the UV.[27] The payload and encapsulation efficiency were then calculated using **Equation 2-5** and **Equation 2-6**:

$$Payload = \frac{m_{oil}}{m_{caps}} \qquad \textbf{Equation 2-5}$$

$$EE(\%) = 100\%\ x\ \frac{m_a}{m_t} = 100\%\ x\ \frac{\frac{m_{oil}}{m_{caps}}}{\frac{m_c}{m_c+m_s}} \qquad \textbf{Equation 2-6}$$

where, m_{oil} represents the mass of core material in microcapsules, m_{caps} mass of capsules, m_a actual loading; m_t theoretical loading; m_c mass of core material used for encapsulation and m_s mass of shell material used for encapsulation.

2.3.6.2 Release profile

The release profile experiment was designed to measure the HS leakage from the microcapsule and establish the permeability of the shell. The experiment was repeated with different shell formation procedures to compare the release data versus time.

For this experiment, 10g of capsule slurry, containing 20% w/w of capsules to water was added to a dialysis tubing. The tubing had its both ends sealed and was charged to a bottle containing 250ml of 36% propanol aqueous solution under magnetic agitation. Then the λ_{max} of the solution at 305 nm was measured over time and the HS mass present in solution obtained using a calibration curve (**Figure 2-16**) using a UV-Vis spectrophotometer.

2.4 Stability and Performance Tests in the Industry

Perfume microcapsules (PMCs) prototypes are tested in industry against two main parameters: *stability* and *performance* in the heavy-duty laundry detergents (HDL) and liquid fabric enhancers (LFE), also known as fabric softeners. In terms of *stability*, it is desirable that

References to this Chapter on pages 89-90

the capsules remain intact without any perfume leakage for at least six months in the finished product. This extended period of time is necessary when supply chain and storage are taken into account along with shelf-life of the product. On the other hand, *performance* measures the capability of the capsule to delivery freshness to the consumer at the correct time. When laundry products (HDL and LFE) are concerned, it is desirable to delivery freshness after washing/drying processes when the consumer handles the fabric.

2.4.1 Pre-assessment: air drying in glass slide

Capsule air-drying in glass slide tests were used to rapidly pre-assess stability and performance of prototypes. The stability was assessed using optical microscopy by the analysis of the shell deformation due to perfume leakage when capsules were air-dried. Performance was assessed through an ofactive assessment of the dried capsules.

The capsule slurry was diluted in DI water 500x and a few drops added to a glass slide and allowed to air-dry overnight at room temperature. Then, the capsules were observed under an optical microscope to check if their structure had collapsed or not (**Figure 2-17**). Capsules that collapse when air-dried are unlikely to be stable in finished products; soft-shell capsules have the tendency to shrink if perfume is leaking out, as they might not be mechanically robust due to thin or incomplete shell formation.

References to this Chapter on pages 89-90

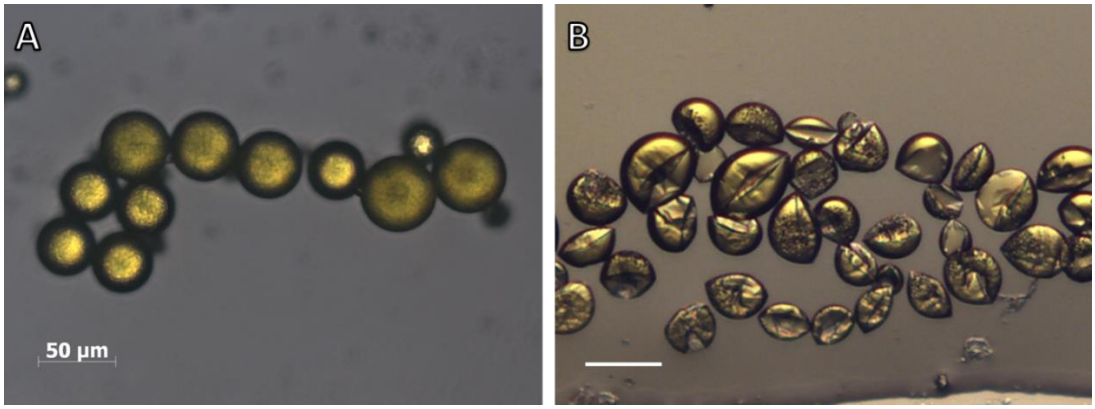

***Figure 2-17**. Optical microscopy images representing the air-drying on glass slide test: (A) non-collapsing capsules, (B) collapsing capsules upon drying. Scale bar: 50µm.*

If the capsules did not collapse after air-drying overnight, they were assessed regarding their performance using an olfactive test:

Step one: each slide was sniffed by at least 3 experts at no more than 5 cm of distance and the odour sense was assessed in the scale: no, low or high odour. Experts were trained in house to assess the intensity of fragrances.

Step two: a second clean glass slide was put on top of the slide containing the dried dilution (from step 1), trapping dry capsules between the slides. The slides were squeezed together to break the capsules. The second glass slide was them removed so the slide containing perfume could be assessed in terms of fragrance intensity against step one (scale: no, low, high).

This test gave a quick pre-screening indication on whether the capsules were mechanically robust, capable of surviving air-drying and retaining the perfume inside their core. It could also indicate whether if the capsules were able to trigger release the perfume when compressive force is used to break their shell.

References to this Chapter on pages 89-90

2.4.2 Stability assessments

Stability assessments were performed at P&G in order to establish if the silica-based capsules were compatible with the desired finished product formulation. As discussed in Chapter 1, fragrances are a mixture of hydrophobic oils and these are the very compounds that detergents are designed to remove from the fabric during the wash, so the shell must be able to prevent the perfume oil from being extracted from the capsule core to the surfactant-rich continuous phase.

2.4.2.1 Microscopy analysis

Similarly, to the air-drying glass slide test, this test aims to visually assess whether the capsules were able to retain perfume when dispersed in the finished product. If the shell was soft, it should shrink as the perfume leaked out (**Figure 2-18B**). On the other hand, if the shell was solid but highly porous, it would retain its shape, however it should be visible that perfume was leaking out (**Figure 2-18D**).

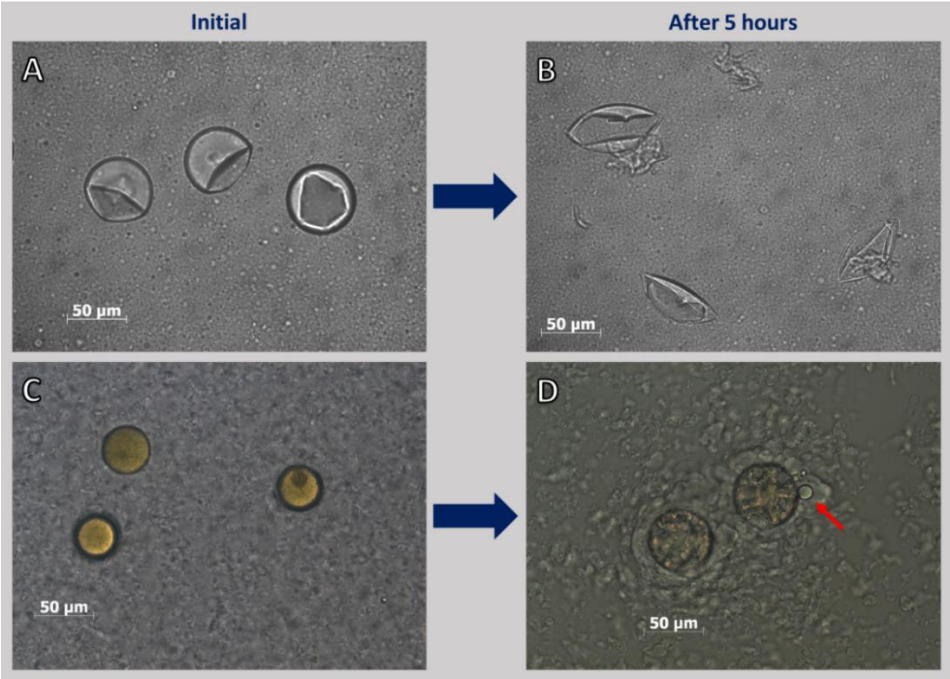

References to this Chapter on pages 89-90

Figure 2-18. *Optical microscopy images illustrating capsules that are instable in a finished product. A and B are capsules with soft shell that deforms upon fragrance leakage. C and D are hard shell capsules that do not deform but it is clear that the fragrance leaks out due to porosity or defects (red arrow).*

2.4.2.2 Perfume headspace using GC-MS

To assess quantitatively the amount of perfume that leaked out from the capsules in the finished product, a perfume headspace study was performed using a gas chromatograph apparatus connected to a mass spectrometry detector (GC-MS). As the perfume formulation is mixture of different perfume raw materials (PRMs), each of these PRMs was individually quantified by the GC-MS and its level assessed against a pure perfume reference.

For this experiment a pre-calculated quantity of slurry containing 0.2g of encapsulated perfume was added to 20g of finished product (HDL, LFE or conditioner). The vial was shaken by hand and left undisturbed under controlled temperature for a desirable period before CG-MS analysis. The obtained percentage of each RPM in the head-space was compared to a sample containing the same amount of fresh free perfume (no capsules), which is the positive control corresponding to 100% leakage. GC-MS used was an Agilent technologies 7890B GC system and 5977B MS detector.

2.4.3 Performance assessment – full scale wash test

This test mimics the wash process for perfume capsules used in laundry applications. After going through washing and drying of fabrics the capsules must retain the perfume, which should be released when mechanical force (e.g. shear and compression) is applied to the dry fabrics as the consumer handles the fabric.

References to this Chapter on pages 89-90

Perfume level calculation

It is assumed that there is a 0.56% perfume activity in the laundry product, with a dosage of 69.2g of water solution containing capsule. This means that 0.39g perfume per wash are necessary (69.2/100*0.56g). The assumed deposition on the fabric is 5% (as calculated for a wash cycle). A typical wash contains 3 kg of load, so 1.29 10^{-4} g perfume is needed per gram of fabric.

Wash test

A laundry product with no perfume was prepared containing a quantity of capsule slurry with the appropriated activity as calculated above. Then, five terry towels (fabric model) were washed using the prepared product in a Miele Softronic W1714 washing machine with the following wash conditions: 30°C, short crease recovery cycle and 1000 rpm. The rest of the load (3 kg) was completed using cotton ballast . After the wash, the terry towels were folded in three and put individually in an aluminium bag for transport to the drying room. The Terry towels were then line dried overnight in the drying room (20°C, 55% humidity).

Evaluation of fabric

The capsule performance was assessed in relation to commercial perfume microcapsules (PMCs) as positive control and free oil samples (samples that were washed in the presence of non-encapsulated perfume oil in the same level as microcapsules) as negative control. A panel of experts performed the ofactive assessment of the fabrics (no, low, high) in three different touch points:

References to this Chapter on pages 89-90

Wet fabric odour (WFO) – Sample were smelled immediately after the wash, for this test a strong fragrance odour is usually expected for the free oil samples as they are not protected by a capsule wall and low odour for samples washed with PMCs.

Dry fabric odour (DFO) – Fabrics were completely dried so any non-encapsulated oil evaporates. For this test, a low fragrance odour is expected for PMCs as they might partially diffuse the fragrance slowly and no odour is expected for the samples washed with free oil, as all fragrance should evaporate as the fabric dries.

Rubbed fabric odour (RFO) – Dried fabrics were rubbed with the intent of breaking the microcapsules in order to release the perfume. A high perfume odour is expected for PMCs and no odour for free-oil samples.

2.5 References

1. H. Isobe and K. Kaneko, *Porous Silica Particles Prepared from Silicon Tetrachloride Using Ultrasonic Spray Method*, *Journal of Colloid and Interface Science*, **1999**, *212*, 234-241.
2. B. Buesser and S. E. Pratsinis, *Design of Nanomaterial Synthesis by Aerosol Processes*, *Annual Review of Chemical and Biomolecular Engineering*, **2012**, *3*, 103-127.
3. L. T. Zhuravlev, *The Surface Chemistry of Amorphous Silica. Zhuravlev Model*, *Colloids and Surfaces A: Physicochemical and Engineering Aspects*, **2000**, *173*, 1-38.
4. R. Xu, *Particle Characterization: Light Scattering Methods*, Springer Netherlands, **2000**.
5. H. C. van de Hulst, *Light Scattering by Small Particles*, Dover Publications, **2012**.
6. E. Kissa, *Dispersions: Characterization, Testing, and Measurement*, CRC Press, **2017**.
7. G. Ghosh, *Handbook of Refractive Index and Dispersion of Water for Scientists and Engineers*, Ghosh, Sujata, **2005**.
8. H. G. Barth, P. J. Elving and J. D. Winefordner, *Modern Methods of Particle Size Analysis*, Wiley, **1984**.
9. Piacentini E. *Droplet Size*. In: Drioli E., Giorno L. (eds) Encyclopedia of Membranes. Springer, Berlin, Heidelberg. **2016**
10. B. Herman and J. J. Lemasters, *Optical Microscopy: Emerging Methods and Applications*, Elsevier Science, **2012**.
11. D. B. Murphy and M. W. Davidson, *Fundamentals of Light Microscopy and Electronic Imaging*, Wiley, **2012**.
12. M. Carter and J. Shieh, in *Guide to Research Techniques in Neuroscience (Second Edition)*, eds. M. Carter and J. Shieh, Academic Press, San Diego, **2015**, pp. 117-144.

13. A. K. Singh, in *Engineered Nanoparticles*, ed. A. K. Singh, Academic Press, Boston, **2016**, pp. 19-76.
14. W. T. J., *Scanning Electron Microscopy and X-Ray Microanalysis, 3rd Edition. By Joseph Goldstein, Dale Newbury, David Joy, Charles Lyman, Patrick Echlin, Eric Lifshin, Linda Sawyer, Joseph Michael Kluwer Academic Publishers, New York (2003) Isbn 0306472929; Hardback; 688; $75.00*, *Scanning*, **2005**, *27*, 215-216.
15. D. B. Williams and C. B. Carter, *Transmission Electron Microscopy: A Textbook for Materials Science*, Springer, **2009**.
16. L. Reimer, *Transmission Electron Microscopy: Physics of Image Formation and Microanalysis*, Springer Berlin Heidelberg, **2013**.
17. J. C. H. Spence, *High-Resolution Electron Microscopy*, OUP Oxford, **2013**.
18. C. Shiu, Z. Zhang and C. R. Thomas, *A Novel Technique for the Study of Bacterial Cell Mechanical Properties*, *Biotechnology Techniques*, **1999**, *13*, 707-713.
19. Z. Zhang, M. A. Ferenczi, A. C. Lush and C. R. Thomas, *A Novel Micromanipulation Technique for Measuring the Bursting Strength of Single Mammalian Cells*, *Applied Microbiology and Biotechnology*, **1991**, *36*, 208-210.
20. J. Blewett, K. Burrows and C. Thomas, *A Micromanipulation Method to Measure the Mechanical Properties of Single Tomato Suspension Cells*, *Biotechnology Letters*, **2000**, *22*, 1877-1883.
21. S. J. D., H. Peter, W. Changxiang and T. C. R., *Determining the Mechanical Properties of Yeast Cell Walls*, *Biotechnology Progress*, **2011**, *27*, 505-512.
22. Z. Zhang, *Mechanical Strength of Single Microcapsules Determined by a Novel Micromanipulation Technique*, *Journal of Microencapsulation*, **1999**, *16*, 117-124.
23. G. Sun and Z. Zhang, *Mechanical Strength of Microcapsules Made of Different Wall Materials*, *International Journal of Pharmaceutics*, **2002**, *242*, 307-311.
24. B. M. Weckhuysen, *In-Situ Spectroscopy of Catalysts*, American Scientific Publishers, **2004**.
25. D. A. Skoog, F. J. Holler, S. R. Crouch, D. M. West, L. Cengage and C. Brooks/Cole Publishing, *Fundamentals of Analytical Chemistry*, Brooks/Cole : Cengage Learning, Belmont, **2014**.
26. R. Mercadé-Prieto, R. Allen, D. York, J. A. Preece, T. E. Goodwin and Z. Zhang, *Determination of the Shell Permeability of Microcapsules with a Core of Oil-Based Active Ingredient*, *Journal of Microencapsulation*, **2012**, *29*, 463-474.
27. H.-Y. Im, J. Kim and H. Sah, *Another Paradigm in Solvent Extraction-Based Microencapsulation Technologies*, *Biomacromolecules*, **2010**, *11*, 776-786.

CHAPTER 3. Pickering Emulsion Stability and PEOS Preparation and Characterization

Abstract

This chapter introduces the basis for the successful formation of silica capsules using Pickering emulsions. This was achieved by considering:

(i) the fundamentals of Pickering emulsion stabilised using silica colloidal nanoparticles (SiO_2 NPs) as Pickering emulsifiers and perfume oils as dispersed phase,

(ii) the possibility of changing the emulsion type from oil-in-water (O/W) to water-in-oil (W/O) by tuning the wetting properties of the SiO_2 NPs,

(iii) the Pickering emulsion's (a) droplet diameter, and (b) size distribution, which was dependent on the concentration of the SiO_2 NPs, due to the limited coalescence phenomenon. Thus, the higher the nanoparticle concentration the smaller the emulsion droplet and the larger the size distribution.

The synthesis and characterization of silica precursor used to form capsules from Pickering emulsions is also reported. The selected precursor was an oil soluble hyperbranched polyethoxysiloxane (PEOS), which is hydrolysed at the oil/water interface from hydrophobic ethoxysilane to hydrophilic silanol groups. This hydrolysis anchors the PEOS to the interface, leading to an interfacial silica layer as the silanol group undergoes a condensation reaction and cross-link affording the capsule wall.

References to this Chapter on pages 119-120

3.1 Introduction

The stability of the Pickering emulsion is the first step towards successful encapsulation of materials, as coalescence can occur if the emulsion is not properly stabilised (Chapter 1 - Section 1.3.1). Ideally, each droplet should retain its form and core until the capsule wall is formed, which can be achieved by thermal annealing[1] or chemical cross-linking of the colloidal particles,[2] among other methods.[3, 4]

In principle, all emulsions tend to coalesce and phase separate, as they are thermodynamically unstable.[5] This instability is due to the large interfacial area between the two immiscible phases (typically water and oil) upon emulsification and formation of the droplets. The large interfacial area in the absence of surfactants leads to an increase in the interfacial Gibbs free energy (ΔG) according to **Equation 3-1**:

$$\Delta G \sim \gamma_{OW} \Delta A_{OW}, \qquad \textbf{\textit{Equation 3-1}}$$

where γ_{OW} is the interfacial tension and ΔA_{OW} is the change in the interfacial area between oil and water. During emulsification ΔA_{OW} increases dramatically, leading ΔG to be positive and the emulsion to be thermodynamically unstable. The presence of surfactants during emulsification can affect ΔG by lowering the interfacial tension and stabilizing the emulsion.[5] Solid particles, on the other hand, do not alter the interfacial tension, but reduce the effective interfacial area A_{OW}, by adsorbing at the water/oil interface.[6]

In addition, when using solid nanoparticles as Pickering emulsifiers, the droplet size and size distribution can be controlled independently of the mixing conditions and the droplet volume fraction, due to the so-called limited coalescence phenomenon.[7]

References to this Chapter on pages 119-120

The limited coalescence phenomenon rationalizes why an excess of oil-water interface is produced when compared to the area that can be covered by the nanoparticles, which must be irreversibly attached to the interface. The droplets coalesce to a limited extent, which reduces the interfacial area between the oil and water, and progressively increases the degree of coverage by the nanoparticles.[7] As a result, a film of nanoparticles is formed at the interface, which kinetically stabilizes the emulsion. The resulting emulsions are stable over months and remarkably monodisperse.

Hyperbranched polyethoxysilane (PEOS) is a silica polymer precursor used to prepare polymer/silica composites. It also has technological interest as processable precursor for silica.[8] It consists of a hydrophobic liquid, with a lower viscosity and much higher solubility in oils when compared to other commercially available linear silica precursor polymers.[9]

PEOS has been investigated as "green-emulsifier" due to its hydrolysis-induced interfacial activity, which leads to an effective O/W stabilisation, without the need of classical surfactants.[10] In addition, it possesses a large number of active groups on the surface that can be easily functionalized.[9] Another key characteristic is that hyperbranched PEOS possesses chemical stability upon long-term storage: up to 2 years, when kept under dry condition.[9]

3.1.1 Aim of this research chapter

In this chapter, two preliminary aims of the research toward creating SiO_2 capsules are addressed and shown graphically in **Figure 3-1**.

Part 1 Aims: the aim is to investigate the stability of Pickering emulsions formed using a commercial perfume oil (PO) or hexyl salicylate (HS) as core materials and hydrophilic silica fumed nanoparticles (SiO_2 NPs) as Pickering emulsifier. The Pickering emulsion stability was

 References to this Chapter on pages 119-120

studied for emulsions made of HS or PO droplets and SiO_2 NPs as Pickering emulsifiers. Some emulsification parameters are modified to understand Pickering stabilization, such as the concentration of SiO_2 NPs to oil, which controls the limited coalescence phenomenon, and the wettability of the SiO_2 NPs which controls the type of emulsion formed (water-in-oil or oil-in-water) as well as the stability of the emulsion in general. As described above, the density and polarity of the oil can also influence the droplet size and stability.

Table 3-1 below describes some key properties of these oils (structure, CLogP and density) which can influence the stability of the Pickering emulsion. The CLogP is an indication of the lipophilicity of the molecule and can affect the interfacial tension between oil and water as well as the solubility of the oil in water. Finally, the density can influence the size of the oil droplet formed. The oils were used in the following chapters for the development of a silica-based encapsulation technology: HS was used as PO model for the development of the encapsulation technology (**Chapter 4**) and the commercial PO was encapsulated using the SiO_2 NPs Pickering stabilisation-based approach in **Chapter 5** and the shell properties were optimized in **Chapter 6**.

***Table 3-1**. Properties of hexyl salicylate and the commercial perfume oil. Perfume oil data were provided by P&G.*

	Structure	**CLogP**	**Density at 25°C (g/cm^3)**	**Interfacial tension (mN.m^{-1})**
Hexyl salicylate (chapter 4)	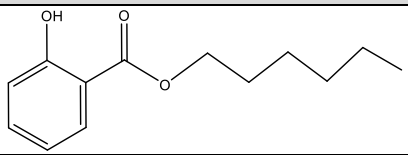	5.7	1.04	3.3
Perfume oil (chapter 5 and 6)	Mixture of 13 components	3.5	0.96	Unknown

References to this Chapter on pages 119-120

Part 2 Aims: PEOS with variable properties (density, viscosity, degree of branching) was prepared by varying the fraction (***f***) of acetic anhydride to PEOS monomer, tetraethoxysilane (TEOS). The different PEOS produced were characterized and used as silica precursor for the formation of the silica shell crosslinking the SiO_2 NPs and sealing the voids between the nanoparticles to form a mechanically stable silica capsule in Chapters 4 to 6.

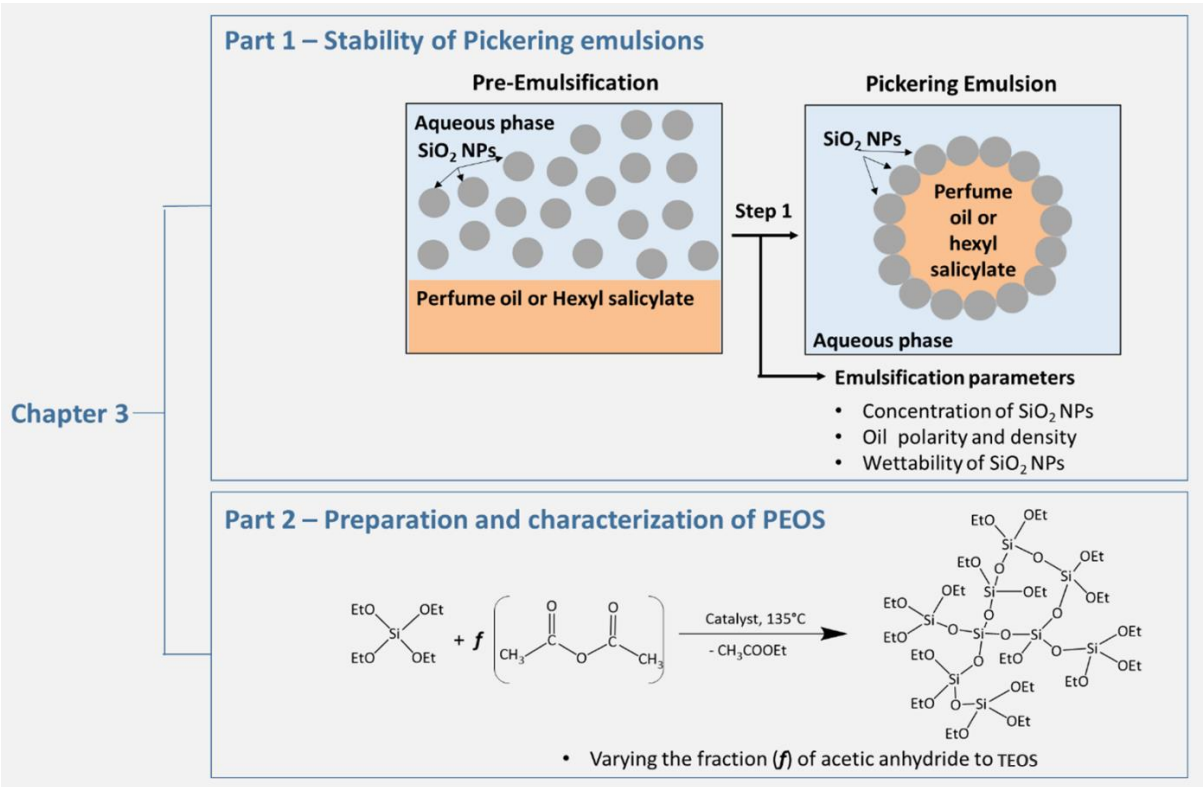

Figure 3-1*. Road map for Chapter 3. In Part 1 of this results chapter, the stability of perfume oil or hexyl salicylate Pickering emulsions using hydrophilic SiO_2 NPs as Pickering emulsifier is described varying the concentration of SiO_2 NPs in relation to the oil phase and the wettability of the SiO_2 NPs. Then, in Part 2, PEOS is prepared using different fraction of acetic anhydride to TEOS and the various PEOS structures are characterized.*

References to this Chapter on pages 119-120

3.2 Results and discussions

3.2.1 Part 1. Pickering emulsion stability using hydrophilic SiO_2 NPs

As described by Binks *et al.*,[11] SiO_2 NPs can successfully form stable Pickering emulsions between water and multiple oils depending on the wettability of the SiO_2 NPs in the interface between water and oil. A simple experiment was used to visually observe the emulsion stability between equal fractions of the commercial perfume oil and deionised (DI) water in the presence, and absence, of hydrophilic SiO_2 NPs after emulsification using a vortex mixer at 2500 RPM for 5 minutes (**Figure 3-2**). An oil soluble dye (PM546 – described in Chapter 2) was added to the perfume oil to visualise the phase separation. Immediately after emulsification (**Figure 3-2A**) an emulsion is formed in both the presence and absence of SiO_2 NPs. However, after 60 seconds (**Figure 3-2B**) there is a clear phase separation in the vial where there are no SiO_2 NPs, whilst in the presence of SiO_2 NPs the emulsion was stabilised. A similar result was observed for HS, and the emulsion was successfully stabilized by the hydrophilic SIO_2 NPs. For both PO and HS the emulsion stabilised by SiO_2 NPs was stable for over a year, indicating that the SiO_2 NPs were irreversibly attached to the interface, protecting the emulsion from coalescence due to electric repulsion.

References to this Chapter on pages 119-120

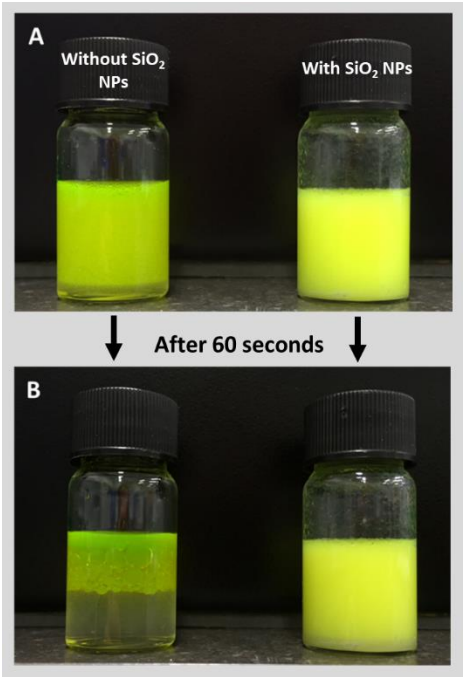

Figure 3-2. *Images showing the comparative study between O/W perfume oil emulsions in the presence and absence of SiO_2 NPs as a function of time: immediately after emulsification (A), and 60 s (B) after emulsification.*

In general, the main reason for the high stability of Pickering emulsions is the irreversibility of the SiO_2 NPs adsorption at the interface of the emulsion droplet when the three-phase contact angle is close to 90°(Section 1.3.1).[11] Therefore, in order to maximise the stability of the emulsion, the hydrophobicity of the surface of the SiO_2 NPs can be tuned to adjust the specific polarity of the oil used. The drop of free energy by placing nanoparticles at the interface becomes less significant with the decrease of the oil/water interfacial tension γ_{ow}, so the Pickering emulsion becomes less stable when γ_{ow} is lower.

Hydrophilic fumed SiO_2 NPs could, however, stabilize the perfume oil/water (and HS/water) emulsion due to the polar character of the oils used as a result of the adsorption of polar oil species onto the surface silanol groups of the SiO_2 NPs.[12] Thus , the stability of a Pickering

References to this Chapter on pages 119-120

emulsion depends on a fine adjustment between nanoparticle surface properties and oil polarity, in addition to other factors such as pH, nanoparticle size and concentration.[11] The hydrophobicity of the SiO_2 NPs on Pickering emulsion stability is examined in *Section 3.2.1.1* below.

3.2.1.1 Limited coalescence phenomenon

The limited coalescence phenomenon was studied herein to verify the possibility of stabilizing perfume oil Pickering emulsion droplets using the hydrophilic SiO_2 NPs, while controlling the droplet mean diameter and the SPAN of the size distribution, which describes the distribution width and is given by **Equation 3-2**. The lower the SPAN value, the more narrowly distributed the emulsion is in terms of size.

$$SPAN = \frac{D[0.9]-D[0.1]}{D[0.5]}, \qquad \textbf{\textit{Equation 3-2}}$$

Where D[0.9], D[0.1] and D[0.5] represent the cumulative mean diameter that falls below 90, 10 and 50% of the total population, respectively.

For the experiment, three emulsions were prepared, at constant stirring speed (2500 RPM) and temperature (25°C) maintaining the same volumes of the aqueous continuous phase (8 ml) and PO (2 ml) but varying the concentration of SiO_2 NPs dispersed in the continuous phase, to give increasing wt% of NPs to PO. **Figure 3-3** shows optical microscopy images of each sample. Clearly, as the concentration of SiO_2 NPs increased the droplet diameter reduced, which is in agreement with the limited coalescence phenomenon theory.[7]

References to this Chapter on pages 119-120

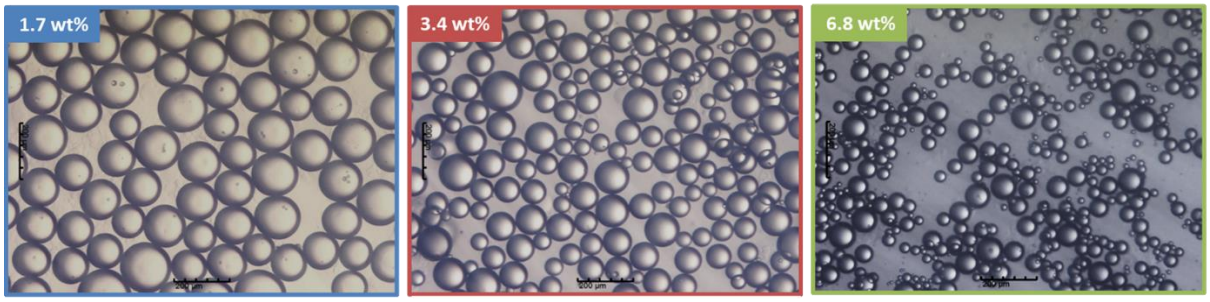

***Figure 3-3**. Optical microscopy images of samples containing 1.7, 3.4, and 6.8 wt% of SiO_2 NPs to perfume oil. It was observed that the higher the concentration of SiO_2 NPS in relation the oil phase, the smaller and more polydispersed the size of the emulsion droplets. Scale bars: 200 µm.*

The mean diameter and SPAN of the distribution can be found in **Table 3-2**. As observed, the SPAN of the size distribution could also be controlled; the sample prepared in the presence of 1.7 wt% SiO_2 NPs had a smaller SPAN when compared to the samples prepared with higher concentrations of SiO_2 NPs. This demonstrates the advantage of using a nanoparticle-poor regime to obtain emulsions with narrow size distributions; as the nanoparticles self-assemble at the interface the droplets coalesce until complete droplet coverage.[13] The possibility of controlling the mean droplet diameter and the particle size distribution (PSD) is an important feature of Pickering emulsions, which suggests that the droplet was successfully stabilized by the SiO_2 NPs.[14] The experiment was repeated for HS droplets stabilised by SiO_2 NPs, and it can be observed in **Table 3-2**, the droplets had a smaller mean diameter overall when compared to the emulsions prepared with perfume oil, this is due to the higher density of HS (1.04 $g.cm^{-3}$) compared to perfume oil (0.96 $g.cm^{-3}$).

References to this Chapter on pages 119-120

Table 3-2. *Pickering Emulsion droplet size and distribution as a function on increasing NPs ratio relative to PO and HS.*

Oil phase	Wt% of SiO_2 NPs to oil phase	Mean diameter (D) µm	SPAN	Specific surface area ($m^2.g^{-1}$) Eq. 3-3	Total surface area (S_{inter}) (m^2) Eq. 3-4	Surface coverage (C) Eq. 3-5	Number of NP layers (*n*) Eq. 3-6
Perfume oil Density 0.96 $g.cm^{-3}$	**1.7**	121.8 ± 21.0	0.984 ± 0.012	0.096	0.017	1.18	1.31
	3.4	80.6 ± 12.8	1.054 ± 0.016		0.025	1.56	1.73
	6.8	41.4 ± 6.1	1.227 ± 0.017		0.049	1.60	1.78
Hexyl salicylate Density 1.04 $g.cm^{-3}$	**1.7**	114.5 ± 4.7	0.919 ± 0.007	0.101	0.018	1.11	1.23
	3.4	77.1 ± 4.8	0.966 ± 0.009		0.026	1.49	1.65
	6.8	39.32 ± 4.2	1.054 ± 0.009		0.051	1.51	1.67

Figure 3-2 shows the reciprocal of average droplet diameter has a linear dependence on the wt% of SiO_2 NPs to oil phase, as would be expected from **Equation 3-3**, where, m_p is the mass of nanoparticles, V_d is the volume of dispersed phase (kept constant) and S_f the specific surface area, which is dependent on the stirring speed.

$$\frac{1}{D} = \frac{s_f m_p}{6V_d}$$ ***Equation 3-3***[7]

This relationship holds providing that all solid nanoparticles are irreversibly attached to the interface, and no free nanoparticles are found free in the continuous phase, and if so it is

References to this Chapter on pages 119-120

possible to control the droplet diameter by adjusting the mass ratio of nanoparticles to dispersed phase.

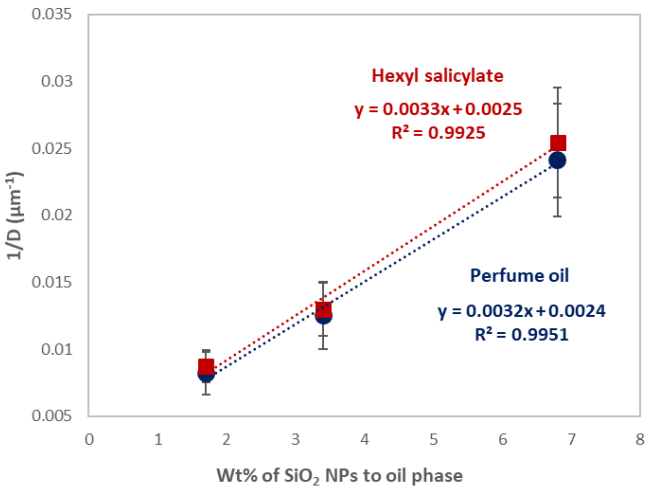

Figure 3-4. *Linear relation between the reciprocal of the droplet diameter and the SiO_2 NPs concentration to perfume oil and hexyl salicylate.*

According to **Equation 3-3**, the slope of the equation depends only on the stirring speed and is proportional to the specific surface area, S_f, *i.e.* the oil droplet surface covered per unit mass of nanoparticles which is constant. The S_f values were 0.096 $m^2.g^{-1}$ for PO and 0.101 $m^2.g^{-1}$ for HS. As the mean size of the HS droplet was smaller, it was expected that a higher surface area could be covered by a specific mass of SiO_2 NPs.

As a derivation from **Equation 3-3**, the number of NPs layers (*n*) could also be estimated by calculating the total surface area formed (**Equation 3-4**) and the theoretical coverage (C) (**Equation 3-5**) of each droplet by the total mass of NPs (m_p). The total droplet surface area (S_i) could be calculated by dividing the volume of the dispersed phase (V_d) by the mean droplet diameter (*D*):

References to this Chapter on pages 119-120

$$S_i = \frac{6V_d}{D}$$ **Equation 3-4**

Assuming that all NPs are adsorbed at the O/W interface, it was possible to define the surface coverage (*C*), which is the ratio between the interfacial area effectively covered by the NPs and the total surface area (S_i).

$$C = \frac{m_p D}{4 d_{NP} \rho_{NP} V_d},$$ **Equation 3-5**

where d_{NP} is the NP diameter and ρ_{NP} the density of the NP, (2.2 g.cm^{-3}, according to the supplier). The number of NP layers (*n*) covering each oil droplet is obtained by dividing the coverage (*C*) by 0.9, which corresponds to the coverage of a dense monolayer of assumed spherical nanoparticles (**Equation 3-6**).[14]

$$n = \frac{C}{0.9}$$ **Equation 3-6**

According to the literature,[14, 15] NPs can adsorb either as a monolayer or multilayer up to 15, depending on the stirring method used. The observed differences can be explained by the fact that the aggregation of the SiO_2 NPs prior to emulsification in aqueous solution, varying their mean diameter when absorbing at the interface. Here, the number of layers is around 1-2 (depending on the state of aggregation of the fumed SiO_2 NPs, between 100-200nm – **Figure 2-1,** note that for simplicity, all images in this thesis are represented using one layer of NPs), suggesting that a monolayer is formed as the energy input of the vortex mixer is relatively low, so high aggregation is expected.

The specific surface area (S_f), total surface area (S_i), coverage (*C*) and number of NP layers (*n*), were calculated for both perfume oil and hexyl salicylate for the three SiO_2 NPs concentrations

 References to this Chapter on pages 119-120

studied using the graph in **Figure 3-4** and **Equations 3-3** to **3-6.** The values can be found in **Table 3-2**. Note that all the calculations were done using the experimental volume mean diameter ([4,3]).

Therefore, it was possible to take advantage of the limited coalescence phenomenon to produce PO and HS emulsions with narrow size distribution using a vortex mixer to produce the emulsions. The differences in terms of ClogP did not interfere in the stabilization of the emulsion, and hydrophilic SiO_2 NPs could be used to stabilise emulsions in this range of polarities.

The initial pH was of these emulsions was **4.7 ± 0.4** and the zeta potential was **-16.0 ± 1.8 mV,** indicating that the droplets surfaces were negatively charged. The emulsions could also be stored for 12 months without coalescence, which indicates that the Pickering emulsion formed were highly stable and could be used as template for the further formation of silica capsules, which is the subject of **Chapter 4**.

1.1.1.1. SiO_2 NPs wettability influence on the type of emulsion

To understand how the wettability of the SiO_2 NPs can affect the type of emulsion formed, emulsions were prepared using equal weight fractions of DI water and perfume oil and SiO_2 NPs of different hydrophilicities. Aerosil 300 was used as hydrophilic nanoparticles while Aerosil R816 was used as hydrophobic nanoparticle. R816 are also fumed silica nanoparticles, however the surface of these NPs is further treated with hexadecylsilane (**Figure 3-5**).

References to this Chapter on pages 119-120

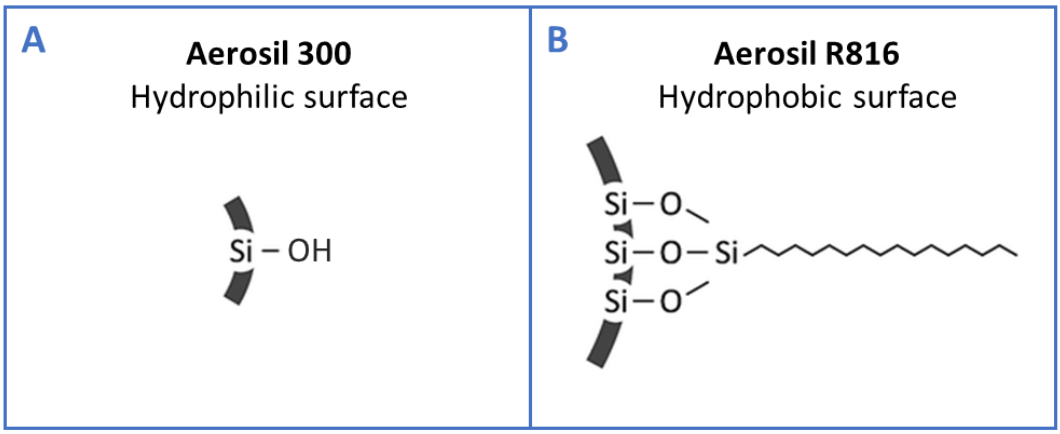

***Figure 3-5**. Scheme representing the surface of the fumed silica nanoparticles used. (A) Aerosil 300 – non-treated hydrophilic surface. (B) Aerosil R816 – hydrophobic surface after treated with hexadecylsilane.*

Interestingly, the surface hydrophobicity of the SiO_2 NPs influenced the emulsion type significantly (O/W or W/O) (**Figure 3-6**). As the hydrophilic nanoparticles were more wetted by the aqueous phase, the nanoparticle contact angle with the water was lower than 90°, and therefore the emulsion had the oil as the dispersed phase (**Figure 3-6A** and **D**). Whereas the opposite was observed for hydrophobic SiO_2 NPs; they were more wetted by the oil phase, and consequently formed emulsions with water as the dispersed phase, as demonstrated by **Figure 3-6C** and **F**.

Interestingly, when a mixture of 50 wt% hydrophobic and 50 wt% hydrophilic nanoparticles was used as Pickering emulsifier, a water-in-oil-in-water emulsion (W/O/W) was formed (**Figure 3-6B** and **E)**, further demonstrating that the type of emulsion formed is highly dependent on the wettability of the colloidal nanoparticles.

References to this Chapter on pages 119-120

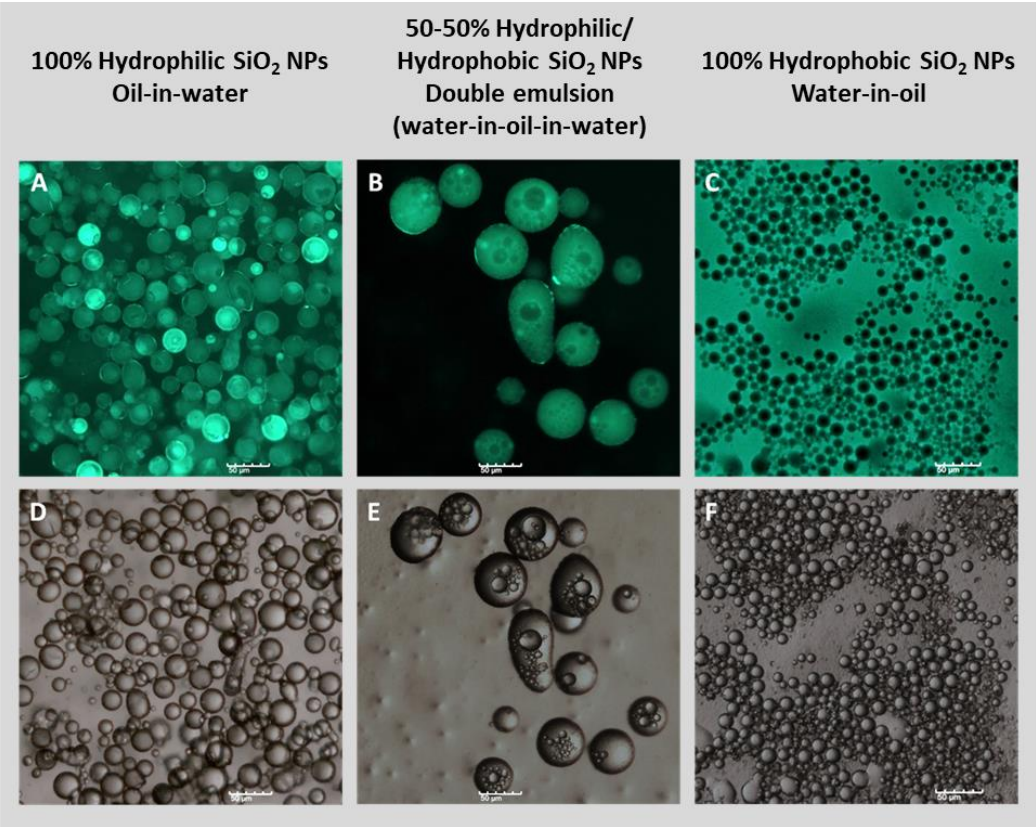

Figure 3-6. *Optical and fluorescence microscopy images of Pickering emulsions formed from SiO_2 NPs, water and perfume oil. Images A and D show stable O/W emulsions using hydrophilic SiO_2 NPs (A300) as Pickering emulsifier. Images C and F show stable W/O emulsions using hydrophobic SiO_2 NPs (AR816 – fumed silica after treated with hexadecylsilane) as Pickering emulsifier. Images B and E show stable W/O/W emulsions using 50% hydrophilic and 50% hydrophobic SiO_2 NPs as Pickering emulsifier.*

In summary, it is possible to use fumed SiO_2 NPs to potentially encapsulate a wide range of actives, from hydrophobic oils to hydrophilic aqueous solutions, by adjusting the surface properties of the nanoparticles, and as consequence, their wettability. Therefore, this methodology is interesting from a commercial point of view, as one single encapsulation

References to this Chapter on pages 119-120

process can be applied for multiple applications. The encapsulation of different actives is explored in **Chapter 6** of this thesis.

3.2.2 Part 2. Preparation and characterization of PEOS

3.2.2.1 PEOS synthesis

The PEOS synthesis process was based on the catalysed condensation reaction of tetraethoxysilane (TEOS) with acetic anhydride as shown in **Equation 3-7**. The catalyst used was tetrakis (trimethylsiloxy) titanium, which catalysed both the condensation reaction and acylation of ethoxysilane enhancing the conversion rate.[9]

$$Si(OC_2H_5)_4 + f(CH_3CO)_2O \xrightarrow{catalyst,135°C} SiO_f(OC_2H_5)_{4-2f} + 2fCH_3C(O)OC_2H_5$$

Equation 3-7

PEOS was produced following the methodology described by Zhu *et al.*[9] (More details in the experimental section). By varying the ratio (*f*) between the acetic anhydride and TEOS (**Equation 3-7**) and keeping the temperature constant at 135°C and stirring speed at 400 RPM, it was possible to produce PEOS with controlled degree of branching, leading to a variable SiO_2 content, density and viscosity (*f* = 1.0, 1.1, 1.15 and 1.2, and for identification purposes, all PEOS produced were named PEOS-*f*, **PEOS 1.0, PEOS 1.1, PEOS 1.15** and **PEOS 1.2**). The proposed generic structure[9] of PEOS using the method described is represented at **Figure 3-7**.

References to this Chapter on pages 119-120

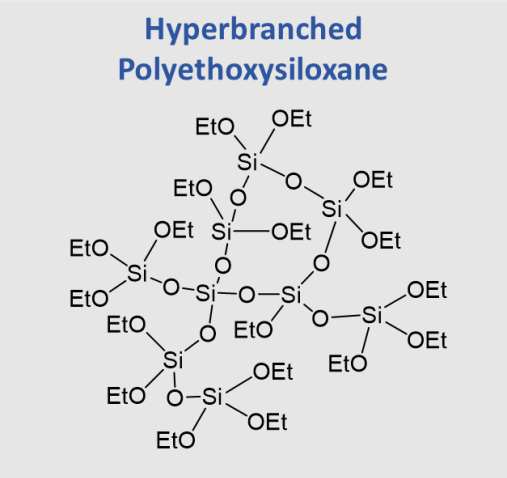

Figure 3-7. *Structure of hyperbranched polyethoxysiloxane as proposed by Zhu et al.*[9]

The physical appearance of the PEOS at all *f* values was a yellow oily liquid.

Figure 3-8 shows the example of PEOS 1.2. The synthesized PEOS was stable for months under a dry nitrogen atmosphere. Its long-term stability is due to the non-hydrolytic character of its synthesis, which avoids the formation of reactive silanol (Si-OH) end groups. However, PEOS reacted with H_2O forming solid silica when in contact with humid environment for over one month, as observed in **Figure 3-8**.

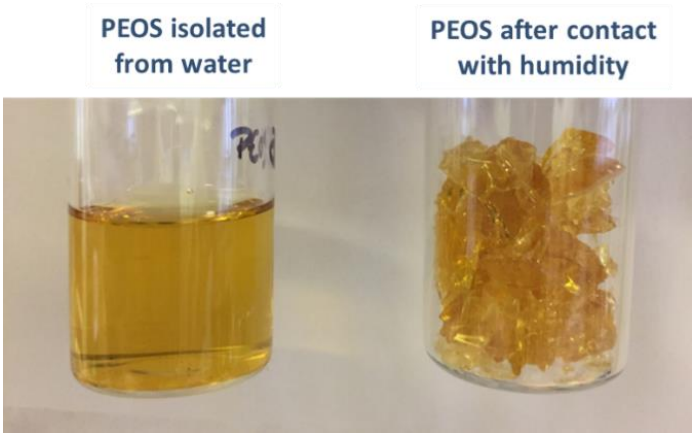

Figure 3-8*. Images of PEOS 1.2 before (left) and after (right) exposure to air humidity for one month.*

References to this Chapter on pages 119-120

PEOS is a polymeric silica precursor that can be hydrolysed in the presence of water as described in section 1.4.2 (**Equation 3-8**). The hydrolysis and cross-linking condensation process liberates water and ethanol:

<u>Hydrolysis:</u> ≡Si−OEt + H_2O → ≡Si−OH + EtOH

<u>Condensation:</u> ≡Si−OH + Si−OEt → ≡Si−O−Si≡ + EtOH

≡Si−OH + Si−OH → ≡Si−O−Si≡ + H2O ***Equations 3-8***

Under limited availability of water, PEOS can be partially hydrolysed.[10] The partially hydrolysed PEOS behaved as an interfacial-active surfactant, similar to hydrolysed long-alkyl-substituted alkoxysilanes.[16, 17] Full hydrolysis can be achieved if the H_2O concentration is increased further (**Figure 3-9**).

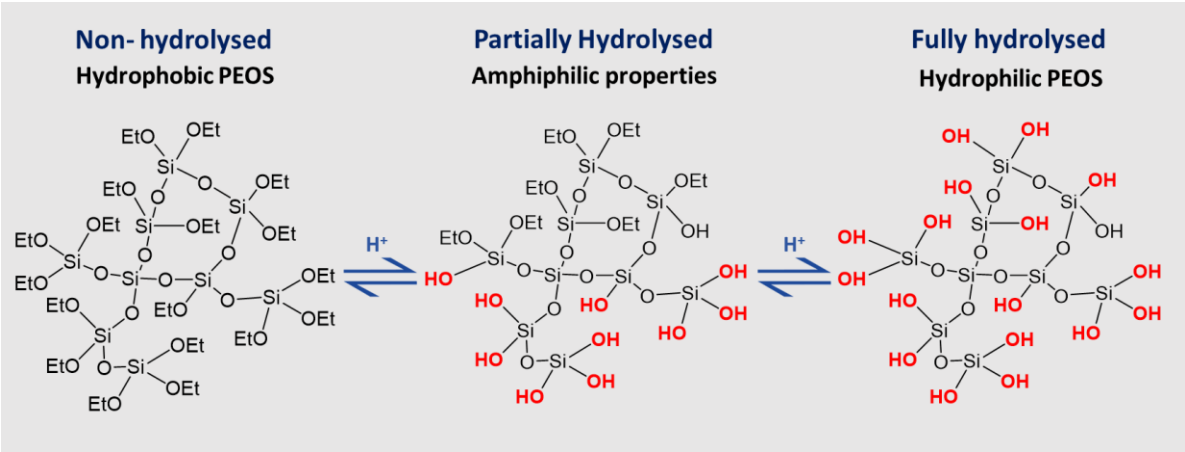

Figure 3-9. *Scheme representing the different hydrolysed stages of PEOS.*

3.2.2.2 PEOS characterisation

The 4 PEOS samples were characterised using standard organic molecular characterization techniques, which are described below. For some experiments, such as IR and ^{1}H NMR, only one example is shown in the results as the spectra are similar for all 4 PEOS types.

References to this Chapter on pages 119-120

3.2.2.3 Infrared spectroscopy

PEOS was first characterized *via* IR spectroscopy (**Figure 3-10**), and the results confirmed that carbonyl functional groups from the acetic anhydride, one at 1825 cm^{-1} (antisymmetric C=O / C=O stetch) and a second one at 1758 cm^{-1} (symmetric C=O/C=O stretch) could not be detected, suggesting that the anhydride was fully consumed by the reaction.

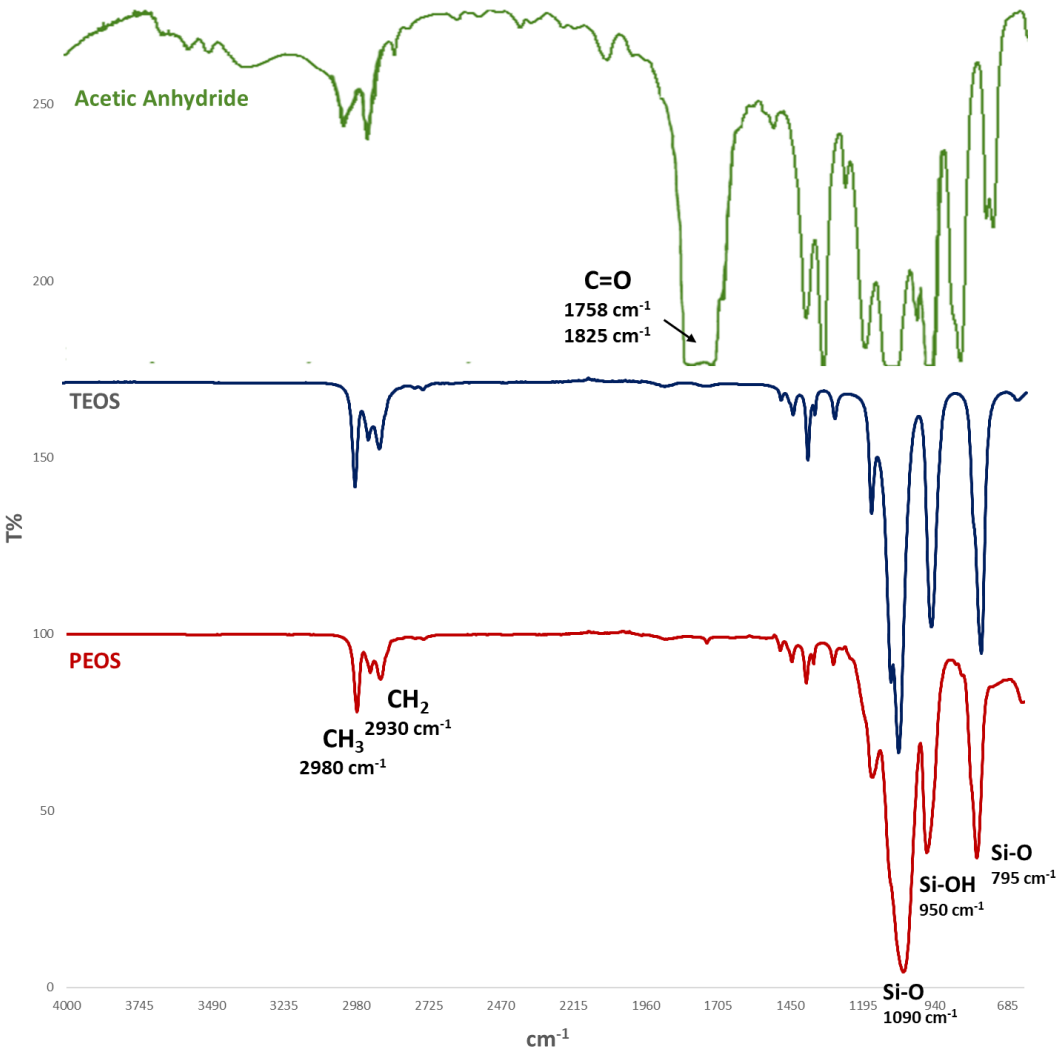

***Figure 3-10**. IR spectra of acetic anhydride PEOS 1.2. Important peaks: Si-O asymmetric vibration – 1090 cm^{-1}, Si-OH asymmetric vibration - 950 cm^{-1}, Si –O symmetric vibration – 795 cm^{-1} and CH_2/CH_3 at the 2980-2850 cm^{-1} region.*

References to this Chapter on pages 119-120

It is also important to notice that the ethoxy group vibrations are present (CH_3 – 2980 cm^{-1} and CH_2 – 2930 cm^{-1}), as well as specific vibrations for alkoxyl silanes (Si-O – 1090 cm^{-1} and 795 cm^{-1}). As PEOS was exposed to air and consequently humidity for this measurement, a Si-OH vibration is also present (950 cm^{-1}).

3.2.2.4 ^1H NMR

Figure 3-11 shows the ^1H NMR spectra of **PEOS 1.2**. The two signals correspond to CH_3 and CH_2 of the ethoxy groups, which is similar to spectra for the TEOS monomer starting material. There were no signals in the acetoxy region, suggesting that the condensation reaction was complete and no acetic anhydride was present in the product, in line with the IR data.

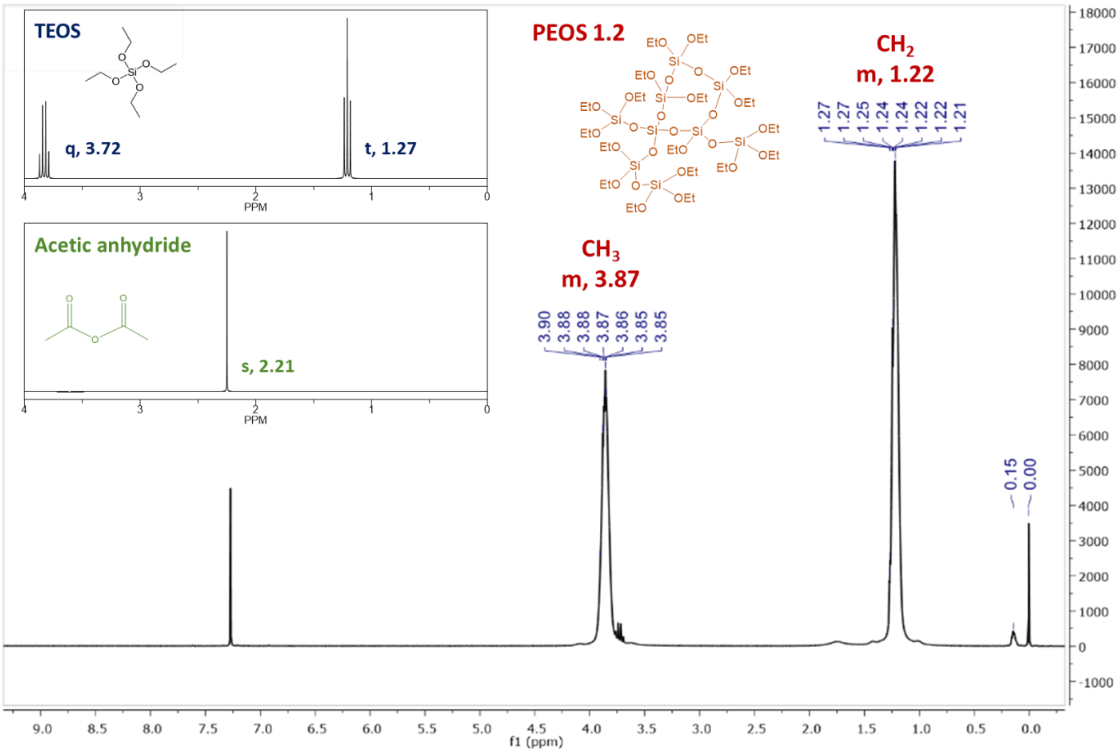

***Figure 3-11**. ^1H NMR spectra of the synthesized PEOS from a molar ratio of 1.2 of acetic anhydride to TEOS and 0.3 mol% of catalyst. The peaks at 7.27 and 0.0 ppm correspond to the*

References to this Chapter on pages 119-120

solvent $CDCl_3$/TMF and the multiplets at 3.87 and 1.22 ppm to the ethoxy groups found in the product (CH_2 and CH_3, respectively).

3.2.2.5 ^{29}Si NMR

When Si NMR for hyperbranched silicon structures is concerned, it is expected to find different groups of peaks depending on the number of silicon atoms bearing the central silicon atom.[9] The ^{29}Si NMR spectra for all four **PEOS** samples are shown in **Figure 3-12**. From the left to right the peaks are: four ethoxy groups Q0 (-82 ppm, TEOS), three ethoxy groups Q1 (-89 ppm, terminal), two ethoxy groups Q2 (- 96 ppm, linear), one ethoxy group Q3 (104 ppm, semidendritic) and no ethoxy group Q4 (-112 ppm, dendritic). TEOS would have only one signal – Q0 for four ethoxty groups, so the Q0 signal observed is proposed to be due to unreacted TEOS that remained in the sample after the reaction, which is in agreement with the results from IR analysis.

References to this Chapter on pages 119-120

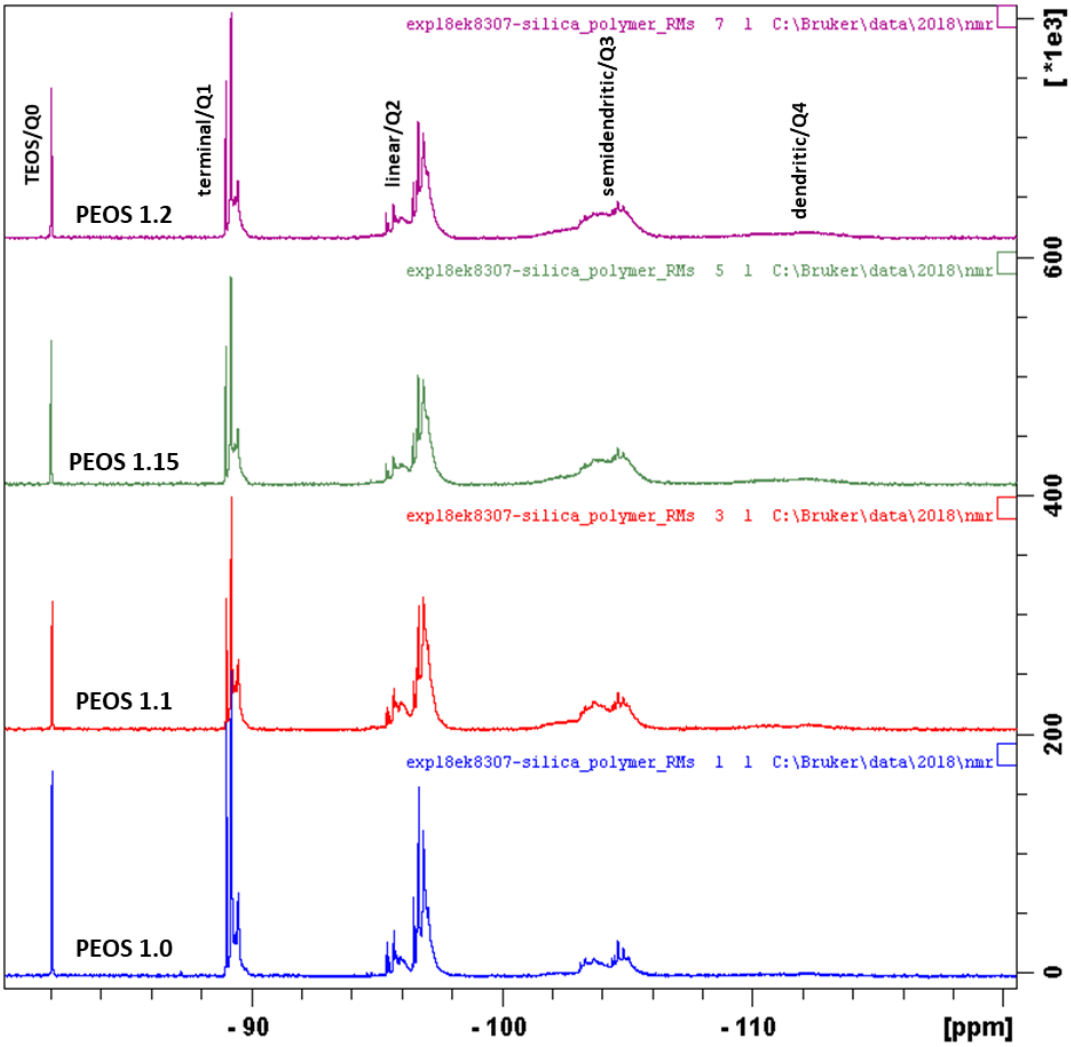

Figure 3-12. *^{29}Si NMR spectra of PEOS synthesised from different acetic anhydride to TEOS molar ratio (f).*

It was possible to calculate the relative amount of each type of silicon atom in the polymer from the integration of the peaks (**Table 3-3**). This information was valuable for the calculation of the degree of branching (DB) of each sample (**Equation 3-9**). DB was expressed as a ratio of the actual growth direction of the polymer (*R*) to the maximum possible growth directions (R_{max}).[18]

$$DB = \frac{R}{R_{max}} = \frac{2Q_4+Q_3}{\frac{2}{3}(3Q_4+2Q_3+Q_2)}$$ ***Equation 3-9***

References to this Chapter on pages 119-120

***Table 3-3**. Summary of the 29Si NMR data for the relative content of each building units of PEOS synthesised from different molar ratios of acetic anhydride to TEOS (f).*

PEOS (*f*)	Units (%)					DB	SiO_2 content (%) from ^{29}Si NMR	Theoretical SiO_2 content (%)
	Q0 TEOS	Q1 terminal	Q2 linear	Q3 semi-dendritic	Q4 dendritic			
1.00	4	26	43	25	4	0.48	45.7	44.8
1.10	2	27	43	32	6	0.53	46.4	47.4
1.15	2	16	39	34	8	0.57	49.6	48.8
1.20	2	15	37	37	8	0.59	50.0	50.3

The silica content values were very similar to the ones obtained theoretically from **Equation 3-7**. As expected, an excess of acetic anhydride could increase the DB and lead to a more cross-linked product.[9] A maximum degree of condensation without gelation, i.e. maximum branching and even intramolecular loop formation, while the product remains in liquid, would be favourable for most applications.[9] Therefore, for the initial encapsulation protocols used in this thesis, **PEOS 1.2** was used as the silica precursor as a degree of branching higher than 0.59 was not possible due to saturation of branching leading to gelation of PEOS.

3.2.2.6 Molecular weight and polydispersity index

PEOS produced from the four different *f* values were analysed using gel permeation chromatography (GPC) with an evaporative light scattering detector (ELS). Polystyrene standards were used to create a calibration curve, in order to estimate the molecular weight of the **PEOS** samples. As observed in **Figure 3-13**, the average molecular weight (M_W) and the polydispersity index (PDI) increased as higher amounts of acetic anhydride were used in the reaction, whilst M_N had a smaller variation across the different samples.

References to this Chapter on pages 119-120

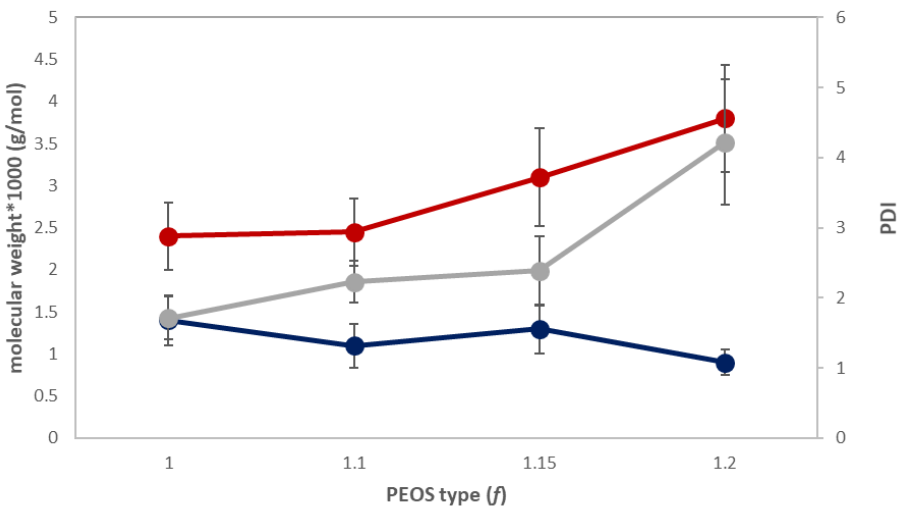

***Figure 3-13**. GPC results for PEOS produced with different molar ratios of acetic anhydride to TEOS illustrating weighted-average (M_W – gray line), and numbered-average (M_N - blue line) molecular weights and PDI (M_W/M_N – red line) for each f used, the experiments were performed in triplicates.*

Clearly as the amount of anhydride increases the polymer grows, as would be expected from the PEOS cross-linking process, whilst at the same time the PDI increases presumably as a result of the DB increasing (**Table 3-3**).

3.2.2.7 Density and viscosity

The different types of PEOS produced were further characterized as neat liquids in terms of viscosity using an AR 550 rheometer/viscometer from TA Instruments (New Castle, DE, USA) and density, estimated by the mass/volume method (**Figure 3-14**). The results agreed with the degree of branching values obtained *via* Si NMR and molecular weight. **PEOS 1.2**, which possessed the highest DB and M_W, also possessed the highest viscosity and density.

References to this Chapter on pages 119-120

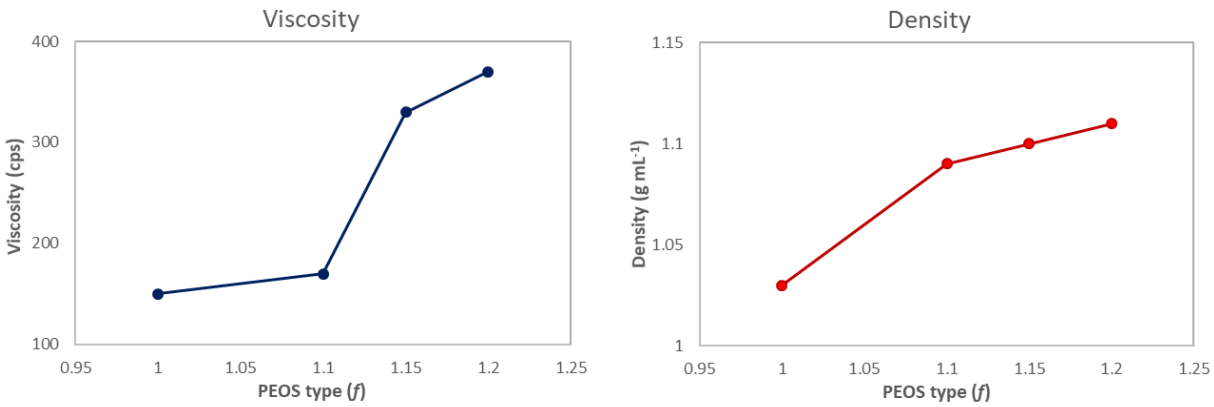

***Figure 3-14**. Viscosity and density values for PEOS samples produced with different fractions of acetic anhydride.*

3.3 Conclusions

In this chapter, the role of emulsion stabilisation was investigated with the support of experiments that demonstrate the Pickering stabilisation phenomenon, as well as the possibility of forming oil-in-water, water-in-oil or double emulsions depending on the wetting properties of the solid SiO_2 nanoparticles. The three-phase contact angle is the key parameter to form highly stable emulsions. However, the stability is also controlled by the size and wettability of the SiO_2 nanoparticles and the polarity of the oil.

It was possible to take advantage of the limited coalescence phenomenon to control the size and size distribution for emulsions formed with both PO and HS using hydrophilic SiO_2 nanoparticles as Pickering emulsifier. As the oil droplet size was finely controlled, it was clear that hydrophilic silica nanoparticles are efficient Pickering emulsifiers for both oils. It was also possible to confirm that a monolayer of SiO_2 is formed around the droplets and the result was in agreement with the literature.[15]

References to this Chapter on pages 119-120

PEOS was synthesised and characterized using multiple techniques (IR, NMR, GPC and Rheology). Si NMR was especially useful to identify the different silicon atom environments and degree of branching, showing that these can be controlled by manipulating the fraction of TEOS to acetic anhydride and to produce PEOS with variable molecular weight, DB, viscosity and density.

Overall it was concluded that it is possible to stabilise PO and HS emulsions using hydrophilic SiO_2 NPs. These Pickering emulsions will be used as templates for the formation of silica capsules together with PEOS as silica precursor to cross-link the SiO_2 NPs and seal the voids between the nanoparticles, with the objective of forming mechanically stable SiO_2 capsules with minimal leakage of the encapsulated oil, which will be discussed in Chapter 4.

3.4 Experimental

3.4.1 Emulsions stability

Two glass vials were charged with DI water (5 ml) and HS containing 0.1wt% of PM546 (oil soluble dye – full description in Chapter 2, Section 2.2.1) (5 ml). SiO_2 NPs (0.1g , A300) were added to one of the vials and both were homogenized using a vortex mixer operating at 2500 RPM for 5 minutes. The resulting emulsions were allowed to stand on the bench top and photographed immediately and after 60 seconds. Microscopy images were also obtained. The same procedure was repeated for the hydrophobic nanoparticles (AR816).

3.4.2 Limited coalescence phenomenon study

Emulsions were prepared by mixing PO or HS (2g) and DI water (8 ml) containing different fractions of Aerosil 300, relatively to the oil phase (1.7, 3.4 and 6.8 wt%), and homogenizing at 2500 RPM using a vortex mixer for 5 minutes. The emulsions were allowed to rest on the

References to this Chapter on pages 119-120

bench top for the limited coalescence phenomenon to take place for 2 hours and optical microscopy and size distribution analysis (Mastersizer) was carried out.

3.4.3 Synthesis of hyperbranched polyethoxysiloxane (PEOS)

Hyperbranched polyethoxysiloxane (**PEOS**) was synthesized as described by Xiaomin *et al.*[9] (**Equation 3-10**). A 250ml two-neck round bottom flask was charged with TEOS (19.5 ml, 0.1 mmol), acetic anhydride (1.0 to 1.2 molar ratio to TEOS) and titanium trimethylsiloxide (0.3 mol% to TEOS), under an N_2 atmosphere. Different molar ratios (f = 1.0, 1.1, 1.15 and 1.2) between TEOS and acetic were used to produce **PEOS** with variable molecular weight. The resulting solution was heated to 135°C and stirred at 400 RPM. As the reaction proceeded, ethyl acetate boiled off over ~24 hours, after which the reaction was allowed to cool to room temperature.

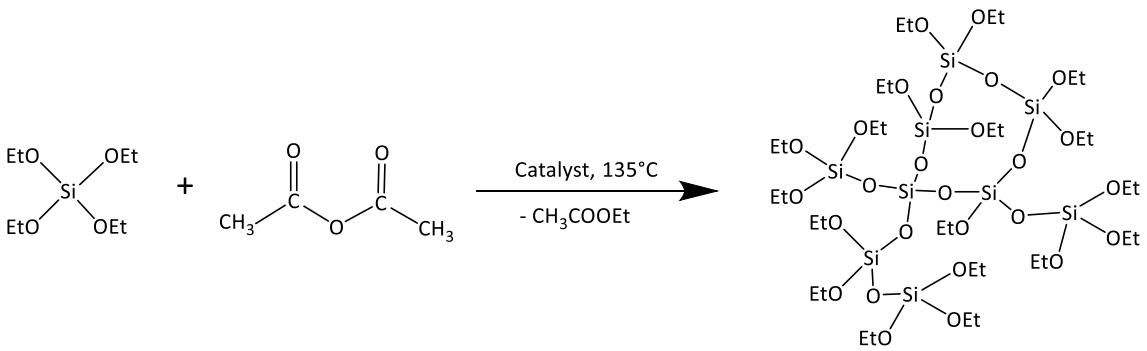

***Equation 3-10**. PEOS formation from the reaction between TEOS and acetic anhydride in the presence of a catalyst at 135°C.*

3.4.4 PEOS characterisation

3.4.4.1 Infrared spectroscopy

IR spectra were recorded as neat oils between the wave numbers 650-4000 cm^{-1} on a PerkinElmer Spectrum 100 PT-IR equipped with an ATR detector and processed by

References to this Chapter on pages 119-120

PerkinElmer Spectrum software. Samples were added directly to the ATR crystal prior measurement. An air background was taken before measuring the samples.

3.4.4.2 ^{1}H NMR

^{1}H NMR spectra were recorded on a Bruker Avance III 300 MHz with the samples dissolved in $CDCl_3$. The data was processed using Topspin software v 2.1. Chemical shifts are reported as δ values relative to $CDCl_3$ at δ_H = 7.27 ppm.

3.4.4.3 ^{29}Si NMR

^{29}Si NMR spectra were obtained using a Bruker 400Hz Avance III HD NMR operating with a Prodigy liquid nitrogen cooled probe, located at Procter and Gamble Great London Innovation Centre, with samples dissolved $CDCl_3$, containing 0.015M chromium acetylacetonate as a relaxation agent.

3.4.4.4 Gel permeation chromatography

To obtain the molecular weight and PDI of the different PEOS molecules, a Waters 2695 GPC equipped with a Waters 2414 Refractive Index Detector and a Wyatt Dawn Heleos II light scattering detector was used. A Toluene solvent system was used with TOSOH TSKGel HHR series ranging from 1,000 Da to 60,000 Da with a pore size of 5 µm and 2 nm. Twelve polystyrene standards were used to create a calibration curve and estimate the molecular weight of the different PEOS molecules based on their elution volumes.

3.4.4.5 Viscosity

Viscosity of liquid PEOS products was measured using an AR 550 rheometer/viscometer from TA Instruments (New Castle, DE, USA), using parallel steel plates of 40 mm diameter and a

References to this Chapter on pages 119-120

gap size of 500 µm. The high shear viscosity at 20 s^{-1} and low shear viscosity at 0.05 s^{-1} was obtained from a logarithmic shear rate sweep from 0.1 s^{-1} to 25 s^{-1} in 3 minutes at 21 °C.

3.4.4.6 Density

Density of PEOS was estimated by the mass/volume method; PEOS was added to a pre-weighted 10 ml volumetric flask. The container was re-weighted and the corresponding mass of PEOS noted. The PEOS mass was divided by the volume of the flask and the density calculated.

3.5 References

1. A. D. Dinsmore, M. F. Hsu, M. G. Nikolaides, M. Marquez, A. R. Bausch and D. A. Weitz, *Colloidosomes: Selectively Permeable Capsules Composed of Colloidal Particles*, *Science*, **2002**, *298*, 1006-1009.
2. M. Williams, B. Olland, S. P. Armes, P. Verstraete and J. Smets, *Inorganic/Organic Hybrid Microcapsules: Melamine Formaldehyde-Coated Laponite-Based Pickering Emulsions*, *Journal of Colloid and Interface Science*, **2015**, *460*, 71-80.
3. Y. Long, B. Vincent, D. York, Z. Zhang and J. A. Preece, *Organic–Inorganic Double Shell Composite Microcapsules*, *Chemical Communications*, **2010**, *46*, 1718-1720.
4. P. H. R. Keen, N. K. H. Slater and A. F. Routh, *Encapsulation of Amylase in Colloidosomes*, *Langmuir*, **2014**, *30*, 1939-1948.
5. D. J. McClements and S. M. Jafari, *Improving Emulsion Formation, Stability and Performance Using Mixed Emulsifiers: A Review*, *Advances in Colloid and Interface Science*, **2018**, *251*, 55-79.
6. Y. Chevalier and M.-A. Bolzinger, *Emulsions Stabilized with Solid Nanoparticles: Pickering Emulsions*, *Colloids and Surfaces A: Physicochemical and Engineering Aspects*, **2013**, *439*, 23-34.
7. S. Arditty, C. P. Whitby, B. P. Binks, V. Schmitt and F. Leal-Calderon, *Some General Features of Limited Coalescence in Solid-Stabilized Emulsions*, *The European Physical Journal E*, **2003**, *11*, 273-281.
8. Y. Abe and T. Gunji, *Oligo- and Polysiloxanes*, *Progress in Polymer Science*, **2004**, *29*, 149-182.
9. X. Zhu, M. Jaumann, K. Peter, M. Möller, C. Melian, A. Adams-Buda, D. E. Demco and B. Blümich, *One-Pot Synthesis of Hyperbranched Polyethoxysiloxanes*, *Macromolecules*, **2006**, *39*, 1701-1708.
10. Y. Zhao, Z. Chen, X. Zhu and M. Möller, *Silica Nanoparticles Catalyse the Formation of Silica Nanocapsules in a Surfactant-Free Emulsion System*, *Journal of Materials Chemistry A*, **2015**, *3*, 24428-24436.

11. B. P. Binks, P. D. I. Fletcher, B. L. Holt, P. Beaussoubre and K. Wong, *Phase Inversion of Particle-Stabilised Perfume Oil-Water Emulsions: Experiment and Theory*, *Physical Chemistry Chemical Physics*, **2010**, *12*, 11954-11966.
12. B. P. Binks and C. P. Whitby, *Nanoparticle Silica-Stabilised Oil-in-Water Emulsions: Improving Emulsion Stability*, *Colloids and Surfaces A: Physicochemical and Engineering Aspects*, **2005**, *253*, 105-115.
13. R. Aveyard, B. P. Binks and J. H. Clint, *Emulsions Stabilised Solely by Colloidal Particles*, *Advances in Colloid and Interface Science*, **2003**, *100–102*, 503-546.
14. M. Baillot, A. Bentaleb, E. Laurichesse, V. Schmitt and R. Backov, *Triggering the Mechanical Release of Mineralized Pickering Emulsion-Based Capsules*, *Langmuir*, **2016**, *32*, 3880-3889.
15. M. Destribats, B. Faure, M. Birot, O. Babot, V. Schmitt and R. Backov, *Tailored Silica Macrocellular Foams: Combining Limited Coalescence-Based Pickering Emulsion and Sol–Gel Process*, *Advanced Functional Materials*, **2012**, *22*, 2642-2654.
16. S. Sakamoto, A. Shimojima, K. Miyasaka, J. Ruan, O. Terasaki and K. Kuroda, *Formation of Two- and Three-Dimensional Hybrid Mesostructures from Branched Siloxane Molecules*, *Journal of the American Chemical Society*, **2009**, *131*, 9634-9635.
17. A. Shimojima, Z. Liu, T. Ohsuna, O. Terasaki and K. Kuroda, *Self-Assembly of Designed Oligomeric Siloxanes with Alkyl Chains into Silica-Based Hybrid Mesostructures*, *Journal of the American Chemical Society*, **2005**, *127*, 14108-14116.
18. D. Hölter, A. Burgath and H. Frey, *Degree of Branching in Hyperbranched Polymers*, *Acta Polymerica*, **1997**, *48*, 30-35.

CHAPTER 4. Preparation and Characterisation of Mechanically Robust SiO_2 Shell Capsules from Oil-in-Water Pickering Emulsions – Encapsulation of Hexyl Salicylate

Abstract

In this chapter, an oil phase composed of hexyl salicylate (HS) and hyperbranched polyethoxysiloxane (PEOS) and an aqueous phase containing hydrophilic fumed silica nanoparticles (SiO_2 NPs) are emulsified forming a stable oil-in-water emulsion. The SiO_2 nanoparticles undergo a spontaneous cross-linking and void-filling of the SiO_2 nanoparticles at the oil-water interface takes place, *via* the hydrolysis of the PEOS at the oil-water interface, followed by subsequent crosslinking of the PEOS and between the SiO_2 nanoparticles. Thus, not only is a mechanically robust SiO_2 shell formed, but also one in which the voids between the SiO_2 nanoparticles are filled, leading to encapsulating the hexyl salicylate in water with very little leakage. In addition, the SiO_2 capsules could be dried and redispersed in water.

The SiO_2 capsules were characterized in terms of mean dimeter, SPAN, shell morphology and thickness, payload, encapsulation efficiency, release profile and mechanical properties. Encapsulation parameters, such as pH, SiO_2 nanoparticles and PEOS concentration were varied in order to establish the optimal conditions for the formation of a shell with improved mechanical properties and size distribution. As a result, capsules produced at lower pH had a narrow size distribution and a well-defined shell. On the other hand, high concentrations of PEOS led to the formation of a more mechanically resistant shell; however, the formed shell was highly porous and hexyl salicylate leaked quickly when the capsules were dispersed in liquid detergent matrix.

 References to this Chapter on pages 162-163

4.1 Introduction

Generally, micron-scale capsules, which have been of intense research interest for many decades,[1-5] are comprised of a shell to separate, control leakage/controlled delivery and protect an 'active' solid, liquid- or gas-filled interior from the surrounding environment. Furthermore, to be functional they need to allow a triggered release of the 'active' at a specified time and place to give the desired functionality. Such structures may be used for the encapsulation of a wide variety of compounds, including fragrances,[1, 2] pharmaceuticals,[3] food additives,[4] or catalysts.[5]

In order to satisfy the sophisticated requirements that the shell must possess, for specific technologies, it has to have chemistries and mechanical properties to control leakage through the shell and rupture of the shell. In terms of fragrance encapsulation for the laundry industry the following properties are important:

(i) The capsules must survive breakage during various processing and handling steps, where mechanical forces are generated in the wash-cycle, such as pumping, mixing washing and drying, but they should break by the mechanical forces generated when the consumer is handling/wearing the fabric to give a sensation of freshness.[6]

(ii) The perfume capsules should not leak during storage (shelf-life) in the liquid detergent matrix, whilst also maintaining the mechanical properties in point (i).

Melamine-formaldehyde capsules were found to accomplish these properties better than other materials.[7] More recently, other types of shell chemistries based on acrylate polymers were also developed and showed good leakage resistance in detergent matrix.[8] However,

 References to this Chapter on pages 162-163

both technologies are based on organic polymers and are considered micro-plastics, hence facing being banned from consumer products in Europe and some Asian countries.[9] This legislation is likely to be followed by the rest of the world. Therefore, there is a need for new technologies to encapsulate perfume for laundry products using more sustainable and ecologically less damaging capsule shells. These could be based on biodegradable polymeric or inorganic shells, or a combination of both.

Pickering emulsions are formed *via* self-assembly of solid nanoparticles at the interface between two immiscible phases such as oil and water.[10] These types of emulsions can advantageously be used as templates for the formation of fully inorganic capsules due to:

(i) their remarkable high resistance to coalesce,

(ii) facile formation,

(iii) low-cost, and

(iv) range of biocompatible and environmentally friendly materials which can be used.[11]

4.1.1 Aim of research in this chapter

In this chapter, the initial aim was to prepare and characterise Pickering emulsion-based SiO_2 capsules encapsulating hexyl salicylate (HS) as perfume model using silica nanoparticles (SIO_2 NPs) as emulsifier (Chapter 3) and PEOS the agent to cross-link (Chapter 3) the interface attached SiO_2 nanoparticles. The concentration of SiO_2 NPs, the concentration of PEOS and the continuous phase pH were varied to understand how these three parameters affect the SiO_2 capsule formation in terms of size, size distribution, mechanical properties and stability in liquid detergents.

References to this Chapter on pages 162-163

Since perfume are complex mixtures of volatile organic oils that usually have variable polarities and densities, which can potentially affect emulsion stability and the formation of the shell, a single fragrance component (one molecular structure) was initially used for the development of an encapsulation method *via* the Pickering emulsion approach using SiO_2 NPs as the emulsion stabiliser, prior to their cross-linking, to afford SiO_2 capsules. HS was selected as the single fragrance component as it is one of the main components of perfume formulations in detergent applications.[12] HS is also a well-defined model found in the literature[13] to describe encapsulation efficiency and release profile.

4.1.2 SiO_2 capsule formation mechanism

The SiO_2 capsule formation mechanism is a delicate interplay between emulsion stability, oil polarity and sol-gel kinetics and can be divided in three key steps:

1. formation of O/W Pickering emulsion;
2. hydrolysis of PEOS at the O/W interface;
3. condensation of PEOS to cross-link the SiO_2 nanoparticles.

Figure 4-1 shows a scheme representing the hypothesised steps for the formation of SiO_2 capsules using the Pickering emulsion plus PEOS approach and HS as core material, which brings both parts of the research described in **Chapter 3** together.

References to this Chapter on pages 162-163

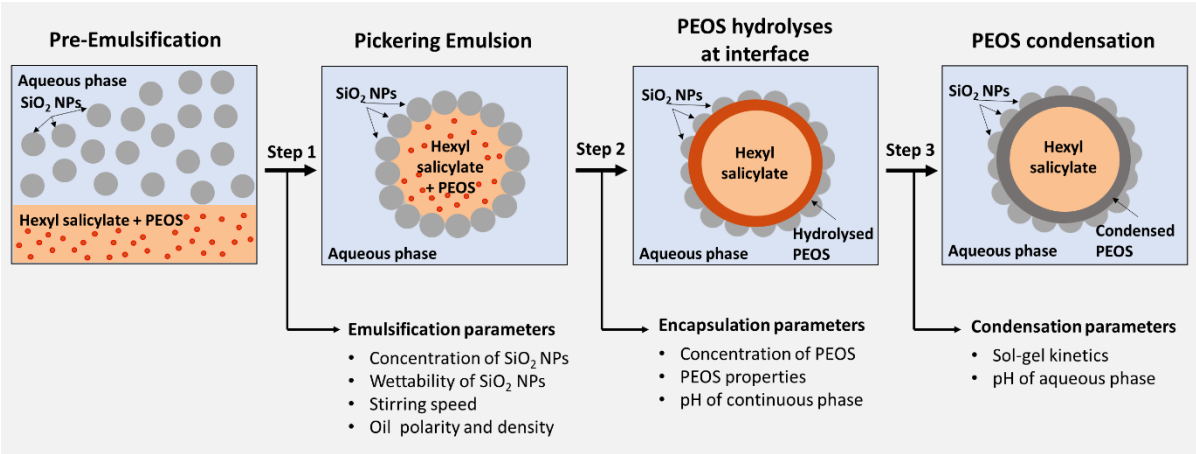

Figure 4-1. *Proposed route for making SiO_2 capsules. Step 1: a Pickering emulsion between hexyl salicylate containing PEOS and an aqueous phase containing SiO_2 NPs was prepared. Step 2: PEOS hydrolyses at the oil-water interface. Step 3: PEOS crosslinks via condensation reaction at the interface, not only linking the SiO_2 NPs, to impart mechanical strength, but also filling the voids between the SiO_2 NPs to reduce HS leakage.*

4.1.2.1 Step 1. Formation of the Pickering emulsion

Starting with the pre-emulsification; the Pickering emulsifier (SiO_2 NPs) is dispersed in the continuous aqueous phase, of known w/v, and PEOS is dispersed in HS, of known v/v to form the dispersed oil phase (**Figure 4-2A**). Then, the Pickering emulsion is formed (**Figure 4-1, Step 1**), *via* the homogenisation of the two phases leading to the formation of an oil-in-water emulsion (**Figure 4-2B**), stabilized by the self-assembly of SiO_2 NPs at the oil-water interface, lowering the interfacial energy, to form the Pickering emulsion (**Figure 4-2C**).

For this step the wettability of the SiO_2 NPs and the oil polarity are key to ensure a high emulsion stability. The concentration ratio of SiO_2 NPs to the oil phase and the stirring method can be varied to control the size and size distribution of the Pickering emulsion droplet.

References to this Chapter on pages 162-163

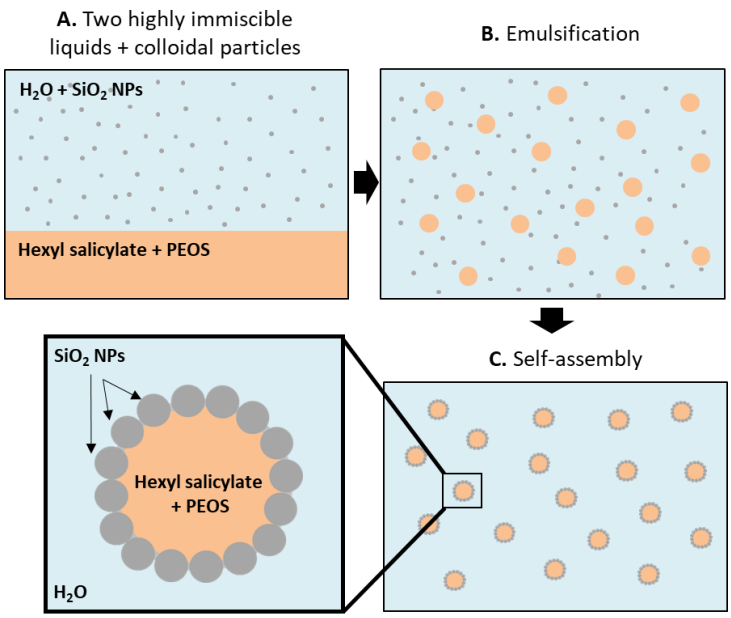

***Figure 4-2**. Simplified scheme of Pickering emulsion formation (**Step 1**) from SiO_2 NPs and PEOS. First, an aqueous dispersion containing SiO_2 NPs is prepared. Then, PEOS is mixed with HS in a separated vial (A). The aqueous and oil phases are then homogenised forming an O/W emulsion (B). The Pickering emulsifiers then self-assemble at the water-oil interface lowering the interfacial energy and stabilising the emulsion (C).*

4.1.2.2 Steps 2 and 3: PEOS hydrolysis and condensation at the O/W interface

During **Step 2**, the PEOS dispersed within the oil phase starts to hydrolyse as it contacts the O/W interface. Upon hydrolysis, the hydrophobic ethoxysilane groups convert to hydrophilic silanol groups, with an affinity towards water, adhering it to the O/W interface (**Figure 4-3A**). The hydrolysed PEOS then cross-links both between itself (ethoxysilane and silanol groups) and the surface of the SiO_2 NPs (silanol groups), creating a polymerised PEOS layer at the interface (**Step 3**), and on the SiO_2 NPs surface, which continues to grow to fill the voids between the SiO_2 NPs (**Figure 4-3B**), leading to a solid shell imparting mechanical strength to the SiO_2 capsule, as well as creating a barrier to stop HS leaking.

References to this Chapter on pages 162-163

Hydrolysis and condensation kinetics play an important role when forming a robust solid SiO_2 capsule shell, as it can affect the quality of the formed SiO_2 capsule in terms of porosity and mechanical properties.[14] The type of silica precursor used can ultimately influence the kinetics, as it must be interfacially active for effective hydrolysis and condensation to take place. Other parameters that can influence the kinetics are the interfacial tension[15] between the oil (controlled by the polarity of the oil) and the water and the pH[16] - both affecting the interfacial activity of PEOS.

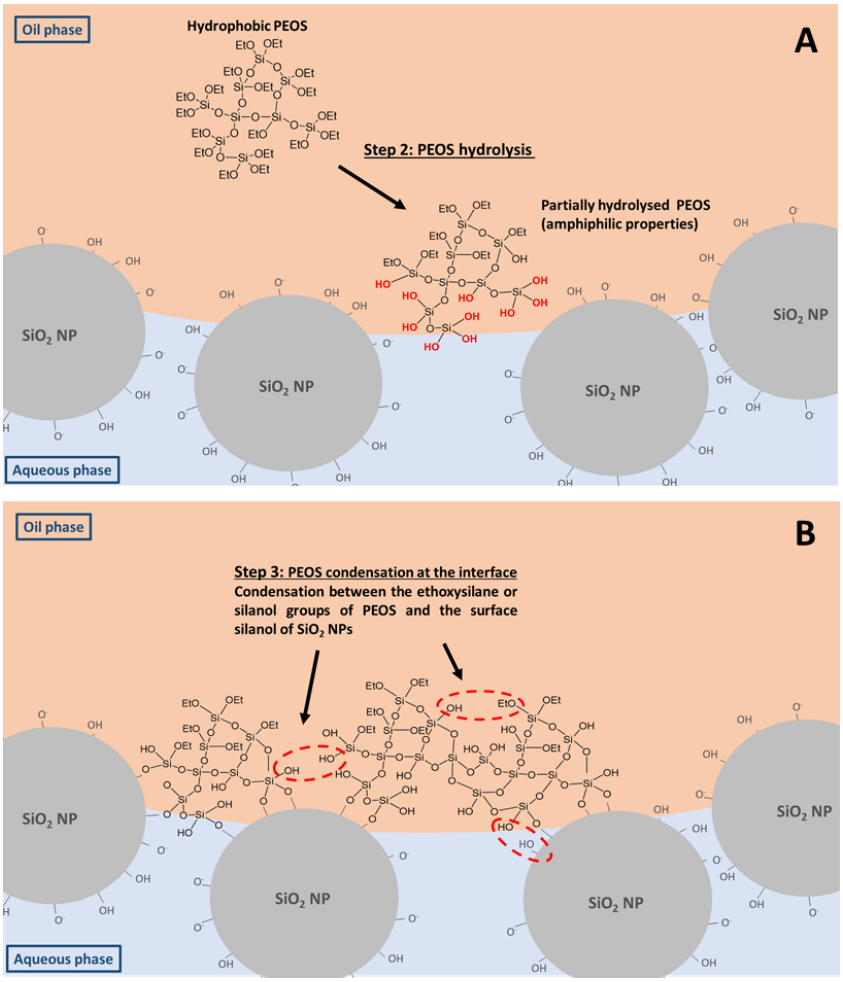

***Figure 4-3**. (A) Scheme representing the hydrolysis of PEOS at the O/W interface as it becomes partially hydrophilic and adherent to the interface (**Step** 2) and (B) condensation process of*

References to this Chapter on pages 162-163

*PEOS at the O/W interface of the droplet solidifies the PEOS, crosslinks the SiO_2 NPs and fills the voids between them (**Step 3**).*

4.1.2.3 The effects of pH

The process as a whole depends strongly on the pH of the aqueous phase, which controls not only the interfacial activity of the PEOS (and its hydrolysis and condensation rates), but also of the SiO_2 nanoparticles, by affecting the surface charge, as shown in **Figure 4-4.**

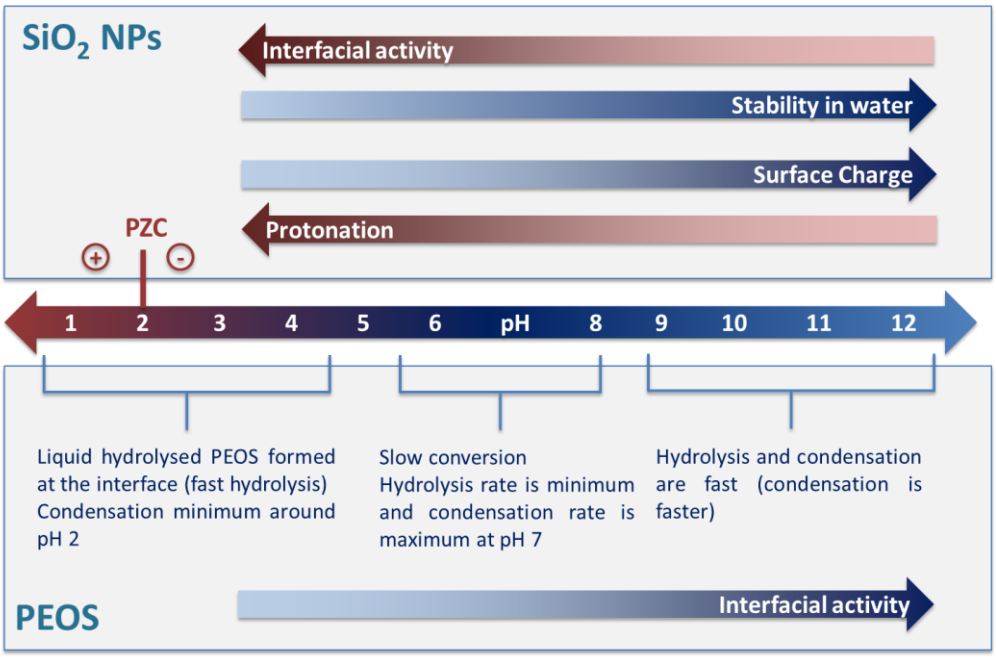

Figure 4-4. *Illustration of the interfacial activity of SiO_2 nanoparticles and PEOS at different pHs, as well as the expected PEOS hydrolysis and condensation rates at the interface. The point of zero charge (PZC) for the SiO_2 nanoparticles is also represented (value from the supplier).*

From **Figure 4-4**, the pH can affect the surface charge of the hydrophilic SiO_2 NPs;[17] at higher pH values the SiO_2 NPs tend to have a negative surface charge (deprotonation of Si-OH groups to Si-O^-), leading to a higher stability in the continuous water phase and, consequently, less interfacial activity. The opposite is true for lower pH values. In this case, the surface silanol

References to this Chapter on pages 162-163

groups become protonated (Si-OH), and increasing the interfacial activity of the SiO_2 NPs until the pH reaches the point of zero charge. Further decrease of the pH leads to further protonation of the surface silanol groups ($Si\text{-}OH_2^+$) and the surface becomes positively charged.[17]

For PEOS the interfacial activity tends to increase with the increase of the pH, as it becomes deprotonated it has more affinity towards the water phase.[18] In addition both the hydrolysis and condensation rates depend on the pH as expected for silicon alkoxides in general (Chapter 1 - section 1.4.3.2).[19] For the hydrolysis step, the maximum rate is obtained at low pH, the minimum at pH 7 and at high pH the rate is high as well. For the condensation step on the other hand, at very low pH (around zero), the condensation rate is high but not as high as the hydrolysis rate. At pH 2 the condensation rate is minimum, after that the rate starts to increase again and it reaches the maximum at pH 7. At higher pH the rate is as high as for the hydrolysis.

Usually acidic or alkaline catalyses are used for the sol-gel process. For PEOS, at a low pH a hydrolysed PEOS layer is formed around the droplet and hydrolysis is complete before condensation starts. At neutral pH (around 7) on the other hand, the condensation rate reaches the maximum and hydrolysis minimum, which leads to the condensation of the PEOS molecules as they undergo hydrolysis. Finally, at high pH both hydrolysis and condensation rates are fast, which could lead to highly porous structures.[14] From these considerations, the ideal pH for the formation of Pickering based SiO_2 capsules using hydrophilic SiO_2 NPs and PEOS could be optimised to ensure high interfacial activity of both SiO_2 NPs and PEOS as well

References to this Chapter on pages 162-163

as an optimal hydrolysis and condensation rate of PEOS leading to the formation of a well-defined silica shell with a low porous structure.

4.2 Results and Discussion

4.2.1 Preparation and characterization of SiO_2 capsules encapsulating HS

SiO_2 capsules were formed using:

(i) HS as the oil phase, containing 20 wt% dispersed PEOS and 0.1 wt% of a green fluorescent dye (PM546), and

(ii) 1 wt% hydrophilic SiO_2 NPS as Pickering emulsifier dispersed in DI water as continuous phase (named, SiO_2 NPs_1-$PEOS_{20}$-HS).

The initial Pickering emulsion was formed *via* the homogenisation of the two phases using a vortex mixer at 2500 RPM for 5 min, at 25°C. The pH of the aqueous phase was 4, as a result of the SiO_2 NPs (Aerosil 300) being naturally acidic, due to their preparation process (see Chapter 2 – section 2.2.2). SiO_2 capsules were then fully characterized, as described below.

4.2.2 Morphology

4.2.2.1 Optical Microscopy

The optical and fluorescence microscope images are shown in **Figure 4-5A** and **B**, respectively. Clearly, it was possible to observe that the SiO_2 NPs_1-$PEOS_{20}$-HS capsules were fluorescing and hence filled with the dye doped HS, and that there was no free HS visible in the continuous aqueous phase after Step 3 in **Figure 4-1** (**Figure 4-5B)**.

References to this Chapter on pages 162-163

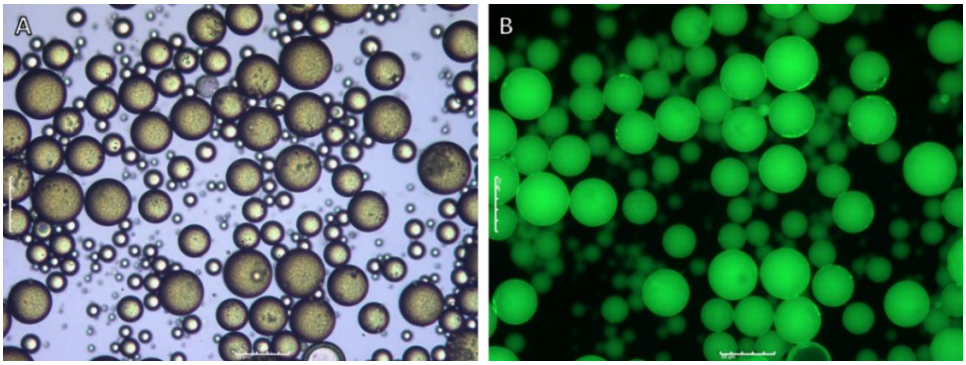

***Figure 4-5**. Optical (A) and Fluorescent (B) images of SiO_2 NPs_1-$PEOS_{20}$-HS loaded with hexyl salicylate containing 0.1 wt% PM546. Scale bar: 50µm*

4.2.2.2 Scanning electronic microscopy (SEM)

SEM is a powerful tool to analyse the surface morphology of a capsule shell. **Figure 4-6** shows the SEM images for the SiO_2 NPs_1-$PEOS_{20}$-HS capsules. First, it is possible to observe that the capsules formed were smooth and spherical indicating there were mechanically stable, as the surface did not shrink under the vacuum imposed by the SEM chamber. In addition, the SEM image of a broken capsule (rare) suggested the formation of a core-shell like structure (**Figure 4-6B**).

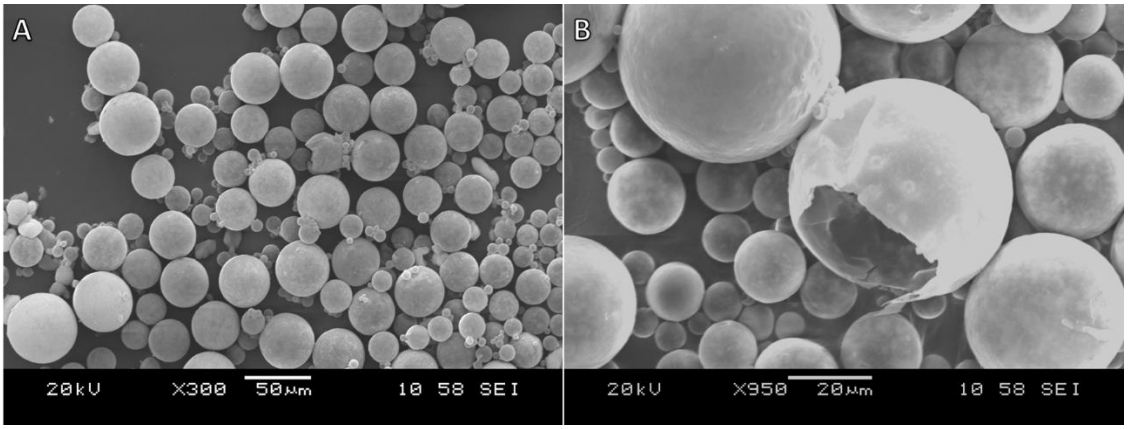

***Figure 4-6**. SEM micrographs of SiO_2 NPs_1-$PEOS_{20}$-HS capsules. Scale bar is 50 µm in micrograph (A) and 20 µm in (B).*

References to this Chapter on pages 162-163

4.2.3 Capsule size distribution

The average mean volume-based diameter and SPAN of the size distribution were 41.1 ± 0.5 µm and 1.032 ± 0.06 for the SiO_2 NPs_1-$PEOS_{20}$-HS capsules, respectively. The size distribution of these SiO_2 capsules was relatively narrow, which demonstrates that even when HS was mixed with PEOS prior to emulsification (**Step 1**,**Figure 4-1**) the size distribution of the emulsion could still be controlled by the concentration of SiO_2 NPs in relation to the volume of oil, in agreement with the observations in Chapter 4 - Section 4.2.1. Moreover, the mean diameter from the Mastersizer was in good agreement with the optical microscopy and SEM images.

4.2.4 Payload and encapsulation efficiency

The Payload and Encapsulation Efficiency (EE) were calculated using **Equation 4-1** and **Equation 4-2,** respectively. The payload estimates what percentage of the total SiO_2 NPs_1-$PEOS_{20}$-HS capsule is composed of core material, while the Encapsulation Efficiency, EE, gives the percentage of oil initially encapsulated during **Step 1 (Figure 4-1**).

$$Payload = \frac{m_{c,samp}}{m_{samp}} \qquad \textbf{\textit{Equation 4-1}}$$

$$EE(\%) = 100\% \times \frac{m_a}{m_o} = 100\% \; x \; \frac{\frac{m_{c,samp}}{m_{samp}}}{\frac{m_c}{m_c+m_s}}, \qquad \textbf{\textit{Equation 4-2}}$$

where $m_{c,samp}$ = mass of core material in the capsules; m_c = mass of core material used for encapsulation; m_a = actual loading; m_o = theoretical loading; m_{samp} = mass of sample and m_s = mass of shell material used for encapsulation. The obtained values were:

- Payload: 82.1 ± 0.6 %

References to this Chapter on pages 162-163

- EE: 99.4 ± 0.4%

The high encapsulation efficiency is expected for Pickering emulsion based SiO_2 capsules as the SiO_2 NPs tend to be trapped at the O/W interface irreversibly, which leads to a high emulsion stability during the capsule formation, allowing the oil to be fully encapsulated.[20]

4.2.5 Shell thickness and inner morphology

The shell thickness was estimated using multiple SEM images of broken SiO_2 NPs_1-$PEOS_{20}$-HS capsules cross-section and ImageJ software. An example of such image can be found at **Figure 4-7**. The average shell thickness was 0.5 ± 0.1 µm. As the SiO_2 NPs used had a primary size of about 10 nm, which form aggregates of about 100 to 200 nm, this result implies that the shell thickness is made mainly of condensed PEOS, so PEOS is not only crosslinking the SiO_2 nanoparticles and filling the voids, but also forming a thick condensed SiO_2 layer. A theoretical calculation was used to validate this speculation as it calculates the thickness of a shell formed only by a condensed SiO_2 precursor (**3**).[21]

$$4\left[\frac{4}{3}\pi {R_c}^3 - \frac{4}{3}\pi(R_c - d_s)^3\right]\rho_s = S\frac{4}{3}\pi(R_c - d_s)^3\,\rho_c, \qquad \textbf{\textit{Equation 4-3}}$$

where R_c = Mean radius of the capsules, ρ_s = Density of hydrated SiO_2, ρ_c = Density of the core material, S = SiO_2 content of PEOS (in this case 50.2% was assumed - from Chapter 3 data), d_S = shell thickness, assuming that the core material is pure and it occupies the whole cavity of the SiO_2 capsule. The shell thickness value from **Equation 4-3** was 0.4 µm, which was very close to the value from the SEM images, confirming that the shell thickness is mainly made of condensed PEOS added to a monolayer of SiO_2 NPs of about 100 nm.

References to this Chapter on pages 162-163

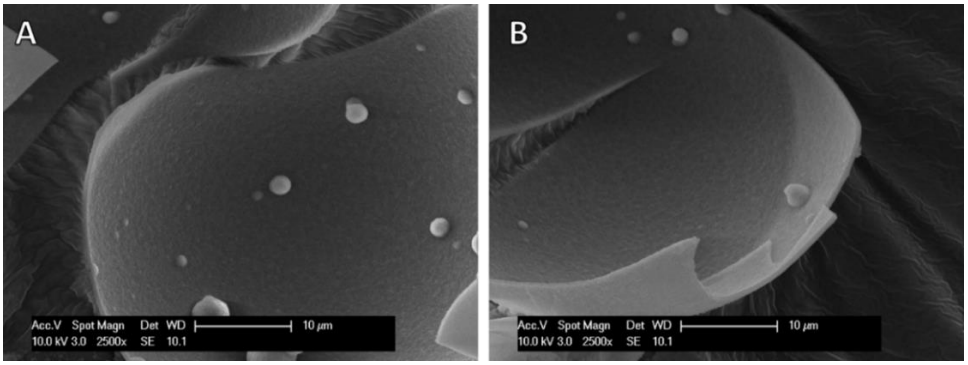

***Figure 4-7**. Close-up SEM images of broken SiO_2 NPs_1-$PEOS_{20}$-HS capsules. Scale bar 10 µm.*

SEM images (**Figure 4-7**) could also give valuable information regarding the inner morphology of the shell. The inner surface was smooth, but also contained some ~1 um globular structure, which might be due to the hydrolysis and condensation of an excess of PEOS in the inner core. According to the literature,[22] the growth of the PEOS layer is from the outside towards the inside of the core, as water migrates through the hydrolysed PEOS layer before full condensation, the globular structures could have been formed as a result of extra water migration in some points of the shell.

4.2.6 Release profile

One of the most important properties of capsules used for consumer goods applications is the capability of the capsule to retain the encapsulated active inside the shell for weeks or months without any leakage. Therefore, it is of great importance to test the shell permeability over time and obtain the release profile of the capsule. Hexyl salicylate has only a small solubility in water (~10^{-6} g mL^{-1}), hence it was preferable to use a solvent capable of increasing the solubility of HS, in order to observe the release profile of HS from the SiO_2 capsules over a shorter timeframe than if just water was used. The chosen solvent should:

(i) not damage the SiO_2 capsule shell;

(ii) be miscible with the slurry continuous phase, in this case water;

(iii) be compatible with the detection method (here UV radiation being adsorbed by the aryl moiety in HS).

The solvent identified to fulfil these criteria were aqueous-base solutions with low molecular weight alcohols. According to the literature,[13] an appropriate solvent is one that the solubility concentration, c_s is around 2 x 10^{-2} to 2 x 10^{-4} g mL^{-1}. The co-solvent used was propan-1-ol at a level of 36 volume %, which gives a c_s of 0.002 g mL^{-1}. The mass HS released from the SiO_2 capsules was obtained using the HS absorbance max at 305 nm and the calibration curve in **Figure 4-24**.

Figure 4-8 shows the release profile of HS in 36% propan-1-ol aqueous solution over time. It was possible to observe that the release over the first 30 days is quasi linear, after which it slows until it reaches 100% HS release after 60 days. Presumably, the mesoporosity of the shell material (as in amorphous SiO_2 materials in general), is the route by which the HS passes into the continuous phase.

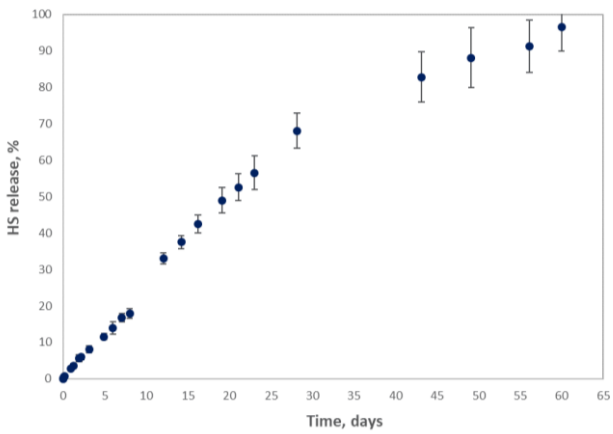

***Figure 4-8**. Release profile of hexyl salicylate in 36% propa-1-ol aqueous solution over time. The absorbance max used was 305 nm.*

References to this Chapter on pages 162-163

Figure 4-9 shows the SiO_2 capsules before and after complete release, which gives further evidence that the SiO_2 capsules were completely emptied while maintaining an intact solid SiO_2 shell, demonstrating that the co-solvent did not mechanically damage the SiO_2 capsule shell during the experiment period.

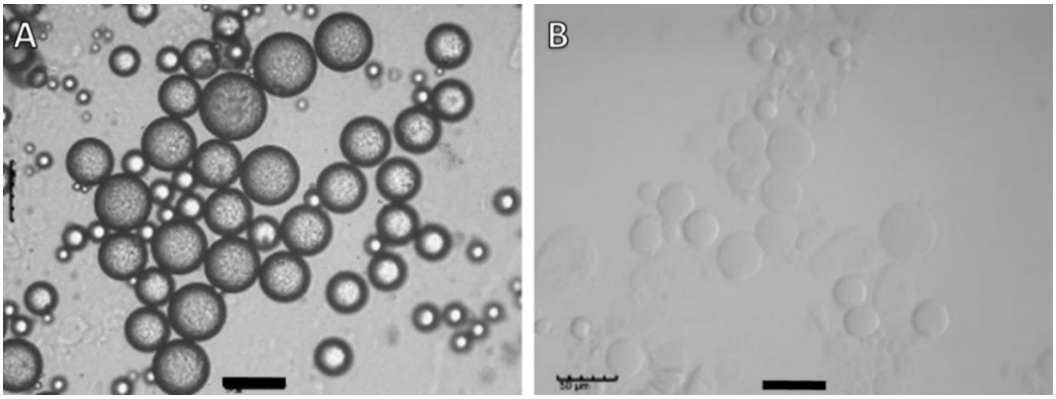

***Figure 4-9**. SiO_2 NPs_1-$PEOS_{20}$-HS capsules before (A) and after (B) release profile experiment using 36% propan-1-ol in water. Scale bar 50 µm.*

The permeability of the SiO_2 capsule can be extracted by fitting **Equation 4-4** to the initial linear region of the HS% release graph[13] (**Figure 4-10**), assuming a relatively narrow size distribution of the SiO_2 capsules as the permeability is a function of the mean diameter of the SiO_2 capsules:

$$R(t) = \frac{6}{d\rho_{oil}} \frac{P}{h} C_s t \qquad \textbf{Equation 4-4}$$

where, *R(t)* is the release as a function of time, *d* the capsule mean diameter, ρ_{oil} the density of the encapsulated oil, *P* the permeability of the shell, *h* the shell thickness, C_s the oil solubility in the continuous phase and *t* the time. Considering a constant shell thickness for

References to this Chapter on pages 162-163

the SiO_2 capsules of 500 nm, the permeability was found to be 5.3 X 10^{-16} m^2s^{-1}. Amorphous SiO_2 materials are known for their high porosity, so the low permeability value is an encouraging result. This low porosity is probably due to a high degree of cross-linking during condensation of PEOS at the interface forming a thick solid SiO_2 capsule shell that was capable of retaining HS for 60 days in water/propan-1-ol media.

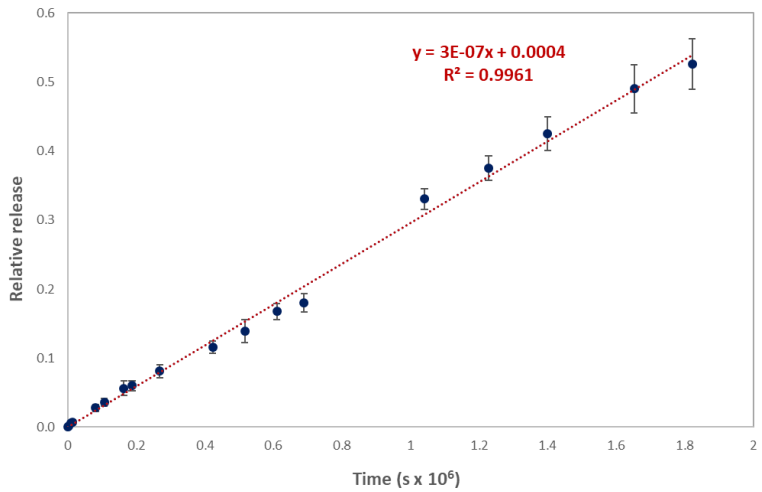

***Figure 4-10**. Relative release of the initial linear regime of Figure 4-8 (R < 0.6). Model parameters: $P/h = 1.07 \times 10^{-9}$ m/s^{-1}, $C_s = 0.002$ $g.mL^{-1}$, $d = 41$ µm and $\rho_{oil} = 1.04$ $g.mL^{-1}$*

4.2.7 Trigger release

For many consumer good applications, such as laundry products, it is necessary that the capsules completely release their content by mechanical force at a desired place/time, *e.g.* by mechanical breakage on cleaned dry garments or hair. To observe the SiO_2 capsules releasing its content over time after their fracture, an experiment was designed using optical microscopy, whereby SiO_2 capsules containing HS and PM546 (fluorescent dye) were placed on the surface of a glass slide, and a glass cover was carefully placed on top of the SiO_2 capsules. Then the glass cover was gently pressed to break the SiO_2 capsules to observe the

References to this Chapter on pages 162-163

oil being released from the fractured capsules (**Figure 4-11**). The images show that the capsule appears to fracture at one point, after which the oil is released, demonstrating the robust core-shell like structure of the capsule.

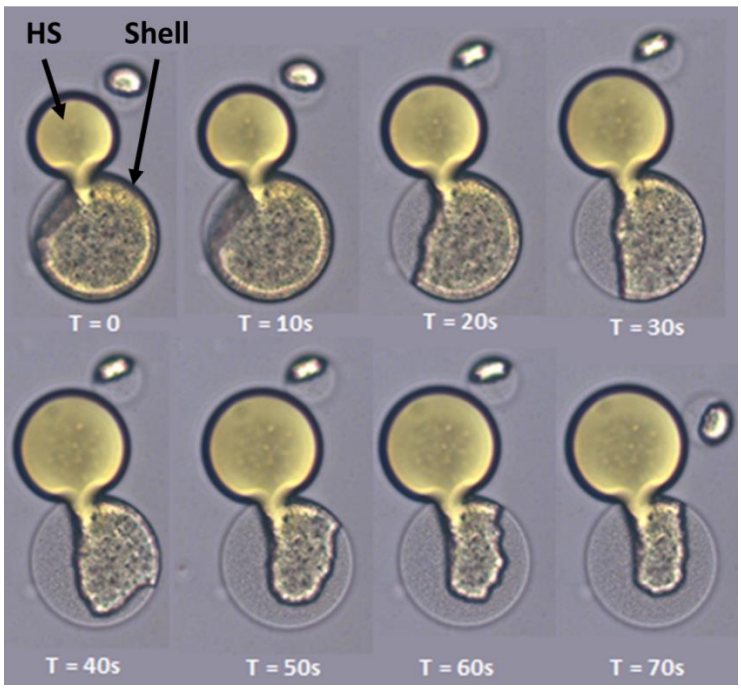

***Figure 4-11**. Optical microscopy images of a single broken SiO_2 capsule releasing HS (yellow oil) taken in 10 seconds intervals. HS is not soluble in water, so as it is released it forms an oil droplet. The diameter of the SiO_2 capsule is approximately 40 µm.*

4.2.8 Mechanical properties

The mechanical strength of capsules is one of the most important parameters for laundry products applications, along with the encapsulation efficiency and release profile of the encapsulated active.[23] With the help of the micromanipulation rig, it was possible to compress single SiO_2 capsules until rupture and obtain the force necessary to break the SiO_2 capsules, as well as the deformation at the rupture. **Figure 4-12** shows images collected by the microscope connected to the micromanipulation rig described in Chapter 2- Section 2.5.5.

References to this Chapter on pages 162-163

The glass probe travels toward the SiO_2 capsule (**Figure 4-12A**), it comes into contact and begins to deform the capsule (**Figure 4-12B**), until the capsule ruptures (**Figure 4-12C**).

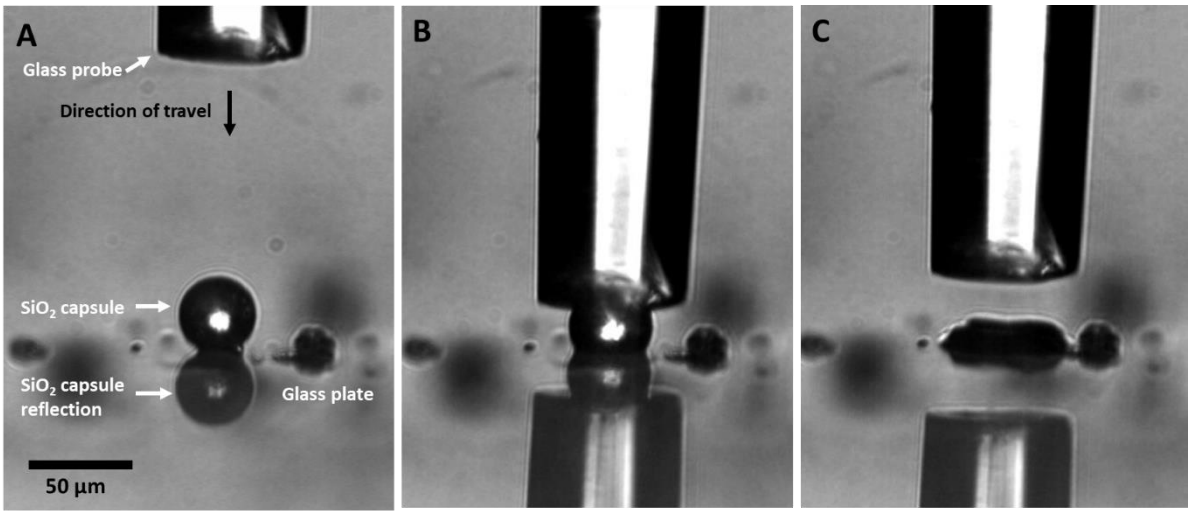

***Figure 4-12**. Images from the side view camera attached to a 10x optical lense. (A) before, (B) during and (C) after fracturing the capsule. The scale bar is 50 µm.*

The graph in **Figure 4-13** shows a curve obtained when compressing a SiO_2 NPs_1-$PEOS_{20}$-HS capsule (30 µm of diameter). Prior to point A (**Figure 4-13**) there was no contact between probe and SiO_2 capsule. The increase in force from displacement 0 µm is the probe coming into contact with the capsule and deforming it (**Figure 4-13**, point B), until the capsule suffers rupture at around 0.06 mN (**Figure 4-13**, point C) with a displacement of about 4 µm, which gives this SiO_2 capsule a nominal deformation of about 13%.

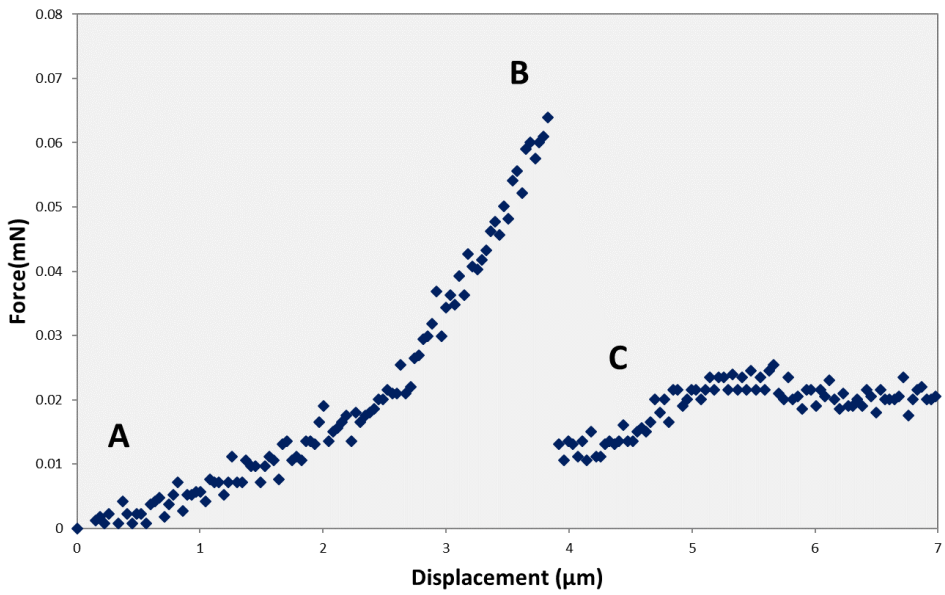

***Figure 4-13**. Resulting force vs displacement curve when compressing a single SiO_2 NPs_1-$PEOS_{20}$-HS capsule (A) before, (B) during and (C) after fracturing the capsule. The clear rupture indicates the formation of a core-shell like structure that suffers rupture under pressure. The capsule diameter is 30 µm.*

The results for a population of SiO_2 NPs_1-$PEOS_{20}$-HS capsules are summarized in **Table 4-1**; the displacement at rupture measures to what extent the SiO_2 capsule shell is deformed before it suffers rupture, and the deformation at rupture represents the ratio of the displacement at rupture to the diameter of the particle. The rupture force is the force required to break the SiO_2 capsule after the deformation and the nominal rupture stress is the ratio of the rupture force to the initial cross-sectional area of individual SiO_2 capsules (Chapter 2 – Section 2.4.6)

References to this Chapter on pages 162-163

Table 4-1. *Mechanical properties summary for a population of 10 SiO_2 NPs_1-$PEOS_{20}$-HS capsules.*

Capsule	Diameter (µm)	Displacement at rupture (µm)	Rupture force (mN)	Deformation at rupture (%)	Nominal rupture stress (MPa)
1	26.9	2.04	0.06	8	0.10
2	28.0	4.81	0.06	17	0.09
3	32.3	7.61	0.10	23	0.12
4	32.3	6.73	0.04	21	0.05
5	32.3	6.34	0.06	19	0.08
6	37.7	5.49	0.05	15	0.04
7	40.9	8.08	0.10	19	0.08
8	43.0	2.36	0.04	5	0.03
9	43.0	3.42	0.06	8	0.04
10	44.1	6.13	0.08	14	0.05
Average ± St Dev	**36.0 ± 6.4**	**5.3 ± 2.1**	**0.06 ± 0.02**	**15 ± 6**	**0.07 ± 0.03**

The values in **Table 4-1** suggest that the SiO_2 capsules, encapsulating HS, are relatively brittle as the deformation at rupture was 15% with a low nominal rupture stress (0.07 MPa) when compared to a typical sample of perfume microcapsule (PMC), which has a deformation at rupture of about 40% and a nominal rupture stress of about 1 MPa (for the same size band – data from P&G).

4.2.9 Varying encapsulation parameters

In order to understand the parameters involved in the formation of SiO_2 capsules using SiO_2 NPs, Pickering emulsions and PEOS, a set of experiments were designed with the objective of varying some of the key emulsification encapsulation parameters, as outlined **Step 1** and **Step**

References to this Chapter on pages 162-163

2 (**Figure 4-1**), in order to obtain SiO_2 capsules with optimized properties when compared to the capsules produced above. The parameters varied were:

(i) concentration of SiO_2 nanoparticles (Step 1);

(ii) concentration of PEOS (Step 2);

(iii) pH of the continuous phase (Step 3).

4.2.9.1 SiO_2 nanoparticles concentration: limited coalescence phenomenon

As observed in **Figure 4-14**, SiO_2 capsules were formed for higher (2 wt%) and lower (0.5 wt%) SiO_2 NPs concentration to the one initially used (1 wt%), with the mean diameter and SPAN related to the concentration of SiO_2 nanoparticles initially dispersed in the continuous phase, as discussed below. Samples were named:

(i) SiO_2 $\underline{NPs_{0.5}}$-$PEOS_{20}$-HS, for SiO_2 capsules produced using <u>0.5 wt%</u> of SiO_2 nanoparticles and 20 wt% of PEOS,

(ii) SiO_2 $\underline{NPs_1}$-$PEOS_{20}$-HS, for SiO_2 capsules produced using <u>1 wt%</u> of SiO_2 nanoparticles and 20 wt% of PEOS (initial sample, discussed in Sections 4.2.1 to 4.2.8), and

(iii) SiO_2 $\underline{NPs_2}$-$PEOS_{20}$-HS for those produced using <u>2 wt %</u> of SiO_2 nanoparticles and 20 wt% of PEOS.

The most interesting property of the SiO_2 capsules formed is the possibility to control the mean diameter and size distribution (SPAN) when different concentrations of SiO_2 NPs were used as observed in **Figure 4-14** and confirmed by the graph at **Figure 4-20A.**

References to this Chapter on pages 162-163

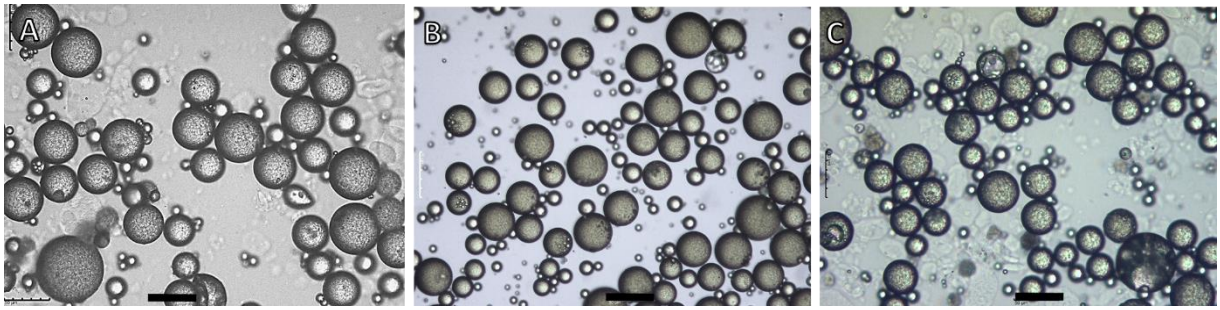

***Figure 4-14**. SiO_2 NPs-PEOS-HS capsules produced with different levels of SiO_2 NPs: (A) 0.5 wt% - SiO_2 $\underline{NPs_{0.5}}$-$PEOS_{20}$-HS (B) 1.0 wt% - SiO_2 $\underline{NPs_1}$-$PEOS_{20}$-HS and (C) 2.0 wt% - SiO_2 $\underline{NPs_2}$-$PEOS_{20}$-HS. Scale bar: 50µm*

4.2.9.2 PEOS concentration

The variation of PEOS concentration was investigated in order to define whether if SiO_2 capsules could still be formed at higher or lower levels of PEOS and the impact on the morphology and mechanical properties of the SiO_2 capsule. **Figure 4-15** shows optical microscopy images of SiO_2 capsules produced using three different levels of PEOS in the oil phase. Samples were named:

(i) SiO_2 NPs_1-$\underline{PEOS_{10}}$-HS, for SiO_2 capsules produced using <u>10 wt% of PEOS</u>,

(ii) SiO_2 NPs_1-$\underline{PEOS_{20}}$-HS, for SiO_2 capsules produced using <u>20 wt% of PEOS</u> (initial sample, discussed in Sections 4.2.1 to 4.2.8), and

(iii) SiO_2 NPs_1-$\underline{PEOS_{40}}$-HS for those produced using <u>40 wt % of PEOS</u>.

References to this Chapter on pages 162-163

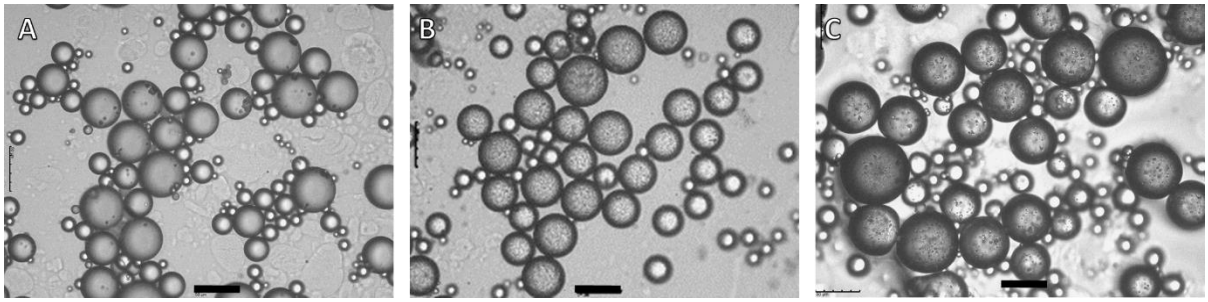

***Figure 4-15**. Capsules produced with different levels of PEOS: (A) 10 wt% - SiO_2 NPs$_1$-PEOS$_{10}$-HS (B) 20 wt% - SiO_2 NPs$_1$-PEOS$_{20}$-HS (c) 40 wt% - SiO_2 NPs$_1$-PEOS$_{40}$-HS. Scale bar: 50µm*

When different concentrations of PEOS were used to produce SiO_2 capsules, the shell morphology changes. SiO_2 NPs$_1$-PEOS$_{10}$-HS capsule (**Figure 4-15A**) surface was much smoother when compared to SiO_2 NPs$_1$-PEOS$_{40}$-HS (**Figure 4-15C**). Moreover, SiO_2 NPs$_1$-PEOS$_{40}$-HS had a higher contrast under the optical microscope, indicating shell thickening, which was confirmed using SEM (**Figure 4-16**). The shell thickness was calculated using image analysis (ImageJ 1.48v software package). From multiple SEM images, the differences regarding shell thickness were noticeable. While SiO_2 NPs$_1$-PEOS$_{10}$-HS capsules formed a thin shell that was strong enough to survive the vacuum imposed by the SEM chamber (**Figure 4-16C**), SiO_2 NPs$_1$-PEOS$_{40}$-HS capsules also survived the vacuum, however the shell formed was much thicker, irregular and porous (**Figure 4-16D**).

References to this Chapter on pages 162-163

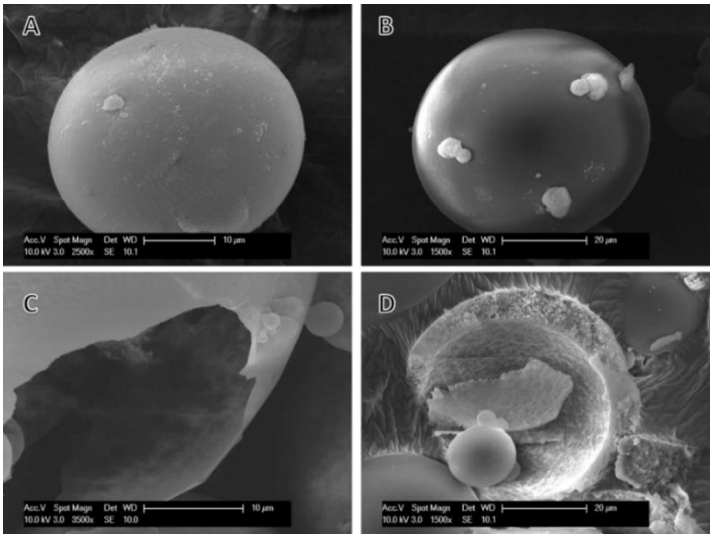

***Figure 4-16**. SEM images of: (A and C) 10 wt% - SiO_2 NPs$_1$-PEOS$_{10}$-HS and (B and D) 40 wt% - SiO_2 NPs$_1$-PEOS$_{40}$-HS. The scale bar is 10 µm (A and C) and 20 µm (B and D).*

The differences in terms of structure for the SiO_2 NPs$_1$-PEOS$_{40}$-HS capsule to SiO_2 NPs$_1$-PEOS$_{10}$-HS and SiO_2 NPs$_1$-PEOS$_{20}$-HS capsules can be explained by the highly porous shell formed for the former one. This difference in terms of shell thickness is because at low pH, all PEOs must hydrolyse before condensation starts. So the PEOS forms a thin and dense layer at the interface and the excess PEOS that remains inside the SiO_2 capsule hydrolyses and condenses slowly by water from the continuous phase diffusing through the still liquid like PEOS layer, before it is fully cross-linked.[22] **Table 4-2** shows the values for three different PEOS levels studied.

***Table 4-2.** Shell thickness from SEM images for different levels of PEOS*

Sample	Wt% of PEOS in the oil phase	Shell thickness (µm)
SiO_2 NPs$_1$-PEOS$_{10}$-HS	**10**	0.15 ± 0.03
SiO_2 NPs$_1$-PEOS$_{20}$-HS	**20**	0.50 ± 0.04
SiO_2 NPs$_1$-PEOS$_{40}$-HS	**40**	7.01 ± 2.05

References to this Chapter on pages 162-163

The SiO_2 capsules prepared with different concentrations of PEOS were stored for a year at RT inside a cupboard, and re-examined optically (**Figure 4-17)**. The SiO_2 NPs$_1$-PEOS$_{10}$-HS capsules were able to retain the oil after one year (A). In contrast, the SiO_2 NPs$_1$-PEOS$_{40}$-HS capsules were mostly empty (B), confirming that the shell structure was presumably more porous, (**Figure 4-16D)**.

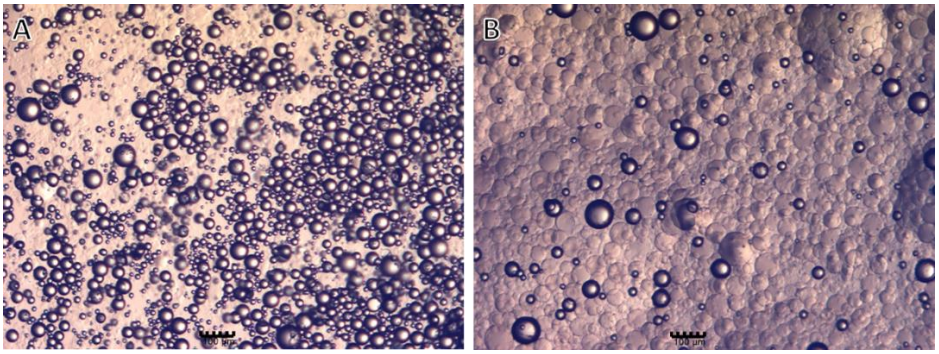

***Figure 4-17**. Optical images taken after one year of (A) 10 wt% - SiO_2 NPs$_1$-PEOS$_{10}$-HS and (B) 40 wt% - SiO_2 NPs$_1$-PEOS$_{40}$-HS. Scale bar: 100µm*

4.2.9.3 pH of the continuous phase

The formation of SiO_2 capsules is extremely dependent on the pH of the continuous phase as it controls the hydrolysis and condensation rate of PEOS, and the surface charges of the SiO_2 NPs.[18] Surprisingly, SiO_2 capsules were formed for all pH tested (from pH 2 to pH 9). Samples were named:

(i) SiO_2 NPs$_1$-PEOS$_{20}$-HS-pH2,

(ii) SiO_2 NPs$_1$-PEOS$_{20}$-HS-pH4 (initial sample, discussed in Sections 4.2.1 to 4.2.8),

(iii) SiO_2 NPs$_1$-PEOS$_{20}$-HS-pH7, and

(iv) SiO_2 NPs$_1$-PEOS$_{20}$-HS-pH9.

References to this Chapter on pages 162-163

In terms of sol-gel, it is an advantage to use acidic or alkaline conditions in order to catalyse the sol-gel process as discussed on Chapter 1 – Section 1.4.3.2, so the rate of hydrolysis and condensation can be finely controlled.[19] **Figure 4-18** below shows SiO_2 capsules obtained in four different pH conditions.

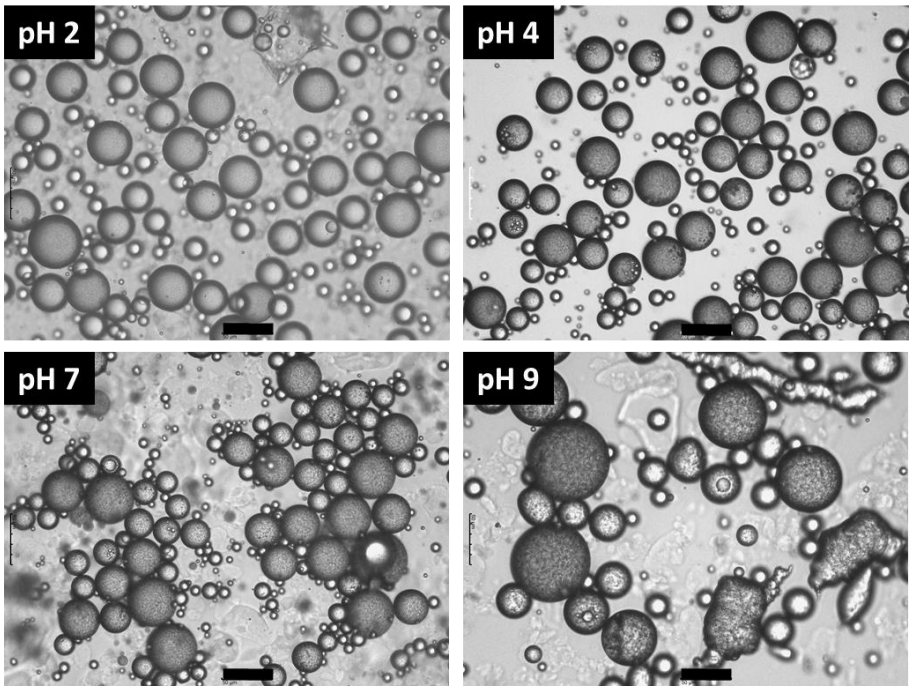

***Figure 4-18**. Optical microscopy images for SiO_2 capsules prepared at pH 2, 4, 7 and 9. As it can be observed, capsules can be formed across all pH values, however at pH 9 they start to lose shape due to the high stability of the SiO_2 NPS in the water phase.*

From **Figure 4-18**, it can be observed that SiO_2 capsules produced at lower pH had a narrower size distribution than those produced at higher pH (**Figure 4-20**). Furthermore, at pH 9, the SiO_2 capsules formed were larger and for many cases not spherical. This can potentially be explained by the fact that at high pH, the surface silanol SiOH group on the SiO_2 nanoparticles are deprotonated, and therefore the nanoparticles carry a negative charge, leading to electrostatic repulsion between theam as well as may be increasing water stability, which

limits the nanoparticles interfacial activity, and hence the Pickering emulsion droplet loses stability.[17]

At pH 7 the SiO_2 capsules formed were spherical, with no mis-formed capsules, indicating the formation of a stable Pickering emulsion; however, capsules in multiple sizes were formed. As the condensation rate reaches the maximum at pH 7, PEOS starts solidifying before the complete formation of a liquid PEOS layer around the whole droplet (**Step 2 - Figure 4-1**), which could lead to a competition for droplet stabilisation between colloidal SiO_2 nanoparticles formed from rapidly condensed PEOS and the SiO_2 NPs (More details in Chapter 1 – Section 1.4.2). At pH 2 and 4 capsules were well defined with a relatively narrow size distribution due to the high surface activity of the SiO_2 NPs at low pH, stabilising the emulsion.

4.2.9.4 Solely PEOS SiO_2 capsules

To understand PEOS amphiphilic properties discussed in **Chapter 3**, SiO_2 capsules were prepared without SiO_2 NPs, *i.e.* solely PEOS SiO_2 capsules maintaining the same PEOS level as the initial experiments: 20% to the oil phase ($PEOS_{20}$-HS). Surprisingly, SiO_2 capsules were successfully produced (**Figure 4-19)**. It was possible to form SiO_2 capsules due to the high stability resulting from a barrier layer formed by partially hydrolysed and partially condensed PEOS on the oil droplet surface, which prevents Ostwald ripening.[18] SiO_2 capsule presented a solid shell that could survive air-drying, as observed at **Figure 4-19C** through the micromanipulation side image and **Figure 4-19D**, which shows a SEM image of a broken shell, showing a core-shell structure. Moreover, the inner shell possessed a larger number of protruding sites when compared to the SiO_2 NPs_1-$\underline{PEOS_{20}}$-HS capsules which corresponded to an excess of PEOS solidifying the inner shell surface.

References to this Chapter on pages 162-163

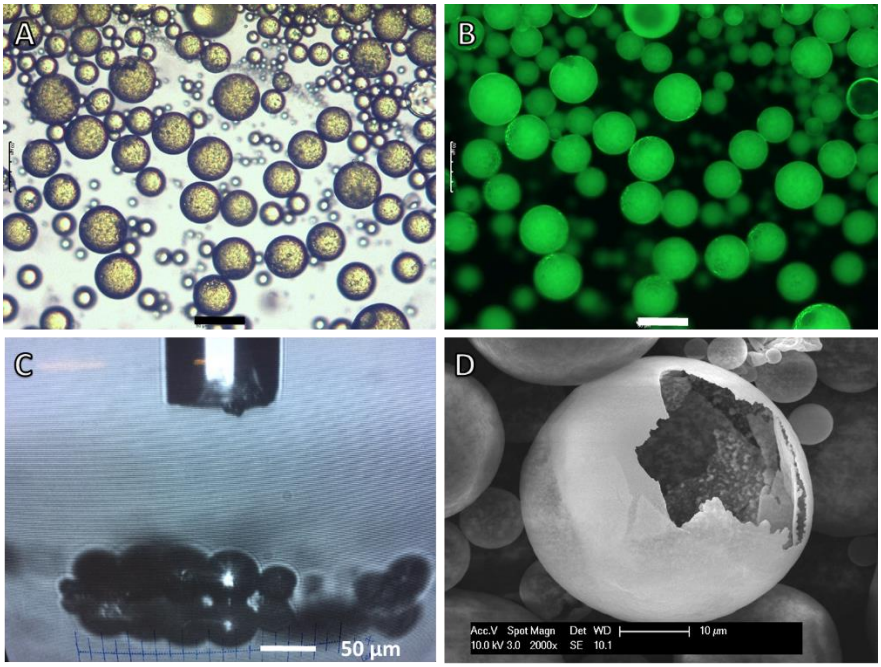

***Figure 4-19**. Optical (A) and Fluorescent (B) images of $PEOS_{20}$-HS containing PM546. The scale bar is 50 µm. (C) Image of $PEOS_{20}$-HS capsules from the micromanipulation rig side view camera (D) SEM image of a broken $PEOS_{20}$-HS capsule showing the core-shell structure.*

4.2.10 Overall size and mechanical properties analysis

For capsules produced with different concentrations of SiO_2 to HS (SiO_2 $NPs_{0.5}$-$\underline{PEOS_{20}}$-HS, SiO_2 NPs_1-$\underline{PEOS_{20}}$-HS and SiO_2 NPs_2-$\underline{PEOS_{20}}$-HS) the different mean diameter and SPAN values can be explained by the limited coalescence phenomenon,[24] which rationalises that the Pickering emulsion droplets will coalesce until the surface of each droplet is fully covered by the solid nanoparticles. Thus, increasing the concentration of SiO_2 NPs will reduce the size of the Pickering emulsion droplets and increase the SPAN (**Figure 4-20A**).

When different PEOS levels to HS were used (SiO_2 NPs_1-$\underline{PEOS_{10}}$-HS, SiO_2 NPs_1-$\underline{PEOS_{20}}$-HS and SiO_2 NPs_1-$\underline{PEOS_{40}}$-HS), the higher the PEOS concentration the higher the mean diameter (**Figure 4-20B**), which can indicate that the amphiphilic properties of PEOS could be

overcoming the Pickering stabilization, and at high PEOS concentration the droplet is stabilized primarily by PEOS.

For the capsules produced at different pH values (pH 2, 4 , 7 and 9) both the mean diameter and SPAN increased with the increase of the aqueous phase pH (**Figure 4-20C**). The mean diameter was particularly large for the pH 9 samples. This data was probably an anomaly as the light scattering detects primarily round shaped-particles, so any non-round SiO_2 capsule will be treated as a sphere leading to a larger size detection. At pH 2 the SPAN and mean diameter had the minimum value. This is due to the high protonation of the SiO_2 NPs surface silanol groups at low pH, which increase their interfacial activity, so they become capable of stabilising the droplet at earlier stages.[18]

References to this Chapter on pages 162-163

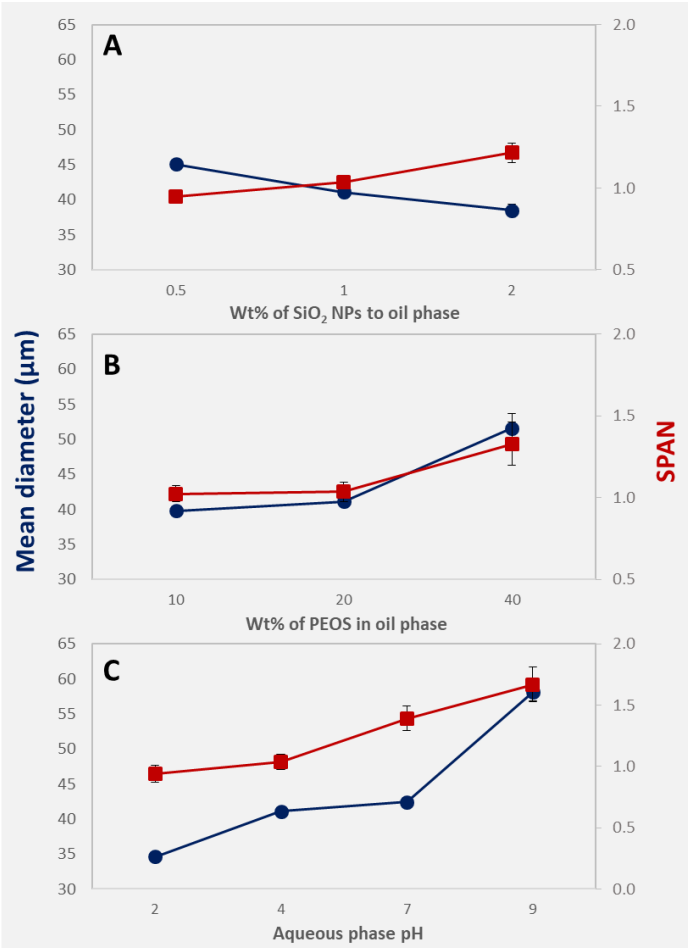

***Figure 4-20**. Mean diameter and SPAN of capsules prepared with (A) variable wt% of SiO_2 NPs to HS, (B) variable wt% of PEOS and (C) variable pH.*

The mechanical properties of the SiO_2 capsules produced in this chapter were compared against a typical PMC used in the industry nowadays. The SiO_2 capsules produced using a higher amount of PEOS (SiO_2 NPs$_1$-PEOS$_{40}$-HS) were the only ones that demonstrated a significant change in terms of rupture force (**Figure 4-21**). The samples produced with 10% PEOS (SiO_2 NPs$_1$-PEOS$_{10}$-HS) and at pH 9 (SiO_2 NPs$_1$-PEOS$_{20}$-HS-pH9) are not included in the graph as their resistance to the transducer probe was too low to be measured using a 0.5 mN transducer.

References to this Chapter on pages 162-163

The mechanical properties of $PEOS_{20}$-HS capsules were comparable to the ones prepared with SiO_2 NPs (SiO_2 NPs_1-$PEOS_{20}$-HS), which confirms that PEOS is the main contributor to the shell thickness and mechanical properties and the SiO_2 NPs serves as Pickering emulsion template.

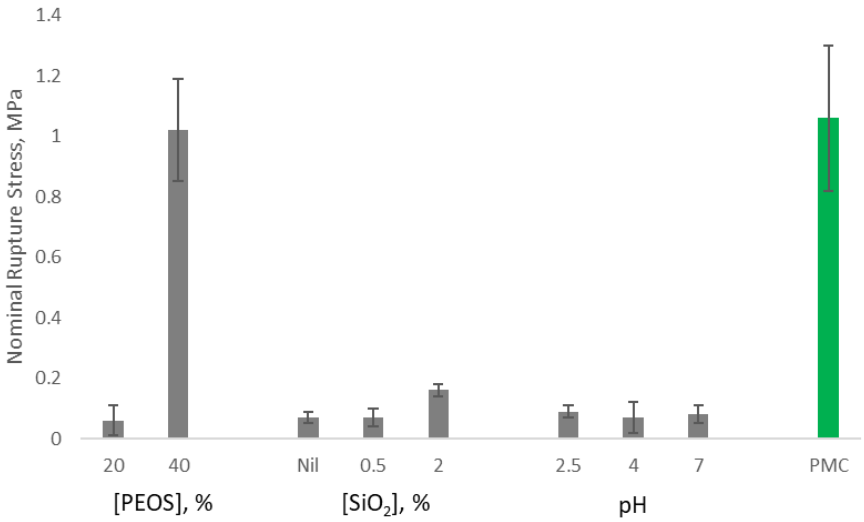

***Figure 4-21**. Nominal rupture stress values of the SiO_2 capsules produced in Section 4.2.9 compared to the expected value of a commercial PMC. All SiO_2 capsules tested had a mean diameter of approximately 35 µm, which is the mean diameter of the PMC example.*

The overall low nominal rupture stress value of the SiO_2 capsules is probably due to the brittleness of the SiO_2 shell, which allows for a small deformation of the shell before failure (around 20-15%). Although the sample containing 40 wt% PEOS had enhanced mechanical properties when compared to the other sample due to its thicker shell, the porous structure of the SiO_2 capsule could be an issue, as for detergent applications the core material needs to be stabilized within the shell with minimum leakage during storage and supply chain of the product. The ideal silica capsule would therefore reconcile the mechanical properties of she sample containing 40 wt% PEOS and the leakage profile of a less porous shell, perhaps a dual-

References to this Chapter on pages 162-163

sell approach could be used to satisfy all the parameters (shell thickness, porosity and leakage).

All SiO_2 capsules produced in Sections 4.2.9 are summarized in **Table 4-3** below, including the mean diameter, SPAN and mechanical properties.

***Table 4-3**. Summary of all SiO_2 capsules produced using hexyl salicylate as oil phase.*

Sample	Wt% of PEOS to HS	Wt% of SiO_2 NPs to HS	pH aqueous phase	Mean diameter (µm)	SPAN	Deformation at rupture (%)	Nominal rupture stress (MPa)
SiO_2 $NPs_{0.5}$-$PEOS_{20}$-HS	20	0.5	4	38.5 ± 0.3	0.95 ± 0.06	14 ± 3	0.07 ± 0.03
SiO_2 NPs_1-$PEOS_{20}$-HS	20	1	4	41.1 ± 0.5	1.04 ± 0.06	15 ± 6	0.07 ± 0.03
SiO_2 NPs_2-$PEOS_{20}$-HS	20	2	4	45.1 ± 0.9	1.22 ± 0.1	24 ± 5	0.16 ± 0.02
SiO_2 NPs_1-$PEOS_{10}$-HS	10	1	4	39.8 ± 0.3	1.02 ± 0.05	-	-
SiO_2 NPs_1-$PEOS_{20}$-HS	20	1	4	41.1 ± 0.5	1.04 ± 0.06	15 ± 6	0.07 ± 0.03
SiO_2 NPs_1-$PEOS_{40}$-HS	40	1	4	51.6 ± 2.1	1.33 ± 0.13	34 ± 2	1.02 ± 0.17
SiO_2 NPs_1-$PEOS_{20}$-HS - pH2	20	1	2.5	34.6 ± 0.2	0.94 ± 0.07	19 ± 2	0.09 ± 0.02
SiO_2 NPs_1-$PEOS_{20}$-HS- pH4	20	1	4	41.1 ± 0.5	1.04 ± 0.06	15 ± 6	0.07 ± 0.03
SiO_2 NPs_1-$PEOS_{20}$-HS - pH7	20	1	7	42.4 ± 0.6	1.39 ± 0.1	14 ± 3	0.08 ± 0.03
SiO_2 NPs_1-$PEOS_{20}$-HS - pH9	20	1	9	58.1 ± 1.2	1.67 ± 0.14	-	-
$PEOS_{20}$-HS	20	-	6	42.8 ± 0.2	1.17 ± 0.08	16 ± 7	0.06 ± 0.02

4.2.11 Stability in liquid detergent

SiO_2 capsules produced with and without SiO_2 NPs (SiO_2 NPs_1-$PEOS_{20}$-HS and $PEOS_{20}$-HS) had their barrier properties tested in liquid detergent (Liquid fabric enhancer - LFE). A simple microscope slide method was used as described in Chapter 2 – Section 2.4.2. **Figure 4-22**

References to this Chapter on pages 162-163

shows the results of the SiO_2 NPs_1-$PEOS_{20}$-HS sample. After just 10 minutes of contact between the SiO_2 capsules and LFE the HS was already coming out of the shell (**Figure 4-22B**), and after 1 hour it was clear that HS was being extracted from the core to the continuous, surfactant rich phase (**Figure 4-22C**). After 24h the SiO_2 capsules looked completely empty, however their structure was intact, suggesting that the SiO_2 shell is solid, but highly porous (**Figure 4-22D**).

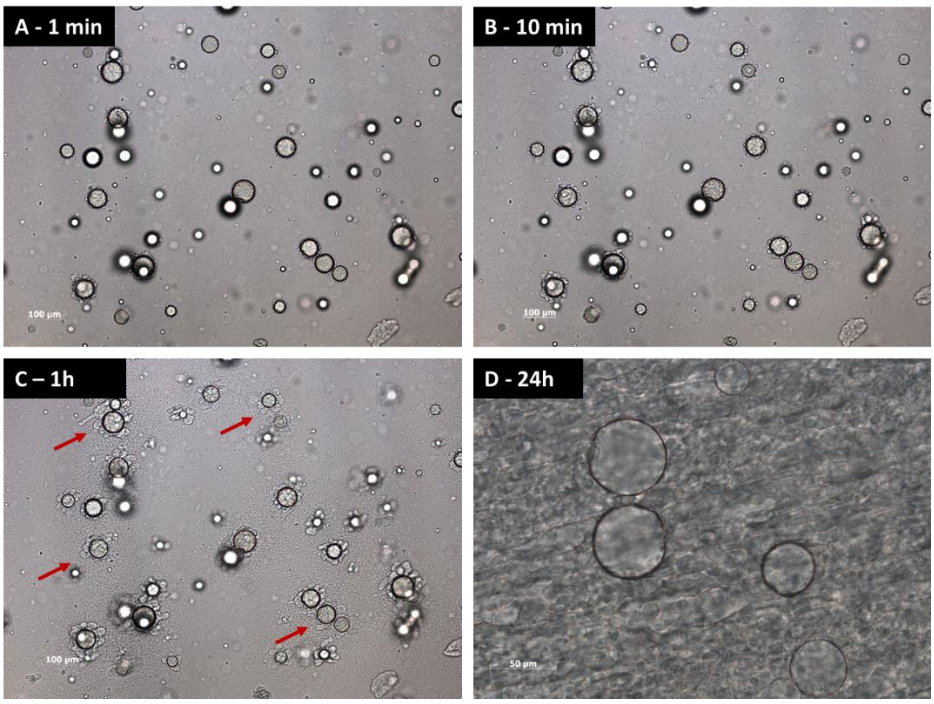

***Figure 4-22**. Optical microscopy images of SiO2 NPs1-PEOS20-HS capsules dispersed in LFE.*

A similar result was observed for the $PEOS_{20}$-HS capsules. In this case, the SiO_2 capsules tested had a fluorescent dye mixed in the HS so the leakage effect was easier to follow. After 1 hour it was possible to clearly observe that some HS had leaked out of the SiO_2 capsule as indicated by the red arrow on **Figure 4-23C** below. After 24 hours the SiO_2 capsule looked mostly empty, but intact, similar to the ones produced with SiO_2 NPs (**Figure 4-23E and F**). It was possible to observe that the continuous phase also had a high concentration of florescent dye, giving

support to the hypothesis that the SiO_2 capsules are highly porous and HS leaks out rapidly in a surfactant-based matrix.

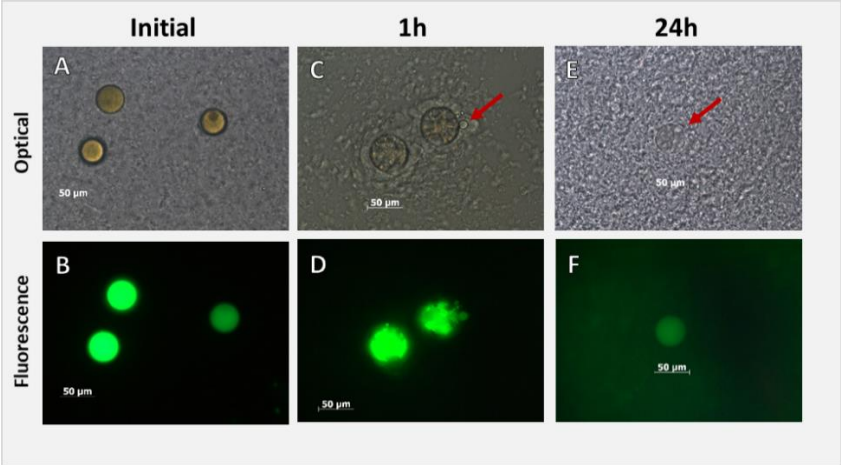

***Figure 4-23**. Optical microscopy images of $PEOS_{20}$-HS capsules dispersed in LFE.*

4.3 Conclusions

As an overall conclusion, it was possible to encapsulate HS in SiO_2 capsules using the Pickering emulsion – PEOS based technique proposed in this chapter. The SiO_2 capsules formed were characterized thoroughly and they possessed a liquid core with a solid shell structure. The release profile of the SiO_2 capsules was very encouraging as the SiO_2 capsules were stable in the slurry for over 1 year and in a stressed environment (36% propan-1-ol) where the HS was released over a period of 60 days. However, when added to a surfactant rich environment (LFE) the SiO_2 capsules were completely emptied in less than 24h, which suggests that the SiO_2 capsules are porous as the HS is rapidly extracted to the surfactant rich matrix. Regarding mechanical properties, the capsules showed a clear rupture, but the force necessary to rupture individual SiO_2 capsules was much lower than for a typical PMC used in the industry, this is probably due to the brittleness of the thin SiO_2 shell.

References to this Chapter on pages 162-163

Emulsification and encapsulation parameters (**Figure 4-1**) were varied to control the mean diameter, SPAN and mechanical properties of the capsules. When the wt% of SiO_2 NPs to HS was varied (HS (SiO_2 $NPs_{0.5}$-$PEOS_{20}$-HS, SiO_2 NPs_1-$PEOS_{20}$-HS and SiO_2 NPs_2-$PEOS_{20}$-HS), the size of the final capsule and the SPAN of the size distribution could be controlled by taking advantage of the limited coalescence phenomenon, however there were no significant differences in terms of mechanical properties.

Capsules could be produced with different wt% of PEOS in the core (SiO_2 NPs_1-$PEOS_{10}$-HS, SiO_2 NPs_1-$PEOS_{20}$-HS and SiO_2 NPs_1-$PEOS_{40}$-HS). However, only the SiO_2 NPs_1-$PEOS_{40}$-HS capsules could have their nominal rupture stress and deformation at the rupture increased significantly, however these capsules were very porous. In terms of size, the higher the PEOS level, the higher the mean diameter, probably due to the stabilization of the droplets by PEOS (amphiphilic).

In terms of pH, well-defined capsules were produced at pH 2, 4 and 7 (SiO_2 NPs_1-$PEOS_{20}$-HS-pH2, SiO_2 NPs_1-$PEOS_{20}$-HS-pH4 and SiO_2 NPs_1-$PEOS_{20}$-HS-pH7). Capsules could not be produced at pH 9 (SiO_2 NPs_1-$PEOS_{20}$-HS-pH9), as the condensation rate of PEOS reaches the maximum. SiO_2 NPs_1-$PEOS_{20}$-HS-pH2 had a low SPAN, showing a narrow size distribution. As the process can be catalysed in acidic conditions, this pH should be further investigated in the next chapters along with higher levels of PEOS.

Surprisingly, stable capsules were formed solely by PEOS ($PEOS_{20}$-HS) as it acts as a surfactant due to its amphiphilic properties, which could make the method even simpler for industrial

References to this Chapter on pages 162-163

applications. Solely PEOS capsules will be further investigated in the following chapters for the encapsulation of a real-world perfume composition.

As an overall conclusion, the mechanisms for the formation of SiO_2 capsules in general from Pickering emulsions and the hydrolysis and condensation of PEOS were elucidated, including some key parameters that can be controlled when forming a solid SiO_2 shell:

i. Wettability of the SiO_2 nanoparticles - determinates the stability of the emulsion as well as the type of emulsion (O/W or W/O);

ii. Concentration of SiO_2 - controls the droplet size and size distribution;

iii. Oil density and polarity – influences the emulsion stability as well as the SiO_2 capsule size and hydrolysis and condensation kinetics;

iv. Concentration of PEOS – The ratio between the encapsulated oil to PEOS could be adjusted in order to control the size of the condensed layer, hence controlling the thickness of the formed wall.

v. Hydrolysis and condensation kinetics – the hydrolysis rate influences the wetting layer formed by the precursor around the droplet, and condensation rate, the solidification of the shell.

vi. pH - controls the interfacial activity of both PEOS and SiO_2 nanoparticles as well as hydrolysis and condensation of PEOS.

References to this Chapter on pages 162-163

4.4 Experimental

4.4.1 Encapsulation of hexyl salicylate

The preparation of the SiO_2 capsules was possible following the following method: HS containing 0.1 wt% of PM546 dye was mixed with PEOS in different proportions depending on the experiment as described in **Table 4-3**. The resulting solution was added to a 1 wt% fumed SiO_2 nanoparticles aqueous dispersion (10g) and emulsified using a vortex mixer for 5 minutes (2500 RPM) forming an O/W Pickering emulsion. Emulsions were then left undisturbed at 25°C for 24 hours to allow hydrolysis and solidification of PEOS at the water-oil interface. The resulting SiO_2 capsules were isolated by centrifugation at 2000 RPM per 10 minutes and re-dispersed in 10 ml of DI water.

4.4.2 Optical microscopy

Optical microscopy images were obtained using two microscopes: a Leica DMRBE, (Leica Microscope & Systems GmbH) equipped with a software package Moticam Pro 3.0 and a CoolLED pE-300 white light source. The resolution of the microscope was 200 nm. The second microscope used was a Zeiss Axio imager 2 pol (Carl Zeiss Microscopy – Germany, resolution 200 nm) also equipped with a UV light source (Kubler codex HXP 120C).

4.4.3 Scanning electron microscopy (SEM)

SEM images were obtained using two different microscopes: a 1000 Tabletop Microscope (Hitachi, Ltd – Japan), magnification 1500X and a Philips XL-30 FEG Environmental SEM with Oxford Inca EDS (Philips UK ltd, Guildford – UK), magnification 3500X.

References to this Chapter on pages 162-163

4.4.4 Size analysis

Mean capsule size and size distribution of the SiO_2 capsules in aqueous dispersion were obtained by static light-scattering using a Mastersizer 2000 instrument (Malvern Instruments Ltd, Malvern - UK). The instrument measures the volume fraction of the SiO_2 capsules in different size bands in the size range of 20 nm to 2000 µm using a Helium-Neon laser connected to a dispersion unit. All experiments were performed at 25°C. The refractive index used was 1.46 (for amorphous SiO_2[25]) and the data analysed using Excel®.

4.4.5 Payload and encapsulation efficiency sample preparation

Capsules were prepared following the method described at Section 4.4.1. After centrifugation, the slurry was added to 50mL of 36% propanol in water (18mL propanol, 32mL DI water) with approximately 15g of glass microbeads (3mm) under magnetic stirring (1000 RPM) per 2 days.

Samples were centrifuged for 20 min (4000 RPM) and the supernatant separated from the solid. 100µl of supernatant was then added to 3ml of 36% propanol in water and the absorbance measured using UV CE 2021, (Cecil Instruments Ltd., UK) at λ = 305 nm and the mass of HS present in solution calculated using a calibration curve (**Figure 4-24**). The mass was used to calculate payload and encapsulation efficiency.

References to this Chapter on pages 162-163

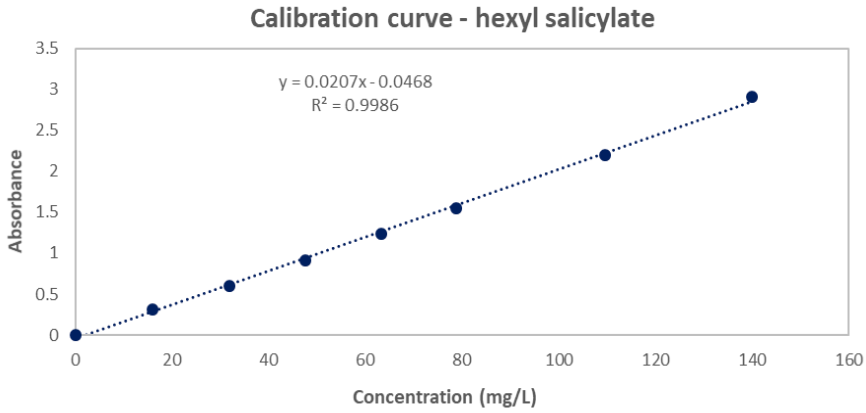

***Figure 4-24**. Calibration curve for hexyl salicylate using different concentrations in 36% propan-1-ol aqueous solution.*

4.4.6 Release profile and permeability

Capsule samples were prepared as described in Section 4.4.1 in triplicates and 10g of SiO_2 capsule suspension containing 20% w/w of SiO_2 capsule to water was added to a dialysis tubing. The tubing had its both ends sealed and was charged to a bottle containing 250ml of 36% propanol aqueous solution under magnetic agitation. Then the λ_{max} of the solution at 305 nm was measured over time and the HS mass present in solution using a calibration curve (**Figure 4-24**). A UV-Vis spectrophotometer (Cecil Instruments, Cambridge, UK) was used to measure the absorbance over time using quartz cuvettes with 3 mL volume capacity and 1 cm of optical path length.

The SiO_2 capsule permeability was determined using the models based on a monodisperse size assumption, which were implemented using commercial spreadsheet software (Excel®, Microsoft).

4.4.7 Trigger release

0.1g of SiO_2 capsule suspension containing 20% w/w SiO_2 capsule to DI water was diluted in 5ml of DI water. One drop of the diluted dispersion was placed onto the surface of a glass micro slide and covered with a cover slide. The cover slide was then pressed gently using a spatula to break the SiO_2 capsules and the oil being released under the optical microscope (Carl Zeiss Microscopy – Germany, resolution 200 nm) observed.

4.4.8 Mechanical properties

The mechanical properties of the SiO_2 capsules were determined by micromanipulation. 0.1g of SiO_2 capsule suspension containing 20% w/w SiO_2 capsule to DI water was first diluted 500x in DI water then a drop of the diluted dispersion was added to a glass slide and left to air dry. The glass containing the SiO_2 capsules was then positioned on the micromanipulation rig stage and observed using the side-view camera equipped with a 10x magnification lense. The glass slide was positioned perpendicular to a glass probe with a diameter of 100 µm mounted on an electronically controlled force transducer (Model 403A, Aurora Scientific Inc., Canada, with a maximum operation limit of 5 mN). A single SiO_2 capsule was compressed by the glass probe travelling at 2 µm s^{-1}. The voltage output generated by the transducer after the compression of the SiO_2 capsule was recorder and converted to force using an excel macro. The sensitivity of the transducer used was 0.5 mN. Ten random SiO_2 capsules were analysed per sample for statistical analysis. Details of the technique can be found in Chapter 2, Section 2.4.6.

References to this Chapter on pages 162-163

4.4.9 Stability in liquid detergent

0.1g of SiO_2 capsule suspension containing 20% w/w SiO_2 capsule to DI water was added to a glass vial containing 5 ml of liquid detergent formulation (LFE). The vial was shaken by hand to ensure well dispersion of the SiO_2 capsules and a drop of the product placed on a glass microslide and covered with a cover glass. Optical microscopy images were taken over time using a Zeiss Axio imager 2 pol (Carl Zeiss Microscopy – Germany, resolution 200 nm) also equipped with a UV light source (Kubler codex HXP 120C).

4.5 References

1. H. Lee, C.-H. Choi, A. Abbaspourrad, C. Wesner, M. Caggioni, T. Zhu and D. A. Weitz, *Encapsulation and Enhanced Retention of Fragrance in Polymer Microcapsules*, *ACS Applied Materials & Interfaces*, **2016**, *8*, 4007-4013.
2. J. J. G. van Soest, in *Flavours and Fragrances: Chemistry, Bioprocessing and Sustainability*, ed. R. G. Berger, Springer Berlin Heidelberg, Berlin, Heidelberg, **2007**, pp. 439-455.
3. R. Gref, Y. Minamitake, M. Peracchia, V. Trubetskoy, V. Torchilin and R. Langer, *Biodegradable Long-Circulating Polymeric Nanospheres*, *Science*, **1994**, *263*, 1600-1603.
4. S. Gouin, *Microencapsulation: Industrial Appraisal of Existing Technologies and Trends*, *Trends in Food Science & Technology*, **2004**, *15*, 330-347.
5. R. Akiyama and S. Kobayashi, *"Microencapsulated" and Related Catalysts for Organic Chemistry and Organic Synthesis*, *Chemical Reviews*, **2009**, *109*, 594-642.
6. D. Caswell, Procter & Gamble, *Laundry System Having Unitized Dosing,* US7534758B2, **2006**
7. J. Ness, Quest International BV, *Perfume Encapsulates,* US7238655B2, **2004**
8. L. F. T. A. S. R. S. B. N. Yan, Encapsys Inc, *Controlled Release Microcapsules,* **2014**
9. E. Kentin, Cham, **2018**.
10. M. Destribats, S. Gineste, E. Laurichesse, H. Tanner, F. Leal-Calderon, V. Héroguez and V. Schmitt, *Pickering Emulsions: What Are the Main Parameters Determining the Emulsion Type and Interfacial Properties?*, *Langmuir*, **2014**, *30*, 9313-9326.
11. Y. Chevalier and M.-A. Bolzinger, *Emulsions Stabilized with Solid Nanoparticles: Pickering Emulsions*, *Colloids and Surfaces A: Physicochemical and Engineering Aspects*, **2013**, *439*, 23-34.
12. K. Bauer, D. Garbe and H. Surburg, *Common Fragrance and Flavor Materials: Preparation, Properties and Uses*, Wiley, **2008**.
13. R. Mercadé-Prieto, R. Allen, D. York, J. A. Preece, T. E. Goodwin and Z. Zhang, *Determination of the Shell Permeability of Microcapsules with a Core of Oil-Based Active Ingredient Journal of Microencapsulation*, **2012**, *29*, 463-474.

14. C. J. Brinker, *Hydrolysis and Condensation of Silicates: Effects on Structure*, *Journal of Non-Crystalline Solids*, **1988**, *100*, 31-50.
15. Y. Zhao, Y. Li, D. E. Demco, X. Zhu and M. Möller, *Microencapsulation of Hydrophobic Liquids in Closed All-Silica Colloidosomes*, *Langmuir*, **2014**, *30*, 4253-4261.
16. Z. Jianing and R. Hans, *Sol–Gel Science, the Physics and Chemistry of Sol–Gel Processing, Ed. By C. J. Brinker and G. W. Scherer, Academic Press, Boston 1990, Xiv, 908 Pp., Bound—Isbn 0-12-134970-5*, *Advanced Materials*, **1991**, *3*, 522-522.
17. B. P. Binks and C. P. Whitby, *Nanoparticle Silica-Stabilised Oil-in-Water Emulsions: Improving Emulsion Stability*, *Colloids and Surfaces A: Physicochemical and Engineering Aspects*, **2005**, *253*, 105-115.
18. Y. Zhao, Z. Chen, X. Zhu and M. Möller, *Silica Nanoparticles Catalyse the Formation of Silica Nanocapsules in a Surfactant-Free Emulsion System*, *Journal of Materials Chemistry A*, **2015**, *3*, 24428-24436.
19. D. Levy and M. Zayat, *The Sol-Gel Handbook: Synthesis, Characterization, and Applications*, Wiley, **2015**.
20. K. L. Thompson, M. Williams and S. P. Armes, *Colloidosomes: Synthesis, Properties and Applications*, *Journal of Colloid and Interface Science*, **2015**, *447*, 217-228.
21. Y. Zhao, Z. Chen, X. Zhu and M. Moller, *Silica Nanoparticles Catalyse the Formation of Silica Nanocapsules in a Surfactant-Free Emulsion System*, *Journal of Materials Chemistry A*, **2015**, *3*, 24428-24436.
22. J. van Wijk, J. W. O. Salari, J. Meuldijk and B. Klumperman, *Determination of the Shell Growth Direction During the Formation of Silica Microcapsules by Confocal Fluorescence Microscopy*, *Journal of Materials Chemistry B*, **2015**, *3*, 7745-7751.
23. G. Sun and Z. Zhang, *Mechanical Strength of Microcapsules Made of Different Wall Materials*, *International Journal of Pharmaceutics*, **2002**, *242*, 307-311.
24. S. A. P. W. P. B. S. Leal-Calderon, *Some General Features of Limited Coalescence in Solid-Stabilized Emulsions*, *The European Physical Journal E*, **2003**, *11*, 273-281.
25. G. Ghosh, *Handbook of Refractive Index and Dispersion of Water for Scientists and Engineers*, Ghosh, Sujata, **2005**.

CHAPTER 5. Encapsulation of a Commercial Perfume Oil in SiO_2 Capsules

Abstract

In this chapter, an oil phase composed of a commercial perfume oil (PO) and hyperbranched polyethoxysiloxane (PEOS) and an aqueous phase containing hydrophilic fumed silica nanoparticles (SiO_2 NPs) are emulsified forming a stable oil-in-water emulsion. The emulsion then undergoes spontaneous formation of a condensed SiO_2 shell to form SiO_2 capsules. The PEOS cross-links the SiO_2 NPs at the oil-water interface, *via* the hydrolysis and condensation of PEOS at the interface. Thus, a mechanically robust SiO_2 shell encapsulating the perfume oil was formed, which could be dried and redispersed in water.

The SiO_2 shell morphology was dependent on the (i) pH of the aqueous phase, (ii) concentration of PEOS, and (iii) the molecular weight of PEOS, which controlled the interfacial activity of PEOS. As described in Chapter 4, the pH of the aqueous phase controls the interfacial activity of both the SiO_2 NPs and PEOS, as well as the hydrolysis and condensation rate of PEOS, which significantly affects the resulting SiO_2 shell, in terms of rigidity.

The SiO_2 capsules were characterized in terms of mean diameter, size distribution, shell morphology and thickness, mechanical properties and *stability* and *performance* in laundry products. Encapsulation parameters, such as pH, SiO_2 NPs concentration, PEOS concentration and PEOs molecular weight were varied to establish the optimal conditions for the formation of a shell with improved mechanical properties, size distribution and stability in the laundry detergents.

References to this Chapter on page 204

5.1 Introduction

As described in earlier chapters perfumes are important elements of a wide range of FMCG products, for a variety of reasons centred around consumer perception and satisfaction of the product. In Chapter 4, a single component fragrance oil, hexyl salicylate (HS), was used as a model for the formulation of SiO_2 capsules from SiO_2 nanoparticles. Herein, SiO_2 capsules are formulated from a complex mixture of fragrance oils that are used commercially. This complex fragrance mixture has organic structures with various chemical functionalities, molecular weights, and densities. Therefore, the hydrophobicity and interfacial properties with water will be modified relative to HS alone, and one might expect the PEOS solubility and interfacial activity to be modified in the fragrance mixture, which may affect the SiO_2 capsule formation, and in turn affect the mechanical robustness and release profiles of the oils. The perfume oil (PO) to be encapsulated is a mixture of thirteen components including a wide range of molecular structures including alcohols, aldehydes, hydrocarbons and terpene.[1] and it is used in laundry products at P&G, which includes a heavy-duty laundry detergent (HDL) and liquid fabric enhancers (LFE). Thus, the complexity of the commercial fragrance oil potentially makes its encapsulation much more challenging than the encapsulation of HS discussed in **Chapter 4**. Thus, the research in this chapter examines how the complex mixture modifies, if at all, any of the observations and results that were found in **Chapter 4**.

5.1.1 Aims of research in this chapter

In this chapter, the initial aim was to evaluate the encapsulation method using Pickering emulsion-based SiO_2 capsules developed in the previous chapter using HS, for the

References to this Chapter on page 204

encapsulation of a 13-component commercial perfume oil (PO) used in P&G laundry products. The chapter is divided in two parts:

<u>Part 1: Encapsulation of PO in SiO_2 capsules using the method developed for HS</u>

The strategy was to produce SiO_2 capsules using the method described in Chapter 4, using PEOS as silica precursor with SiO_2 NPs (**part 1A**) and without SiO_2 NPs (**part 1B**). SiO_2 capsules were characterized in terms of mean diameter, size distribution, mechanical properties and stability in liquid detergents. The results were compared to HS SiO_2 capsules produced in Chapter 4. **Figure 5-1** provides a simplified roadmap of **Part 1** of the chapter:

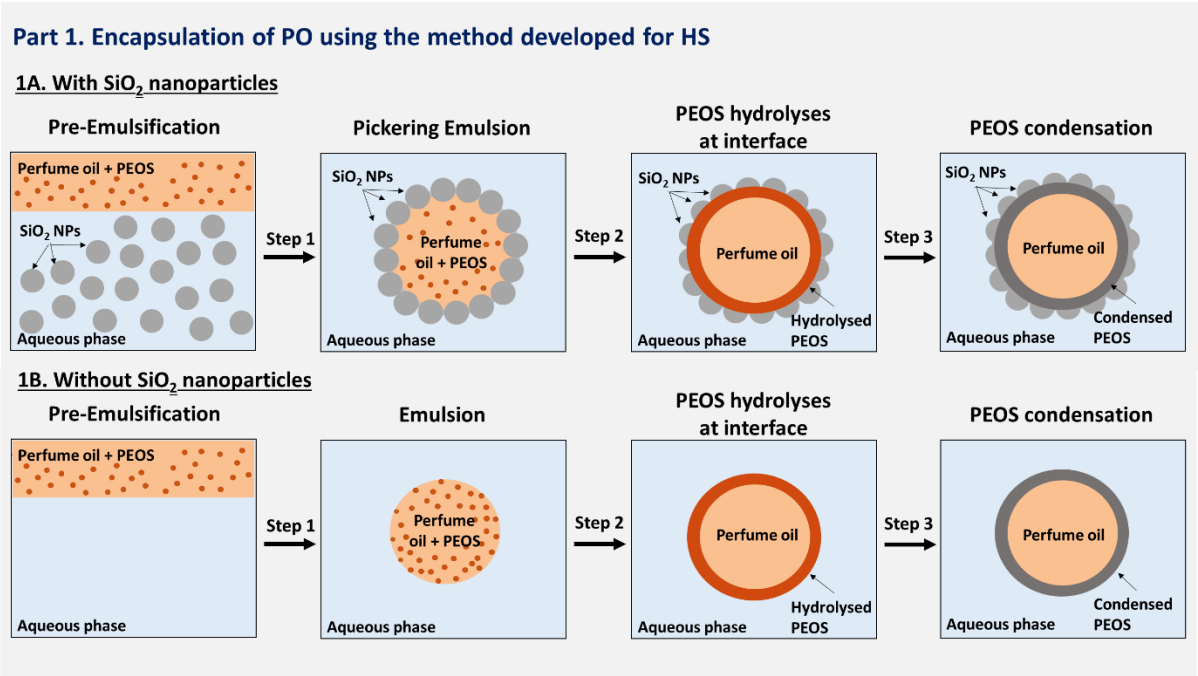

***Figure 5-1**. Proposed route for making SiO_2 capsules with SiO_2 NPs (Part 1A) or without SiO_2 NPs (Part 1B). Step 1: an emulsion between PO containing PEOS and an aqueous phase with or without SiO_2 NPs is prepared. Step 2: PEOS hydrolyses at the oil-water interface. Step 3: PEOS crosslinks via condensation reaction at the interface, forming a solid SiO_2 shell.*

References to this Chapter on page 204

Part 2. Optimization of the PO SiO_2 capsules to meet the industry needs

In **Part 2** the encapsulation process was optimized to meet the industry needs in terms of:

(i) SiO_2 capsule mean diameter;

(ii) mechanical properties;

(iii) stability and performance in LFE.

To optimize the solid SiO_2 shell formation the following parameters were varied (**Figure 5-2.**):

(i) emulsification method (stirring speed);

(ii) concentration of SiO_2 NPs to PO;

(iii) pH of aqueous phase;

(iv) concentration of PEOS;

(v) PEOS molecular weight.

The roadmap for **Part 2** can be found in **Figure 5-2.** The emulsification method and concentration ratio of SiO_2 NPs to PO are varied in Step 1, while the pH of aqueous phase, concentration and molecular weight of PEOS are varied in Step 2.

References to this Chapter on page 204

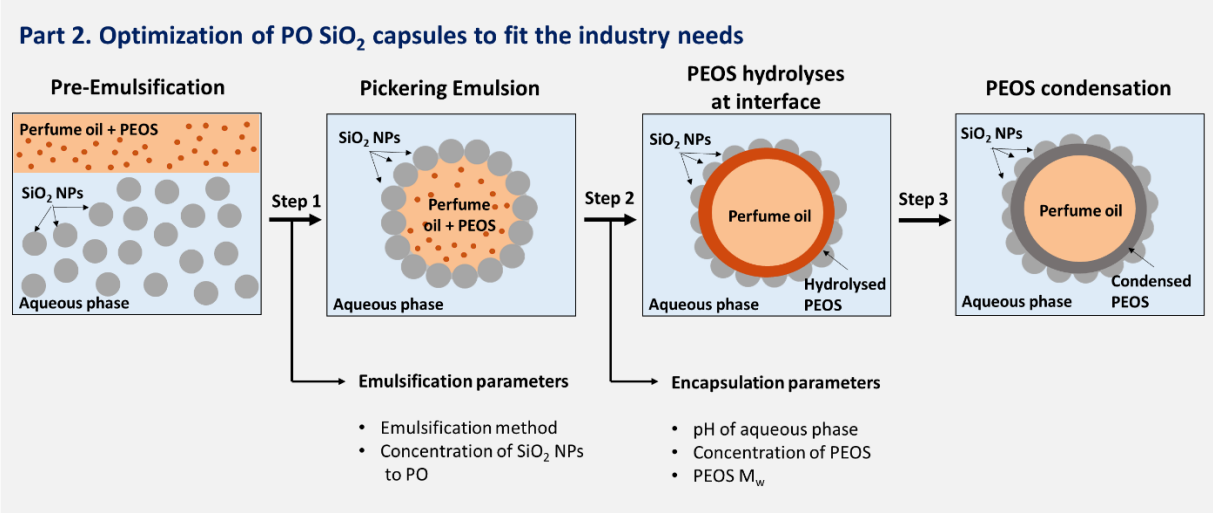

***Figure 5-2**. Proposed route for making improved SiO_2 capsules (Part2). Step 1: an emulsion between PO containing PEOS and an aqueous phase with SiO_2 NPs is prepared by varying the emulsification method and the concentration of SiO_2 NPs. Step 2: PEOS hydrolyses at the oil-water interface, varying the pH and concertation and molecular weight of PEOS. Step 3: PEOS crosslinks via condensation reaction at the interface, forming a solid SiO_2 shell.*

To help with the assessment of the newly developed encapsulation technology, the mean diameter, mechanical properties, *stability* and *performance* for **Part 2** were assessed against a commercially available polymeric perfume microcapsules (PMCs), encapsulating the same PO used in liquid detergent formulations nowadays, in order to identify whether the PO SiO_2 capsule prototypes could be potential sustainable alternative.

5.1.1.1 Commercial polymeric perfume microcapsules (PMCs)

The SiO_2 capsules must have comparable *performance* and *stability* properties to PMCs currently used in industry. Melamine-Formaldehyde (MF) capsules were used as PMCs references for this project with the following properties that must be matched or improved:

References to this Chapter on page 204

(i) stability: no more than 2% perfume leakage in the laundry product after 1 week at 35C°;

(ii) performance: survive the wash and deliver freshness after the fabric is air-dried (noticeable dried fabric odour – DFO).

In terms of physical and mechanical properties, MF capsules have:

(i) mean size between 10 to 35 µm;

(ii) nominal rupture stress around 1.5 – 2.5 MPa;

(iii) deformation at rupture of 40-45%.

SiO_2 capsules encapsulating perfume oil produced in **Part 2** were assessed against the above parameters. The PMCs encapsulating the same perfume oil used in this project were used as benchmark for the SiO_2 capsules development. Commercial MF PMC data was courtesy of P&G.

5.2 Results and discussions

5.2.1 Part 1. Preparation and characterization of perfume oil SiO_2 capsules With and Without SiO_2 Nanoparticles

5.2.1.1 Encapsulation method

The procedure for the encapsulation of the commercial PO was adapted from the experiment designed for the encapsulation of HS. As it was possible to stabilise HS emulsions solely with PEOS, the initial experiments for PO made use of PEOS as silica precursor to form SiO_2 capsules in the presence and absence of SiO_2 NPs, with DI water as continuous phase.

References to this Chapter on page 204

5.2.1.2 Structural and morphological characterization With and Without SiO_2 Nanoparticles

With SiO_2 nanoparticles (capsule ID: SiO_2NPs-PEOS-PO): Using the method developed for the encapsulation of HS with SiO_2 NPs in **Chapter 4**, it proved possible to encapsulate the PO, but with a significant difference that the capsules appeared not spherical but deflated or crumpled[2] (**Figure 5-3A**), as if they had lost some PO. For these experiments, the pH of the continuous phase was found to be 4.5 ± 0.4, which is due to the fumed SiO_2 nanoparticles used to stabilise the droplets, which act as a weak acid with a negative surface charge in neutral pH. One hypothesis for this apparent deflation/crumpling is that as ethanol is released at the interface it increases the solubility of some component oils in the complex PO at the interface, causing the core to lose volume, through solubilisation into the continuous phase, of the more hydrophilic oils in the PO. When PO was stabilised solely by SiO_2 NPS (i.e without PEOS) in **Chapter 3**, Section 3.2.1, there were no signs of deflation, which supports that the ethanol formation is, at least in part, responsible for the deflation of SiO_2NPs-PEOS-PO capsules.

Without SiO_2 nanoparticles (capsule ID: PEOS-PO): Using the method developed for the encapsulation of HS without SiO_2 nanoparticles in Chapter 4, it proved possible to encapsulate the PO (**Figure 5-3B**), with apparently less deflation than when SiO_2 NPs were used (**Figure 5-3A**). Overall, the SiO_2 capsules had a spherical shape with noticeable absence of deflated or crumpled sites. An explanation for this is that PEOS was completely hydrolysed before condensation started, forming a film of hydrolysed PEOS around the droplet before condensation, which could accommodate the loss in volume due to PEOS migration to the interface and ethanol formation that could drive up perfume solubility in water. When the

References to this Chapter on page 204

shell started to solidify the volume was already adjusted and no crumples were present. The pH in this case was found to be 5.9 ± 0.2.

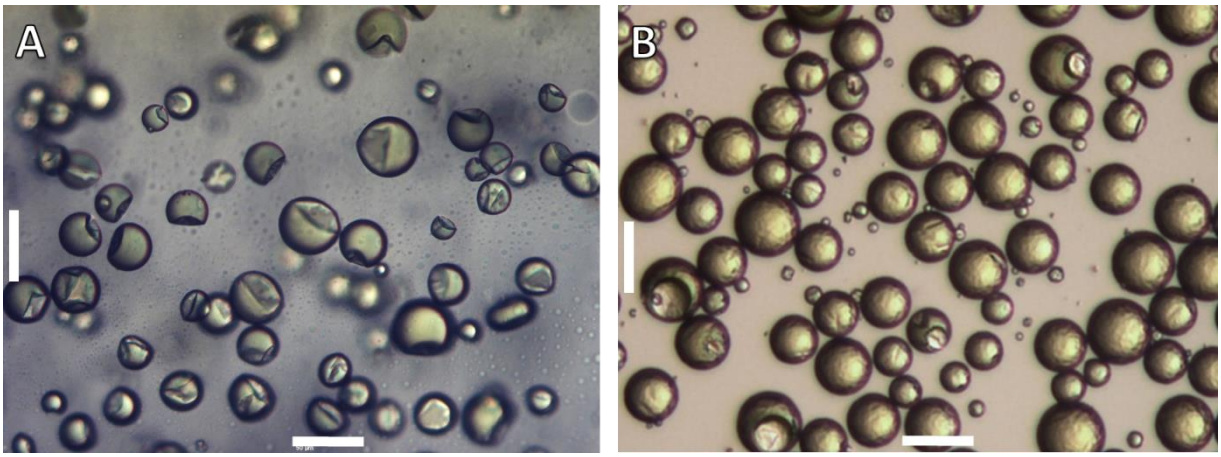

***Figure 5-3**. Optical microscopy images of (A) SiO_2NPS-PEOS-PO (B) PEOS-PO capsules. Scale bar: 50µm*

5.2.1.3 Morphological Comparison of SiO_2 capsule formation with and without SiO_2 nanoparticles, and with PO or HS as the fragrance oil Component.

The SEM images of SiO_2NP-PEOS-PO and PEOS-PO capsules are shown in **Figure 5-4A** and **B**. Interestingly, for both cases, a rough surface structure was observed, in direct contrast to when HS alone was used (**Figure 5-4C** and **D**) due to shrinking of the shell upon drying. This result implies some significant difference is occurring in the formation of the capsules as a result of the nature of the PO relative to HS. Clearly, as shrinking is observed for PEOS SiO_2 capsules prepared with and without SiO_2 NPs, the PEOS layer is responsible for the phenomena, which indicates that some components of the PO interact with PEOS, preventing the formation of a well-defined SiO_2 shell.

References to this Chapter on page 204

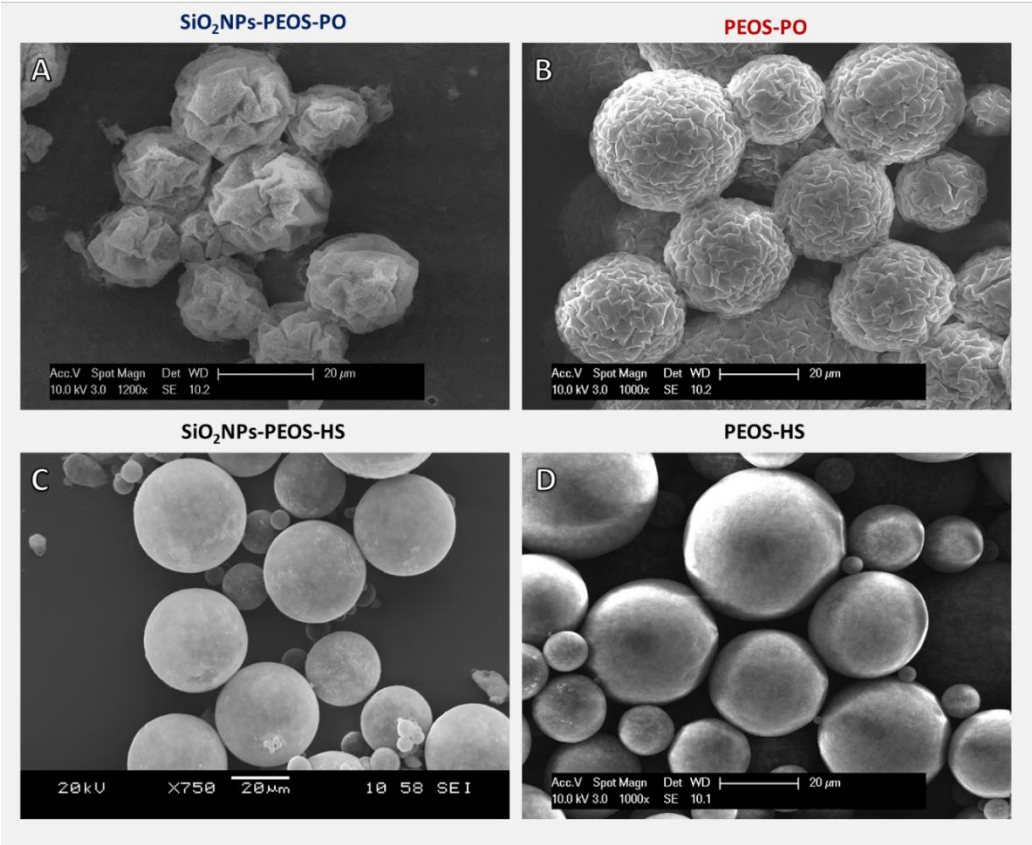

***Figure 5-4**. SEM images of PO SiO_2 capsules (A) SIO_2 NPs-PEOS-PO (B) PEOS-PO, showing clear signs of shell shrinking when dried for the SEM experiments, and HS SiO_2 capsules (C) SIO_2 NPs-PEOS-HS (D) PEOS-HS (Chapter 4), showing a well-defined shell that survives air-drying. The scale bar is 20 µm.*

The shrinking phenomena observed when PO is used could be explained by considering the differences in polarity between PO and HS, whereby PO's is lower (ClogP of PO: 3.5, HS: 5.1). Thus, the interfacial activity of PEOS will be less when PO is used, and hence the density of the SiO_2 cross-linking will be less, and in turn the SiO_2 capsule wall strength will be lower, and hence, upon drying, the shell shrinks when PO is used as a core. The SiO_2NPs-PEOS-PO surface was observed in detail in **Figure 5-5**, where the surface looks much more porous than when HS was used, supporting the reduction in PEOS cross-linking.

References to this Chapter on page 204

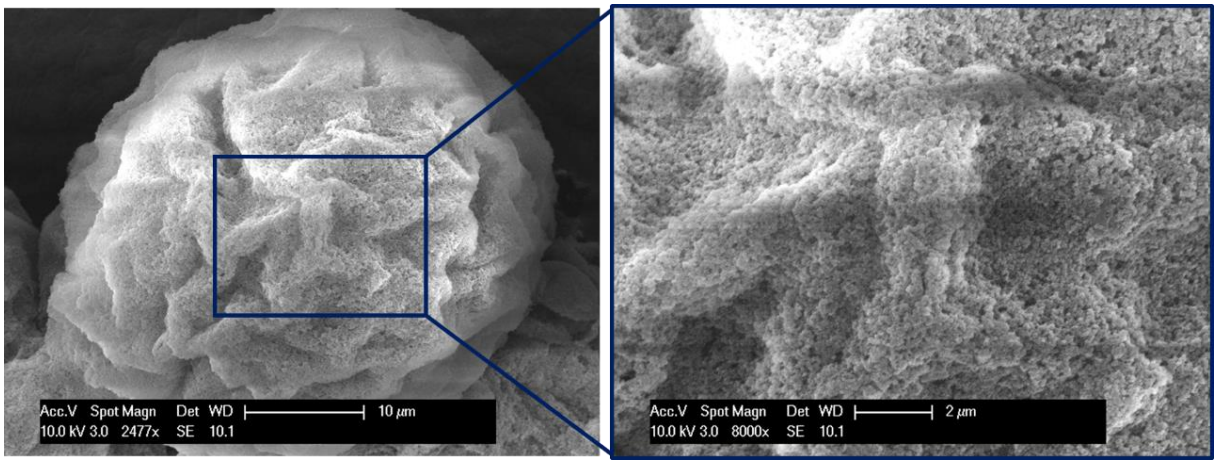

***Figure 5-5**. SEM close up of a SiO_2NPs-PEOS-PO showing a porous structure relative to when HS was used as the single component fragrant oil.*

5.2.1.4 Physical and mechanical properties

The average diameter, SPAN and mechanical properties of both SiO_2NPs-PEOS-PO and PEOS-PO capsules using the Mastersizer and the micromanipulation rig were summarized in Table 5-1**.** It was clear that when maintaining all other parameters fixed, SiO_2 NPs-PEOS-PO capsules were around 8 µm smaller than PEOS-PO capsules. This difference in terms of size is due to the limited coalescence phenomenon that controls the droplet diameter after the Pickering emulsion is formed.[3] There was no significant changes in terms of SPAN, suggesting that PEOS is an efficient emulsifier for PO in these conditions as observed for HS. It is clear that the SiO_2NPs-PEOS-PO had a marginally higher rupture force and nominal rupture stress, while there was no significant difference in terms of deformation at rupture. It was also clear that the mean diameter from the micromanipulation rig, where SiO_2 capsules are air-dried, was much lower than the one from the Mastersizer (where capsules are in solution), supporting the hypothesis that the capsules were shrinking in size upon drying.

References to this Chapter on page 204

Table 5-1. *Comparison of mechanical properties of SiO_2 capsules produced with (SiO_2NPs-PEOS-PO) and without (PEOS-PO) SiO_2 NPs.*

Sample	Mean diameter[a]	SPAN	Micromanipulation Mean diameter[b]	Displacement at rupture	Rupture force	Deformation at rupture	Nominal rupture stress
	µm		µm	µm	mN	%	Mpa
SiO_2NPs-PEOS-PO	42.6 ± 3.9	1.12 ± 0.15	37.1 ± 5.4	8.1 ± 1.5	0.57 ± 0.19	21.7 ± 3.3	0.53 ± 0.08
PEOS-PO	54.9 ± 2.3	0.99± 0.17	36.9 ± 5.7	9.0 ± 1.6	0.50 ±0.15	24.5 ± 2.9	0.47 ± 0.06

[a] *From Mastersizer 2000*
[b] *Mean diameter From side-view camera of the Micromanipulation rig*

When dealing with capsules in general, usually the rupture force increases linearly with the diameter of a capsule.[4] **Figure 5-6** shows the graph for both type of SiO_2 capsules, where it is possible to observe that there is visible increase of rupture force with the increase of the diameter. Moreover, from the experiments using HS (**Chapter 4**), it was suggested that the condensed PEOS layer is responsible for the mechanical properties of the capsule, so the PEOS-HS capsules had comparable rupture force to the SiO_2NPs-PEOS-HS capsules. However, for the capsules prepared using PO as core, there was a small increase in terms of nominal rupture stress for the SiO_2NPs-PEOS-PO capsules when compared to PEOS-PO capsules. This small increase in terms of nominal rupture stress could be due to the cross-linking between PEOS and SiO_2 NPs and the lower pH when acidic SiO_2 NPs were present in solution, accelerating PEOS hydrolysis at the interface.[5]

References to this Chapter on page 204

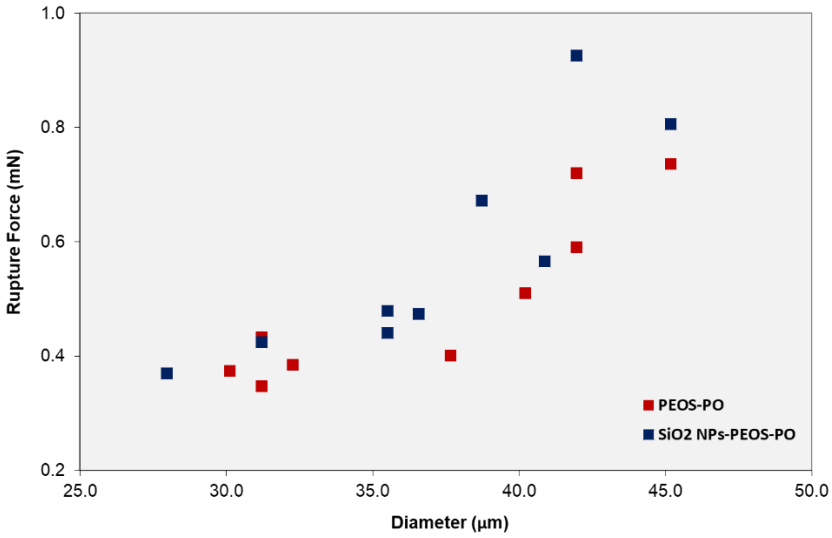

***Figure 5-6**. Diameter versus rupture force values for the SiO_2 NPs-PEOS-PO and PEOS-PO capsules.*

As discussed previously, the SiO_2 capsules shrank in size upon drying, which could contribute to a higher nominal rupture stress for the PO SiO_2 capsules when compared to the HS SiO_2 capsules (**Figure 5-7**). The noticeable difference is reflected by the fact, upon drying, the PO SiO_2 capsules did not have a well–defined core–shell structure compared to HS SiO_2 capsules produced under the same conditions. PO SiO_2 capsules were also compared to a commercial PMC with similar size, and the nominal rupture stress and deformation at rupture were about half the values of the PMC (**Figure 5-7**).

References to this Chapter on page 204

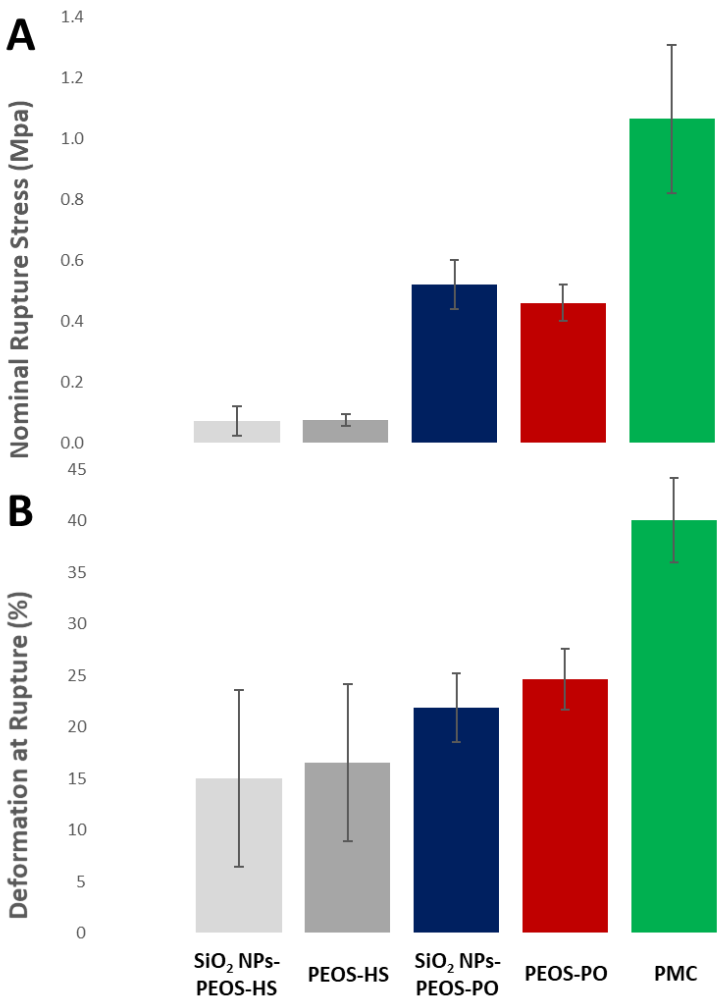

***Figure 5-7**. Nominal rupture force and percentage of deformation at rupture for the SiO_2 capsules with PO core compared to the ones with HS core and a commercial PMC.*

The mechanical trigger release properties of the SiO_2 capsule were also tested using the same method described for the HS SiO_2 capsules. Capsules containing PO were placed on the surface of a glass slide and a glass cover was carefully placed on top of the SiO_2 capsules under an optical microscope. The glass cover was gently pressed to break the SiO_2 capsules in order to observe the PO being released (**Figure 5-8**). The PO was released in a similar fashion to HS in **Chapter 4**. PO was released from the SiO_2 capsules, which confirms the core-shell like

References to this Chapter on page 204

structure of SiO_2 capsules despite the highly rugged shell surface observed in the SEM images and side-view camera in the micromanipulation rig.

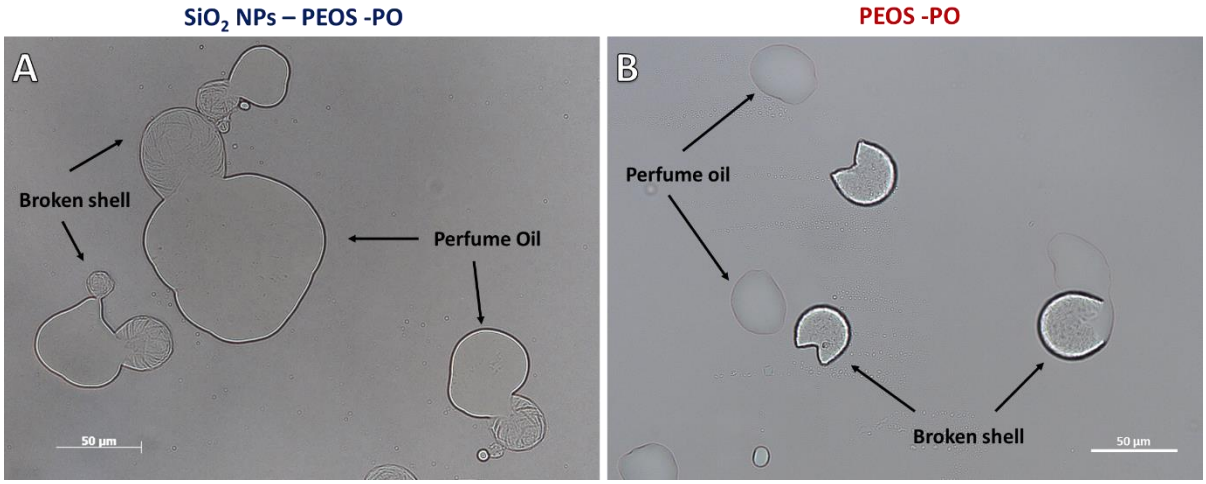

***Figure 5-8**. Optical microscopy of SiO_2NPs-PEOs-PO and PEOS-PO capsules that were gently broken using a glass cover, releasing liquid PO. The scale bar is 50 µm.*

5.2.1.5 Stability in laundry detergent

The stability of the PO SiO_2 capsules in fabric softer matrix (LFE) was assessed using the GC-MS method (Chapter 2 – section 2.5). SiO_2 capsules were dispersed in the liquid detergent matrix and divided in two batches; one stored at room temperature (25°C) and a second one stored at 35°C. Capsules tend to have a higher leakage rate when stored at higher temperature, so it can give a good indication on the stability of the capsules in the detergent matrix when compared to the ones stored at room temperature. It was found that there was 100% leakage after 24h for both samples (the same result was obtained for the HS capsules – Chapter 4), suggesting that the SiO_2 shell formed is highly porous, with or without SiO_2 nanoparticles in the shell.

References to this Chapter on page 204

5.2.2 Part 2. Optimization of the emulsification method to meet the industry needs

5.2.2.1 Emulsification method

For the industrial application, it is desirable that the capsule mean size is between 15-35 µm using a method that can be easily scaled-up for industrial production. This research was then taken to P&G to investigate the possibility of using the methodology described in the previous sections for the preparation of PO SiO_2 capsules in the 15-20 µm size range using methods used in the company to produce PMCs. An ultra-turrax emulsifier operating at 8000 RPM, which is the standard speed used at P&G to produce PMC prototypes, was tested for the SiO_2 capsules in order to produce droplets (and capsules) in the correct size. A new emulsification process needed to be used as the maximum operation speed of the vortex mixer used previously in this project was 2500 RPM.

5.2.2.2 Limited coalescence phenomenon

The limited coalescence phenomenon was investigated using the same method described in **Chapter 3** for vortex mixing. Herein, four different ratios of SiO_2 NPs to PO were investigated. It was possible to obtain droplets in the desired size range of 15 – 35 µm as observed in **Table 5-2**.

***Table 5-2**. Pickering Emulsion droplet size and distribution as a function of increasing SiO_2 NPs ratio relative to PO using the ultra-turrax at 8000 RPM (Step 1).*

Wt% of SiO_2 NPs to PO	Mean diameter, µm	SPAN
0.75	45.6 ± 0.8	0.72 ± 0.07
1.5	30.1 ± 0.4	0.81 ± 0.07
3	18.3 ± 0.5	0.96 ± 0.08
6	12.13 ± 0.72	1.53 ± 0.11

References to this Chapter on page 204

As observed in **Figure 5-9**, the PO droplet size and SPAN of the size distribution could be controlled, by taking advantage of the limited coalescence phenomenon. Moreover, it was possible to obtain a liner relationship between the reciprocal of the mean dimeter and the concentration of SiO_2 NPs in relation to PO with a specific surface area (PO droplet surface covered per unit mass of nanoparticles) of 0.345 m^2g^{-1}. This value is 3.5x more than the observed for the droplets produced using the vortex mixer at 2500 RPM (0.096 m^2g^{-1}, data from Chapter 3).

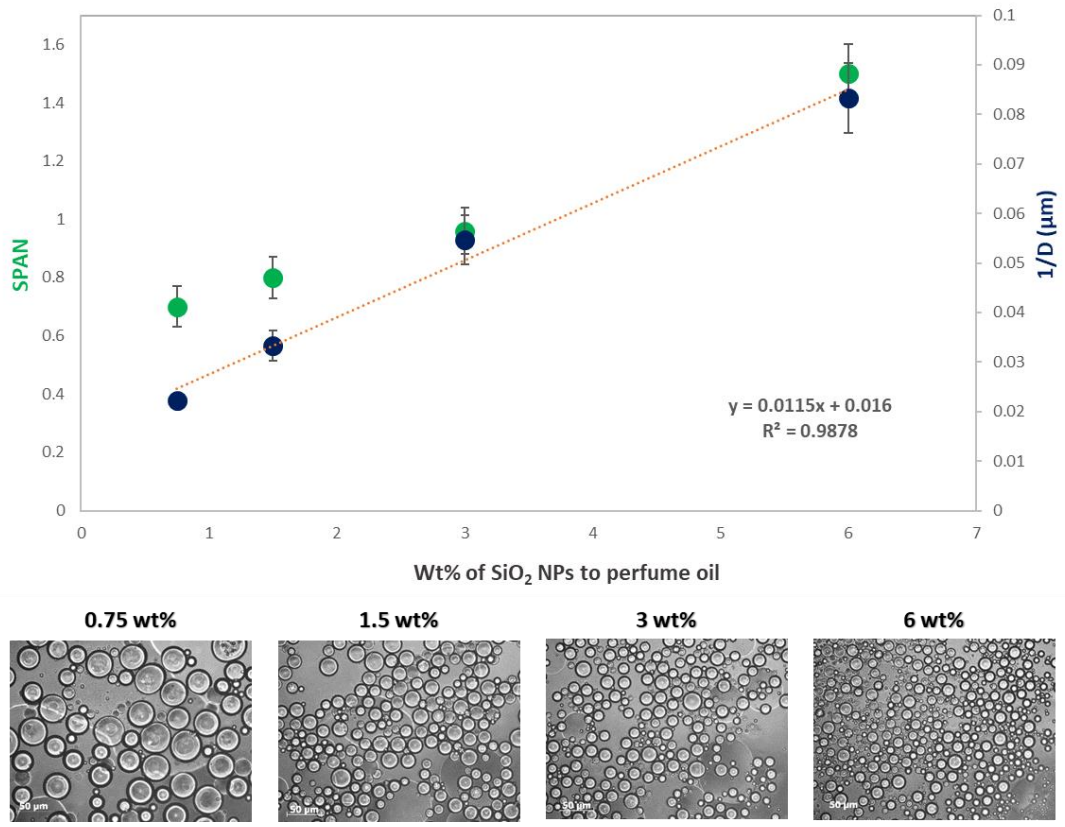

***Figure 5-9**. The graph shows the linear relation between the reciprocal of the droplet diameter and the SiO_2 NPs concentration to PO. Optical microscopy images of samples containing 0.75, 1.5, 3 and 6 wt% of SiO_2 NPs to PO when prepared using the ultra-turrax at 8000 RPM. Scale bars: 200 µm*

References to this Chapter on page 204

5.2.2.3 Preparation of SiO_2 capsules using the ultra-turrax

The possibility of using a higher shear rate to prepare the emulsions was tested for the formation of SiO_2 capsules with and without SiO_2 NPs to stabilise the emulsion, as well as for different quantities of PEOS in the oil phase (varying from 20% to 40% in weight of the oil phase). As observed in **Figure 5-10**, it was possible to produce emulsions with 20% and 40% in weight of PEOS in the oil phase when SiO_2 NPs were used to stabilise the emulsion (**Figure 5-10A and B**). Interestingly, the emulsions formed with 40% PEOS in the oil phase sediment straight after the emulsification: the density of these droplets was 1.02 gcm^{-3}, as it was made of 40 wt% PEOS (density: 1.11 g cm^{-3}) and 60 wt% PO (density: 0.96 g cm^{-3}). The density of hydrolysed silica is 1.65 g cm^{-3}, so as PEOS started to hydrolyse at the interface, the density of the SiO_2 capsule increased further and overcame the emulsion stability provided by the negatively charged SiO_2 NPs covering the surface of the droplets.

For the emulsions prepared with solely PEOS as emulsifier, an inverse emulsion was formed (**Figure 5-10C**), suggesting that PEOS was not an efficient emulsifier at higher shear rates. As a result, the following experiments were designed for PO capsules formed using SiO_2 NPs to stabilise the emulsion, and 20 or 40 wt% of PEOS in the oil phase.

References to this Chapter on page 204

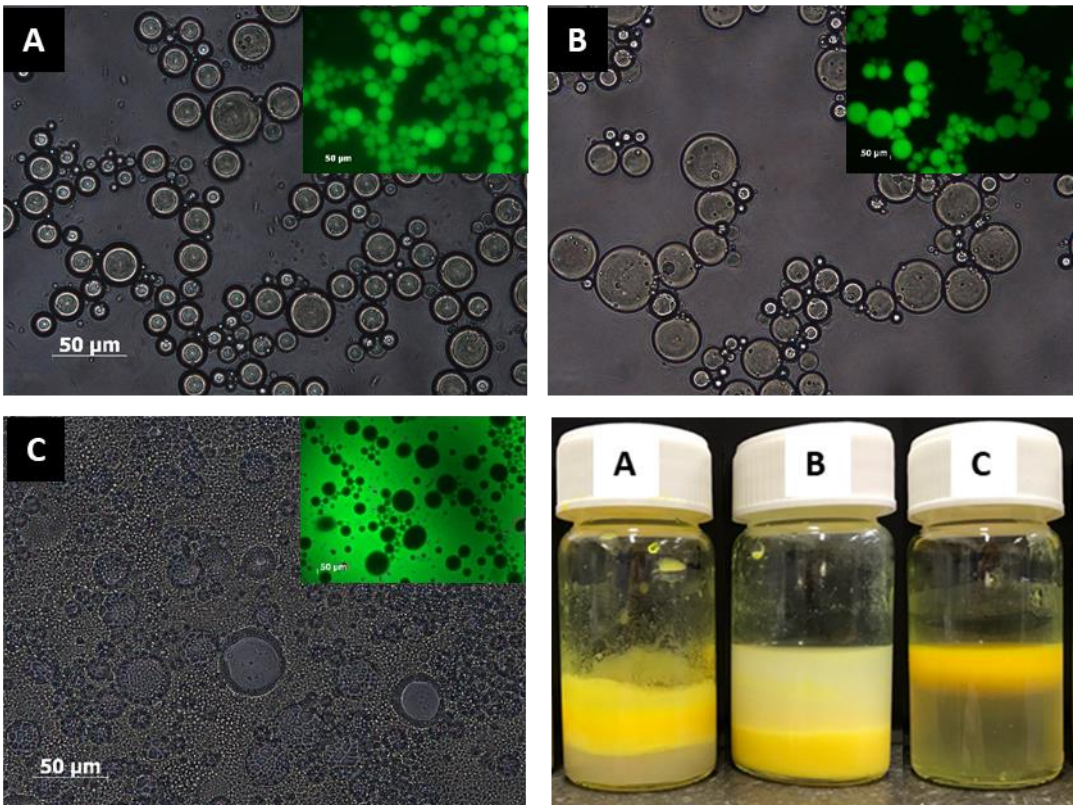

***Figure 5-10**. Optical microscopy images of emulsions prepared using the ultra-turrax operating at 8000 RPM. (A) emulsion between 1 wt% SiO_2 NPs in DI water and PO containing 20 wt% PEOS, (B) emulsion between 1 wt% SiO_2 NPs in DI water and PO containing 40 wt% PEOS and (C) emulsion between DI water and PO containing 20 wt% PEOS. (D) Optical image of the prepared emulsions. Scale bars are 50 µm.*

5.2.3 Optimization of SiO_2 shell formation

5.2.3.1 Effect of the PEOS level

As described in **Chapter 4** for the HS SiO_2 capsules, by increasing the concentration of PEOS in the oil phase, it was possible to increase the shell thickness of the capsule. In addition, the samples prepared with 40wt% PEOS had improved mechanical properties when compared to the ones prepared with 20wt%. This improvement in terms of mechanical properties could

References to this Chapter on page 204

be due to the increase in terms of shell thickness, leading to the formation of capsules that are more resistant or core gelation due to the high concentration of PEOS. PO SiO_2 capsules were produced with different concentrations of PEOS in relation to the oil phase and DI water as continuous phase (**Figure 5-11)**. When no PEOS was used (**Figure 5-11A**), as expected, the emulsion did not survive air drying. When 20 wt% PEOS was used (**Figure 5-11B**), the result was similar to the capsules formed from vortex emulsification at 2500 RPM (**Figure 5-4**). On the other hand, when 40 wt% PEOS was used there was no sign of shell shrinking (**Figure 5-11C**), which suggests that the shell was more mechanically stable. However, the SEM image of a broken capsule (**Figure 5-11D**), suggested that the whole core was gelled, probably due to the high porosity of the material, allowing water to migrate to the interior of the core before full hydrolysis and condensation of the shell. As the surface area was much higher when capsules were prepared at 8000 RPM, the complete solidification of the shell took 5 days at RT.

References to this Chapter on page 204

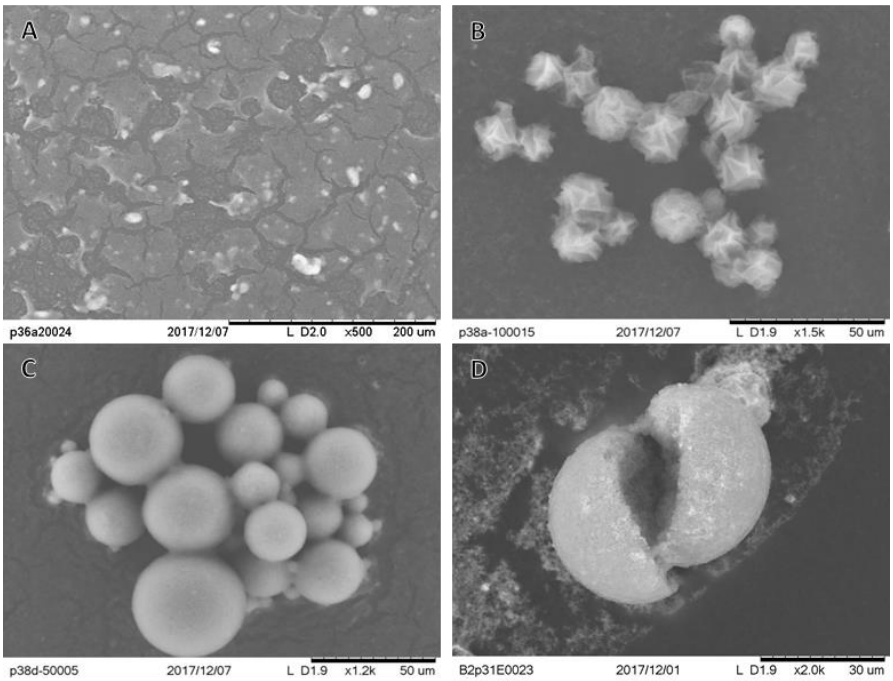

***Figure 5-11**. SEM images of PO SiO_2 capsules prepared in DI water as continuous phase (pH 4.6). (A) initial Pickering emulsion, showing that without PEOS, the emulsion does not survive air-drying, (B) PO SiO_2 capsules prepared with 20 wt% of PEOS (SiO_2NPS-PEOS 1.2-20%-PO-pH 4.6), (C) PO SiO_2 capsules prepared with 40 wt% of PEOS (SiO_2NPS-PEOS 1.2-20%-PO-pH 4.6) and (D) close-up of a broken SiO_2NPS-PEOS 1.2-20%-PO-pH 4.6 capsule. Images obtained after 5 days of capsule preparation.*

5.2.3.2 Effect of pH

The pH of the aqueous phase was varied when optimizing the formation of HS SiO_2 capsules (Chapter 4 – Section 4.2.9.3). It was concluded that an acidic pH leads to the formation of more well-defined capsules, with more narrow size distribution (lower SPAN), which can be explained by the increased surface activity of the SiO_2 NPs at lower pH, due to the protonation of the surface silanol groups (**Figure 4-4**), producing more stable Pickering emulsions. A low pH also catalyses the hydrolysis of PEOS, which could contribute to the formation of a more

References to this Chapter on page 204

robust shell. Herein, PO SiO_2 capsules were produced in different low pH values (1.2, 0.65 and 0.55), to assess the best conditions of the formation of a well-defined SiO_2. The PEOS concentration in the oil phase was kept as 20 and 40 wt% (**Figure 5-12**).

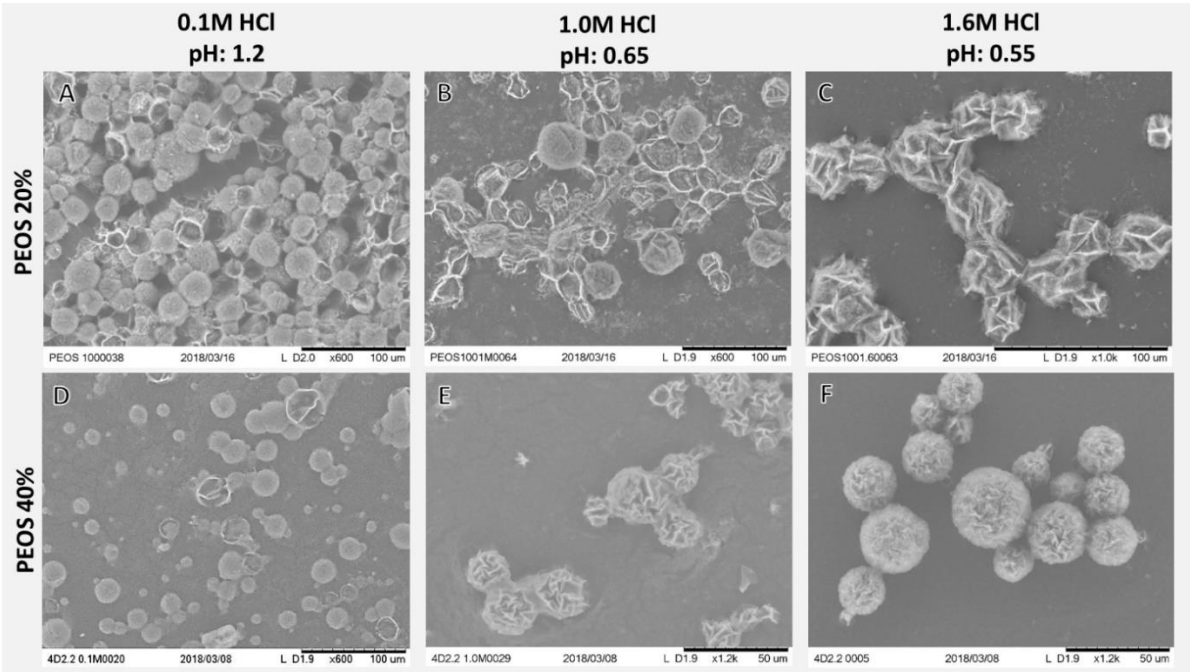

***Figure 5-12**. SEM images of PO SiO_2 capsules produced in different conditions: with 20wt% PEOS: (A) pH 1.2 (SiO_2 NPs dispersed in 0.1M $HCl_{(aq)}$), (B) pH 0.65 (SiO_2 NPs dispersed in 1.0M $HCl_{(aq)}$) and (C) pH 0.55 (SiO_2 NPs dispersed in 0.55M $HCl_{(aq)}$). With 40wt% PEOS: (D) pH 1.2 (SiO_2 NPs dispersed in 0.1M $HCl_{(aq)}$), (E) pH 0.65 (SiO_2 NPs dispersed in 1.0M $HCl_{(aq)}$) and (F) pH 0.55 (SiO_2 NPs dispersed in 0.55M $HCl_{(aq)}$). All images where obtained after 24h of the emulsification.*

From **Figure 5-12**, it is clear that capsules could be formed in all acid pH tested. In addition, the lower pH accelerated the shell formation time (from 5 days in DI water to 3 days in 0.1M HCl and 1 day for 1.6M HCl). However, when the pH was below 1, there was a clear shell shrinking effect, probably because at this point both the hydrolysis and condensation of PEOs

References to this Chapter on page 204

are at the maximum rate, so porous structures are likely to be formed, regardless of the PEOS concentration. Moreover, at such low pH, the slurry started to become yellow, likely due to degradation of PO. At pH 1.2 however, there was no shell shrinking for most of the capsules and no colour change was observed, so this pH was selected for the following optimization experiments.

5.2.3.3 Effect of PEOS M_w

The shell shirking and crumpling effect observed for capsules produced with PEOS 1.2 clearly indicate that PEOS might not be as surface active in PO as in HS. PEOS becomes surface active as it starts to hydrolyse, increasing its affinity towards the water phase.[6] The amphiphilic properties of PEOS also depend on the interfacial tension between oil and water. The higher the surface tension between the two phases, the more surface active PEOS is as it hydrolyses, accumulating at the interface before condensation. As the ClogP for PO (3.5) is lower than the ClogP of HS (5.7), the surface tension between perfume oil and water is lower, so PEOS is less surface active, condensing in the oil phase before reaching the interface.

The shell properties can be improved by varying the molecular weight of PEOS, changing the surface activity of PEOS. PEOS can become more surface active not only by increasing the surface tension between water and oil, but also by increasing the rate at which PEOS becomes amphiphilic, i.e. the rate that PEOS becomes hydrolysed enough to accumulate at the interface. An approach to make PEOS more surface active would be to lower its molecular weight with the objective of forming a partially hydrolysed molecule that is surface active in the perfume oil/water interface, before full condensation of PEOS due to diffusion of water into the core.

References to this Chapter on page 204

In Chapter 3 – Section 3.3, four different PEOS samples were prepared (**Table 3-5**), varying in terms of molecular weight, degree of branching, density and viscosity. In addition, the possibility of preparing capsules using PEOS 1.0, 1.1 and 1.15 as silica precursor, which have a lower molecular weight when compared to PEOS 1.2, and could, in theory, be more surface active, was investigated. All types of PEOS could successfully form SiO_2 capsule at pH 1.2. However, the samples prepared with the lowest molecular weight polymer, named PEOS 1.0, demonstrated the best result in terms of shell formation and mechanical properties. Capsules were prepared using 20% (SiO_2 NPS-PEOS 1.0-20%-PO) and 40% of PEOS 1.0 (SiO_2 NPS-PEOS 1.0-40%-PO) and their shell properties were compared to the capsules produced using PEOS 1.2 using 20% (SiO_2NPS-PEOS 1.2-20%-PO) and 40% of PEOS 1.2 (SiO_2NPS-PEOS 1.2-40%-PO). SiO_2 NPS-PEOS 1.0-20%-PO had remarkably narrow size distributions (**Figure 5-13**) that could be finely controlled by the SiO_2 NPs content in relation to the oil phase by taking advantage of the limited coalescence phenomenon during emulsification (**Table 5-2**)

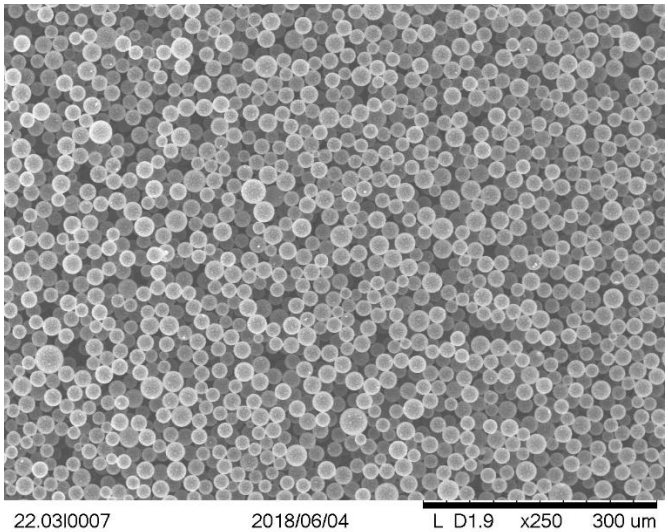

***Figure 5-13**. SEM image of SiO_2 NPS-PEOS 1.0-20%-PO showing a remarkable narrow size distribution.*

References to this Chapter on page 204

When SiO_2 capsules were prepared at pH 1.2 using PEOS 1.0, a solid SiO_2 shell that was able to survive air-drying as completely formed only after a 6-weeks period, which is much slower when compared to the 3 days required for the samples prepared with PEOS 1.2. This is likely due to the more advanced degree of condensation of PEOS 1.2 molecules and the lower number of hydrolysable moieties present in PEOS 1.2. It was not possible to produce capsules using PEOS 1.0 at pH 4.6, as the shell formation was extensively slow (more than 4 months). The reason for the faster shell formation at pH 1.2 is the same as the capsules prepared using PEOS 1.2: at pH 1.2, the hydrolysis step is catalysed, allowing for the formation of a hydrolysed PEOS film at the interface before condensation starts.

5.2.3.4 Shell properties comparison

SiO_2 capsules prepared using 20 wt% or 40 wt% of PEOS 1.2 and 1.0 at pH 1.2 had their shell morphology compared using optical microscopy and SEM. The optical microscopy images show that for the samples produced using PEOS 1.2 in 0.1M HCl aqueous solution (**Figure 5-14A** SiO_2 NPS-PEOS 1.2-20%-PO and **B** SiO_2 NPS-PEOS 1.0-40%-PO) a core-shell structure is formed. However, the solid shell was not completely filled with perfume oil and presented crumples, as observed for the capsules produced using PEOS 1.2 in DI water (**Figure 5-3**. Optical microscopy images of (A) SiO_2NPS-PEOS-PO (B) PEOS-PO capsules. Scale bar: 50µm). The best hypothesis to explain the morphology of the shell is that the side product from the hydrolysis and condensation of PEOS is ethanol, which could drive up the solubility in water of some PO components, causing the core to lose volume before full solidification.

The SiO_2 capsules produced using PEOS 1.0 did not present crumples on the shell, which were completely round. However, from **Figure 5-14C** and **D**, it was clear that the shell was not

References to this Chapter on page 204

completely filled with perfume oil and a void was observed. The presence of a well-defined shell suggests that PEOS 1.0 was indeed more surface active than PEOS 1.2, as all hydrolysed PEOS 1.0 solidified at the interface, avoiding crumples of the shell due to core loss at the early stages of shell formation. Nevertheless, the presence of a void inside the shell suggests that perfume oil could still escape from the shell, probably due to the silica shell being highly porous, so some PO components with higher solubility towards water might have diffused to the aqueous phase, as the shell was slowly forming, probably due to the formation of ethanol.

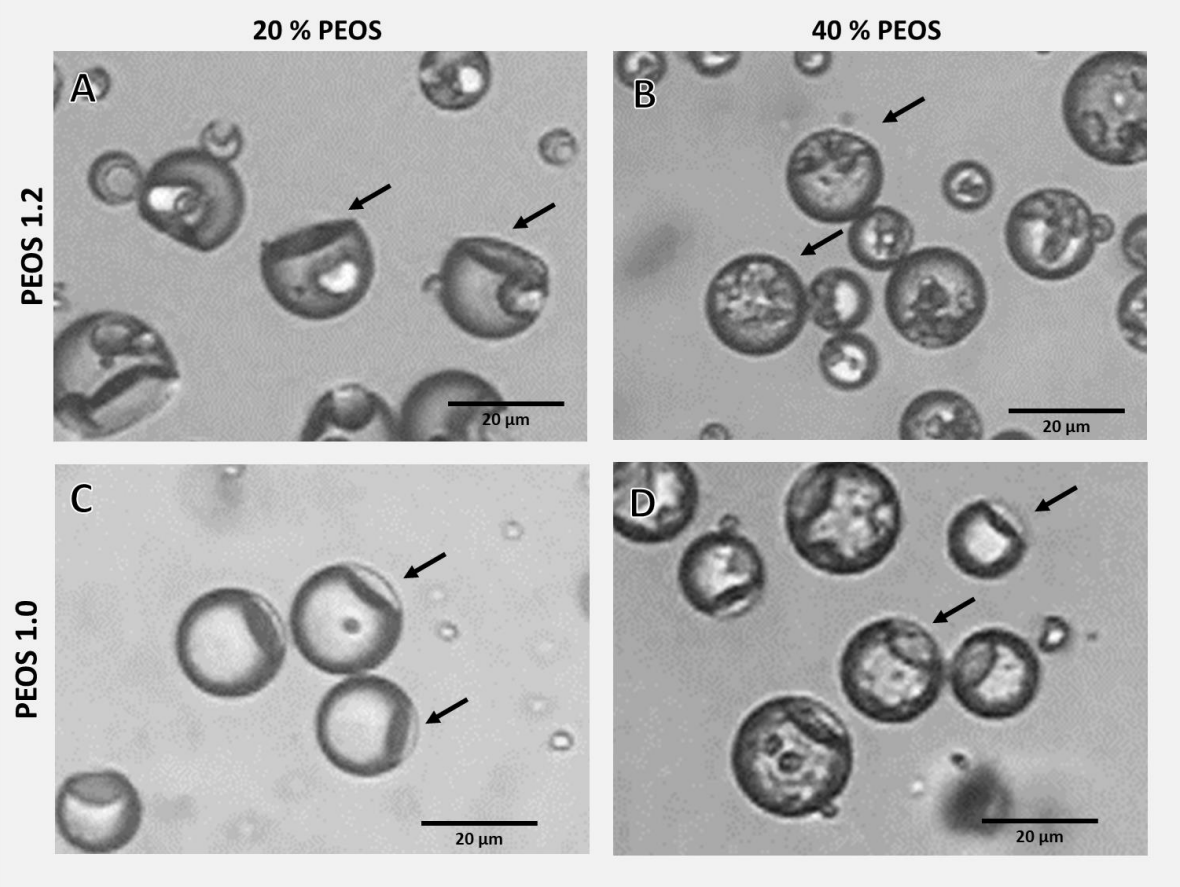

***Figure 5-14**. Optical microscopy images of SiO_2 capsules produced with (A) SiO_2 NPS-PEOS 1.2-20%-PO; (B) SiO_2 NPS-PEOS 1.2-40%-PO; (C) SiO_2 NPS-PEOS 1.0-20%-PO and (D) SiO_2 NPS-PEOS 1.0-40%-PO. The scale bar is 20 µm.*

References to this Chapter on page 204

Figure 5-15 compares the inner shell morphology of capsules produced with 20 and 40 wt% PEOS 1.0 or 1.2. It is clear that the samples SiO_2 NPS-PEOS 1.2-20%-PO and SiO_2 NPS-PEOS 1.2-40%-PO had no significant difference in terms of shell thickness and the excess of PEOS condensed inside the shell (**Figure 5-15A** and **B**). A probable explanation is that the rate of water diffusion through the SiO_2 NPs/hydrolysed PEOS shell is faster than the hydrolysis and condensation rate of PEOS at the interface, which indicates a low surface activity of PEOS in perfume oil. The insert of the images shows an intact SiO_2 capsule where the crumple described above is clearly observed. On the other hand, the SiO_2 NPS-PEOS 1.0-20%-PO and SiO_2 NPS-PEOS 1.0-40%-PO capsules possess a well-defined shell that could have its thickness controlled by the amount of PEOS used (**Figure 5-15C** and **D**), the insert images of intact SiO_2 capsules show no signals of shell deformation.

References to this Chapter on page 204

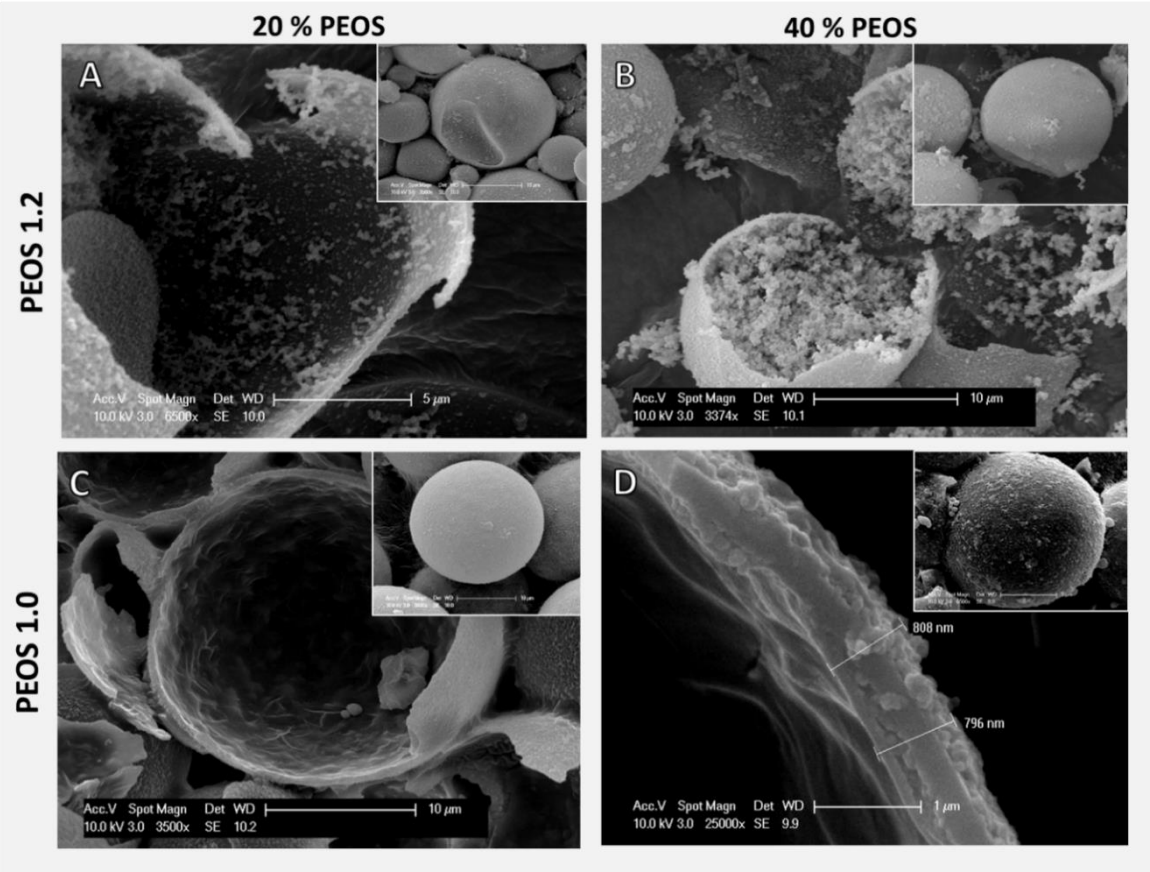

***Figure 5-15**. SEM images of SiO_2 capsule shells comparing samples produced with (A) SiO_2 NPS-PEOS 1.2-20%-PO; (B) SiO_2 NPS-PEOS 1.2-40%-PO; (C) SiO_2 NPS-PEOS 1.0-20%-PO and (D) SiO_2 NPS-PEOS 1.0-40%-PO. The insert shows intact capsules.*

As the only variable between the above samples is the molecular weight of the PEOS used as silica precursor, it was clear that the surface activity of PEOS could be tailored simply by varying the molecular weight. This variation leads to an efficient formation of a well-defined core-shell structure encapsulating a complex oil with a lower interfacial tension with water when compared to HS. The formation of a well-defined shell at pH 1.2 is likely to be due to a high hydrolysis rate in comparison to the condensation, so all the PEOS hydrolyses at the interface before condensation starts.[7] The consequence is that hydrolysed PEOS molecules

References to this Chapter on page 204

are allowed to rearrange at the interface before solidification, allowing for the formation of a well-defined shell, as all PEOS is fully hydrolysed.[5]

The mean diameter, SPAN, experimental shell thickness and theoretical calculation of the PEOS layer from **Equation 4-5**, for the capsules prepared using PEOS 1.2 at pH 4.6 and 1.2 and the capsules prepared using PEOS 1.0 are described in **Table 6-4**. Increasing the amount of PEOS in the oil phase from 20 to 40 wt% did not change significantly the mean diameter of the capsules or the SPAN of the size distribution.

References to this Chapter on page 204

***Table 5-3**. Mean diameter, SPAN, average shell thickness values and mechanical properties for the capsules produced at pH 1.2 with 20% and 40% in weight of PEOS 1.2 or 1.0 formulated in the oil phase.*

Sample	pH	SiO_2 precursor		Shell structure	Shell solidification time	Mean diameter	SPAN	Average shell thickness	Theoretical PEOS condensed layer thickness (from Eq. 4-5)	Deformation at rupture	Nominal rupture stress
		Type	Conc.			µm	µm	nm	nm	%	Mpa
SiO_2NPS-PEOS 1.2-20%-PO-pH 4.6	4.6	PEOS 1.2	20 wt%	Core/shell (shrinking upon drying)	5 days	22.2 ± 1.9	1.23 ± 0.11	-[a]	232	18.85 ± 2.6	0.22 ± 0.06
SiO_2NPS-PEOS 1.2-40%-PO-pH 4.6	4.6	PEOS 1.2	40 wt%	Gelled core/shell	5 days	26.8 ± 1.9	1.10 ± 0.13	-[a]	574	24.81 ± 2.7	0.89 ± 0.16
SiO_2NPS-PEOS 1.2-20%-PO	1.2	PEOS 1.2	20 wt%	Core/shell	3 days	18.8 ± 1.2	1.02 ± 0.05	308 ± 28	232	21 ± 6	0.32 ± 0.14
SiO_2NPS-PEOS 1.2-40%-PO	1.2	PEOS 1.2	40 wt%	Gelled core/shell	3 days	19.0 ± 1.1	1.05 ± 0.08	383 ± 26	574	15 ± 5	0.79 ± 0.10
SiO_2NPS-PEOS 1.0-20%-PO	1.2	PEOS 1.0	20 wt%	Core/shell	6 weeks	17.0 ± 1.0	0.99 ± 0.03	375 ± 41	174	20 ± 9	0.30 ± 0.09
SiO_2NPS-PEOS 1.0-40%-PO	1.2	PEOS 1.0	40 wt%	Core/shell	6 weeks	17.1 ± 1.1	1.21 ± 0.23	750 ± 25	437	15 ± 5	1.04 ± 0.43

[a] Shell thickness could not be measured experimentally

References to this Chapter on page 204

(a) PO SIO_2 capsule produced with PEOS 1.2

The shell thickness for both samples at pH 1.2 was higher than the theoretical shell thickness from **Equation 4-5**, which considers the capsule mean diameter, the density of the oil phase and full conversion of PEOS into SiO_2. The shell thickness for the SiO_2 NPS-PEOS 1.2-20%-PO capsules (232 nm) was in relative agreement with the experimental data (308 nm); the difference is due to the SiO_2 NPs layer that is not taken into account when theoretically calculating the condensed PEOS layer. As the fumed SiO_2 NPs form aggregates of around 100 nm, the experimental shell thickness was good agreement with the theoretical calculation. The SiO_2 NPS-PEOS 1.2-40%-PO capsules had a much larger theoretical condensed PEOS thickness (574 nm) than the experimental value (383 nm), which is in agreement with the SEM images (**Figure 5-15**), showing that the excess of PEOS solidifies inside the shell. Interestingly, there seems to be a limited thickness of the condensed PEOS layer, as the shell thickness using 20 or 40 wt% PEOS was relatively similar due to water migration into the hydrated PEOS layer limited by complete hydrolysis and condensation of PEOS.[6]

(b) PO SIO_2 capsule produced with PEOS 1.0

The experimental shell thickness for samples prepared with PEOS 1.0 was higher than the theoretical calculation (**Equation 4-5)**. For the SiO_2 NPS-PEOS 1.0-20%-PO capsules, the experimental shell thickness was 375 nm while the theoretical condensed PEOS thickness was 174 nm. There was a difference of about 200 nm, which could imply that the condensed PEOS layer was highly porous, as the calculation is based on an assumption of a dense structure. For the SiO_2NPS-PEOS 1.0-40%-PO capsules, the experimental average shell thickness was

References to this Chapter on page 205

about 750 nm and the theoretical calculation returned a value of 437 nm. The difference again could be due to the formation of a porous structure, as from the SEM images of the shell (**Figure 5-15D**), the SiO_2 NPs layer is much thinner when compared to the condensed PEOS layer and could not contribute significantly to the overall shell thickness.

5.2.3.5 Overall mechanical properties

Bar charts in **Figure 5-16** compare (A) the nominal rupture stress and (B) the deformation at rupture of capsules at pH 1.2 using PEOS 1.0 and PEOS 1.2 containing 20 or 40 wt% PEOS as silica precursor. It is possible to observe that for both samples prepared with 20% PEOS (SiO_2 NPS-PEOS 1.2-20%-PO and SiO_2 NPS-PEOS 1.0-20%-PO), there was no significant difference in terms of nominal rupture stress, and the values were about 3X smaller than the one of the commercial PMC (**Figure 5-16A**). The experimental shell thickness for these samples was quite similar (308 nm for PEOS 1.2 and 375 nm for PEOS 1.0), which is a plausible explanation for their similar mechanical properties.

There was a significant increase in terms of nominal rupture stress for the samples produced using 40 wt% of PEOS compared to the ones produced using 20 wt%. The value for SiO_2 NPS-PEOS 1.0-40%-PO capsules was comparable to the PMC values for capsules with similar sizes. This difference in terms of nominal rupture stress is likely due to the shell thickening effect observed when more PEOS was used to form the shell, forming more mechanically strong SiO_2 capsules. The SiO_2 NPS-PEOS 1.2-40%-PO capsules also saw an increase in terms of nominal rupture stress when compared to the samples produced using 20 wt%. However, as observed in **Figure 5-15B**, there is an excess of PEOS condensing in the core and forming a

References to this Chapter on page 205

solid matrix, which provides the capsule more resistance to the force imposed by the probe during the micromanipulation experiment for a given deformation.

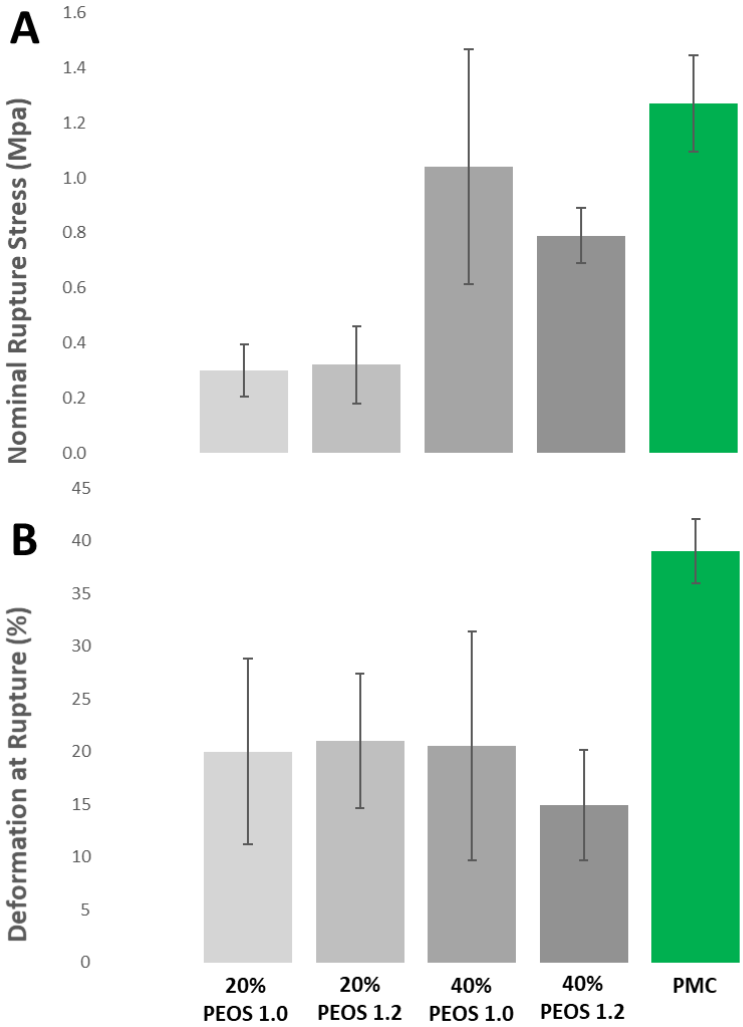

***Figure 5-16**. (A) Nominal rupture force and (B) percentage of deformation at rupture for the SiO_2 capsules with PEOS 1.0 or 1.2 (20 wt% and 40 wt%) produced at pH 1.2 compared to a commercial PMC.*

In terms of percentage of deformation at rupture (**Figure 5-16B**), capsules deformed around 20% of their size, which is about half of the deformation observed for PMCs (40%). It can be explained by the brittle character of the SiO_2 shell, leading to a small deformation before

References to this Chapter on page 205

breaking, which explains the overall lower nominal rupture stress when compared to PMCs. The highly deformable shell found in PMCs can also improve their nominal rupture stress as the deformation can accommodate the force opposed by the probe before rupture.

5.2.3.6 Overall stability and performance in laundry detergents

(a) Pre-assessment: air drying in glass slide

Capsule air-drying in glass slide tests were used to rapidly pre-assess stability and performance of prototypes capsules. The stability was assessed using optical microscopy by the analysis of the shell deformation due to perfume leakage when capsules were air-dried. Performance was assessed through an olfactive assessment of the dried capsules by breaking the capsules when pressing a second glass slide against the one where the capsules were dried (method described in Chapter 2).

For this test, all capsules produced could survive air-drying. However, only the capsules produced using PEOS 1.0 (SiO_2 NPS-PEOS 1.0-20%-PO and SiO_2 NPS-PEOS 1.0-40%-PO) could retain perfume after drying for 24h, which could be smelled when the capsules were broken using a second glass slide. This result indicates that PEOS 1.0 could form robust structures capable of protecting the perfume from escaping the shell during the drying process.

(b) Perfume headspace using GC-MS

To assess quantitatively the amount of perfume that leaked out from the capsules in the laundry product (LFE – laundry fabric enhancer), a perfume headspace study was performed using a gas chromatograph system connected to a mass spectrometry detector (GC-MS). As the perfume formulation is a mixture of different perfume raw materials (PRMs), each of these PRMs was individually quantified by the GC-MS and its level was assessed against a pure

References to this Chapter on page 205

perfume reference. Perfume headspace was measured after 24h from the addition of the capsules to the laundry product.

As expected, capsules produced with PEOS 1.2, which could not retain perfume using the above test, also had 100% leakage when the perfume headspace was tested using GC-MS. Unfortunately, even the samples prepared using PEOS 1.0 (SiO_2 NPS-PEOS 1.0-20%-PO and SiO_2 NPS-PEOS 1.0-40%-PO, that could retain the perfume after air-drying, could not prevent perfume leakage when the capsules were added to a detergent matrix (LFE) and had 100% leakage after 24h in the detergent matrix.

Figure 5-17 shows optical images of capsules produced using PEOS 1.0 dispersed in LFE at the initial moment and after 24h. It is possible to see that initially the contrast of the SiO_2 capsules with the background suggests that the capsules were filled with perfume oil. After 24h the perfume had leaked out and the contrast was almost completely lost and the shell looks empty.

References to this Chapter on page 205

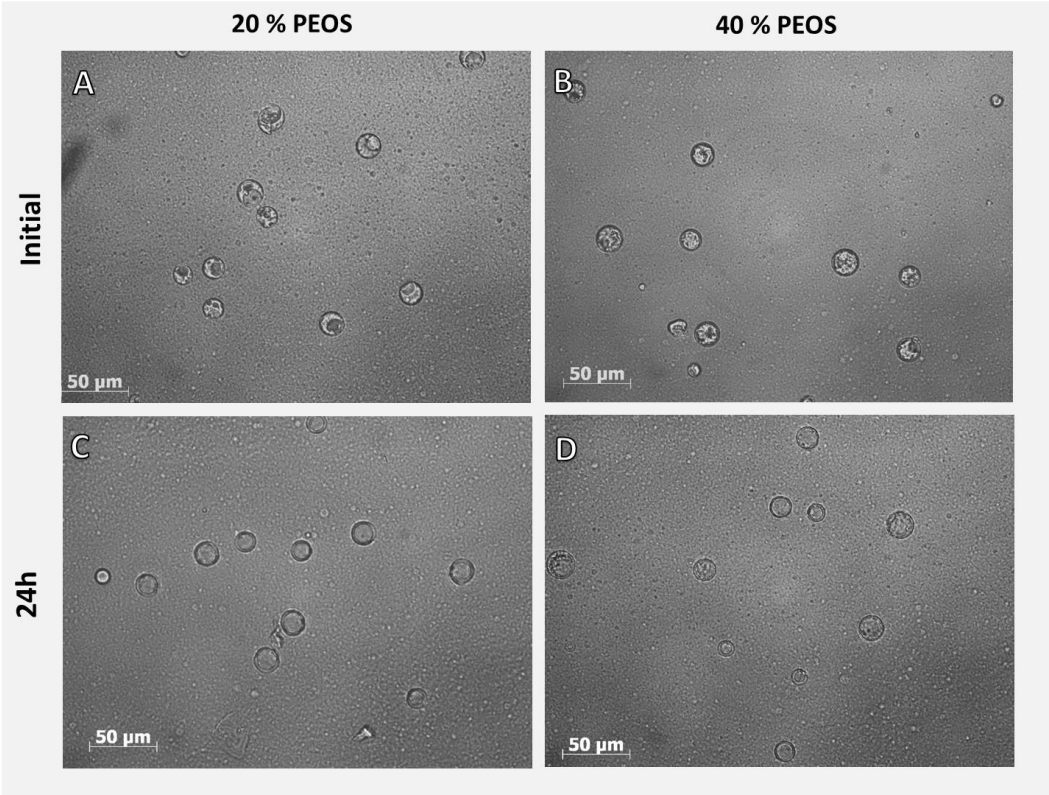

***Figure 5-17**. Optical microscopy images of SiO_2 NPS-PEOS 1.0-20%-PO and SiO_2 NPS-PEOS 1.0-40%-PO capsules when initially dispersed in LFE and after 24h at RT. The scale bar is 50 µm.*

5.3 Conclusions

SiO_2 capsules formed using hydrophilic SiO_2 fumed nanoparticles and PEOS as shell material and a commercial perfume oil as core were successfully produced. SiO_2 capsules were synthesised and characterized using the method described for the encapsulation of HS (Chapter 4). Although the perfume oil could be successfully encapsulated, the capsules were much larger in size when compared to commercial PMCs (MF capsules) currently used in laundry products. Moreover, the SiO_2 capsule wall was not rigid and started to shrink when air-dried, which made it difficult to measure the mechanical properties and shell thickness. In terms of performance and stability, these SiO_2 capsules could not retain the perfume oil inside the shell when added to a liquid detergent matrix.

References to this Chapter on page 205

A new emulsification method was used to match the capsule size requirements of the P&G commercial capsules and the pH of the continuous phase was adjusted to catalyse the hydrolysis of the silica precursor polyethoxysiloxane (PEOS), and produce a more rigid shell that did not experience shrinking upon drying, producing capsules with a well-defined SiO_2 shell. When capsules were produced in a low pH media (pH 1.2) the shell was well-defined and did not shrink upon drying as the hydrolysis step is much faster than the condensation, allowing reorganization of hydrolysed PEOS molecules at the interface, leading to the formation of a well-defined shell.

The molecular weight of the PEOS was also varied. The results suggested that the surface activity of PEOS could be tailored simply by varying the molecular weight. This simple variation leads to an efficient formation of a well-defined core-shell structure encapsulating a complex oil with a lower interfacial tension with water when compared to HS. There are three hypotheses to explain the different shell morphologies by varying the pH of the aqueous phase and the molecular weight of PEOS:

(i) the side product from the hydrolysis and condensation of PEOS is ethanol, which could drive up the solubility in water of some PRM components, causing the core to lose volume at early stages of shell formation (most likely);

(ii) as PEOS condenses, it is no longer part of the oil core volume, as the droplet is covered with solid SiO_2 NPs, and therefore, the core volume is depleted of the volume occupied by PEOS (around 20%);

References to this Chapter on page 205

(iii) the solid shell is formed rapidly and some components of the perfume oil with higher solubility in water might diffuse to the aqueous phase due to the high porosity of the wall, independently of the presence of ethanol.

Hypothesis (i) is more likely to explain the morphology of SiO_2 capsules produced using PEOS 1.2 and it is valid for capsules produced using both DI water and 0.1M HCl as aqueous phase. Hypothesis (ii) is less likely as the capsules produced using HS as core material did not present shell crumpling, suggesting that the morphology observed for SiO_2 capsules produced using perfume oil as a core is likely due to the loss of PRM components, and not due to PEOS condensation. Hypothesis (iii) explains the morphology of the capsules produced using PEOS 1.0, that has a higher surface activity hence all PEOS condenses at the interface, however some PRM still leaks out, possibly due to the porosity of the formed shell.

Capsules produced with PEOS 1.0 had a much slower shell solidification kinetics when compared to capsules prepared using PEOS 1.2, likely to be due to the more advanced stage of condensation of PEOS 1.2 molecules and the lower number of hydrolysable moieties on the surface of PEOS 1.2, which accelerates the sol-gel process. Nevertheless, the smaller molecular weight of PEOS 1.0 molecules compared to PEOS 1.2, contributes to the easy rearrangement of the PEOS molecules at the interface and the formation of a well-defined shell, where all PEOS solidifies at the interface.

The ratio of PEOS to oil was also varied in order to enhance the shell mechanical properties. When PEOS 1.0 was used to form the shell, by increasing the PEOS concentration it was possible to increase the shell thickness and as consequence, the nominal fracture strength, which had a comparable value to a commercial PMC. For SiO_2 capsules produced with PEOS

 References to this Chapter on page 205

1.2, there was no significant increase in terms of shell thickness, independently of the pH and the excess of PEOS solidified in the core of the capsule, due to the low surface activity.

Although it was possible to produce SiO_2 capsules with enhanced mechanical properties and capable of retaining perfume inside the shell when the capsule was air-dried, the capsules produced using PEOS 1.0 were not able to prevent the release of perfume oil when the capsules were added to a detergent matrixes (LFE), which could be explained by the porosity of the shell that released 100% of the encapsulated perfume in less than 24 hours.

As a final conclusion, the SiO_2 capsules produced at this stage could successfully match the size required by the P&G in a remarkable narrow size distribution and enhanced nominal rupture stress by controlling the shell thickness. However, due to the brittleness of the SiO_2 shell, the capsules exhibited a lower deformation at the rupture than the polymeric capsules counterparts. In addition, these capsules had 100% PO leakage after 24h when dispersed in a liquid detergent matrix (LFE).

5.4 Experimental

5.4.1 Encapsulation of perfume oil

5.4.1.1 Using the vortex mixer

A 1 wt% Aerosil 300 dispersion in DI water was prepared. In a separate vial, 0.1g of PEOS was dissolved in 0.4g of the perfume oil containing 0.1wt% of PM546. The perfume oil and PEOS mixture was then added to the water phase containing SiO_2 nanoparticles (or only DI water for the experiments without SiO_2 nanoparticles) and the mixture was then emulsified using a vortex mixer at 2500 RPM for 5 minutes. The vial was then left to stand on the bench top

References to this Chapter on page 205

(25°C) and centrifuged at 2000 RPM for 10 minutes to isolate the capsules after condensation was complete (variable for each sample).

5.4.1.2 Using the ultra-turrax

A 2.5 wt% Aerosil 300 dispersion in water was prepared. In a separate vial, 0.5g of PEOS was dissolved in 2 g of the PO (1g of PEOS for experiments with 40%PEOS in the core). The PO and PEOS mixture was then added to the water phase containing SiO_2 nanoparticles and the mixture was then emulsified using an IKA Ultra-Turrax T25 basic homogeniser (IKA-Werke GmbH & Co – Germany) filled with a dispersing head of 10 mm diameter operating at 800 RPM for 5 minutes. The vial was then left to stand on the bench top (25°C) for the condensation step to be completed.

5.4.2 Size analysis

Mean capsule diameter and SPAN of the size distribution of the capsules in aqueous dispersion were obtained by static light-scattering using a Mastersizer 2000 instrument (Malvern Instruments Ltd, Malvern - UK). The instrument measures the volume fraction of the capsules in different size bands in the size range of 20 nm to 2000 µm using a Helium-Neon laser connected to a dispersion unit. All experiments were performed at 25°C. The refractive index used was 1.46 (for amorphous silica[8]) and the data analysed using Excel®.

5.4.3 Optical microscopy

Optical microscopy images were obtained using two microscopes: a Leica DMRBE, (Leica Microscope & Systems GmbH) equipped with a software package Moticam Pro 3.0 and a CoolLED pE-300 white light source. The resolution of the microscope was 200 nm. The second

References to this Chapter on page 205

microscope used was a Zeiss Axio imager 2 pol (Carl Zeiss Microscopy – Germany, resolution 200 nm) also equipped with a UV light source (Kubler codex HXP 120C).

5.4.4 Scanning Electron Microscopy

SEM images were obtained using two different microscopes: a 1000 Tabletop Microscope (Hitachi, Ltd – Japan), magnification 1500X and a Philips XL-30 FEG Environmental SEM with Oxford Inca EDS (Philips UK ltd, Guildford – UK), magnification 3500X.

5.4.5 Trigger release

0.1g of SiO_2 capsule suspension containing 20% w/w capsule to DI water was diluted in 5ml of DI water. One drop of the diluted dispersion was placed onto the surface of a glass micro slide and covered with a cover slide. The cover slide was then pressed gently using a spatula to break the SiO_2 capsules and observe the oil being released under the optical microscope (Carl Zeiss Microscopy – Germany, resolution 200 nm).

5.4.6 Mechanical properties

The mechanical properties of the SiO_2 capsules were determined by micromanipulation. 0.1g of SiO_2 capsule suspension containing 20% w/w SiO_2 capsule to DI water was fist diluted 500x in DI water, then a drop of the diluted dispersion was added to a glass slide and left to air dry. The glass containing the capsules was then positioned on the micromanipulation rig stage and observed using the side-view camera equipped with a 10x magnification lens. The glass slide was positioned perpendicular to a glass probe with a diameter of 100 µm mounted on an electronically controlled force transducer (Model 403A, Aurora Scientific Inc., Canada, with a maximum operation limit of 5 mN). A single SiO capsules was compressed by the glass probe travelling at 2 µm s^{-1}. The voltage output generated by the transducer after the compression

References to this Chapter on page 205

of the capsule was recorder and converted to force using a excel macro. The sensitivity of the transducer used was 0.5 mN/V. Ten random capsules were analysed per sample for statistical analysis. Details of the technique can be found in Chapter 2, Section 2.4.6.

5.4.7 Stability in liquid detergent

5.4.7.1 Microscopy analysis

0.1g of capsule suspension containing 20% w/w capsule to DI water was added to a glass vial containing 5 ml of liquid detergent formulation (HDL). The vial was shaken by hand to ensure well dispersion of the capsules and a drop of the product placed on a glass microslide and covered with a cover glass. Optical microscopy images were taken over time using a Zeiss Axio imager 2 pol (Carl Zeiss Microscopy – Germany, resolution 200 nm) also equipped with a UV light source (Kubler codex HXP 120C).

5.4.7.2 Perfume headspace using GC-MS

The leakage of perfume raw materials (PRM) from the capsules was assessed using GC-MS. A pre-calculated quantity of slurry containing 0.2g of encapsulated perfume was added to 20g of finished product (HDL or LFE). The vial was shaken by hand and left undisturbed under controlled temperature for a desirable period before CG-MS analysis. The obtained percentage of each RPM in the head-space was compared to a sample containing the same amount of fresh free perfume (no capsules), which is the positive control corresponding to 100% leakage. GC-MS used was an Agilent technologies 7890B GC system and 5977B MS detector.

References to this Chapter on page 205

5.5 References

1. G. Fráter, J. A. Bajgrowicz and P. Kraft, *Fragrance Chemistry*, *Tetrahedron*, **1998**, *54*, 7633-7703.
2. S. S. Datta, H. C. Shum and D. A. Weitz, *Controlled Buckling and Crumpling of Nanoparticle-Coated Droplets*, *Langmuir*, **2010**, *26*, 18612-18616.
3. S. Arditty, C. P. Whitby, B. P. Binks, V. Schmitt and F. Leal-Calderon, *Some General Features of Limited Coalescence in Solid-Stabilized Emulsions*, *The European Physical Journal E*, **2003**, *11*, 273-281.
4. X. Pan, D. York, J. A. Preece and Z. Zhang, *Size and Strength Distributions of Melamine-Formaldehyde Microcapsules Prepared by Membrane Emulsification*, *Powder Technology*, **2012**, *227*, 43-50.
5. Y. Zhao, Z. Chen, X. Zhu and M. Moller, *Silica Nanoparticles Catalyse the Formation of Silica Nanocapsules in a Surfactant-Free Emulsion System*, *Journal of Materials Chemistry A*, **2015**, *3*, 24428-24436.
6. A. Shimojima, Z. Liu, T. Ohsuna, O. Terasaki and K. Kuroda, *Self-Assembly of Designed Oligomeric Siloxanes with Alkyl Chains into Silica-Based Hybrid Mesostructures*, *Journal of the American Chemical Society*, **2005**, *127*, 14108-14116.
7. C. J. Brinker, *Hydrolysis and Condensation of Silicates: Effects on Structure*, *Journal of Non-Crystalline Solids*, **1988**, *100*, 31-50.
8. G. Ghosh, *Handbook of Refractive Index and Dispersion of Water for Scientists and Engineers*, Ghosh, Sujata, **2005**.

CHAPTER 6. Optimization of Perfume Capsules Stability and Performance in Liquid Detergent and Encapsulation of Other Actives

Abstract

In this study, the main objective was to improve the stability and performance of the perfume oil-silica capsules, produced in **Chapter 5**, in detergent matrixes. Two new approaches are taken to reduce the leakage rate of the perfume oil in this Chapter:

1. by adding a core modifier to the perfume oil, increasing hydrophobicity of the core, reducing diffusion of perfume oil to water, and
2. by coating the already formed capsules with an extra silica layer, with the objective of sealing the porous silica structure.

It was observed that by using a core modifier (isopropyl myristate (IPM)) the stability in liquid detergent was not substantially improved, however, surprisingly the PEOS sol-gel kinetics, shell thickness and mechanical properties were enhanced, probably due to the formation of less porous structures when the core modifier was present in high quantities.

Two coating materials were used as silica precursor for the formation of an extra silica layer around the already formed SiO_2 capsules:

1. tetraethoxysiloxane (TEOS): commonly used silica precursor, forming $[Si(OH)_4]$ when hydrolysed in aqueous solution, leading to silica condensation at the capsule surface due to heterogeneous nucleation.

References to this Chapter on pages 245-246

2. sodium silicate (Na_2SiO_3): a water-soluble salt, which precipitates as SiO_2 at pH lower than 9.

It was observed that when a controlled addition of both silica precursor to the capsule dispersion, the SiO_2 capsule could be coated by an extra silica layer. Moreover, when coated with sodium silicate, the SiO_2 capsules had their stability in liquid detergent greatly increased, suggesting that the porous structure was successfully coated. These SiO_2 capsules also demonstrated enhanced performance in full wash tests, which is an encouraging result for silica-based perfume capsules.

Finally, the technology developed for the encapsulation of perfume oils was expanded to the encapsulation of other strategic actives for industry. Firstly, a eutectic oil mixture of menthol and menthyl lactate was used (cooling agent), and secondly a water-soluble dye (allura red). Both were successfully encapsulated using the approach developed in this thesis, showing not only that the technology has flexibility in terms of the type of active being encapsulated, but also a wider applicability for the encapsulation of aqueous actives.

6.1 Introduction

As discussed previously, and recapped here, microencapsulation is a powerful technology used in the fabric and home care industry for the introduction of fragrances into liquid detergents,[1] in order to enhance consumer experience when using laundry products giving a prolonged freshness sensation while maximizing the fragrance delivery to the fabric.[2] It can provide enhanced active ingredients stability in the surfactant base matrix,[3] aid deposition of the active to an specific substrate,[4] and provide prolonged and controlled release of active ingredients.[5] Controlled release encapsulation technologies usually rely on diffusion of active

 References to this Chapter on pages 245-246

ingredients from the core through a permeable shell to the desired site.[6] However, permeability of capsules wall can also lead to loss of active ingredients from the core during processing and storage, and this is especially problematic for volatile core materials such as perfume oils.[3] For laundry applications, such capsules should retain the encapsulated perfume oil inside the shell in all processing steps from manufacturing to washing, deposition on fabric surface after washing, until they are ruptured by mechanical rubbing and friction with fabric at end-use applications to release the perfume.[7]

Perfume microcapsules (PMCs) prototypes are tested in industry against two main parameters: *stability* and *performance* in the heavy-duty laundry detergents (HDL) and liquid fabric enhancers (LFE), also known as fabric softeners. In terms of *stability*, it is desirable that the capsules remain intact without any perfume leakage for at least six months in the finished product to avoid phase-separation. This extended period is necessary when supply chain and storage are considered along with shelf-life of the product. On the other hand, *performance* measures the capability of the capsule to deliver the perception of freshness to the consumer at the correct time. When it comes to laundry products (HDL and LFE), it is desirable to deliver freshness after washing/drying processes when the consumer handles the fabric.

In the work reported in the **Chapter 5**, a commercial perfume oil was successfully encapsulated in SiO_2 capsules. The method was based on the Pickering emulsion stabilisation using fumed SiO_2 nanoparticles followed by the hydrolysis and condensation of polyethoxysiloxane to form a robust SiO_2 shell/perfume oil core composite. The SiO_2 capsule had exceptional narrow size distribution and the mechanical properties could be tailored by controlling the shell thickness. However, these SiO_2 capsules were not stable in liquid

 References to this Chapter on pages 245-246

detergent formulations, and the encapsulated oil leaked out completely in a matter of hours. Therefore, a method to reduce leakage of the active ingredient from SiO_2 capsules and increase the mechanical stability of the wall is required.

6.1.1 Aims of research in this chapter

This chapter is divided in two parts:

- Part 1. Optimisation of the shell properties of perfume oil capsules in terms of mechanical properties, stability and performance in the finished product (**Figure 6-1**)
- Part 2. Application of the encapsulation method developed for hexyl salicylate and perfume oil to other actives with industrial application (**Figure 6-2**).

For part 1, the aim is to minimize leakage of the perfume oil out of the silica capsules produced in Chapter 5 in a surfactant containing formulation (liquid detergents), and bloom noticed by consumers when the finished product formulation is utilized in fabric care applications. Two strategies are presented to obtain optimized SiO_2 capsules **(Figure 6-1**):

- Part 1A. Use isopropyl myristate (IPM) as a core modifier. In encapsulation, core modifiers are used to drive up the hydrophobicity of the oil and make it more stable in the core of the capsule. Here, IPM is investigated at varying concentrations to optimise the stability of perfume oil capsules in liquid detergent matrixes.
- Part 1B. Formation of an extra SiO_2 layer on the surface of the capsules *via* mineralization using sodium silicate or TEOS, to seal the porous shell, to avoid the leakage of perfume oil in liquid detergent matrixes.

The SiO_2 capsules encapsulating perfume oil (PO) were characterized and compared to a benchmark polymeric perfume microcapsule (PMC).

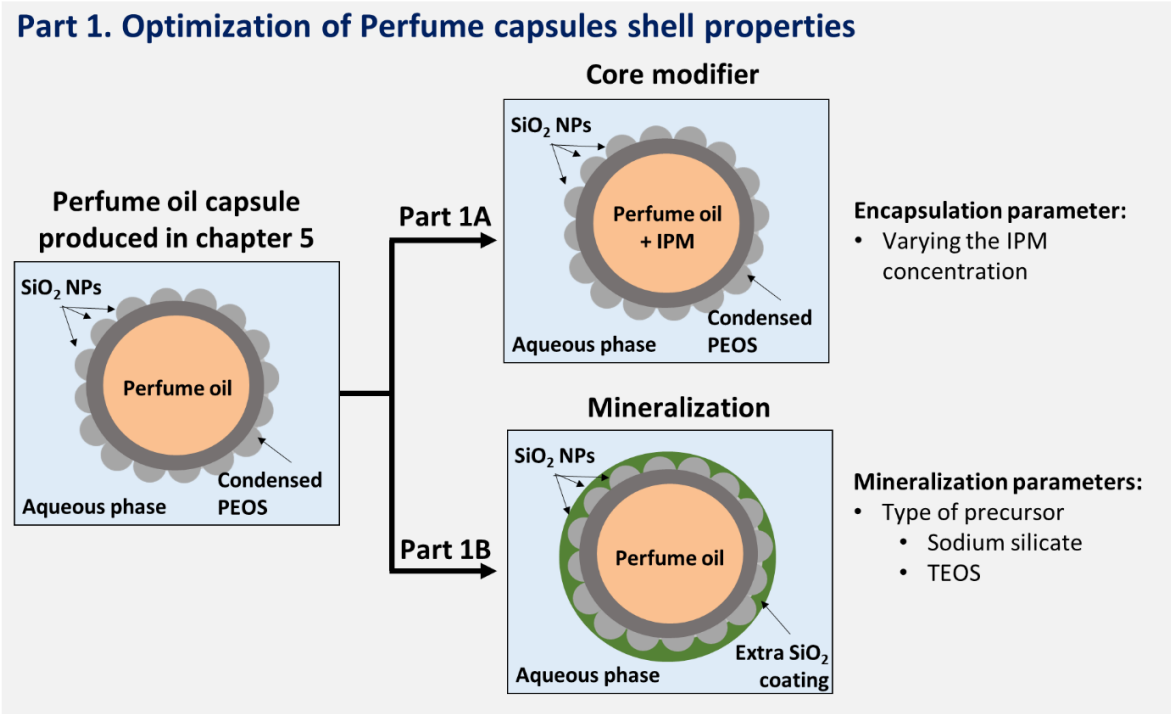

***Figure 6-1**. Road map for Part 1 of Chapter 6: Optimization of PO SiO_2 capsules shell properties using two routes. Part 1A. Using a core modifier to drive up the hydrophobicity of the core, making the perfume more stable inside the SiO_2 capsule. Part 1B. Mineralizing the SiO_2 capsules with a SiO_2 precursor with the objective of depositing an extra silica layer on top of the capsules optimising stability and performance.*

In the second part of the chapter, an exploration of the encapsulation of other actives with potential commercial application as a proof of concept is made.

- Part 2A. Encapsulation of menthol menthyl lactate (MML). MML is a cooling agent used in consumer goods to give a "freshness" sensation. It finds applications in tooth paste and shampoos, for example.

- Part 2B. Encapsulation of a water-soluble active (allura red dye). Here, the idea is to use the Pickering emulsion stabilisation, that hydrophobic colloidal particles are more preferentially wetted by the oil phase and create water-in-oil emulsions to produce silica capsules based on the condensation of PEOS from the continuous phase. Allura red was used as the model dye, but the encapsulation of water-soluble actives can be extended to other actives such as hueing dyes, enzymes and bleach.

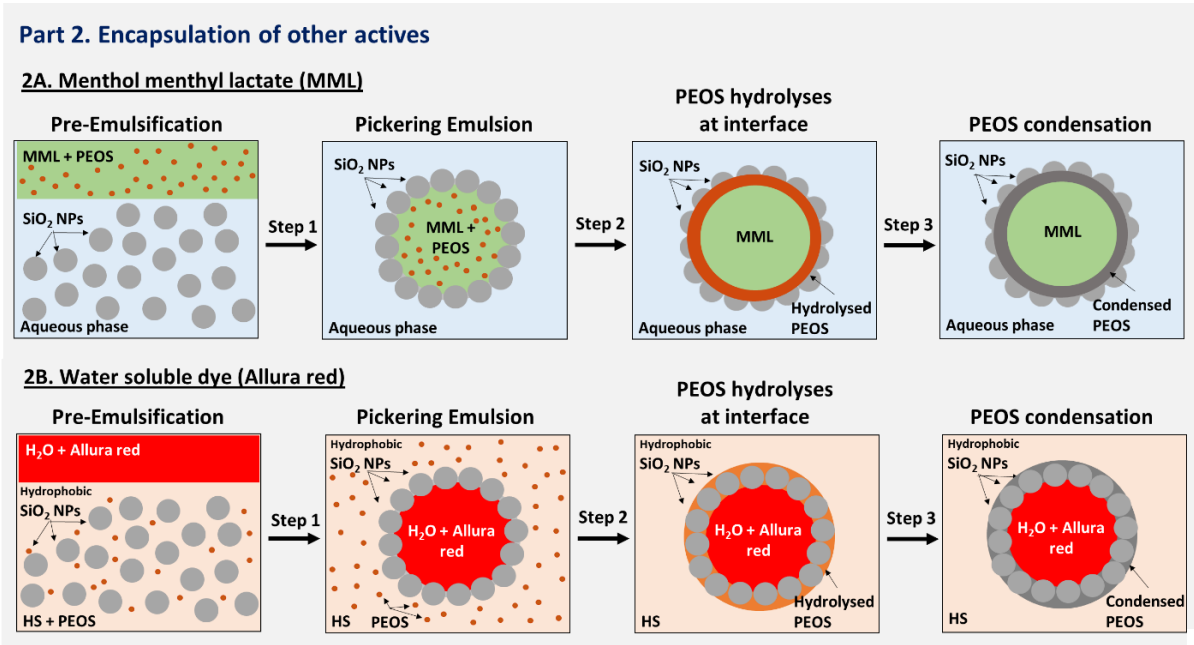

***Figure 6-2**. Road map for the Part 2 of Chapter 6: Encapsulation of other actives. Part 2A – encapsulation of menthol menthyl lactate (MML). Part 2B – encapsulation of a water-soluble dye (allura red).*

6.2 Results and Discussions

6.2.1 Part 1A. IPM as core modifier

Isopropyl myristate (IPM) (**Figure 6-3**) is a fatty acid ester, prepared *via* conventional esterification of isopropanol with myristic acid.[8] It finds many applications in food, cosmetic

and pharmaceutical industries as an emollient, thickening agent, or lubricant.[9] IPM is used in cosmetics as a substitute for natural oils because it has excellent spreading properties and is absorbed easily into the skin. In many topical and transdermal preparations, IPM is also used as a co-solvent with skin penetration enhancement properties of active ingredients[10]

IPM is also a common solvent for perfume encapsulation, as it can modify the partition coefficient of the perfume oil, making the core more hydrophobic and bring more stability to the encapsulated perfume in liquid detergent matrixes.[11] The ClogP of IPM is 7.2 and the density at 25^0C is 0.85 g/cm^3.

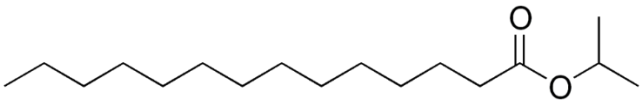

***Figure 6-3**. Chemical structure of isopropyl myristate*

The level of IPM in the core can vary depending on the type of perfume or detergent matrix, in order to maximize the stability of the encapsulated perfume in the laundry product. IPM was used here to optimise the SiO_2 capsules produced in **Chapter 5**, by making the core less likely to leak out the porous SiO_2 shell when capsules are added to a surfactant rich matrix (LFE or HDL).

6.2.1.1 Free energy of particle detachment

IPM has a higher ClogP (7.2) than hexyl salicylate (5.7, Chapter 4) and perfume oil (3.5, Chapter 5), so according to the Pickering emulsification theory, hydrophilic fumed SiO_2 NPs would be less efficient stabilizing an IPM-water emulsion as IPM is more hydrophobic. To understand the emulsion stabilization at different contact angles, the free energy of particle

detachment (ΔG_d) theoretical calculation was studied using IPM, hydrophilic fumed SiO_2 NPs and DI water.

Experimental determination of the three-phase contact angle between a solid particle and the oil-water interface can be challenging, especially for polydispersed and partially aggregated fumed SiO_2 NPs.[12] However, it was possible to obtain an approximated calculation using the Young equation (**Equation 6-1**):

$$\cos\theta = \frac{\gamma_{so} - \gamma_{sw}}{\gamma_{ow}} \qquad \textbf{\textit{Equation 6-1}}$$

For a solid nanoparticle (*s*) located at the water-oil interface, the interfacial tensions are related to the contact angle (θ), measured in the water phase. The interfacial tension between water and oil (γ_{ow}) is relatively easy to obtain, however there is no direct measure for γ_{sw} and γ_{so}. Bink and co-workers[12] have estimated the interfacial tension between hydrophilic fumed SiO_2 NPs with water and IPM by expressing the surface tension γ as a sum of polar forces (γ^p) and dispersion forces (γ^d) (**Equation 6-2**):

$$\gamma = \gamma^p + \gamma^d \qquad \textbf{\textit{Equation 6-2}}$$

The interfacial tension between the phases could then be calculated for solid-water, solid-oil and oil-water using **Equations 6-3.**

$$\gamma_{sw} = \gamma_{sa} + \gamma_{aw} - 2\sqrt{\gamma_s^d \gamma_w^d} - 2\sqrt{\gamma_s^p \gamma_w^p}$$

$$\gamma_{so} = \gamma_{sa} + \gamma_{oa} - 2\sqrt{\gamma_s^d \gamma_o^d} - 2\sqrt{\gamma_s^p \gamma_o^p}$$

$$\gamma_{ow} = \gamma_{oa} + \gamma_{aw} - 2\sqrt{\gamma_o^d \gamma_w^d} - 2\sqrt{\gamma_o^p \gamma_w^p} \qquad \textbf{\textit{Equation 6-3}}$$

References to this Chapter on pages 245-246

The calculated values are summarized in **Table 6-1**. Thus, utilising **Equation 6-1, Equation 6-2** and **Equation 6-3**, it was possible to calculate the contact angle of the hydrophilic fumed SiO_2 NPs with water in a water/IPM emulsion as θ = 62°. The value is below 90°, which is expected for the formation of oil in water emulsions using hydrophilic nanoparticles.

***Table 6-1**. Dispersion forces, polar forces and interfacial tension for IPM, Di water and fumed SiO_2 NPs.*[12]

	Dispersion forces (mN)		Polar forces (mN)		Interfacial tension with air (mN m^{-1})		Interfacial tension (mN m^{-1})	
IPM	γ_{do}	26.1	γ_{po}	3.2	γ_{oa}	29.3	γ_{ow}	28.5
DI water	γ_{dw}	21.5	γ_{pw}	50.4	γ_{wa}	71.9	γ_{sw}	5.01
Fumed SiO_2 NPs	γ_{ds}	42	γ_{ps}	34	γ_{sa}	76	γ_{os}	18.22

As mentioned previously, to form stable emulsions, the three-phase contact angle (θ) between the particle and the immiscible phases (**Figure 1-4**) should be close to 90°,[13] because the larger adsorption energy for particles at the oil-water interface results in a higher energy input required for desorption. The minimum energy required for particle detachment to the continuous phases, ΔG_d (free energy of particle detachment) could be calculated according to **Equation 6-4**:[14]

$$\Delta G_d = \pi r^2 \gamma_{ow} (1 \pm cos\theta)^2, \qquad \textbf{\textit{Equation 6-4}}$$

where ΔG_d is the free energy, *r* is the particle radius, γ_{ow} is the interfacial tension between the oil and water phases, θ the three-phase contact angle, and the '+' term refers to the desorption of the particle into oil, whilst the '-' term refers to the desorption of the particle

References to this Chapter on pages 245-246

into water. The calculated ΔG_d for hydrophilic SiO_2 NPs in the water/IPM interface was estimated using **Equation 6-4** and the value was $\Delta G_d = 626\ kT$, which is much greater than the thermal energy kT (the Boltzmann constant, k times the temperature, T), indicating the formation of a stable emulsion.

The free energy of detachment to the oil and water was plotted against the contact angle for the IPM/water system (**Figure 6-4)**. As the nanoparticles used were hydrophilic, the free energy of particle detachment into water (triangles) was smaller than that into oil (circles). The opposite would be true if hydrophobic SiO_2 NPs were used.[15] Overall, the minimum necessary energy for particle detachment (dashed line) was zero at 0° and 180° and maximum at 90°.

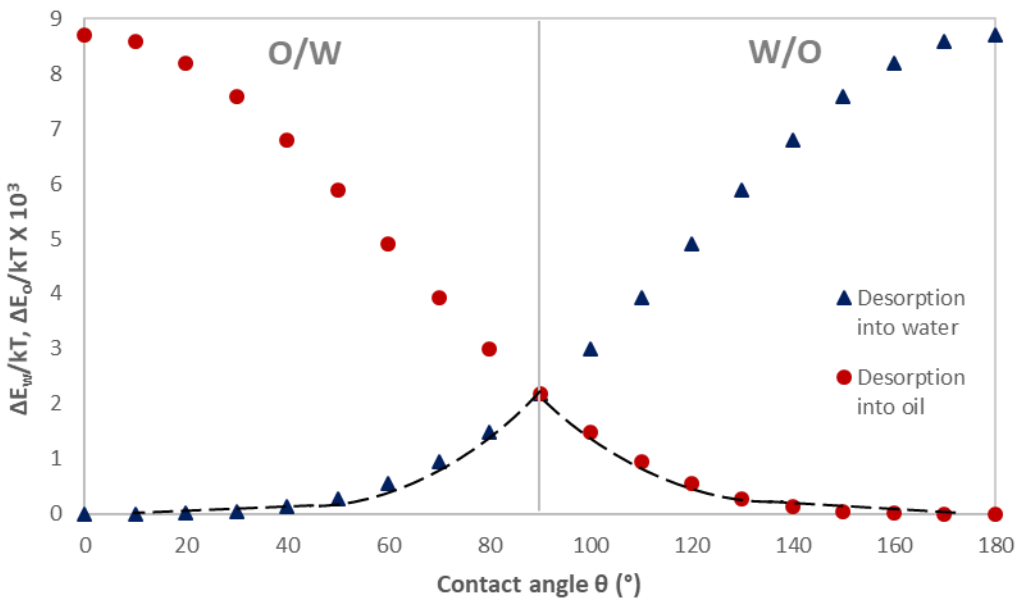

Figure 6-4. *Free energy of detachment of a spherical particle into water (triangles) and into oil (circles) calculated by* ***Equation 6-4*** *with r = 10 nm and γ_{ow} = 50 mN m^{-1} versus particle contact angle ϑ.*

References to this Chapter on pages 245-246

The energy of particle attachment to the fluid interface, $\Delta G_a = - \Delta G_d$, is negative for all contact angles (except close to 0° and 180°), hence the particle attachment is usually thermodynamically favourable. Therefore, solid colloidal particles with chemically homogeneous surfaces can spontaneously attach to fluid interfaces and are surface active.[15]

6.2.1.2 IPM SiO_2 capsules

It was clear from the free energy of detachment calculations presented above that, in theory, it would be possible to stabilise IPM droplets using hydrophilic SiO_2 nanoparticles, even with the high ClogP of the oil. To validate experimentally the calculations, SiO_2 capsules were produced using solely IPM as core material and the encapsulation procedure presented in **Chapters 4** and **5** based on the Pickering stabilisation of the oil droplets, followed by the hydrolysis and condensation of PEOS at the interface (IPM_{100} SiO_2 capsules).

As observed in **Figure 6-5**, IPM_{100} SiO_2 capsules were successfully produced. Moreover, the stability to coalescence of the emulsion was remarkable, most of the water was released producing a high stable cream that could be dried and redispersed in water. As observed in **Figure 6-5D**, IPM_{100} SiO_2 capsules had a well-defined and smooth shell.

References to this Chapter on pages 245-246

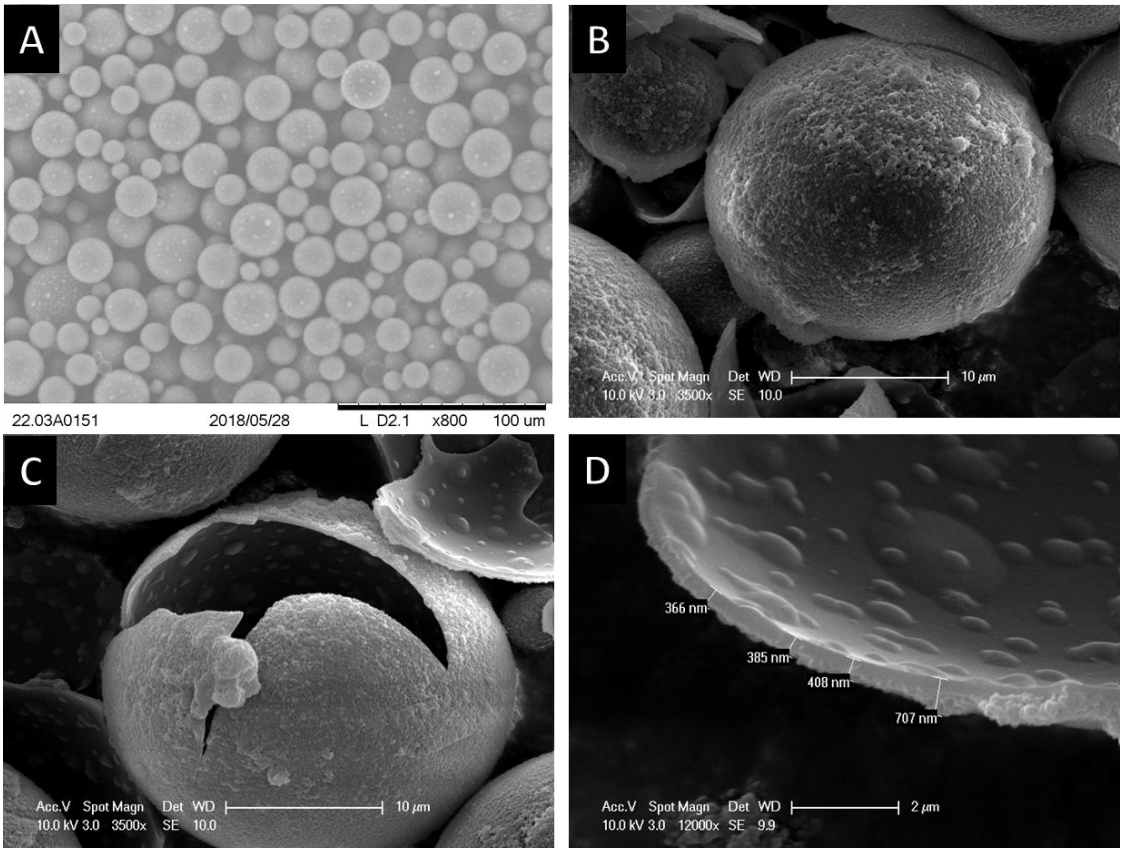

***Figure 6-5**. SEM images of SiO_2 capsules encapsulating IPM produced using 20 wt% PEOS 1.0 under acidic conditions (IPM_{100} SiO_2 capsules) showing (A) a population of capsules, (B and C) the capsule structure and (D) shell thickness.*

6.2.1.3 IPM + PO SiO_2 capsules

IPM was tested as core modifier for perfume oil at different concentration with the perfume oil, with the objective of producing capsules with higher stability in liquid detergent matrixes leading to an optimized performance in the finished product. Capsules were produced having a core composition of:

- 80% IPM / 20% PO ($IPM_{80}PO_{20}$ SiO_2 capsules)
- 40% IPM / 60% PO ($IPM_{40}PO_{60}$ SiO_2 capsules)

SiO_2 capsules could be produced using both compositions. The inner shell morphology was analysed and compared to IPM_{100} SiO_2 capsules and PO_{100} SiO_2 capsules (SiO_2 NPs-PEOS 1.0-20%-PO in Chapter 5) using SEM microscopy (**Figure 6-6**). Interestingly, the inner shell morphology changed depending on the composition of the core. A smooth surface was observed for the IPM_{100} SiO_2 capsules (**Figure 6-6A**) and was still present for $IPM_{80}PO_{20}$ SiO_2 capsules (**Figure 6-6B**). However, when the level of PO used was higher ($IPM_{40}PO_{60}$ SiO_2 capsules - **Figure 6-6C**), the inner surface became rough and more similar to the surface of PO_{100} SiO_2 capsules (**Figure 6-6D**).

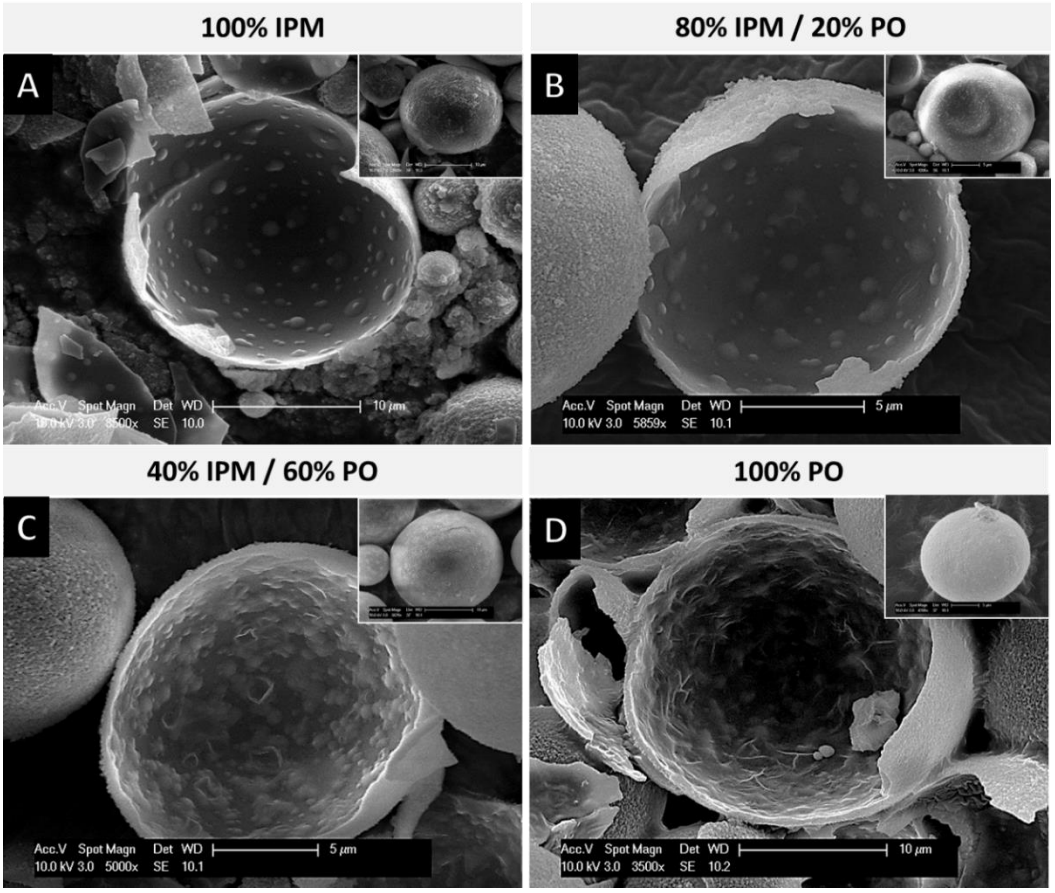

***Figure 6-6**. SEM images comparing the inter shell structure for capsules produced using different levels of IPM and PO: (A) IPM_{100} SiO_2 capsules, (B), $IPM_{80}PO_{20}$ SiO_2 capsules, (C) $IPM_{40}PO_{60}$ SiO_2 capsules and (D) PO_{100} SiO_2 capsules.*

References to this Chapter on pages 245-246

An explanation for these observations is that the PO is composed of 13 different perfume raw material (PRM) components, including aldehydes, alcohols, esters and hydrocarbons (according to P&G), some of which could have higher solubility towards the water phase, especially as ethanol is generated during hydrolysis and condensation of PEOS.

Optical microscopy images (**Figure 6-7**) were used to confirm that some PRMs of the PO could indeed be solubilised to the water phase, perhaps due to the ethanol generation during the hydrolysis and condensation of PEOS at the interface. IPM_{100} SiO_2 capsules were completely full of oil after the solidification of the shell (**Figure 6-7A**). However, when PO was added to the core, the capsules were not completely filled with oil, which indicates the loss of PO during the emulsification process. Even for the $IPM_{80}PO_{20}$ SiO_2 capsules the effect was observed (**Figure 6-7B**), however, as expected the void inside the shell was much smaller when compared to the $IPM_{40}PO_{60}$ SiO_2 capsules. (**Figure 6-7C** and **D**)

References to this Chapter on pages 245-246

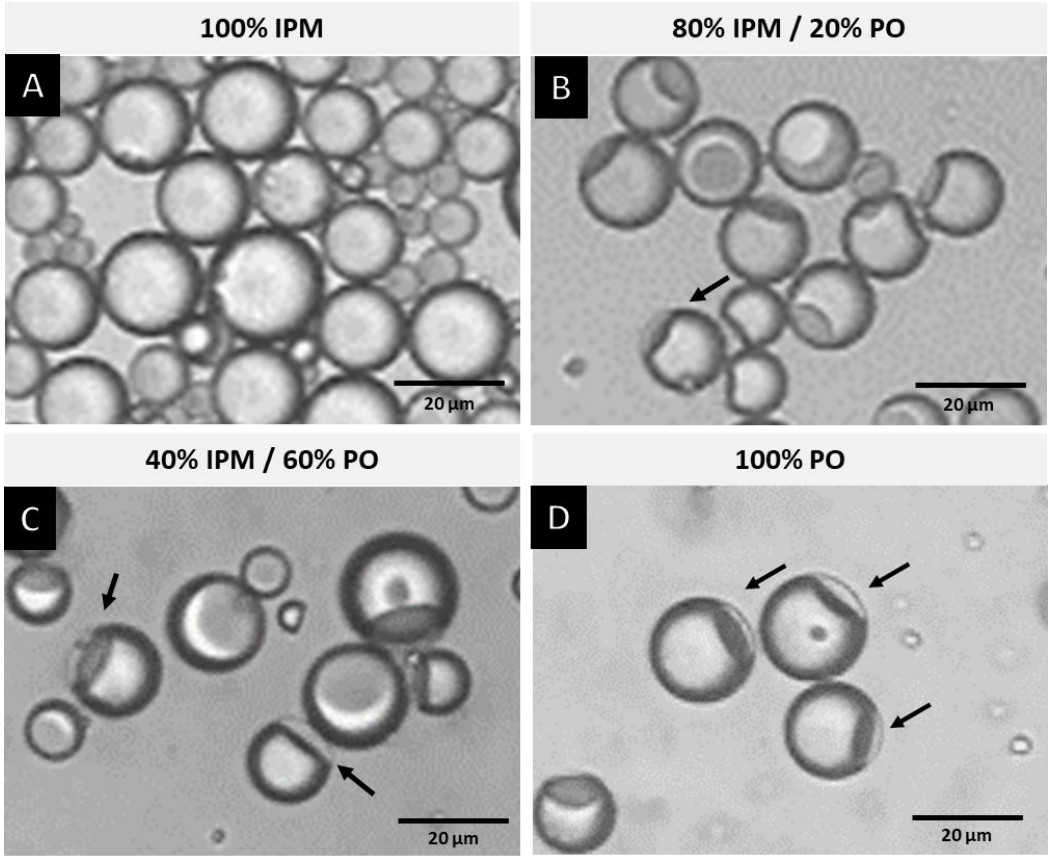

***Figure 6-7**. Optical microscopy images comparing the capsules produced using different levels of IPM and PO: (A) 100% IPM, (B), 80% IPM and 20% PO, (C) 40% IPM and 60% PO and (D) 100% PO.*

SiO_2 capsules produced with different levels of IPM and PO also had their mean diameter and SPAN of the size distribution measured. As observed in **Table 6-2**, the composition of the oil did not impact significantly the mean diameter and the SPAN of the size distribution.

The average shell thickness changed significantly when the core composition was varied. The values are summarized in **Table 6-2**, along with the theoretical thickness of the PEOS condensed layer calculated theoretically. It was observed that as the level of IPM increased, the average shell thickness decreased. This result was the opposite of what was expected

from the theoretical calculation, which considers the density of the core material and the mean diameter of the capsule.

As discussed in **Chapter 4** and **5**, the theoretical condensed PEOS layer does not take into account the SiO_2 nanoparticles layer, which should be approximately 100 nm, so the experimental shell thickness is in fact the theoretical condensed layer in addition to the SiO_2 nanoparticles layer. The experimental and theoretical values for the $IPM_{100}SiO_2$ capsules were very similar, indicating that all PEOS is hydrolysed and condenses to form the SiO_2 shell. On the other hand, capsules formed with different levels of PO in the core had different values of shell thickness.

The differences observed between the experimental and theoretical shell thickness values are likely connected to the different inner shell morphologies observed in **Figure 6-6**, and it was hypothesised that some components of the PO might become more water-soluble as the shell is forming and ethanol is released from the hydrolysis and condensation of PEOS. This process could lead to the formation of a more porous SiO_2, reflecting on a thicker shell for the SiO_2 capsules produced with a higher level of PO even if the same concentration of PEOS was used to form all the capsules.

Table 6-2. *Core density, capsule mean diameter, SPAN of the capsule size distribution and experimental and theoretical shell thickness of capsules produced using different levels of IPM and PO.*

References to this Chapter on pages 245-246

Sample	Mean diameter	SPAN	Core density	Average shell thickness (from SEM images)	Theoretical PEOS condensed layer thickness (from Equation 4-5)
	µm	µm	$g.cm^{-3}$	nm	nm
PO_{100} SiO_2 capsules	17.0 ± 1.0	0.99 ± 0.03	0.96	375 ± 41	174
$IPM_{40}PO_{60}$ SiO_2 capsules	20.4 ± 1.3	0.92 ± 0.07	0.92	355 ± 29	222
$IPM_{80}PO_{20}$ SiO_2 capsules	21.2 ± 1.2	0.93 ± 0.07	0.87	330 ± 63	221
IPM_{100} SiO_2 capsules	21.4 ± 1.9	0.98 ± 0.14	0.85	314 ± 26	216

6.2.1.4 Sol-gel kinetics

The higher the concentration of IPM in the core, the faster the SiO_2 shell solidification. This result is illustrated in **Figure 6-8**, which contains SEM images of the PO/IPM SiO_2 capsules after 3 days of the capsule synthesis. It was observed that for the IPM_{100} SiO_2 capsules (**Figure 6-8A**) and $IPM_{80}PO_{20}$ SiO_2 capsules (**Figure 6-8B**) a solid SiO_2 shell was already formed, and the shell could survive air-drying and the vacuum imposed by the SEM. The SiO_2 capsules were still collapsing for the $IPM_{40}PO_{60}$ SiO_2 capsules (**Figure 6-8C**) and PO_{100} SiO_2 capsules (**Figure 6-8D**), however, the $IPM_{40}PO_{60}$ SiO_2 capsules seemed to be in a more advanced shell formation stage than PO_{100} SiO_2 capsules, as a clear deflated shell is observed. As discussed in Chapter 5, PO_{100} SiO_2 capsules were completely formed after 6 weeks.

References to this Chapter on pages 245-246

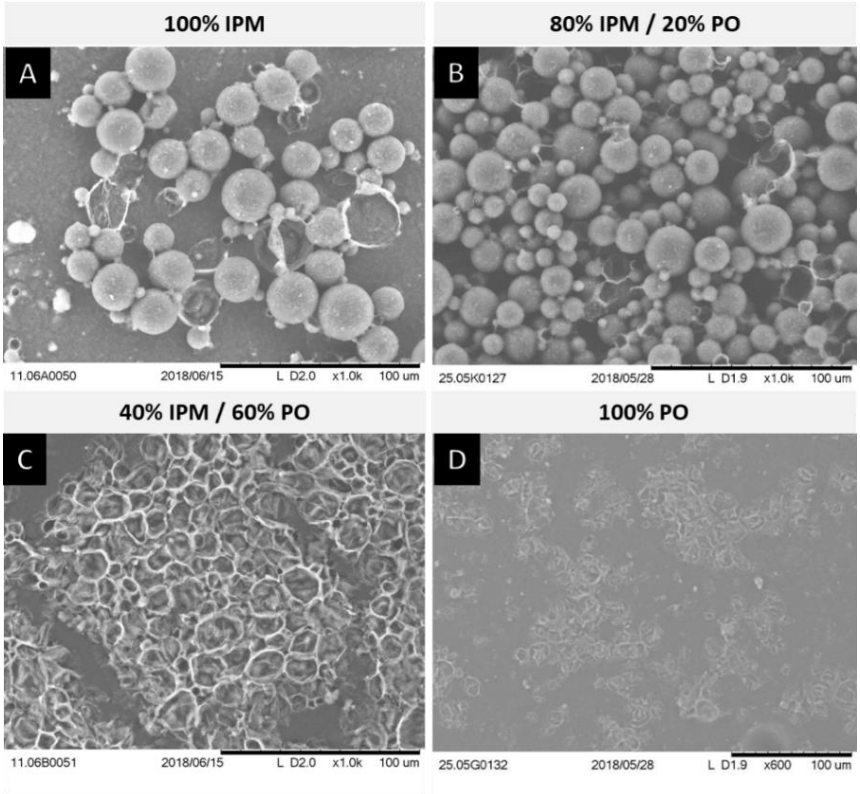

***Figure 6-8**. SEM images comparing the SiO_2 shell formation for capsules produced using different levels of IPM and PO: (A) IPM_{100} SiO_2 capsules, (B), $IPM_{80}PO_{20}$ SiO_2 capsules, (C) $IPM_{40}PO_{60}$ SiO_2 capsules and (D) PO_{100} SiO_2 capsules. Images were obtained after 3 days of the capsule synthesis.*

The explanation for the differences observed in **Figure 6-8** is likely connected to the interactions between ethanol, IPM and PO, which were responsible for the different shell morphologies and thickness discussed in the above section (6.1.1.3). If ethanol has affinity with some PRM components, the equilibrium constant of the PEOS hydrolysis and condensation is higher, leading to a slower sol-gel kinetics when compared to IPM. IPM has a higher ClogP (higher surface tension with water), which contributes to the greater surface activity of PEOS, hence more efficient shell formation.

6.2.1.5 Mechanical properties

The mechanical properties of the SiO_2 capsules containing a core-modifier were evaluated using the micromanipulation technique described in **Chapter 2** (**Figure 6-9**). Surprisingly, $IPM_{100}SiO_2$ capsules had a notable higher nominal fracture strength when compared to $PO_{100}SiO_2$ capsules (**Figure 6-9A**). Interestingly, the nominal rupture stress increased as the content of IPM increased. However, even with a content as high as 80% IPM ($IPM_{80}PO_{20}SiO_2$ capsules), the nominal rupture stress was much lower when compared to the $IPM_{100}SiO_2$ capsules.

The density of the shell discussed above can explain the higher nominal rupture stress observed for the $IPM_{100}SiO_2$ capsules, as the condensed PEOS layer was denser and more resistant to the pressure imposed by the force transducer, when compared to the samples prepared using different levels of PO in the core. In terms of deformation at the rupture (**Figure 6-9B**), the $IPM_{100}SiO_2$ capsules and $IPM_{80}PO_{20}SiO_2$ capsules had a slightly smaller deformation, compared to the capsules with a higher level of PO, indicating that theses shells are more brittle, probably due to the lower porosity of the SiO_2 shell.

References to this Chapter on pages 245-246

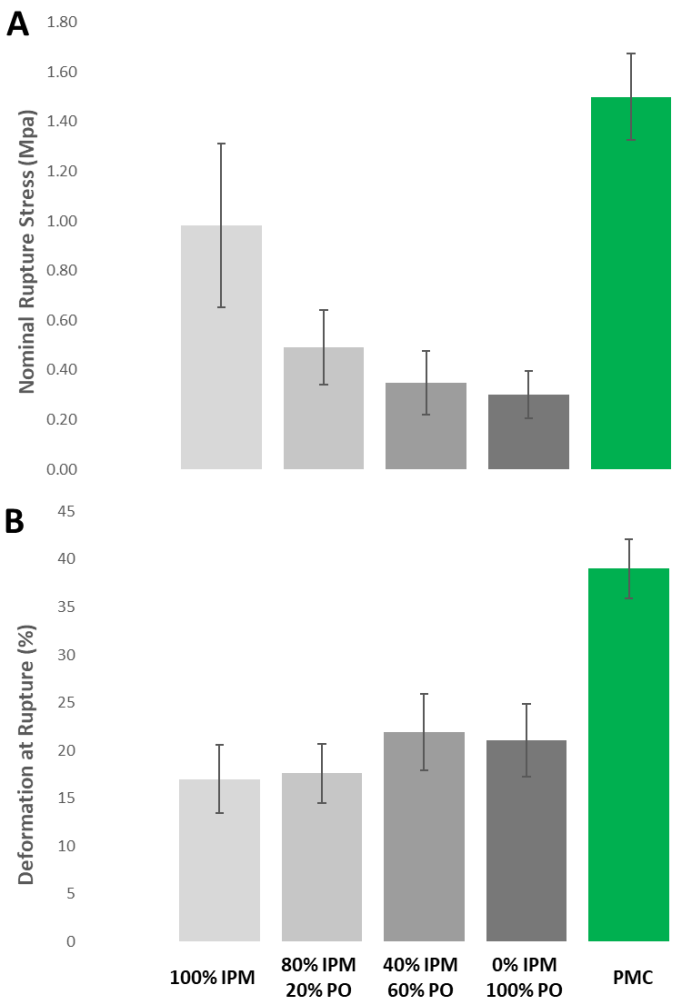

***Figure 6-9**. Nominal rupture stress (A) and percentage of shell deformation at the rupture (B) for capsules produced using different levels of IPM and PO in the core.*

6.2.1.6 Stability in LFE

The stability of the SiO_2 capsules produced containing different levels of IPM as core modifier was tested in LFE matrix. **Figure 6-10** shows SiO_2 capsules initially dispersed in LFE and after 6h and 30 hours. It was observed that for the IPM_{100} SiO_2 capsules (**Figure 6-10A - C**), there is no significant change in the capsule core, and no IPM leaks to the surfactant rich LFE matrix after 30 hours. For the $IPM_{80}PO_{20}$ SiO_2 capsules (**Figure 6-10D - F**) it can be seen that from the beginning the shell is not completely full of oil, as observed in **Figure 6-7B**, after 6 hours the

apparent void seems to be enlarged indicating the loss of core material l(**Figure 6-10E**). After 30 hours, no significant change was found (**Figure 6-10F**). A similar behaviour was observed for the $IPM_{40}PO_{60}$ SiO_2 capsules (**Figure 6-10G - I**). A void is observed initially, in agreement with **Figure 6-7C**, and it is then much larger after 6 and 30 hours (**Figure 6-10H** and **I**) indicating that PO is the component leaking out of the shell.

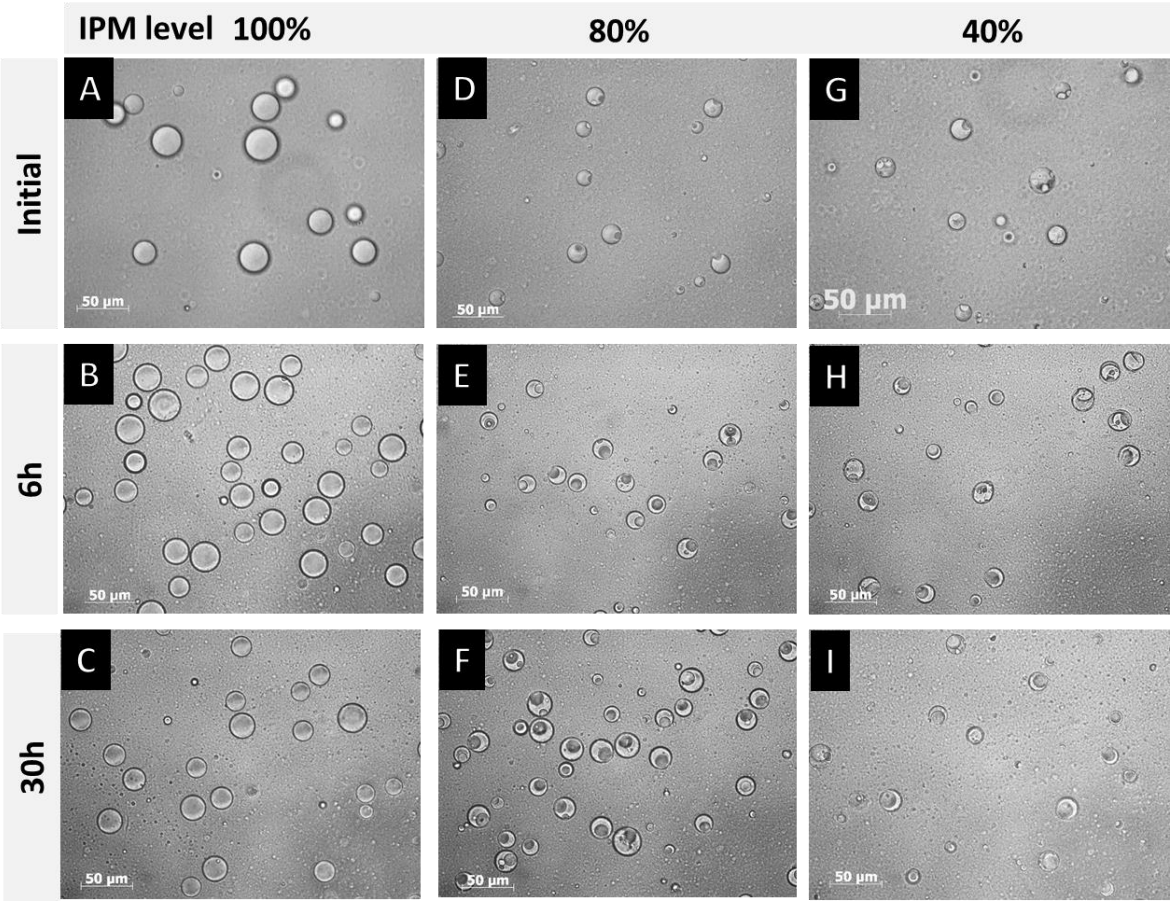

***Figure 6-10**. Optical microscopy images of SiO_2 capsules with different IPM levels to PO in the core (100, 80 and 40%) dispersed in LFE initially and after 6h and 30h.*

The optical microscopy images were compared to GC-MS data of PO leakage at P&G. Both capsules produced using IPM as core-modifier for PO ($IPM_{80}PO_{20}$ SiO_2 and $IPM_{40}PO_{60}$ SiO_2

capsules) had 100% leakage of PO after 24h in the LFE matrix, suggesting that the SiO_2 capsule shell is still permeable to the PO, even if a core modifier was used.

6.2.2 Part 1B. Mineralization using Na_2SiO_3 and TEOS

6.2.2.1 Experiment design

The stability experiments in **Chapter 5** and Part 1A of this chapter confirmed that the encapsulated PO leaked out of the SiO_2 capsules when added to a liquid detergent matrix, with and without IPM, suggesting that the SiO_2 shell was porous, allowing perfume to be solubilised by the surfactant rich continuous phase. To minimize this porosity of the shell, a mineralization experiment was designed with the objective of depositing SiO_2 on the surface of the already formed SiO_2 capsules, sealing the pores and avoiding PO leakage in liquid detergent. Two SiO_2 precursors were chosen for the experiment: tetraethoxysiloxane (TEOS) and sodium metasilicate (Na_2SiO_3).

6.2.2.2 Mineralization using Na_2SiO_3

The advantage of using crystalline silicates like sodium metasilicate for the deposition of amorphous silica on the surface of the SiO_2 capsules is that they are readily soluble in water. For example, the solubility for anhydrous sodium metasilicate is 210 g/l at 20 °C.[16] Depending on both pH and concentration of Na_2SiO_3, the Na_2SiO_3 aqueous solutions can contain varying proportions of monomeric tetrahedral ions, oligomeric linear or cyclic silicate ions (di- or trisilicate ions) and polysilicate ions of three-dimensional structure. These ions are in a constant dynamic equilibrium and the degree of polymerisation of the silicate anions increases with increasing concentration.[17]

The pH of the medium also has a strong impact on the polymerisation-depolymerisation equilibrium of Na_2SiO_3; above a pH 11 stable solutions of monomeric and polymeric silicate ions exist and no insoluble amorphous SiO_2 is present. Acidification below pH 11 leads to increasing precipitation of amorphous SiO_2, which is characterised by the loss of interstitial alkali ions from the three-dimensional network.[17] Precipitation rapidly increases when the pH is lowered to 9. Leading to the deposition of a silica coating on the porous SiO_2 capsules Na_2SiO_3 could be used. At pH values below 9 only a low but constant amount remains in solution as monomeric silicate ions. By considering the high dissociation constants of silicic acid (pK_a 9.9 - 12 at 30 °C),[16] when the Na_2SiO_3 solution is added to a 0.1M HCl solution (pH 1.2), only a small proportion of silicate ions is in solution and amorphous SiO_2 should precipitate onto the surface of the SiO_2 capsules.

Due to the alkaline character of sodium silicate, a limited amount of Na_2SiO_3 could be added to the capsule dispersion before it solubilises the SiO_2 shell of the capsules. A Na_2SiO_3 titration was used to identify what is the maximum amount of a 10wt% Na_2SiO_3 solution which can be added to a 0.1M HCl solution before the pH changes. The curve can be found in **Figure 6-11**, and it can be observed that 0.5g of a 10wt% Na_2SiO_3 solution could be added to 10g of 0.1M HCl while maintaining the pH around 2.

References to this Chapter on pages 245-246

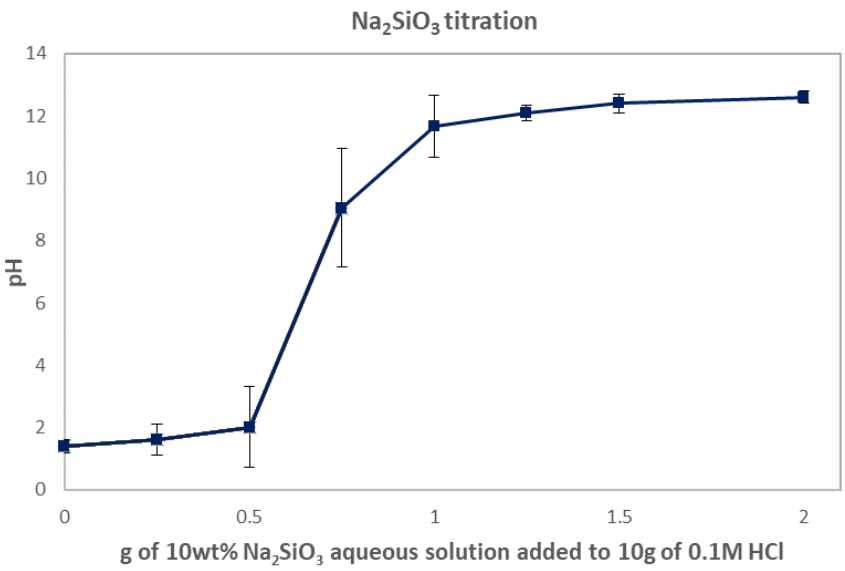

***Figure 6-11**. Graph indicating the pH change when different amounts of a 10wt% Na_2SiO_3 aqueous solution are added to 10g of a 0.1M HCl solution. The initial pH of the 10wt% Na_2SiO_3 aqueous solution was pH 13 and the 0.1M HCL aqueous solution 1.2. The experiment was repeated 3x (error bars).*

It was calculated that if 1g of capsule slurry was added to the 10g of 0.1M HCl and taking into account the surface area of the capsules, it would be necessary that 0.01g of 10wt% Na_2SiO_3 solution is required to cover all surface area of the capsules with at least one layer of SiO_2 molecules. Therefore, the 0.5 g limit from the titration curve (**Figure 6-11**) would be enough to cover the capsules with about 50 layers of SiO_2 molecules. For the experiment, a syringe pump (Havard PHD 4000) was used to control the addition of Na_2SiO_3 to the slurry at a rate of 10 µl per minute.

Figure 6-12 compares the surface morphology of the PO_{100} SiO_2 capsule before (**Figure 6-12A**) and after (**Figure 6-12B**) mineralization with Na_2SiO_3. Significant difference is observed in the close-up images, in **Figure 6-12D** (close-up before mineralization) the SiO_2 nanoparticles are

clearly observed, including the voids between them. After mineralization (**Figure 6-12E**) the surface was much smoother and no individual SiO_2 nanoparticles or clear voids are observed, which indicates a successful mineralization.

6.2.2.3 Mineralization using TEOS

TEOS was controllably added to the SiO_2 capsules dispersion with the help of a syringe pump at a rate of 10 µl per minute. The slow addition was necessary to avoid phase separation or the necessity of pre-hydrolysis of TEOS. Moreover a high [TEOS] induces a high [$Si(OH)_4$] within the surrounding continuous water phase, which promotes the generation of monoliths rather than deposition of SiO_2 on the surface of the capsules. Below the TEOS concentration threshold of about 2.2M/m^2 the silica condensation mostly takes place at the capsule surface, which is covered with SiO_2 nanoparticles, favouring heterogeneous nucleation of TEOS at the interface and minimizing the nucleation enthalpy. [18]

Mineralization using TEOS also took place in 0.1M HCl aqueous solution (pH approx. 1.2, below the silica isoelectric point – approx. 2.). A low pH was chosen, not only to catalyse the hydrolysis step, but also because at high pH values, where the particulates may have a high solubility in the sol, more porous SIO_2 structures are obtained. At low pH values fine pore networks and dense structure are formed due to low dissolution re-precipitation rate of TEOS.[19] **Figure 6-12** compares the surface morphology of the PO_{100} SiO_2 capsule before mineralization with TEOS . Significant difference is observed in the close-up images, in **Figure 6-12D** (close-up before mineralization) the SiO_2 nanoparticles are clearly observed, including the voids between them. After mineralization (**Figure 6-12F**) the surface morphology has

References to this Chapter on pages 245-246

changed, but the surface is not as clearly covered by a SiO_2 layer as observed for the Na_2SiO_2 mineralization.

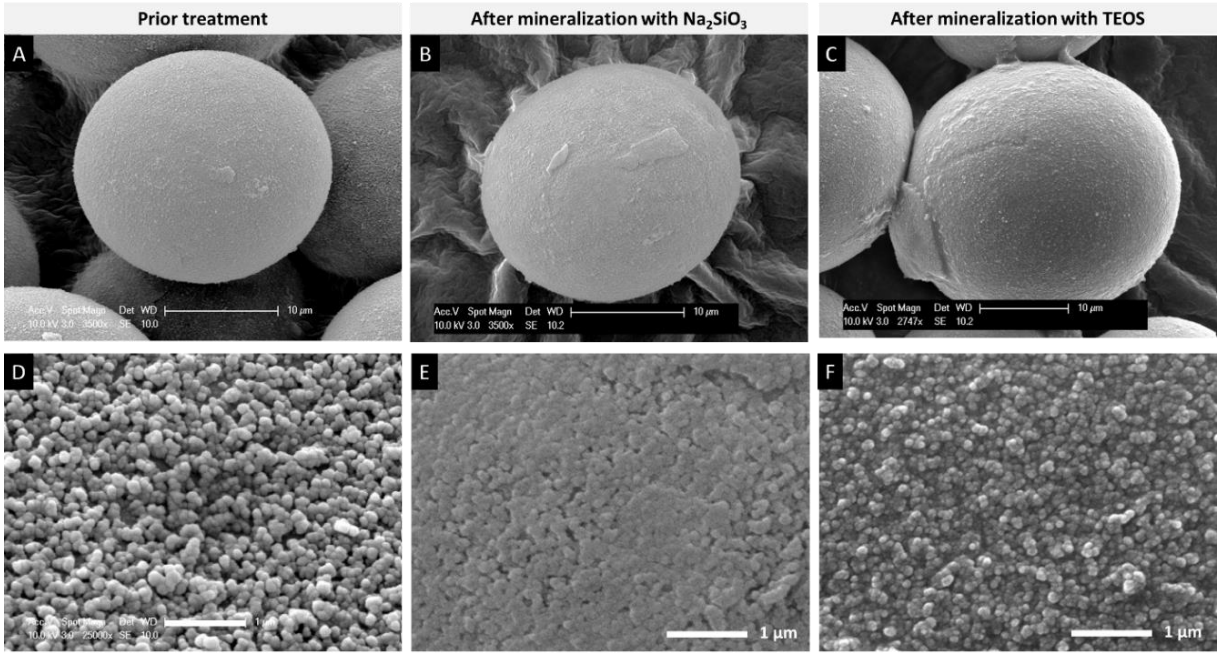

Figure 6-12. *SEM images of a SiO_2 capsule before (A) and after mineralization using TEOS (B) and Na_2SiO_3 (C). D-F shows the close-up of the surface of each capsule, respectively.*

6.2.2.4 Stability in liquid detergent

SiO_2 capsules mineralized with both TEOS and Na_2SiO_3 were dispersed in LFE matrix and their stability tested as function of perfume oil leakage percentage using the headspace GC-MS method discussed in **Chapter 2**. The results are in **Figure 6-13.** There was a clear decrease in terms of PO leakage when the capsules were treated with both Na_2SiO_3 and TEOS mineralization when compared to the original sample (PO_{100} SiO_2 capsules) (**Table 6-3**).

References to this Chapter on pages 245-246

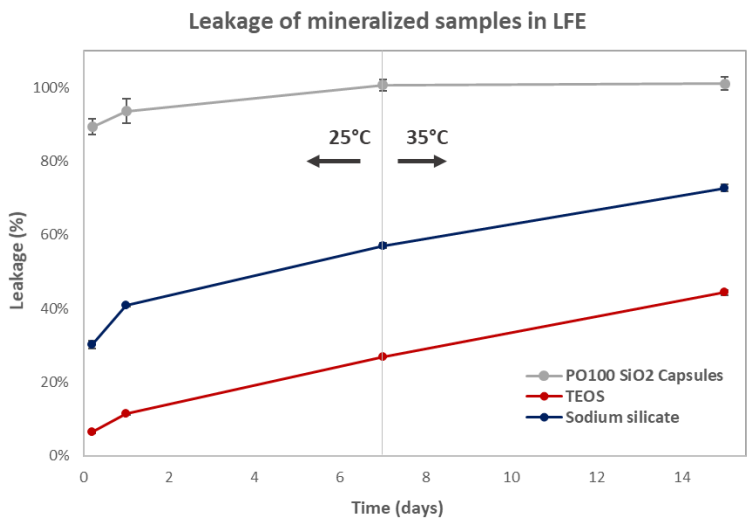

***Figure 6-13**. Graph of leakage in LFE for PO SiO_2 capsules compared to capsules mineralized with Na_2SiO_3 and TEOS. The first 7 days capsules were left at 25°C then put in a stability room at 35°C for an extra week.*

The first measurement was obtained after 5h the capsules were dispersed in LFE at 25°C. At this point, the registered PO leakage was 89% for non-mineralized capsules and 6.4% and 30% for capsules mineralized with Na_2SiO_3 and TEOS, respectively. After 24h the PO leakage was 94% for non-mineralized capsules, while for the capsules mineralized with Na_2SiO_3 was 11% and TEOS 41%, suggesting that the mineralization could in fact close the voids. The capsules were kept at 25°C for 7 days, and then put in a stability room at 35°C for additional 8 days to accelerate the leakage process; perfume kept diffusing through the shell and at 15 days the leakage was 44% for mineralization with Na_2SiO_3 and 73% for TEOS. At this point, the capsules were completely broken using a magnetic stirring bar, to release all the remaining perfume and confirm that no PO was lost during mineralization process, both mineralized samples had 100% encapsulation efficiency from this experiment, confirming the success of the experiment.

References to this Chapter on pages 245-246

***Table 6-3**. Leakage percentage of PO in LFE for the mineralized capsules compared to a non-mineralized reference.*

Sample	Days			
	0.2 (25°C)	1 (25°C)	7 (25°C)	8-15 (35°C)
PO_{100} SiO_2 capsule-Na_2SiO_3 min	6.4 ± 0.2%	11.4 ± 0.3%	26.87 ± 0.2%	44.4 ± 0.7%
PO_{100} SiO_2 capsule-TEOS min.	30.1 ± 1.1%	40.8 ± 0.4%	57.12 ± 0.6%	72.7 ± 1.0%
PO_{100} SiO_2 Capsules	89.3 ± 2.1%	93.7 ± 3.2%	100.76 ± 1.5%	101.1 ± 1.8%

The results show that both Na_2SiO_2 and TEOS mineralization process has reduced the PO leakage significantly, in particular for the Na_2SiO_3 mineralization. **Figure 6-14** shows SiO_2 capsules mineralized with Na_2SiO_3, dispersed in LFE for 24h. In **Figure 6-14A** the SiO_2 capsule in LFE. The capsule was then compressed with a second glass slide (**Figure 6-14B**) and it was observed that liquid PO was coming out of the broken shell, suggesting that PO was stable inside the capsule when dispersed in LFE confirming the data presented in **Figure 6-13**.

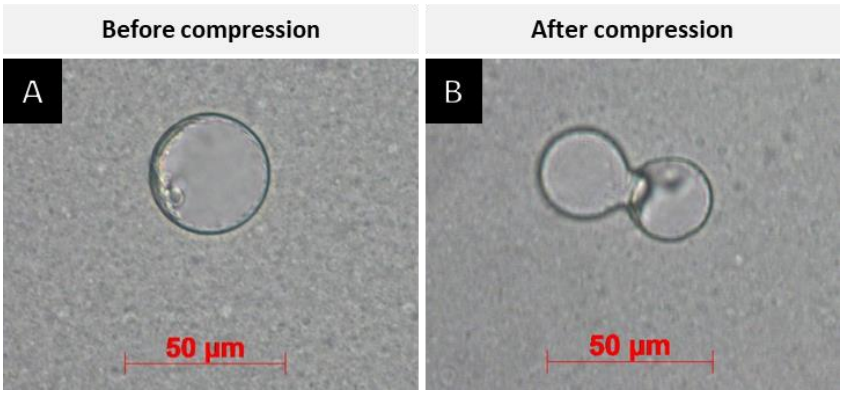

***Figure 6-14**. Optical images of a PO_{100} SiO_2 capsule mineralized with Na_2siO_3 dispersed in LFE matrix after 24h at 25°C. (A) SiO_2 capsule before being compressed by a second glass slide and (B) after compression, where it is possible to observe perfume oil being released. The scale bar is 50 µm.*

References to this Chapter on pages 245-246

6.2.2.5 Performance in full scale wash test

Olfactive performance of the SiO_2 capsules mineralized with both TEOS and Na_2SiO_3 was assessed by:

(i) laundering fabrics using a capsule slurry containing liquid fabric softener (LFE),

(ii) indoor line-drying the fabrics for 24 hours, and

(iii) recording the rubbed fabric odour (RFO) by expert perfumers.

The final perfume activity was calculated to be approximately the same amount as expected in a commercial LFE product (0.66% - data from P&G). Terry towels were used as model fabric for the wash, which was performed in a Miele Softronic W1714 washing machine, at 30°C, using a short crease recovery cycle and 1000 RPM rotation speed. The capsules were dispersed in LFE 1 hour before the wash test to minimize PO leakage. **Figure 6-15** shows SEM image of SiO_2 capsules depositing in terry towel.

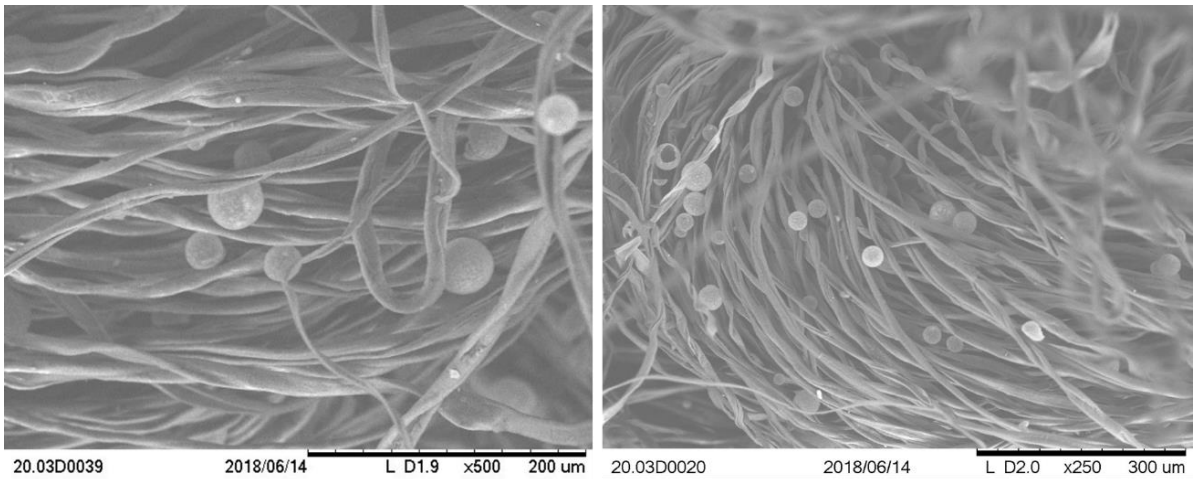

***Figure 6-15**. SEM images of PO_{100} SiO_2 capsules mineralized with Na_2SiO_3 depositing in terry towels.*

References to this Chapter on pages 245-246

The olfactive assessment was relative to the commercial PMC (RFO = 100), and the results are summarized in **Figure 6-16**. It was observed that, the PO_{100} SiO_2 capsules without mineralization did not delivery significant freshness after the towels were dried (RFO = 2). This result was expected as the PO_{100} SiO_2 capsules had 100% PO leakage when added to LFE. The mineralized samples, however, had encouraging results. PO_{100} SiO_2 capsules mineralized with TEOS had a RFO result of 19 and the ones mineralized with Na_2SiO_3 had RFO = 50, indicating that these capsules were capable of surviving the wash and drying conditions and delivery freshness when broken by the perfumers, releasing the perfume oil.

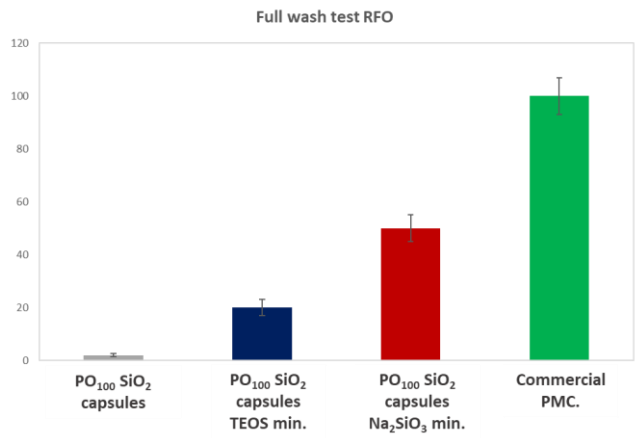

***Figure 6-16**. Full-scale wash test RFO performance for SiO_2 capsules using a commercial PMC as reference. Terry towels were used as fabric models and LFE as detergent matrix.*

6.2.3 Overall results for SiO_2 capsules with PO as core

Overall results for the PO SiO_2 capsules produced in Chapter 6 are summarized in **Table 6-4**. It was possible to produced SiO_2 capsules with comparable mean diameter as the commercial PMC. The overall SPAN was lower than that of the PMC, indicating that the SiO_2 capsules have a narrower size distribution. Adding variable amounts of IPM to the core or the mineralization treatment with Na_2SiO_3 or TEOS did not alter the mean diameter and SPAN considerably. In

addition, the commercial PMC had a shell thickness of about 100 nm (data from P&G), which is about 3x less than the SiO_2 capsules.

Mineralization of SiO_2 capsules had a huge impact on the PO stability in liquid detergent and performance in a full wash test. Moreover, there was a small increase of the nominal rupture stress for the SiO_2 mineralized capsules (both with Na_2SiO_3 and TEOS). However, as the stability in LFE increased significantly, there is an indication that for both mineralization processes there was a shell densification (closing the voids in the SiO_2 shell) by the deposition of extra layers of silica on the capsule surface.

References to this Chapter on pages 245-246

***Table 6-4**. Overall results for SiO_2 capsules developed in Chapter 6 compared to a commercial polymeric PMC.*

	Core material	SiO_2 precursor	Shell solidification time	Mean diameter	SPAN	Average shell thickness	Deformation at rupture (%)	Nominal rupture stress	glass slide test	Stability in LFE (24h) – head space leakage	Performance full scale wash
				Mm		nm	%	Mpa		%	
SiO_2 NPs-PEOS 1.0-20% -PO (PO_{100} SiO_2 capsule)	100% PO	PEOS 1.0 20%	6 weeks	17.0 ± 1.0	0.99 ± 0.03	375 ± 41	20 ± 9	0.30 ± 0.09	High	93%	No
$IPM_{40}PO_{60}$ SiO_2 capsule	40% IPM/60% PO	PEOS 1.0 20%	3 weeks	20.4 ± 1.3	0.92 ± 0.07	355 ± 29	22 ± 4	0.35 ± 0.13	High	97%	-[a]
$IPM_{80}PO_{20}$ SiO_2 capsule	80% IPM/20% PO	PEOS 1.0 20%	10 days	21.2 ± 1.2	0.93 ± 0.07	330 ± 63	18 ± 3	0.49 ± 0.15	High	100%	-[a]
PO_{100} SiO_2 capsule-TEOS min.	100% PO	PEOS 1.0 20%	6 weeks	18.0 ± 1.4	0.91 ± 0.03	383 ± 57	14 ± 5	0.39 ± 0.12	High	41%	Low
PO_{100} SiO_2 capsule-Na_2SiO_3 min	100% PO	PEOS 1.0 20%	6 weeks	17.4 ± 1.1	0.90 ± 0.05	362 ± 45	18 ± 5	0.59 ± 0.26	High	11%	Medium
Commercial PMC	**?**	**-**	**-**	**18.2 ± 2.7**	**1.53**	**100**	**40 ± 3**	**1.50 ± 0.18**	**High**	**2%**	**High**

[a] *Capsules not evaluated using the wash test*

References to this Chapter on pages 245-246

6.2.4 Part 2. Encapsulation of other actives – proof of concept

6.2.4.1 Part 2A. Encapsulation of Menthol Menthyl Lactate (MML)

Menthol and menthyl lactate (MML) is a eutectic mixture used in cosmetics, personal care, food and pharma industry as cooling and flavouring agent.[20] Menthol is a naturally occurring terpene compound, has a very long history of being used in food and medical-related products. Menthyl lactate on the other hand, is synthesized from menthol and lactic acid and it has also been used as cooling agent for skin products, chewing gun and tabaco.[21] Encapsulation of MML could bring more stability to the mixture in aqueous based products such as shampoos and toothpaste.

As observed in **Figure 6-17**, it was possible to produce SiO_2 shell/MML core capsules using the technology developed for the encapsulation of HS and PO. The capsules had a remarkable narrow size distribution as observed in **Figure 6-17A**. The mean diameter was 63.6 µm, the SPAN of the size distribution 0.68 and the average shell thickness 460 ± 39 nm.

Some of the capsules had almost perfectly spherical fractures as a result of drying, due to LaPlace pressure:[22] as the capsule dries, the differences in terms of pressure causes the shell to break. The fractures had a narrow size distribution across and the fractured part of the shell always ended up inside the capsule (**Figure 6-17C** and **D**). Capsules were intact in solution as no free oil was observed, so it was possible to encapsulate MML in SiO_2 capsules, however, for dry applications the shell mechanical properties must be optimized.

References to this Chapter on pages 246-247

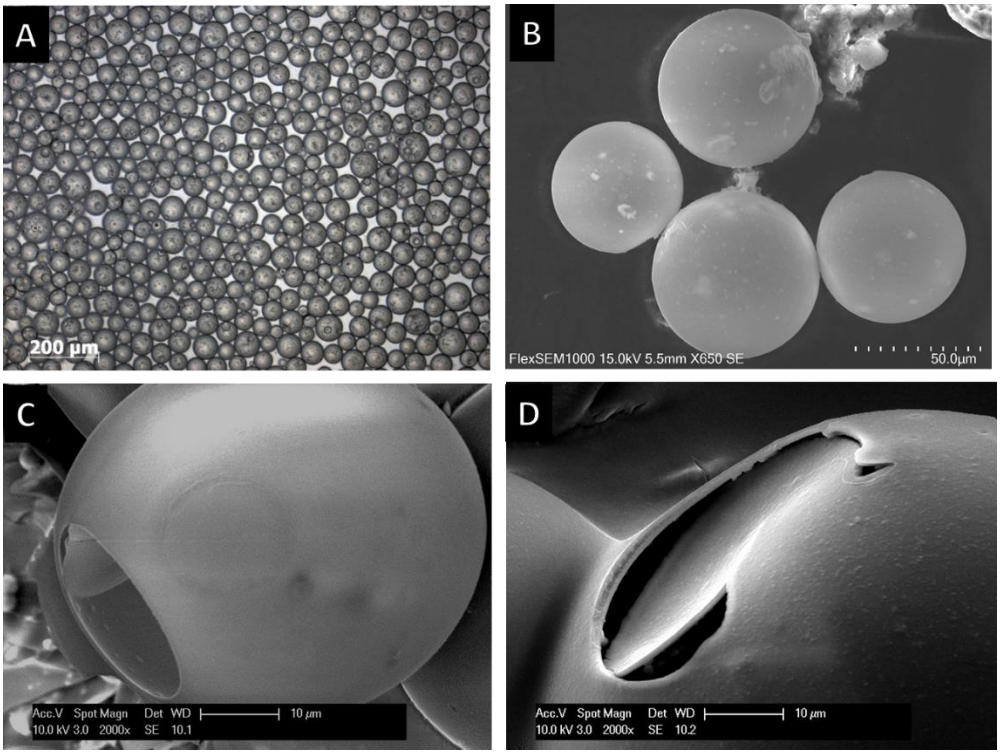

***Figure 6-17**. Optical microscopy (A) and SEM (B-D) images of Pickering emulsion-based silica capsules encapsulating menthol menthyl lactate.*

6.2.4.2 Part 2B. Encapsulation of a water-soluble dye from W/O Pickering emulsions

The technology developed for the encapsulation of a commercial perfume oil was also tested for the encapsulation of a water-soluble active using Allura red, a food-grade dye, as model active for the proof of concept. The objective was to use the Pickering emulsion theory, which rationalises the possibility of shaping the type of emulsion (water-in-oil or oil-in-water) depending on the wettability of the Pickering emulsifiers[12] (Chapter 3 – Section 3.2.1.1). For the formation of water-in-oil emulsions, hydrophobic fumed SiO_2 nanoparticles previously modified with hexadecylsilane were used as Pickering emulsifier (Aerosil R8160). These SiO_2

nanoparticles must stabilize effectively w/o emulsions while a portion of free silanol groups are still available at the particle surface for reaction with PEOS.

Figure 6-18 shows the water-soluble core capsules. It was observed that allura red was clearly encapsulated and shell showed sign of crumpling suggesting that some core material is lost, probably due to the sol-gel process (**Figure 6-18A**), as observed when encapsulating PO. Nevertheless, robust capsules that could survive air-drying were formed, confirming the water-soluble encapsulation prototype was successful (**Figure 6-18B**).

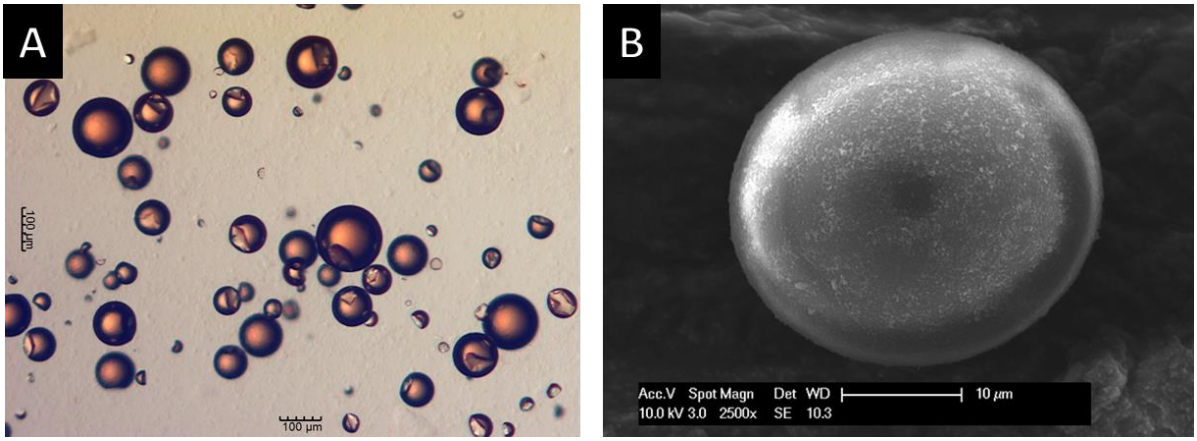

***Figure 6-18**. Optical microscopy (A) and SEM (B) images of Pickering emulsion-based SiO_2 capsules encapsulating an aqueous solution of 0.1 wt% of Allura red.*

6.3 Conclusions

For the optimization of the PO-SiO_2 capsules stability and performance in liquid detergent matrixes, two approaches were studied:

(i) the use of a core-modifier, to make the core more hydrophobic and less likely to be solubilise by the surfactant rich detergent matrix, and

(ii) the mineralization of the SiO_2 capsule to seal the shell voids and pores.

When IPM was used as core-modifier, it was observed that the mechanical properties and shell thickness were dependant on the final level of IPM in the core. Interestingly, when solely IPM was encapsulated ($IPM_{100}SiO_2$ Capsules), the nominal rupture stress was 3.5x higher than the one observed for the $PO_{100}SiO_2$ capsules and 2.3x higher than the $PO_{20}IPM_{80}SiO_2$ capsules. The difference is probably due to the higher affinity of PO towards the water phase in the early stages of shell formation leading to the formation of a porous wall. Unfortunately, IPM did not have a significant positive impact on the stability of the capsules in liquid detergent matrix and all PO leaked out after 24h and only IPM remained inside the shell. Interestingly however, the shell formation kinetics were greatly improved when IPM was used as core material, minimising the time necessary for complete shell formation.

Mineralization of the shell using Na_2SiO_3, could successfully overcome PO leakage of the SiO_2 capsules in liquid detergent, and encouraging results were obtained. These mineralised capsules could also survive a full-scale wash test, depositing on Terry towels, and releasing perfume oil when mechanical force was applied to the towels. Mineralization with TEOS also improved the stability of the SiO_2 capsules in liquid detergent. However, the performance in the full-wash test was much lower. These results were very encouraging, as for the first time SiO_2 capsules encapsulating PO were capable of delivering freshness after a full wash cycle.

Finally, it was possible to use the technique developed throughout this thesis for the encapsulation of other actives with potential application in the consumer goods industry. Herein, we have shown the examples of the encapsulation of a eutectic mixture (MML) and a water-soluble dye (allura red). The technology is versatile and has the potential to be used in many fields by tuning the shell properties for the desirable application.

 References to this Chapter on pages 246-247

6.4 Experimental

6.4.1 Encapsulation of PO and IPM

A 2.5 wt% Aerosil 300 SiO_2NPs dispersion in 0.1M HCl aqueous solution was prepared. In a separate vial, PEOS (0.5 g) was dissolved in PO/IPM (2 g) in different proportions depending on the experiment, as described in **Section 6.2.13**. The oil phase (PO/IPM/PEOS) was then added to 8 g of the aqueous phase containing SiO_2 NPs and the resulting mixture was emulsified using an IKA Ultra-Turrax T25 basic homogeniser (IKA-Werke GmbH & Co – Germany) equipped with a dispersing head of 10 mm diameter operating at 8000 RPM for 5 minutes. The vial was then left undisturbed at 25°C for the condensation step to be completed (1 to 6 weeks, depending on the core composition).

6.4.2 Mineralization using Na_2SiO_3

A 100 ml glass vial was charged with 0.1M HCl aqueous solution (20mL) and SiO_2 capsule slurry (1 g) containing 20% of PO in weight. Then, a 10 wt% Na_2SiO_3 aqueous solution was added to the SiO_2 capsules/0.1M HCl dispersion using a HAVARD PHD 4000 syringe pump at a rate of 10 µl per minute, for a total of 1 hour and 30 minutes (0.9 mL). The dispersion was continuously mixed using an IKA overhead stirrer at 400 RPM for the duration of the Na_2SiO_3 addition. The dispersion was left under stirring (300 RPM) for 24h at 25°C, and then centrifuged at 2000 RPM for 10 minutes to isolate the mineralized SiO_2 capsules, after decant the liquid.

6.4.3 Mineralization using TEOS

A 100 ml glass vial was charged with 20 mL of a 0.1M HCl aqueous solution and 1 g of SiO_2 capsules containing 2% of PO in weight. Then, TEOS was controllably added to the SiO_2

References to this Chapter on pages 246-247

capsules/0.1M HCl dispersion using a HAVARD PHD 4000 syringe pump at a rate of 10 µl per minute, for a total of 1 hour and 30 minutes (0.9 mL). The dispersion was continuously mixed using an IKA overhead stirrer at 400 RPM for the duration of TEOS addition. The dispersion was left under stirring (300 RPM) for 24h at 25°C, and then centrifuged at 2000 RPM per 10 minutes to isolate the mineralized SiO_2 capsules, after decanting the liquid.

6.4.4 Size analysis

Mean capsule diameter and SPAN of the size distribution of the capsules in aqueous dispersion were obtained by static light-scattering using a Mastersizer 2000 instrument (Malvern Instruments Ltd, Malvern - UK). The instrument measures the volume fraction of the capsules in different size bands in the size range of 20 nm to 2000 µm using a Helium-Neon laser connected to a dispersion unit. All experiments were performed at 25°C. The refractive index used was 1.46 (for amorphous silica[23]) and the data analysed using Excel®.

6.4.5 Optical microscopy

Optical microscopy images were obtained using two microscopes: a Leica DMRBE, (Leica Microscope & Systems GmbH) equipped with a software package Moticam Pro 3.0 and a CoolLED pE-300 white light source. The resolution of the microscope was 200 nm. The second microscope used was a Zeiss Axio imager 2 pol (Carl Zeiss Microscopy – Germany, resolution 200 nm) also equipped with a UV light source (Kubler codex HXP 120C).

6.4.6 Scanning Electron Microscopy

SEM images were obtaneide using two different microscopes: a 1000 Tabletop Microscope (Hitachi, Ltd – Japan), magnification 1500X and a Philips XL-30 FEG Environmental SEM with Oxford Inca EDS (Philips UK ltd, Guildford – UK), magnification 3500X.

References to this Chapter on pages 246-247

6.4.7 Mechanical properties

The mechanical properties of the microcapsules were determined by micromanipulation. 0.1g of capsule suspension containing 20% w/w capsule to DI water was first diluted 500x in DI water, and then a drop of the diluted dispersion was added to a glass slide and left to air dry. The glass containing the capsules was then positioned on the micromanipulation rig stage and observed using the side-view camera equipped with a 10x magnification lense. The glass slide was positioned perpendicular to a glass probe with a diameter of 100 µm mounted on an electronically controlled force transducer (Model 403A, Aurora Scientific Inc., Canada, with a maximum operation limit of 5 mN). A single capsule was compressed by the glass probe travelling at 2 µm s^{-1}. The voltage output generated by the transducer after the compression of the capsule was recorded and converted to force using an excel macro. The sensitivity of the transducer used was 0.5 mN/V. Ten random capsules were analysed per sample for statistical analysis. Details of the technique can be found in Chapter 2, Section 2.4.6.

6.4.8 Perfume headspace using GC-MS

The leakage of perfume raw materials (PRM) from the capsules was assessed using GC-MS. A pre-calculated quantity of slurry containing 0.2g of encapsulated perfume was added to 20g of finished product (HDL, LFE or conditioner). The vial was shaken by hand and left undisturbed under controlled temperature for a desirable period before CG-MS analysis. The obtained percentage of each RPM in the head-space was compared to a sample containing the same amount of fresh free perfume (no capsules), which is the positive control corresponding to 100% leakage. GC-MS used was an Agilent technologies 7890B GC system equipped with a 5977B MS detector.

References to this Chapter on pages 246-247

6.4.9 Full wash-scale performance

A laundry product with no perfume was prepared containing a quantity of capsule slurry with the appropriated activity as calculated above. Then, five terry towels (fabric model) were washed using the prepared product in a Miele Softronic W1714 washing machine with the following wash conditions: 30°C, short crease recovery cycle and 1000 rpm. The rest of the load (3 kg) was completed using Calderon load. After the wash, the terry towels were folded in three and put individually in an aluminium bag for transport to the drying room. The Terry towels were then line dried overnight in the drying room (20°C, 55% humidity).

The capsule performance was assessed in relation to commercial perfume microcapsules (PMCs) as positive control. A panel of expert perfumers performed the ofactive assessment of the fabrics in relation to the Rubbed fabric odour (RFO), where dried fabrics are rubbed with the intent of breaking the capsules in order to release the perfume.

6.4.10 Encapsulation of MML

A 2.5 wt% Aerosil 300 SiO_2 NPs dispersion in water was prepared. In a separate vial, 0.5g of PEOS was dissolved in 2g of MML. The MML and PEOS mixture was then added to the water phase containing SiO_2 NPs (8g) and the mixture was then emulsified using an IKA Ultra-Turrax T25 basic homogeniser (IKA-Werke GmbH & Co – Germany) equipped with a dispersing head of 10 diameter operating at 8000 RPM for 5 minutes. The vial was then left to stand at 24h at 25°C and centrifuged at 2000 RPM for 10 minutes to isolate the capsules.

6.4.11 Encapsulation of a water-soluble dye

0.1g of PEOS was mixed with a 1 wt% Aerosil R816 SiO_2 NPs dispersion in HS (total of 5g). In a separate vial, a 0.1wt% allura red in water was prepared. The allura red solution (1g) was

References to this Chapter on pages 246-247

then added to the oil phase (5g) and the mixture emulsified using vortex mixer at 2500 RPM for 5 minutes at 25°C. The vial was then left to stand for 4 weeks at 25°C and centrifuged at 2000 RPM for 10 minutes to isolate the capsules.

6.5 References

1. M. Giamberini, S. F. Prieto, B. Tylkowski, N. A. G. Bandeira, K. A. Bogdanowicz, R. Garcia-Valls, T. Gumi, R. Jastrzab, L. Marteaux and G. Palumbo, *Microencapsulation: Innovative Applications*, De Gruyter, **2015**.
2. J. O. D. J Smets, A Pintens, S J Guinebretiere, A K Druckrey ,P D Sands Procter and Gamble Co *Benefit Agent Containing Delivery Particle,* **2007**
3. S. Bône, C. Vautrin, V. Barbesant, S. Truchon, I. Harrison and C. Geffroy, *Microencapsulated Fragrances in Melamine Formaldehyde Resins*, *CHIMIA International Journal for Chemistry*, **2011**, *65*, 177-181.
4. R. Mercadé-Prieto, X. Pan, A. Fernández-González, Z. Zhang and S. Bakalis, *Quantification of Microcapsules Deposited in Cotton Fabrics before and after Abrasion Using Fluorescence Microscopy*, *Industrial & Engineering Chemistry Research*, **2012**, *51*, 16741-16749.
5. H. N. Yow and A. F. Routh, *Formation of Liquid Core–Polymer Shell Microcapsules*, *Soft Matter*, **2006**, *2*, 940-949.
6. G. B. Sukhorukov, A. Fery, M. Brumen and H. Möhwald, *Physical Chemistry of Encapsulation and Release*, *Physical Chemistry Chemical Physics*, **2004**, *6*, 4078-4089.
7. X. Pan, D. York, J. A. Preece and Z. Zhang, *Size and Strength Distributions of Melamine-Formaldehyde Microcapsules Prepared by Membrane Emulsification*, *Powder Technology*, **2012**, *227*, 43-50.
8. *Monographs on Fragrance Raw Materials: Isopropyl Myristate*, *Food and Cosmetics Toxicology*, **1976**, *14*, 323-325.
9. R. N. Vadgama, A. A. Odaneth and A. M. Lali, *Green Synthesis of Isopropyl Myristate in Novel Single Phase Medium Part I: Batch Optimization Studies*, *Biotechnology Reports*, **2015**, *8*, 133-137.
10. P. Klaffenbach and D. Kronenfeld, *Analysis of Impurities of Isopropyl Myristate by Gas-Liquid Chromatography*, *Journal of Chromatography A*, **1997**, *767*, 330-334.
11. A. S. N. P. B. Claudie, Firmenich Sa, *Process for Preparing Aminoplast Microcapsules,* **2015**
12. B. P. Binks, P. D. I. Fletcher, B. L. Holt, P. Beaussoubre and K. Wong, *Phase Inversion of Particle-Stabilised Perfume Oil-Water Emulsions: Experiment and Theory*, *Physical Chemistry Chemical Physics*, **2010**, *12*, 11954-11966.
13. R. Aveyard, B. P. Binks and J. H. Clint, *Emulsions Stabilised Solely by Colloidal Particles*, *Advances in Colloid and Interface Science*, **2003**, *100–102*, 503-546.
14. E. Dickinson, *Use of Nanoparticles and Microparticles in the Formation and Stabilization of Food Emulsions*, *Trends in Food Science & Technology*, **2012**, *24*, 4-12.
15. *Colloidal Particles at Liquid Interfaces*, Cambridge University Press, Cambridge, **2006**.

16. L. D. a. F. HPR, *Crc Handbook of Chemistry and Physics*, Boca Raton, 75th Edition edn., **1995**.
17. J. G. VAIL, *Soluble Silicates*, *Soil Science*, **1952**, *74*, 407.
18. M. Destribats, V. Schmitt and R. Backov, *Thermostimulable Wax@Sio2 Core−Shell Particles*, *Langmuir*, **2010**, *26*, 1734-1742.
19. C. J. Brinker, *Hydrolysis and Condensation of Silicates: Effects on Structure*, *Journal of Non-Crystalline Solids*, **1988**, *100*, 31-50.
20. Y. Yu, W. Zhang, X. Han, X. Huang, J. Zhao, Q. Ren and H. Luo, *Menthol-Based Eutectic Mixtures: Novel Potential Temporary Consolidants for Archaeological Excavation Applications*, *Journal of Cultural Heritage*, **2019**.
21. S. S. Bharate and S. B. Bharate, *Modulation of Thermoreceptor Trpm8 by Cooling Compounds*, *ACS chemical neuroscience*, **2012**, *3*, 248-267.
22. J. van Wijk, J. W. O. Salari, J. Meuldijk and B. Klumperman, *Determination of the Shell Growth Direction During the Formation of Silica Microcapsules by Confocal Fluorescence Microscopy*, *Journal of Materials Chemistry B*, **2015**, *3*, 7745-7751.
23. G. Ghosh, *Handbook of Refractive Index and Dispersion of Water for Scientists and Engineers*, Ghosh, Sujata, **2005**.

CHAPTER 7. Conclusion and Future Work

7.1 Overall conclusion

The main objective of this research was to evaluate the possibility of encapsulating a commercial perfume oil in SiO_2 capsules with desirable structural and mechanical properties, providing stability, protection and triggered release for laundry applications. Therefore, an encapsulation method based on SiO_2 NPs as Pickering emulsion templates and the hydrolysis and condensation of hyperbranched polyethoxysilane (PEOS) was investigated for the formation of a robust SiO_2 shell. The technology development was divided in 4 main steps:

1. Understanding the stability of hexyl salicylate (HS) and perfume oil (PO) Pickering emulsion stabilised by SiO_2 NPs followed by the synthesis and characterization of PEOS (**Chapter 3**);
2. development of the encapsulation method using a perfume model as core material (HS) (**Chapter 4**);
3. encapsulation of the commercial PO in the SiO_2 capsules varying key parameters to obtain a robust SiO_2 shell (**Chapter 5**);
4. optimization of the SiO_2 capsule shell for laundry applications (**Chapter 6**).

PO SiO_2 capsules were successfully produced and the results were encouraging, demonstrating that the technology has potential to substitute commercial polymer microcapsules (PMCs) in the future. The summary of the physical, mechanical properties, stability and performance of the SiO_2 capsules produced throughout this research compared to a commercial PMC used for laundry products applications can be found in **Table 7-1.**

References to this Chapter on page 255

Table 7-1. *Summary of physical, mechanical properties, stability and performance data for the PO SiO_2 capsules.*

	Ch.	Core material	SiO_2 precursor	Mean size (µm)	SPAN	Average shell thickness (nm)	Deformation at rupture (%)	Nominal rupture stress (Mpa)	glass slide test	Stability in LFE (24h at RT) – head space leakage %	Performance full scale wash
SiO_2NPS-PEOS 1.2-20%-PO-pH 4.6	**5**	100% PO	PEOS 1.2 20%	22.21 ± 1.94	1.23 ± 0.11	-[a]	19 ± 3	0.22 ± 0.06	No	100%	-
SiO_2NPS-PEOS 1.2-40%-PO-pH 4.6	**5**	100% PO	PEOS 1.2 40%	26.77 ± 1.86	1.10 ± 0.13	-[a]	25 ± 3	0.89 ± 0.16	No	100%	-
SiO_2 NPs-PEOS 1.2-20% -PO	**5**	100% PO	PEOS 1.2 20%	18.76 ± 1.24	1.02 ± 0.05	308 ± 28	21 ± 6	0.32 ± 0.14	No	100%	No
SiO_2 NPs-PEOS 1.2-40% -PO	**5**	100% PO	PEOS 1.2 40%	19.01 ± 1.08	1.05 ± 0.08	383 ± 26	15 ± 5	0.79 ± 0.10	No	100%	No
SiO_2 NPs-PEOS 1.0-20% -PO (PO_{100} SiO_2 capsule)	**5**	100% PO	PEOS 1.0 20%	17.00 ± 1.01	0.99 ± 0.03	375 ± 41	20 ± 9	0.30 ± 0.09	High	93%	No
SiO_2 NPs-PEOS 1.0-40% -PO	**5**	100% PO	PEOS 1.0 40%	17.09 ± 1.08	1.21 ± 0.23	750 ± 25	15 ± 5	1.04 ± 0.43	High	100%	No
$IPM_{40}PO_{60}$ SiO_2 capsule	**6**	40% IPM/60% PO	PEOS 1.0 20%	20.41 ± 1.27	0.92 ± 0.07	355 ± 29	22 ± 4	0.35 ± 0.13	High	97%	No
$IPM_{80}PO_{20}$ SiO_2 capsule	**6**	80% IPM/20% PO	PEOS 1.0 20%	21.22 ± 1.23	0.93 ± 0.07	330 ± 63	18 ± 3	0.49 ± 0.15	High	100%	No
PO_{100} SiO_2 capsule-TEOS min.	**6**	100% PO	PEOS 1.0 20%	18.04 ± 1.44	0.91 ± 0.03	383 ± 57	14 ± 5	0.39 ± 0.12	High	41%	Low
PO_{100} SiO_2 capsule-Na_2SiO_3 min	**6**	100% PO	PEOS 1.0 20%	17.45 ± 1.13	0.90 ± 0.05	362 ± 45	18 ± 5	0.59 ± 0.26	High	11%	Medium
Commercial PMC	**-**	**?**	**-**	**18.20 ± 2.72**	**1.53**	**100**	**40 ± 3**	**1.50 ± 0.18**	**High**	**2%**	**High**

References to this Chapter on page 255

7.1.1 Emulsion stability

PO and HS droplets could successfully be stabilized using hydrophilic fumed silica nanoparticles as Pickering emulsifiers. Pickering emulsions were stable for over 6 months. It was possible to take advantage of the limited coalescence phenomenon to control the mean size and the SPAN of the size distribution for emulsions.[1] As the oil droplet mean diameter could be controlled by the concentration of SiO_2 NPs to oil, it was clear that hydrophilic silica nanoparticles are efficient Pickering emulsifiers for both oils.[2]

7.1.2 SiO_2 capsule formation

(a) The effect of the pH

The silica sol-gel process is extremely dependent on the pH,[3] which affects the surface activity of the SiO_2 NPS and the hydrolysis and condensation rate of PEOS.[4] As the SiO_2 NPs used in this project were hydrophilic with a surface covered with Si-OH groups, a low pH was favourable for the formation of stable Pickering emulsions, as the surface silanol groups become protonated and less stable in the water phase, giving preference to the water-oil interface. A low pH was also ideal for a proper hydrolysis and condensation rates of PEOS; in these conditions both hydrolysis and condensation are fast, however, all PEOS hydrolyses before condensation starts, forming a film around the droplet,[5] that can accommodate re-arrangements and the formation of a well-defined shell.

(b) The effect of the PEOS concentration

SiO_2 capsules could be formed with three different concentrations of PEOS in relation to the oil phase tested: 10, 20 and 40 wt%. By increasing the concentration of PEOS in the oil phase to 40 wt%, the SiO_2 capsules had a higher nominal rupture stress compared to ones produce

References to this Chapter on page 256

with 10 or 20 wt%. The observed variations in terms of mechanical properties were due to two main factors: the formation of a thicker SiO_2 shell or the solidification of an excess of PEOS inside the core. When PEOS 1.0 was used to form the shell, by increasing the PEOS concentration it was possible to increase the shell thickness and as consequence, the nominal fracture strength, which had a comparable value to a commercial PMC.[6] For SiO_2 capsules produced with PEOS 1.2, there was no significant increase in terms of shell thickness independently of the pH and the excess of PEOS solidified in the core of the capsule, due to the fast condensation rate, high viscosity and low surface activity of PEOS 1.2.

(c) The effect of PEOS molecular weight (M_w)

Two different PEOS batches produced in our laboratory were tested for the encapsulation of PO: PEOS 1.2 (M_w: 3700 g/mol) and PEOS 1.0 (M_w: 2500 g/mol). PEOS 1.2 also had a more advanced degree of condensation, as identified by the degree of branching calculations (0.59 for PEOS 1.2 and 0.48 for PEOS 1.0). It was observed that capsules produced using PEOS 1.0 as silica precursor (SiO_2 NPs-PEOS 1.0-20% -PO and SiO_2 NPs-PEOS 1.0-40% -PO), had consistently more well-defined shells and no PEOS condensed inside the core. The opposite was observed for PEOS 1.2, where when 40 wt% of PEOS was used (SiO_2 NPs-PEOS 1.2-40% -PO), core solidification was observed. These observations suggest that PEOS 1.0 was more surface active, i.e. had more amphiphilic properties when partially hydrolysed, so all PEOS 1.0 condensed at the interface. PEOS 1.2 in the other hand had a more advanced degree of condensation (i.e. less hydrolysable moieties when compared to PEOS 1.0, so the condensation rate is faster)[7] and a higher viscosity, so part of it started to condensate before reaching the interface. In terms of performance, capsules produced with PEOS 1.0 had a more promising results when compared to the ones produced using PEOS 1.2; when PEOS 1.0 was

References to this Chapter on page 256

used, capsules could survive airdrying and release perfume when mechanical force was applied to them, which was not observed for capsules produced using PEOS 1.2. However, the shell formation of SiO_2NPs-PEOS 1.0 capsules was much slower than for the ones prepared with PEOS 1.2, probably due to the slow condensation rates.

(d) The effect of the oil polarity

Four oils were successfully encapsulated using the silica-based encapsulation technology described in this thesis: hexyl salicylate (ClogP 5.7), perfume oil (ClogP 3.5), isopropyl myristate (IPM) (ClogP 7.2) and menthol menthyl lactate (MML) (CloP 3.0). The polarity of the oil had an impact in the inner shell surface as well as the shell thickness of the capsule, therefore, contributing to the mechanical properties of the capsule. The polarity of the oil also influenced the shell solidification time; the solidification was faster when the core oil was less polar, which contributed to high interfacial tension between the oil and the water and promoting the surface activity of PEOS.

(e) The effect of the mineralization

A post treatment of the silica capsules with a slow addition of TEOS or sodium silicate seemed to have contributed for the formation of SiO_2 layer around the pre-formed SiO_2 capsules, minimising the porosity of the shell therefore, minimising leakage of PO from the capsule core. Mineralization of the shell using Na_2SiO_3, could successfully overcome the stability problems of the SiO_2 capsules in liquid detergent, and encouraging results were obtained. These mineralised capsules could also survive a full-scale wash test, depositing on terry towels, and releasing perfume oil when shear was applied to the towels. Mineralization with TEOS also improved the stability of the SiO_2 capsules in liquid detergent but the performance

References to this Chapter on page 256

in the full-wash test was much lower. These results were very encouraging, as for the first time all SiO_2 capsules encapsulating PO could deliver freshness (release perfume oil) after a full wash cycle.

(f) Encapsulation of other actives

It was possible to use the technique developed throughout this thesis for the encapsulation of other actives with potential application in the consumer goods industry. Herein, we have shown the examples of the encapsulation of a single oil component (HS), a mixture of perfume raw materials (PO), a eutectic mixture (MML) and a water-soluble dye, Allura red. The technology is versatile and has the potential to be used in many fields by tuning the shell properties for the desirable application.

7.1.3 Overall size and size distribution results

The advantage of using Pickering emulsions as templates for the formation of silica capsules is that the mean size could be finely controlled by taking advantage of the limited coalescence phenomenon.[1] Moreover, as an overall, the SPAN of the size distribution was much lower for the SiO_2 capsules when compared to the commercial PMC, which could be interesting when while designing a encapsulation technology for different applications with targeted delivery.

7.1.4 Overall mechanical properties results

The mechanical properties of the capsules produced during this project could be controlled by two main parameters: the concentration of PEOS used to form the capsules and the composition of the oil phase. It was noticed that the higher the concentration of PEOS the thicker the SiO_2 shell, leading to a higher nominal rupture stress. The composition of the oil phase also had an impact on the mechanical properties. When IPM was used as core-modifier,

References to this Chapter on page 256

it was observed that the mechanical properties and shell thickness were dependant on the final level of IPM in the core. Interestingly, when solely IPM was encapsulated (IPM_{100} SiO_2 Capsules), the nominal rupture stress was 3.5x higher than the one observed for the PO_{100} SiO_2 Capsules) and 2.3x higher than the $PO_{20}IPM_{80}SiO_2$ capsules, while the shell thickness was lower. The difference is probably due to the higher affinity of some components of PO towards the water phase in the early stages of shell formation leading to the formation of a porous wall and a void inside the shell as observed in the PO_{100} SiO_2 Capsules.

7.1.5 Overall performance and stability results

SiO_2 capsules produced in chapters 4 and 5 (**Table 7.1**) were very porous when added to a surfactant rich matrix (LFE), as all oil phase quickly leaked out of the SiO_2 shell. In chapter 6, when IPM was used in combination with PO in the oil phase, it was observed that the perfume oil still leaked completely out, while IPM remained stable inside the SiO_2 capsule shell, as it is more hydrophobic than the PO. Mineralization using TEOS or sodium silicate improved the stability of perfume oil in silica capsules in LFE. These mineralised capsules could also survive a full-scale wash test, depositing on Terry towels, and releasing perfume oil when shear was applied to the towels.

7.1.6 Have we developed a promising alternative perfume oil encapsulation technology for laundry products application?

Promising. Nevertheless, there is a long way to go. According to P&G, for the first time it was possible to produce all-silica capsules encapsulating a complex commercial perfume oil, which are low leaking in a surfactant rich matrix and able to delivery freshness benefit after a full wash test. These results are extremely encouraging, however, there are many

References to this Chapter on page 256

challenges associated with bringing this technology to the market, such as bringing the leakage percentage down to maximum 2% for a prolonged period (6 months), matching the performance of the current PMCs in full scale wash tests and industrial scale production.

7.2 Future work and recommendations

This thesis has demonstrated the possibility of encapsulating a complex perfume oil in silica capsules for laundry applications. To further develop the technology, it is necessary to further understand the mechanistic transformations leading to the formation of the SiO_2 shell, such as the sol-gel kinetics of PEOS at the water/oil interface, parameters controlling intrinsic reactivity of PEOS at the interface and understand the interactions of PEOS with SiO_2 NPs and the different components of the PO. Gaining fundamental understanding of the microstructure of the capsules wall need to be fully characterized and studied to produce optimal SiO_2 capsules with low porosity and higher nominal rupture stress in an acceptable time frame.

Cleary the time necessary for the capsules to be fully solidified is not suitable for an industrial application, so the capsule curing process must be optimised. Initial experiments done in last month of the project suggested that by curing the capsule at 50°C for 3 weeks is enough to obtain fully solidified capsules. Temperature should be investigated further if it doesn't cause degradation of the perfume oil. Other sol-gel acceleration procedures might be tested such as the use of a sol-gel catalyst and surface modified silica nanoparticles.

By adding the mineralization step after the encapsulation process it was possible to minimize leakage; however, the percentage of PO leaking out of the capsule is still high for the

References to this Chapter on page 256

application (11% after 24h at room temperature). Therefore, the mineralization process must me optimized to reach acceptable leakage levels for commercial applications (less than 2%).

For industrial applications, a new technology must be scalable to be produced at the plant. Therefore, the technology developed herein, in the millilitres scale, must be optimized for the production in the tons scale, especially for laundry applications which is P&G's largest business operating worldwide.

Finally, it was possible to encapsulate different oils using technology developed throughout this project (hexyl salicylate, perfume oil, isopropyl myristate and menthol menthyl lactate) and preliminary experiments suggested that it is possible to encapsulate water-soluble actives as well. These studies could be extended to the encapsulation of other strategic actives for the industry, such as enzymes, bleaching agents and dyes.

7.3 References

1. S. Arditty, C. P. Whitby, B. P. Binks, V. Schmitt and F. Leal-Calderon, *Some General Features of Limited Coalescence in Solid-Stabilized Emulsions*, *The European Physical Journal E*, **2003**, *11*, 273-281.
2. R. Aveyard, B. P. Binks and J. H. Clint, *Emulsions Stabilised Solely by Colloidal Particles*, *Advances in Colloid and Interface Science*, **2003**, *100–102*, 503-546.
3. D. Levy and M. Zayat, *The Sol-Gel Handbook: Synthesis, Characterization, and Applications*, Wiley, **2015**.
4. Y. Zhao, Y. Li, D. E. Demco, X. Zhu and M. Möller, *Microencapsulation of Hydrophobic Liquids in Closed All-Silica Colloidosomes*, *Langmuir*, **2014**, *30*, 4253-4261.
5. Y. Zhao, Z. Chen, X. Zhu and M. Moller, *Silica Nanoparticles Catalyse the Formation of Silica Nanocapsules in a Surfactant-Free Emulsion System*, *Journal of Materials Chemistry A*, **2015**, *3*, 24428-24436.
6. G. Sun and Z. Zhang, *Mechanical Strength of Microcapsules Made of Different Wall Materials*, *International Journal of Pharmaceutics*, **2002**, *242*, 307-311.
7. C. J. Brinker, *Hydrolysis and Condensation of Silicates: Effects on Structure*, *Journal of Non-Crystalline Solids*, **1988**, *100*, 31-50.